

UNIVERSITY OF BELGRADE
FACULTY OF CIVIL ENGINEERING

Ahmed A. Alalikhhan

DETECTION AND LOCALIZATION OF
DAMAGE OF CIVIL STRUCTURES BASED
ON AMBIENT VIBRATION
MEASUREMENTS

Doctoral thesis

Belgrade, 2016.

UNIVERZITET U BEOGRADU
GRAĐEVINSKI FAKULTET

Ahmed A. Alalikhani

DETEKCIJA I LOKALIZACIJA OŠTEĆENJA
GRAĐEVINSKIH KONSTRUKCIJA NA
OSNOVU REGISTROVANIH
AMBIJENTALNIH VIBRACIJA

Doktorska disertacija

Beograd, 2016.

University of Belgrade
Faculty of Civil Engineering

Doctoral thesis:

**DETECTION AND LOCALIZATION OF DAMAGE OF CIVIL
STRUCTURES BASED ON AMBIENT VIBRATION
MEASUREMENTS**

Candidate:

Ahmed A. Alalikhhan

Supervisor:

Associate Professor Dr. Zoran Mišković

University of Belgrade, Faculty of Civil Engineering

Examining Committee members:

Professor Dr. Milenko Stegić,

University of Zagreb, Faculty of Mechanical Engineering and Naval Architecture

Associate Professor Dr. Ratko Salatić,

University of Belgrade, Faculty of Civil Engineering

Assistant Professor Dr. Nataša Prašćević,

University of Belgrade, Faculty of Civil Engineering

Belgrade,

2016.

Univerzitet u Beogradu

Građevinski Fakultet

Doktorska disertacija:

**DETEKCIJA I LOKALIZACIJA OŠTEĆENJA GRAĐEVINSKIH
KONSTRUKCIJA NA OSNOVU REGISTROVANIH
AMBIJENTALNIH VIBRACIJA**

Kandidat:

Ahmed A. Alalikhhan

Mentor:

V. prof. dr. Zoran Mišković,

Univerzitet u Beogradu, Građevinski Fakultet

Članovi komisije za ocenu i odbranu:

Prof. dr. Milenko Stegić,

Univerzitet u Beogradu, Građevinski Fakultet

V. prof. dr. Ratko Salatić,

Univerzitet u Beogradu, Građevinski Fakultet

V. prof. dr. Nataša Praščević,

Univerzitet u Beogradu, Građevinski Fakultet

Beograd,

2016.

ACKNOWLEDGEMENTS

The work that presented in this thesis required large efforts, financial resources and logistic supports which facilitated the implementing of this work for the sake of scientific research.

The author would like to thank Serbian government represented by Science and Technology Development of Republic of Serbia for PhD scholarship within the project "World in Serbia" and for partial financial support through the Technology Development Project TR- 36048.

Special thank for the Ministry of Higher Education and Scientific Research of Republic of Iraq for providing the opportunity to get PhD scholarship and financial supports.

Author would like to thank and gratitude the great role of the mentor A. Professor Dr. Zoran Mišković for his wise suggestions and supervising the present work to reach the extreme level of knowledge containment.

Also, special thanks for the examining committee members Professor Dr. Milenko Stegić and A. Professor Dr. Ratko Salatić for their useful advises and suggestions that have been raised the present work to a higher level.

Author thanks all colleagues who helped directly or indirectly in completing this work throughout the period of study.

Finally, thanks for His Excellency Dr. Falah Alsaady, the Iraqi ambassador in the Belgrade for his logistic help during the beginning period of study.

Belgrade, 2016.

The author

DETECTION AND LOCALIZATION OF DAMAGE OF CIVIL STRUCTURES BASED ON AMBIENT VIBRATION MEASUREMENTS

ABSTRACT

Generally, damage detection of different types of steel structures is the main aspect that has been studied in the present work. Damage could be detected by different ways which depend on different procedures existed in literature. In the present work, the adopted concept of damage detection depends on the procedure of comparison between the updated modal parameters (natural frequencies and mode shapes) of the FE model with their corresponding experimental values. Hence, estimating of structural modal parameters experimentally and numerically are another aspects that are adopted in the present work. Based on ambient vibration measurements (AVM) that implemented upon different types of steel structures, experimental modal parameters are extracted using ARTeMIS software according to the frequency domain decomposition (FDD) technique. On the other hand, modal analysis by ANSYS software is implemented to compute the numerical values of modal parameters which required during the procedure of damage detection. The process of damage detection is executed with the aid of proposed Tabu Search (TS) optimization procedure to detect the location and severity of damage. This technique is relatively new and was not used before in the field of civil structure damage detection which satisfies the state of the art in the present work. The proposed procedures of TS optimization are written and performed in MATLAB environment. MATLAB has the ability of simultaneously handling the experimentally extracted modal parameters with their corresponding numerical values which are continuously updated by ANSYS software. The comparison between the estimated experimental and numerical modal parameters is executed according to values obtained by a certain proposed form called "objective function" which produces the value of error that used in the comparison. Minimum value of error reflects the optimum value that indicates the closest result to the target (actual) value.

For the sake of damage detection, another important aspect had been adopted in the present work which is the calibration process by updating of FE model. Due to several reasons,

mismatch between modal parameters of the experimental and numerical model is usually exist leading to erroneous results in the procedure of damage detection. Hence, calibration process is aimed to produce numerical (updated) values of structural modal parameters as close as possible to their corresponding experimental values. In this way, the convergence between the compared modal parameters is achieved which allows the procedure of damage detection to be implemented with more accurate results.

Four types of steel structures are modeled in the present work to study the behavior of 1D, 2D and 3D structural models during the procedures of calibration process and damage detection . A simply supported overhang beam model is adopted to study the behavior of 1D structural model while a grid-bridge model has plate action is used to represent 2D structural model in the proposed procedures. For the 3D structural model, two models are adopted: Vierendeel bridge model and 10-storey building model which represent the most complex structural models in the present work. This verifies the ability of applying the proposed procedures, calibration by FE model updating and damage detection, upon the complex structures.

Present study discovered that the proposed TS optimization procedure is an efficient and robust technique for using in the both fields of calibration by FE model updating and damage detection of complex civil structures.

Keywords: damage detection, ambient vibration measurements, modal parameters, Tabu Search, steel structures

Scientific field: Civil Engineering

Narrow scientific field: Vibration of steel structures

UDK: 624.014.2(043.3)

DETEKCIJA I LOKALIZACIJA OŠTEĆENJA GRAĐEVINSKIH KONSTRUKCIJA NA OSNOVU REGISTROVANIH AMBIJENTALNIH VIBRACIJA

REZIME

Općenito, u radu je razmatrana detekcija oštećenja različitih tipova čeličnih konstrukcija. Oštećenje se može otkriti na različite načine, koji zavise od različitih postupaka navedenih u literaturi. Detekcija oštećenja zavisi od postupka poredjenja između ažuriranih modalnih parametara (prirodnih frekvencija i oblika) modela KE s odgovarajućim eksperimentalnim vrednostima. Procenjuju se modalni strukturni parametri, eksperimentalno i numerički. Na osnovu merenja ambijentalnih vibracija (MAV), na različitim vrstama čeličnih konstrukcija, eksperimentalni modalni parametri se određuju pomoću ARTeMIS softvera u skladu s tehnikom frekvencijskog razlaganja (FR). S druge strane, primenom ANSYS softvera, izračunavaju se numeričke vrednosti modalnih parametara potrebnih u postupku otkrivanja oštećenja. Detekcija oštećenja vrši se uz pomoć predložene Tabu (TS) optimizacije za otkrivanje lokacije i ozbiljnost oštećenja. Tehnika TS optimizacije je relativno nova i nije ranije korišćena u detekciji oštećenja građevinskih konstrukcija. Predložene procedure TS optimizacije su napisane i izvedene u MATLAB okruženju. MATLAB ima sposobnost za istovremeno razmatranje eksperimentalno dobijenih parametara modela, i odgovarajućih numeričkih vrednosti koje se kontinualno ažuriraju uz pomoć ANSYS softvera. Poređenje između procenjenih eksperimentalnih i numeričkih parametara modela se vrši u skladu s vrednostima dobijenih predloženom "objektivnom funkcijom" (treba "funkcija kriterijuma" ili "funkcija cilja") koja određuju vrednost greške. Minimalna vrednost greške odražava optimalnu vrednost koja ukazuje na najbliži rezultat ciljne (stvarne) vrednosti.

U cilju detekcije oštećenja usvojen je još jedan važan korak, tj. kalibracija s ažuriranjem FE modela. Iz više razloga, neslaganje između modalnih parametara eksperimentalnog i numeričkog modela je obično dovodi do pogrešnih rezultata u postupku otkrivanja oštećenja. Stoga, proces kalibracije ima za cilj da proizvede (ažurira) numeričke vrednosti strukturnih parametara modela, što je moguće bliže , odgovarajućim

eksperimentalnim vrednostima. Na ovaj način je ostvarena konvergencija između odnosa modalnih parametara, što omogućava postupak detekcije oštećenja.

Modelirane su četiri vrste čeličnih konstrukcija kako bi se proučavalo ponašanje 1D, 2D i 3D konstruktivnih modela u toku procesa kalibracije i detekcije oštećenja. Model slobodno oslonjene grede s prepustima je usvojen za proučavanje ponašanja 1D modela, dok model rešetke se koristi za predstavljanje 2D modela. Za 3D model, usvojena su dva modela: Vierendeel model mosta i model 10-spratne zgrade. Ovo potvrđuje sposobnost primene predložene procedure, kalibracije FE modela ažuriranja i detekcije oštećenja na složene konstrukcije.

Predstavljena studija otkrila je da je predloženi postupak TS optimizacije efikasna i snažna tehnika za korišćenje u obe oblasti kalibracije FE modela ažuriranja i detekcije oštećenja složenih građevinskih objekata.

Ključne reči: otkrivanje oštećenja, merenje ambijentalnih vibracija, modalni parametri, TS optimizacija, čelične konstrukcije

Naučna oblast: Građevinarstvo

Uža naučna oblast: Vibracije čeličnih konstrukcija

UDK: 624.014.2(043.3)

I. LIST OF CONTENTS

LIST OF FIGURES.....	x
LIST OF TABLES.....	xxi
SYMBOLS AND ABBREVIATIONS.....	xxvi
1. INTRODUCTION.....	1
1.1. General.....	1
1.2. Objective and scope.....	3
1.3. Innovative aspect of the research.....	5
1.4. Layout of the dissertation.....	5
2. METHODS OF DAMAGE DETECTION IN CIVIL STRUCTURES.....	7
2.1. Introduction.....	7
2.2. Theory of damage.....	8
2.2.1. Crack theory.....	8
2.2.2. Effect of damage on structural elements.....	9
2.2.3. Damage sources.....	10
2.3. Levels of damage detection.....	11
2.4. Description of some damage detection methods.....	12
2.4.1. Damage detection according to the integrity of the tested model.....	13
2.4.1.1. Destructive tests.....	13
2.4.1.2. Non-destructive tests.....	14
2.4.2. Damage detection based on static displacements.....	15
2.4.3. Vibration based damage detection.....	16
2.4.3.1. Damage detection according to strain energy.....	17
2.4.3.2. Damage detection using modal flexibility method.....	21
2.4.3.3. Damage detection using frequency response function (FRF).....	22
2.4.3.4. Damage detection using natural frequencies and mode shapes.....	23
2.4.3.4.1. Change in natural frequencies.....	24
2.4.3.4.2. Changes in mode shapes.....	25

3. CIVIL STRUCTURE MODAL PROPERTIES IDENTIFICATION BASED ON AMBIENT VIBRATION MEASUREMENTS.....	27
3.1. Introduction.....	27
3.2. Applications of Ambient Vibration Measurements (AVM) technique.....	27
3.3. Adopted techniques of extraction dynamic properties from AVM recorded data.....	32
3.3.1. ARTeMIS software capabilities.....	32
3.3.2. Frequency Domain Decomposition (FDD).....	34
3.3.3. Enhanced Frequency Domain Decomposition (EFDD).....	37
3.3.4. Stochastic Subspace Identification (SSI).....	38
3.4. Equipments needed for AVM tests.....	42
3.4.1. Accelerometers.....	42
3.4.2. Data Acquisition System.....	43
3.4.3. PC computer.....	44
3.4.4. Simulation of ambient vibrations - Low frequency and low level shaker excitation.....	46
3.4.5. Other complementary devices.....	47
3.5. Adopted damage detection procedure of civil structures based on ambient vibration measurements.....	48
3.5.1. Adopted procedure of damage detection.....	48
3.5.2. Objective function.....	51
3.5.2.1. General.....	51
3.5.2.2. Adopted objective functions.....	53
4. APPLICATION OF OPTIMIZATION PROCEDURES IN DAMAGE DETECTION OF CIVIL STRUCTURES.....	55
4.1. Introduction.....	55
4.2. Optimization techniques.....	56
4.2.1. Genetic Algorithm (GA) technique.....	57
4.2.2. Simulated Annealing (SA) technique.....	59
4.2.3. Artificial Neural Network (ANN) technique.....	61

4.2.4. Tabu Search (TS) technique.....	62
4.3. Review of application of optimization methods in damage detection.....	63
4.3.1. GA procedure in damage detection.....	63
4.3.2. SA procedure in damage detection.....	65
4.3.3. ANN procedure in damage detection.....	65
4.3.4. TS procedure in damage detection.....	66
4.4. Tabu Search - Adopted optimization technique in the study.....	67
4.4.1. General.....	67
4.4.2. Objectives of selecting TS technique in the present work.....	67
4.4.3. Characteristics of the adopted TS algorithm.....	68
4.4.3.1. Tabu list.....	68
4.4.3.2. Candidate list.....	68
4.4.3.3. Termination criteri.....	69
4.4.4. Adopted TS procedure.....	69
5. EXPERIMENTAL RESEARCH ON STRUCTURAL MODELS OF DIFFERENT CONFIGURATIONS - RESEARCH PROGRAM AND RESULTS.....	72
5.1. Introduction.....	72
5.2. Simply supported overhang beam model.....	72
5.2.1. Experimental program - model erection.....	73
5.2.2. Preparing the requirements of AVM and experimental analysis.....	73
5.2.3. Implementing of AVM upon the overhang beam model.....	75
5.2.4. Processing the configuration input file and AVM data by ARTeMIS software.....	76
5.2.5. Intact case of the overhang beam model.....	78
5.2.5.1. Results of the extracted modal parameters using FDD technique.....	78
5.2.5.2. Verifying the extracted modal parameters using EFDD technique.....	82
5.2.5.3. Verifying the extracted modal parameters using SSI technique.....	83
5.2.6. Damaged case of the overhang beam model.....	87
5.2.6.1. First adopted overhang damage case AODC-1.....	87
5.2.6.2. Second adopted overhang damage case AODC-2.....	90

5.3. Grid-bridge model.....	92
5.3.1. Experimental program.....	92
5.3.1.1. Scale considerations.....	92
5.3.1.2. Model erection.....	93
5.3.2. States of mass applications.....	96
5.3.3. Preparing requirements of AVM and experimental analysis.....	97
5.3.4. Implementing AVM upon the grid-bridge model.....	98
5.3.5. Processing the configuration input file and AVM data by ARTeMIS software.....	98
5.3.6. Intact case of the grid-bridge model.....	100
5.3.6.1. State of model without additional mass.....	100
5.3.6.1.1. Results of the extracted modal parameters using FDD technique.....	100
5.3.6.1.2. Verifying the extracted modal parameters using EFDD technique.....	103
5.3.6.1.3. Verifying the extracted modal parameters using SSI technique.....	104
5.3.6.2. Results of the extracted modal parameters using FDD technique for the model with additional mass state.....	105
5.3.7. Damaged case of the grid-bridge model.....	106
5.3.7.1. State of the model without additional mass.....	106
5.3.7.1.1. First adopted right side damage case RAGDC-1.....	107
5.3.7.1.2. Second adopted right side damage case RAGDC-2.....	108
5.3.7.1.3. Adopted left side damage case LAGDC-1.....	109
5.3.7.2. State of the model with additional mass.....	110
5.3.7.2.1. Adopted right side damage case with mass RAGDC-1M.....	110
5.3.7.2.2. First adopted left side damage case with mass LAGDC- 1M.....	110
5.3.7.2.3. Second adopted left side damage case with mass LAGDC- 2M.....	111

5.3.8. Repairing the damaged model.....	111
5.4. Vierendeel bridge model.....	112
5.4.1. Experimental program.....	112
5.4.1.1. Scale considerations.....	112
5.4.1.2. Model erection.....	113
5.4.2. States of mass applications.....	115
5.4.3. Preparing requirements of AVM and experimental analysis.....	115
5.4.4. Implementing of AVM upon the Vierendeel bridge model.....	116
5.4.5. Processing the configuration input file and AVM data by ARTeMIS software.....	117
5.4.6. Intact case of the Vierendeel bridge model.....	117
5.4.6.1. State of the model without additional mass.....	118
5.4.6.1.1. Results of the extracted modal parameters using FDD technique.....	118
5.4.6.1.2. Verifying the extracted modal parameters using EFDD technique.....	120
5.4.6.2. Results of the extracted modal parameters using FDD technique for the state of model with additional mass.....	121
5.4.7. Damaged case of the Vierendeel bridge model.....	123
5.4.7.1. State of the model without additional mass AVDC-1.....	123
5.4.7.2. State of the model with additional mass AVDC-1M.....	125
5.4.8. Repairing the damaged model.....	127
5.5. Multi-storey building model.....	127
5.5.1. Experimental program.....	127
5.5.2. Preparing the requirements of AVM and experimental analysis.....	130
5.5.3. Implementing of AVM upon the MSB model.....	133
5.5.4. Processing the configuration input file and AVM data by ARTeMIS software.....	133
5.5.5. Intact case of the MSB model.....	133
5.5.6. Damaged case of the MSB model ABDC-1.....	136

5.5.7. Repairing the damaged model.....	137
6. NUMERICAL MODELLING AND ADJUSTMENT OF NUMERICAL RESULTS OBTAINED BY FEM AND EXPERIMENTAL RESULTS.....	138
6.1. Introduction.....	138
6.2. Numerical modal analysis of FE model.....	138
6.3. Calibration process by FE model updating.....	139
6.3.1. General.....	139
6.3.2. Structural parameters for FE model updating process.....	140
6.3.3. Adopted method for Calibration of FE model.....	141
6.4. Numerical calculations of the simply supported overhang beam model.....	142
6.4.1. FEM analysis of the initial intact model.....	143
6.4.2. Calibration process by FE overhang model updating.....	145
6.4.3. Simulation of damaged element in FE model.....	148
6.5. Numerical calculations of the grid-bridge model.....	148
6.5.1. FEM analysis of the initial intact model.....	148
6.5.1.1. Initial FE model without additional mass state.....	148
6.5.1.2. Initial FE model with additional mass state.....	152
6.5.2. Calibration process by updating of FE grid-bridge model.....	154
6.5.2.1. Calibration of the grid-bridge model without additional mass state.....	155
6.5.2.2. Calibration of the grid-bridge model with additional mass state.....	159
6.5.3. Equivalent of severity of damage with respect to the used length of element in FE model.....	162
6.5.4. Simulation of damaged elements in FE model.....	165
6.6. Numerical calculations of the Vierendeel bridge model.....	165
6.6.1. FEM analysis of the initial intact model.....	165
6.6.1.1. Initial FE model without additional mass state.....	165
6.6.1.2. Initial FE model with additional mass state.....	170
6.6.2. Calibration process by updating of FE Vierendeel bridge model.....	172

6.6.2.1. Calibration of the Vierendeel bridge model without additional mass state.....	172
6.6.2.1.1. Including of five modes in the objective function.....	173
6.6.2.1.2. Including of four modes in the objective function.....	174
6.6.2.2. Calibration of the Vierendeel bridge model with additional mass state.....	179
6.6.3. Equivalent of severity of damage with respect to the used length of element in FE model.....	183
6.6.4. Simulation of damaged elements in FE model.....	184
6.7. Numerical calculations of the Multi-storey building (MSB) model.....	184
6.7.1. FEM analysis of the initial intact model.....	184
6.7.2. Calibration process by updating of FE MSB model.....	189
6.7.3. Equivalent of severity of damage with respect to the used length of element in FE model.....	196
6.7.4. Simulation of damaged elements in FE model.....	197
7. VERIFICATION OF THE PROPOSED NUMERICAL MODEL, DETECTION AND LOCALIZATION OF DAMAGE USING TABU-SEARCH OPTIMIZATION METHOD.....	198
7.1. Introduction.....	198
7.2. Damage detection in the overhang beam model.....	198
7.2.1. Creating the form of objective function.....	199
7.2.2. Application of the objective function.....	202
7.2.2.1. Objective function through damage case of AODC-1.....	202
7.2.2.2. Objective function through damage case of AODC-2.....	203
7.2.3. Damage detection using the proposed TS optimization procedure.....	203
7.2.3.1. Application of TS procedure for damage detection of AODC-1.....	204
7.2.3.2. Application of TS procedure for damage detection of AODC-2.....	205
7.3. Damage detection in the grid-bridge model.....	206
7.3.1. Creating the form of objective function.....	206
7.3.2. Application of the objective function.....	207

7.3.2.1. Objective function through damage case of RAGDC-1.....	207
7.3.2.2. Objective function through damage case of RAGDC-2.....	208
7.3.2.3. Objective function through damage case of LAGDC-1.....	209
7.3.2.4. Objective function through damage case of RAGDC-1M.....	210
7.3.2.5. Objective function through damage case of LAGDC-1M.....	211
7.3.2.6. Objective function through damage case of LAGDC-2M.....	212
7.3.3. Damage detection in the grid-bridge model using the proposed TS optimization procedure.....	213
7.3.3.1. Application of TS procedure for damage detection of RAGDC-1.....	214
7.3.3.2. Application of TS procedure for damage detection of RAGDC-2.....	215
7.3.3.3. Application of TS procedure for damage detection of LAGDC-1.....	217
7.3.3.4. Application of TS procedure for damage detection of RAGDC-1M.....	218
7.3.3.5. Application of TS procedure for damage detection of LAGDC-1M.....	220
7.3.3.6. Application of TS procedure for damage detection of LAGDC-2M.....	221
7.4. Damage detection in the Vierendeel bridge model.....	223
7.4.1. Creating the form of objective function.....	223
7.4.2. Application of the objective function.....	223
7.4.2.1. Objective function through damage case of AVDC-1.....	223
7.4.2.2. Objective function through damage case of AVDC-1M.....	224
7.4.3. Damage detection in Vierendeel bridge model using the proposed TS optimization procedure.....	225
7.4.3.1. Application of TS procedure for damage detection of AVDC-1.....	225
7.4.3.2. Application of TS procedure for damage detection of AVDC-1M.....	227
7.5. Damage detection in the MSB model.....	228
7.5.1. Creating the form of objective function.....	228
7.5.2. Application of the objective function during damage case ABDC-1.....	229

List of contents

7.5.3. Damage detection in MSB model using the proposed TS optimization procedure.....	230
8. CONCLUSIONS AND RECOMMENDATIONS FOR FUTURE RESEARCH.....	232
9. REFERENCES.....	237
10. APPENDICES.....	247
APPENDIX A. Configuration input file (CFG).....	247
APPENDIX B. The acceleration data file (ASC file).....	257
APPENDIX C. Relations between recorded data and time of AVM tests.....	259
1. Model without additional mass.....	259
2. Model with additional mass.....	264
Author biography	
Copyright assignment	
Declaration of identity the printed and electronic versions of doctoral thesis	
Statement on the use	

II. LIST OF FIGURES

Figure 2.1: Crack modes.....	8
Figure 2.2: Sub-divisions of the beam [20].....	18
Figure 3.1: Tested part of GAZELA Bridge	28
Figure 3.2: Accelerometers handling and installation in test of structure of GAZELA bridge.....	29
Figure 3.3: Layout of GAZELA bridge test points for AVM of the tested approach [61].....	30
Figure 3.4: Average of the normalized singular values of spectral density matrices (SDMs) (for simple overhang model).....	36
Figure 3.5: Selection and linking process for the structural modes exist in each data measurement (Intact Pedestrian bridge model).....	40
Figure 3.6: MAC comparison between different modes estimated by FDD approach.....	42
Figure 3.7: Converting energy by the accelerometer.....	42
Figure 3.8: Installed accelerometers in two perpendicular directions of measurements.....	43
Figure 3.9: QuantumX measuring amplifier.....	44
Figure 3.10: Various output graphs via PC computer during the AVM test.....	45
Figure 3.11: Monitoring of results during the test.....	45
Figure 3.12: Electric shaking device.....	47
Figure 3.13: Damage detection general procedure [30].....	50
Figure 4.1: Global and local (maximum or minimum) values in the function.....	56

List of figures

Figure 4.2: Selection, crossover and mutation processes in GA procedure.....	58
Figure 4.3: Flow chart of GA optimization procedure with stopping criteria.....	59
Figure 4.4: Structure of multi-layer neural network.....	61
Figure 4.5: Flow chart of damage detection by Tabu Search optimization.....	70
Figure 5.1: Simple overhang beam model.....	73
Figure 5.2: Overhang beam model during AVM test.....	74
Figure 5.3: Locations of the installed accelerometers.....	74
Figure 5.4: Complete assembly for AVM test.....	75
Figure 5.5: Flow chart of the configuration input file of the overhang beam model.....	77
Figure 5.6: Geometry, distribution and measured directions of accelerometers throughout the overhang beam model.....	78
Figure 5.7: Normalized singular values of spectral density matrices of the overhang beam model data set using FDD peak-picking.....	79
Figure 5.8: Comparison of the first four extracted modes using MAC bar chart.....	80
Figure 5.9: Comparison of the first three extracted modes using MAC bar chart.....	81
Figure 5.10: Normalized singular values of spectral density matrices of the overhang beam model data set using EFDD peak-picking.....	82
Figure 5.11: Stability diagram of CVA.....	84
Figure 5.12: Candidate stable, unstable and noise modes throughout the frequency domain.....	85
Figure 5.13: Complete selection of the first three modes by SSI technique.....	85

List of figures

Figure 5.14: Values of natural frequencies extracted by FDD, EFDD and SSI techniques.....	87
Figure 5.15: (a) Damage location, (b) Formation of damage case AODC-1.....	88
Figure 5.16: Increasing the crack depth of the model (overturned model position).....	90
Figure 5.17: Reinstalling model for the test of second damage scenario.....	91
Figure 5.18: Preparing the main steel sections of the grid-bridge model.....	93
Figure 5.19: Top view sketch of the grid-bridge model with dimensions.....	94
Figure 5.20: The complete manufactured model of the grid-bridge (overturned position)..	94
Figure 5.21: Supports and the painted model (overturned position).....	95
Figure 5.22: Grid-bridge model on concrete supports.....	95
Figure 5.23: Grid-bridge model in the additional mass state.....	96
Figure 5.24: Preparing the devices of AVM tests.....	97
Figure 5.25: Accelerometers mesh of measurements for the grid-bridge model.....	98
Figure 5.26: Flow chart of the configuration input file of the grid-bridge model.....	99
Figure 5.27: Normalized singular values of spectral density matrices of the grid-bridge model without additional mass state using FDD peak-picking.....	100
Figure 5.28: Comparison of the first five extracted modes of the grid-bridge model without additional mass using MAC bar chart.....	102
Figure 5.29: Candidate stable, unstable and noise modes throughout the frequency domain.....	105
Figure 5.30: Formation of damage case RAGDC-1.....	107

List of figures

Figure 5.31: Formation of damage case LAGDC-2.....	109
Figure 5.32: Fences of the Vierendeel bridge model.....	113
Figure 5.33: Vierendeel bridge model.....	114
Figure 5.34: Details of the experimental Vierendeel bridge model.....	114
Figure 5.35: Masses distribution along the bridge deck for the model with additional mass state.....	115
Figure 5.36: Accelerometers mesh of measurements for the Vierendeel bridge model.....	116
Figure 5.37: Vierendeel bridge model during AVM.....	117
Figure 5.38: Normalized singular values of spectral density matrices of the Vierendeel bridge model without additional mass state using FDD peak-picking.....	118
Figure 5.39: Comparison of the first five extracted modes of the intact Vierendeel bridge model without additional mass using MAC matrix bar chart.....	120
Figure 5.40: Comparison of the first five extracted modes of the intact Vierendeel bridge model with additional mass using MAC matrix bar chart.....	123
Figure 5.41: (a) Beam damage location, (b) formation process of the scenario AVDC-1.....	124
Figure 5.42: Damage in the lower part of column AVDC-1M.....	125
Figure 5.43: Dimensions of damage scenario AVDC-1M.....	126
Figure 5.44: Details of the multi-storey building MSB model.....	128
Figure 5.45: MSB model fixed on rigid support.....	129
Figure 5.46: Details of beam-column joint.....	130
Figure 5.47: Installing of accelerometers on the tower part of the MSB model.....	131

List of figures

Figure 5.48: Accelerometers, locations and directions on the 3D mesh of measurement for MSB.....	132
Figure 5.49: Installed shaker on the rigid steel base of the MSB model.....	132
Figure 5.50: Normalized singular values of spectral density matrices of the intact MSB model data sets using FDD peak-picking.....	133
Figure 5.51: Column damage scenario ABDC-1.....	137
Figure 6.1: Flowchart of the proposed calibration procedure of FE model updating.....	142
Figure 6.2: Overhang FE model.....	143
Figure 6.3: Parameters of mass moment of inertia.....	144
Figure 6.4: Differences between experimentally estimated and numerically computed natural frequencies for different values of modulus of elasticity.....	147
Figure 6.5: Details of initial FE grid-bridge model	149
Figure 6.6: Grid-bridge FE model without additional mass created in ANSYS.....	150
Figure 6.7: Grid-bridge FE model with additional mass state created in ANSYS.....	153
Figure 6.8: Improvement of FE model based on minimum objective function value by TS optimization procedure for grid-bridge model without additional mass state.....	156
Figure 6.9: Change of structural parameters during the improvement of objective function minimum value of the model without additional mass state.....	156
Figure 6.10: Errors of initial and calibrated FE modal frequencies respect to experimental values of the grid-bridge model without additional mass state.....	158
Figure 6.11: Convergence between experimental and numerical updated values of natural frequencies for the grid-bridge model without additional mass state using TS procedure.....	158

List of figures

Figure 6.12: Improvement of FE model correlation based on minimum objective function value by TS optimization procedure for grid-bridge model with additional mass state.....159

Figure 6.13: Change of structural parameters during the improvement of objective function minimum value of the model with additional mass state.....160

Figure 6.14: Errors of initial and calibrated FE modal frequencies respect to experimental values of the grid-bridge model with additional mass.....161

Figure 6.15: Convergence between experimental and numerical updated values of natural frequencies for the grid-bridge model with additional mass state using TS procedure.....162

Figure 6.16: Equivalent damage value for the cantilevered 42mm element model.....164

Figure 6.17: (a) Details of the initial FE Vierendeel bridge model, (b) Vierendeel bridge FE model without additional mass created in ANSYS.....167

Figure 6.18: Vierendeel bridge FE model with additional mass state created in ANSYS..171

Figure 6.19: Improvement of FE model correlation based on minimum objective function value by TS optimization procedure for Vierendeel model without additional mass state using five modes.....174

Figure 6.20: Improvement of FE model correlation based on minimum objective function value by TS optimization procedure for Vierendeel model without additional mass state using four modes.....176

Figure 6.21: Change of structural parameters during the improvement of objective function minimum value of the Vierendeel model without additional mass state.....177

Figure 6.22: Errors of initial and calibrated FE modal frequencies respect to experimental values of the Vierendeel bridge model without additional mass state.....178

List of figures

Figure 6.23: Convergence between experimental and numerical updated values of natural frequencies for the Vierendeel model without additional mass state using TS procedure.....179

Figure 6.24: Improvement of FE model correlation based on minimum objective function value by TS optimization procedure for Vierendeel model with additional mass state using four modes.....180

Figure 6.25: Change of structural parameters during the improvement of objective function minimum value of the Vierendeel model with additional mass state.....181

Figure 6.26: Errors of initial and calibrated FE modal frequencies respect to experimental values of the Vierendeel bridge model with additional mass state.....182

Figure 6.27: Convergence between experimental and numerical updated values of natural frequencies for the Vierendeel model with additional mass state using TS procedure.....183

Figure 6.28: (a) Details of the initial FE Vierendeel bridge model, (b) MSB FE model created in ANSYS.....185

Figure 6.29: Improvement of FE model correlation based on minimum objective function value by TS optimization procedure for MSB model - Advanced iterative calibration method.....191

Figure 6.30: Change of structural parameters during the improvement of objective function minimum value of the MSB model.....192

Figure 6.31: Optimum mass distribution in levels 9 and 10 of the FE MSB model during the classical method of calibration process.....193

Figure 6.32: Errors of initial and calibrated FE modal frequencies respect to experimental values of the MSB model.....195

Figure 6.33: Modification of FE MSB model and the convergence between experimental and numerical values of natural frequencies, using TS procedure.....195

List of figures

Figure 6.34: Equivalent damage value for the cantilevered 30 mm element model.....196

Figure 7.1: Flow chart of the creating process of the applicable objective function.....200

Figure 7.2: Behavior of the objective function for damage case AODC-1.....202

Figure 7.3: Behavior of the objective function for damage case AODC-2.....203

Figure 7.4: Improvement of objective function minimum value during iterations of the proposed TS based damage detection of the overhang model in AODC-1 damage case.....205

Figure 7.5: Improvement of objective function minimum value during iterations of the proposed TS based damage detection of the overhang model in AODC-2 damage case.....205

Figure 7.6: Behavior of the objective function for damage case RAGDC-1.....208

Figure 7.7: Behavior of the objective function for damage case RAGDC-2.....209

Figure 7.8: Behavior of the objective function for damage case LAGDC-1.....210

Figure 7.9: Behavior of the objective function for damage case RAGDC-1M.....211

Figure 7.10: Behavior of the objective function for damage case LAGDC-1M.....212

Figure 7.11: Behavior of the objective function for damage case LAPDC-2M.....213

Figure 7.12: Improvement of objective function minimum value during iterations of the proposed TS based damage detection of the grid-bridge model in RAGDC-1 damage case.....214

Figure 7.13: The distribution of the explored solutions in the tested space using TS optimization procedure for damage case RAGDC-1.....215

List of figures

Figure 7.14: Improvement of objective function minimum value during iterations of the proposed TS based damage detection of the grid-bridge model in RAGDC-2 damage case.....216

Figure 7.15: The distribution of the explored solutions in the tested space using TS optimization procedure for damage case RAGDC-2.....216

Figure 7.16: Improvement of objective function minimum value during iterations of the proposed TS based damage detection of the grid-bridge model in LAGDC-1 damage case.....217

Figure 7.17: The distribution of the explored solutions in the tested space using TS optimization procedure for damage case LAGDC-1.....218

Figure 7.18: Improvement of objective function minimum value during iterations of the proposed TS based damage detection of the grid-bridge model in RAGDC-1M damage case.....219

Figure 7.19: The distribution of the explored solutions in the tested space using TS optimization procedure for damage case RAGDC-1M.....219

Figure 7.20: Improvement of objective function minimum value during iterations of the proposed TS based damage detection of the grid-bridge model in LAGDC-1M damage case.....220

Figure 7.21: The distribution of the explored solutions in the tested space using TS optimization procedure for damage case LAGDC-1M.....221

Figure 7.22: Improvement of objective function minimum value during iterations of the proposed TS based damage detection of the grid-bridge model in LAGDC-2M damage case.....222

Figure 7.23: The distribution of the explored solutions in the tested space using TS optimization procedure for damage case LAGDC-2M.....222

List of figures

Figure 7.24: Behavior of objective function for damage case AVDC-1.....	224
Figure 7.25: Behavior of objective function for damage case AVDC-1M.....	224
Figure 7.26: Improvement of objective function minimum value during iterations of the proposed TS based damage detection of the Vierendeel model in AVDC-1 damage case.....	226
Figure 7.27: The distribution of the explored solutions in the tested space using TS optimization procedure for damage case AVDC-1.....	226
Figure 7.28: Improvement of objective function minimum value during iterations of the proposed TS based damage detection of the Vierendeel model in AVDC-1M damage case.....	227
Figure 7.29: The distribution of the explored solutions in the tested space using TS optimization procedure for damage case AVDC-1M.....	228
Figure 7.30: Behavior of the objective function for damage case ABDC-1.....	229
Figure 7.31: Improvement of objective function minimum value during iterations of the proposed TS based damage detection of the MSB model in damage case ABDC-1.....	230
Figure 7.32: The distribution of the explored solutions in the tested space using TS optimization procedure for damage case ABDC-1.....	231
Figure 10.1: Acceleration measurements of set 1.....	259
Figure 10.2: Acceleration measurements of set 2.....	260
Figure 10.3: Acceleration measurements of set 3.....	261
Figure 10.4: Acceleration measurements of set 4.....	262
Figure 10.5: Acceleration measurements of set 5.....	263

List of figures

Figure 10.6: Acceleration measurements of set 1.....	264
Figure 10.7: Acceleration measurements of set 2.....	265
Figure 10.8: Acceleration measurements of set 3.....	266
Figure 10.9: Acceleration measurements of set 4.....	267
Figure 10.10: Acceleration measurements of set 5.....	268

III. LIST OF TABLES

Table 5.1: Total masses of cubes and accelerometers on the overhang beam model.....	73
Table 5.2: Estimated candidate values of natural frequencies and their mode shapes.....	79
Table 5.3: MAC matrix for the extracted candidate modes.....	80
Table 5.4: Adopted modes by FDD peak-picking for the intact overhang beam model.....	81
Table 5.5: Estimated values of natural frequencies and damping ratios by EFDD technique.....	83
Table 5.6: Estimated modal parameters of the overhang beam model using SSI technique.....	86
Table 5.7: Differences of values of natural frequencies extracted by FDD, EFDD and SSI techniques.....	86
Table 5.8: Values of extracted natural frequencies for damage case AODC-1.....	88
Table 5.9: Normalized displacements for the second mode shapes of the intact and damage cases of the overhang beam model.....	89
Table 5.10: Normalized displacements for the three mode shapes of the intact and damage cases.....	90
Table 5.11: Values of extracted natural frequencies for damage case AODC-2.....	91
Table 5.12: Values of natural frequencies of the grid-bridge model without additional mass extracted by FDD technique based on different values of frequency lines.....	101
Table 5.13: MAC matrix for the extracted modes of the grid-bridge model without additional mass.....	102
Table 5.14: Values of natural frequencies and mode shapes of the intact grid-bridge model without additional mass.....	103

List of tables

Table 5.15: Values of natural frequencies of the grid-bridge model without additional mass extracted by EFDD technique based on different values of frequency lines.....	104
Table 5.16: Values of natural frequencies, mode shapes and mode shape characters for the first five modes of the intact grid-bridge model with additional mass state.....	106
Table 5.17: Extracted values of natural frequencies for damage case RAGDC-1.....	108
Table 5.18: Extracted values of natural frequencies for damage case RAGDC-2.....	108
Table 5.19: Extracted values of natural frequencies for damage case LAGDC-1.....	109
Table 5.20: Extracted values of natural frequencies for damage case RAGDC-1M.....	110
Table 5.21: Extracted values of natural frequencies for damage case LAGDC-1M.....	111
Table 5.22: Extracted values of natural frequencies for damage case LAGDC-2M.....	111
Table 5.23: Values of natural frequencies, mode shapes and mode shapes characters for the first five modes of the intact Vierendeel bridge model without additional mass.....	119
Table 5.24: Values of natural frequencies for the first five modes of the intact Vierendeel bridge model without additional mass extracted by EFDD technique.....	120
Table 5.25: Values of natural frequencies, mode shapes and mode shapes characters for the first five modes of the intact Vierendeel bridge model with additional mass.....	122
Table 5.26: Extracted values of natural frequencies for damage case AVDC-1.....	124
Table 5.27: Extracted values of natural frequencies for damage case AVDC-1M.....	126
Table 5.28: Values of natural frequencies, mode shapes and mode shapes characters for the first five modes of the intact MSB model.....	134
Table 5.29: MAC matrix for the extracted modes of the intact MSB model.....	136
Table 5.30: Extracted values of natural frequencies for damage case ABDC-1.....	137

List of tables

Table 6.1: Experimentally extracted and numerically computed values of natural frequencies of the intact overhang beam model.....	144
Table 6.2: Experimentally extracted and numerically computed mode shapes of the intact overhang beam model.....	145
Table 6.3: Modal frequencies computed based on different values of modulus of elasticity.....	146
Table 6.4: Experimentally extracted and numerically computed values of natural frequencies of the intact initial FE grid-bridge model without additional mass state.....	150
Table 6.5: Experimentally extracted and numerically computed mode shapes of the intact initial grid-bridge model without additional mass state.....	151
Table 6.6: Experimentally extracted and numerically computed values of natural frequencies of the intact initial FE grid-bridge model with additional mass state.....	153
Table 6.7: Total number of the included values of adopted structural parameters in the FE model updating procedure for the grid-bridge model.....	155
Table 6.8: Comparison between experimental, numerical initial and numerical updated values of natural frequencies of the grid-bridge model without additional mass state.....	157
Table 6.9: Comparison between experimental, numerical initial and numerical updated values of natural frequencies of the grid-bridge model with additional mass state.....	161
Table 6.10: Equivalent damage severity.....	164
Table 6.11: Experimentally extracted and numerically computed values of natural frequencies of the intact initial FE Vierendeel model without additional mass state.....	168
Table 6.12: Experimentally extracted and numerically computed mode shapes of the intact initial Vierendeel bridge model without additional mass state.....	169

List of tables

Table 6.13: Experimentally extracted and numerically computed values of natural frequencies of the intact initial FE Vierendeel model with additional mass state.....	171
Table 6.14: Total number of the included values of adopted structural parameters in the FE model updating procedure for the Vierendeel bridge model using five modes.....	173
Table 6.15: Total number of the included values of adopted mass density in the FE model updating procedure for the Vierendeel bridge model using four modes.....	175
Table 6.16: Implementing TS optimization process using three and four included structural parameters upon FE Vierendeel without additional mass state using four modes only.....	176
Table 6.17: Comparison between experimental, numerical initial and numerical updated values of natural frequencies of the Vierendeel bridge model without additional mass state.....	177
Table 6.18: Implementing TS optimization process using three and four included structural parameters upon FE Vierendeel with additional mass state using four modes only.....	179
Table 6.19: Comparison between experimental, numerical initial and numerical updated values of natural frequencies of the Vierendeel bridge model with additional mass state.....	182
Table 6.20: Equivalent values of densities for the applied masses and the steel plate.....	187
Table 6.21: Experimentally extracted and numerically computed values of natural frequencies of the intact initial FE MSB model.....	187
Table 6.22: Experimentally extracted and numerically computed mode shapes of the intact initial MSB model.....	188
Table 6.23: Total number of the included values of adopted structural parameters in the FE model updating procedure for the MSB model.....	190

List of tables

Table 6.24: Optimum updated values of the included structural parameters during the proposed TS optimization process upon the FE model of MSB.....	192
Table 6.25: Comparison between experimental, numerical initial and numerical updated values of natural frequencies of the MSB model.....	194
Table 7.1: Studied values of weighting factors in objective function during the trial and error method according to equation (7.1).....	201
Table 7.2: Studied values of weighting factors in modifying of equation (7.1).....	206
Table 10.1: Acceleration data of the ASC file.....	257

IV. SYMBOLS AND ABBREVIATIONS

1. Symbols

Latin uppercase

A	State matrix in the equation of stochastic state space vectors
B	Input matrix in the equation of stochastic state space vectors
C	Output matrix in the equation of output vector of the stochastic state space system
C_B	Boltzmann's constant
D	Mass density
D	Damping ratio
D	Density parameter
D	The norm of the difference between the experimental and numerical normalized mode shapes
D	Input matrix in the equation of output vector of the stochastic state space system
$D1$	Density parameter of steel members and plates
$D2$	Density parameter of steel plates and concrete block of 4.5 kg
$D3$	Density parameter of steel plates and concrete block of 10.5 kg
$D4$	Density parameter of steel plates and steel block of 13.5 kg
$D5$	Density parameter of steel plates and steel block of 16.2 kg
D_{initial}	Initial value of mass density
D_N	Value of equivalent density
E	Material modulus of elasticity
E_{initial}	Initial value of modulus of elasticity
E_{optim}	Optimum value of modulus of elasticity
F	Flexibility matrix
F_D	Flexibility matrix in damage state

Symbols and abbreviations

F_d	Direct difference between the experimentally and numerically estimated values of natural frequencies
F_{ij}	Fractional energy
F_r	Relative difference between the experimentally and numerically estimated values of natural frequencies
F_u	Flexibility matrix in intact state
G_{uu}	Power spectral density matrix of the input
G_{yy}	Power spectral density matrix of the output
$H(\omega)$	Frequency response function
I	Moment of inertia
I_y	Mass moment of inertia
K	Structural stiffness matrix
K	Certain number of neighbouring solutions
L_{hollow}	Side length of the hollow square cross section
L_{solid}	Side length of the solid square cross section
L_{stif}	The length of the longer side of the stiffened element cross section
M	Mass matrix
M_{CS}	Mass of the additional concrete or steel block
M_p	Mass of steel plate
N_d	Total number of division
N_{MOVE}	Total allowable moves
$N(S_i)_j$	Candidate lists
N_T^{TS}	Maximum number of iterations
P_l	Acceptance probability
R	Certain number of subsets
R. Err.	Relative error

R_{Err}	Relative error between experimental and numerical values of natural frequencies
S_0	Initial solution
T	Sampling interval
T_I	Temperature of the system at recent solution
$T_{initial}$	Initial temperature
T_{new}	New temperature
U	Strain energy
V_p	Volume of steel plate
W_d	Weighting factor for the participation of the normalized mode shapes in the objective function
W_f	Weighting factor for the participation of natural frequencies in the objective function
W_m	Weighting factor for the participation of modal assurance criterion in the objective function
X^h	Crack position
Z_k	Normalized damage index

Latin small letters

a_j	Limit of certain region of beam
d	Distance from the centre of mass to the center of beam thickness,
f	natural frequency
$f(t)$	External force term in the equation of motion
f^{BEST}	Best solution
f_i^E	Experimental value of natural frequency
f_{ik}	Fractional energy
f_i^N	Numerical value of natural frequency

f_i^T	Tested value of natural frequency
f_i^U	Updated value of natural frequency
i	Number of certain mode
j	Number of certain region of beam
j	Component number of certain mode shape
k	Certain sub-region
l	Total length
m	Number of included modes
n	Number of degree of freedom
n	Number of adopted modes
p_k	The updated parameter
t	Thickness of sides of hollow section beam
v_t	Noise of the measurements of the stochastic state space system
w_t	Noise of the process of the stochastic state space system
$x(t)$	Displacement term in the equation of motion time series
$x(t)$	Time series
x_t	State space vector at step t in the stochastic state space system
\vec{x}_t	Recent solution
\vec{x}_{t+1}	New solution
y_t	Output vector in the stochastic state space system

Greek uppercase

ΔF	Change in the flexibility
Φ_{ij}^E	Experimentally estimated normalized mode shape vector
Φ_{ij}^N	Numerically estimated normalized mode shape vector

Greek small letters

β	Damage index
β_k	Damage index for the k sub-region
$\bar{\beta}_k$	Mean of damage indices
δK	Amount of change in stiffness
$\delta\lambda_i$	Change in eigenvalue
$\delta\phi_t$	Change in eigenvector
$\varepsilon_i^{X_n}$	Error function
λ	Eigenvalue
σ_k	Standard deviation of damage indices
ϕ	Mass normalized mode shape vectors
ϕ_t	Mode shape
ϕ_{ij}^e	The j^{th} component of the i^{th} experimentally estimated mode shape
ϕ_{ij}^m	The j^{th} component of the i^{th} numerically estimated mode shape
ϕ_t	Eigenvector
ω	Natural frequency
$\psi_i(x)$	A certain i^{th} mode shape

2. Abbreviations

1D	One dimension
2D	Two dimension
3D	Three dimension
ABDC	Adopted Building damage case
ANN	Artificial neural network
AODC	Adopted overhang damage case
AVDC	Adopted Vierendeel damage case
AVM	Ambient vibration measurement

Symbols and abbreviations

CVA	Canonical variate analysis
<i>DI</i>	Damage index
DOF	Degree of freedom
EFDD	Enhanced frequency domain decomposition
ET	Element type
FDD	Frequency domain decomposition
FE	Finite elements
FRF	Frequency response function
GA	Genetic algorithm
Hz	Hertz
LAGDC	Left adopted grid damage case
MAC	Modal assurance criteria
MEMS	Micro electro mechanical system
MP	Material properties
MSB	Multi storey building
MSE	Modal strain energy
Obj_Func	Objective function
PC	Principle component
RAGDC	Right adopted grid damage case
RC	Real constant
SA	Simulated annealing
SDM	Spectral density matrix
SDOF	Single degree of freedom
SHM	Strength health monitoring
SSI	Stochastic subspace identification
SVD	Singular value decomposition
TS	Tabu search
UPC	Unweighted principal component

1. INTRODUCTION

1.1 General

Due to several wars that took place in Iraq, the need for the concept of structural damage detection become very urgent in order to control propagation of damages that affected on structures. Such unusual reason represented by wars or even the usual reasons like the effect of moisture, rains, exposure to chemical materials ...etc, all cause deterioration in elements of structure which reduce the service life of those structures. Damages in the structure can be likened to the diseases in the human body, and in the field of structural engineering, the required inspection method that is needed to detect those diseases is called Structural Health Monitoring (SHM).

Structural health monitoring (SHM) can be described as an occasional operation that is necessary to be applied on structures to detect any existence of damage throughout the service life of the structure. The damage is defined as changes that happened with the time on the material and/or geometric properties of the structural system which reduces the performance and efficiency of that structural system and may lead to the failure. Different techniques are existed for SHM [1] and this work interests with the technique that uses the concept of periodically observed dynamic response measurements. These measurements are obtained from an array of sensors in order to determine the current state of the vibrated system respect to the original state [2].

On the other hand, the dynamic response measurements can be obtained according to different methods with respect to the method of excitation. This work adopts the ambient vibration as an exciter for the examined system. Ambient vibration measurements can be defined in general as a certain process that applied on a naturally excited structure due to ambient agents in order to obtain modal characteristics of that structure, which include natural frequencies, corresponding mode shapes and damping estimates [3]. Ambient excitation agents include, wave loads (offshore structures), wind loads (buildings) or traffic loads (bridges), often excite large civil engineering structures [4]. The ambient vibration

tests describe the linear behavior of structures [5] since the amplitudes of the vibrations are small.

In general, damage inspection process should be implemented periodically on structures. This period depend on type and age of structure, ambient condition and many other requirements that governs the need of inspection. Codes have recommendations related with this article. For example, bridges and significant highways need between 1 to 6 years as a period between two inspections [6]. Others [7] limited the period by few months rather than years.

Damage can cause disaster if it is not be controlled, and hence, it should be inspected properly and intensively due to the probability of being tiny and hence likely to be grow with the time. In this case, non-concentrated inspection process may not give indications for damage assessments in the time of inspection and the damage will grow allowing to make collapse. For example, The I-35W Mississippi River bridge (officially known as Bridge 9340) was constructed in 1967 crossing river of Mississippi in Minneapolis, Minnesota, United States. It had eight lanes and carrying 140000 vehicle per day. Although of processes of inspections that had performed and repeated for 40 years, the bridge had collapsed in August 1, 2007 due to the presence of steel flow in some sections [8]. This case may also be happened in airplanes when the damage exists in some parts of the main frame, although this case need a special attention and frequent schedules for maintenance is usually implemented. For example, the distress of Aloha Airlines flight 243, April 29th, 1988, was mainly due to corrosion that insufficiently controlled by maintenance [9].

Damage can occur due to several reasons, properties of materials which should be strong enough to make the structure able to support internal and external loads. Also, the instability of structure which occurs either due to the selection of material or designation, will produce fatigues or corrosions that make the structure fails. Manufacturing errors and lack of considerations of unexpected problems are other reasons that cause damages which affect directly on service life of structures. Although the importance of damage monitoring is an important issue even in normal cases when the structures subjected to normal conditions, the need becomes more urgent when abnormal conditions exist. Explosions, earthquakes, hurricanes, or any similar condition, make the structure needs to be examined

intensively for the sake of public safety. In such cases the time and cost of training have a crucial role and the lack of each of them may affect negatively in the inspection and assessment process [10].

1.2 Objective and scope

This dissertation contains the work of the author during the period 2011-2016 in the field of experimental modal testing and theoretical vibrational analysis of civil engineering steel structures.

The main objective of this work is to specify location and assessing the damage that may take place in various types of steel structures. There are several methods of damage identification applied in literature depend on various parameters. In general, two methods can be classified as a base of damage identification, local damage detection and global damage detection. Local damage detection technique mainly refers to non-destructive methods where the location of local damage could be detected. Methods of damage detection in this case are either visual or localized experimental methods such as ultrasonic, acoustic, magnetic field, radiography, eddy current or thermal field methods. All of these experimental techniques require that a portion of the structure being inspected is readily accessible [11].

Usually, this method is applicable for simple structures and it is adequate if there is some knowledge about the existence of damage. Global damage detection technique has more general ability in damage detection regardless the size and shape of the whole structure. This technique is known as vibration-based damage detection technique using one or more of the dynamic characteristics which include frequency response functions FRFs, natural frequencies, modal shapes and damping ratios [12]. This technique is adopted in this work due to its novelty and generality. Several other aspects have taken under consideration in this work and studied intensively during the period of the research that has a relationship with the main purpose of this work. Those aspects can be summarized as following:

- Highlighting the most appropriate methods that can be used for damage detection according to the philosophy of damage detection, method of excitation,

measurements, destructive or non-destructive state, the study will adopt the most suitable and applicable method.

- A review on several existing optimization techniques that are needed as an auxiliary and complementary tool is used in damage detection procedure. In this thesis, the need for a recent method that did not used before is aimed for the originality of research and state-of-the-art considerations.
- Selecting models that are needed to apply damage numerically and experimentally. In this case, the novelty and generality of the selected model should also be taken in the consideration for the sake of research originality.
- Preparing analysis requirements represented by software that are needed for analyzing data for both experimental and numerical cases. The most efficient and adequate software are adopted to produce best results.
- In each part of the damage detection procedure, there are aspects affect on the whole process and govern, in some way, the results directly or indirectly. Some of these aspects include:
 - Applying the concept of calibration on the numerical finite element (FE) model in order to coincide with the experimental model, and hence, closest state between the two models will be reached. This process is very important in the procedure of damage detection and should be applied for the sake of results accuracy.
 - The role of each of the adopted dynamic properties in the detection process for the investigated model, which include natural frequencies and normalized mode shapes. Each of them has a certain weight that affect on the final result.
 - The governing equation that used as an indicator for the degree of convergence between comparative results. This equation is known as "objective or target function", which governs the behavior of the optimization process. In this article, several forms are investigated intensively.
 - Several parameters exist in the experimental process, which include: the proper technique for modal extraction, appropriate number of measuring sets, testing

time, accuracy of the treated data that have several options to produce the parameter, and other else are taken in the consideration in this work.

- Giving conclusions about the results of each model. This include the best form that gives good indication for the location and severity of damage.

1.3 Innovative aspect of the research

In this thesis, some particularly innovative aspects of this work which deserve to be mentioned, are summarized as following:

- This work selects a modern optimization method to be used in the fields of civil engineering damage detection and model calibration process. This optimization method, which is called Tabu Search method, did not ever used before in the field of civil engineering damage detection or calibration process, and hence, this work applies and improves the procedure of this technique as a first participation.
- Modifying some objective functions to be adequately used with the adopted models and give recommendations about each of them.
- Using some special models that should have general behavior represented by the presence of both, axial and flexural action in their members. Although in this case the model will be more complicated, but it will be more general and objectivity.
- Covering different types of steel structures in one work. This will facilitate the mission of handling such models for the sake of future academic researches.

1.4 Layout of the dissertation

This dissertation is divided into ten chapters starting from the introduction that describes the general aims and the innovative aspects of the study. In chapter two, a review of the previously adopted techniques in the field of damage detection is considered and these techniques are related with the subject of this dissertation. Ambient vibration measurements based modal identification techniques are highlighted in chapter three with all requirements needed to implement the test and extract structural modal properties. In the same chapter, a review is considered upon the adopted procedure of damage detection and the required objective function to perform this procedure. In chapter four, some previously adopted optimization techniques are reviewed and their role in the field of structural

damage detection is briefly described. This revision is required to give a comparison and impression about the innovative use of the proposed Tabu Search (TS) optimization technique in the field of damage detection. The experimental programs that implemented upon all the adopted models in this work are explained in chapter five. Details of each case study and the related processes of erecting, testing and extracting results are described in this chapter. Chapter six of this dissertation contains the numerical calculations which are the required complementary part for the experimental measurements of the adopted models. The numerical calculations include numerically modal identification and the applied technique of calibration process upon each adopted model in this work. Results of application the proposed procedure of TS optimization technique are discussed in chapter seven. The observed conclusions of this work are declared in chapter eight which contains also the recommendations for future researches. Finally, the adopted references are listed in chapter nine while the appendices are summarized in chapter ten of this dissertation.

2. METHODS OF DAMAGE DETECTION IN CIVIL STRUCTURES

2.1 Introduction

It is important to understand the general definition of the damage which is related with civil structures. As it was defined in the previous chapter, the damage could be understood as the intensive or non intensive negatively changes affect on the Young's modulus, Poisson's ratio and density of the material that used in the structural system. Together or separately, these changes may also include the geometry of structural members leading to the reduction in their original designed characteristics, from which, the whole current or future structural efficiency will be reduced [13]. The process of damage detection, which is a part of structural health monitoring, in structural systems has a significant importance represented by increasing the safety and reliability of structural components. If the damage is able to be located and its evolution is under control, then the damaged structural elements can be repaired or replaced before some critical limit is reached and dangerous or costly failure occurs. Hence, damage detection process has an important role in satisfying public safety by preventing or reducing injury and loss of life and the associated cost of liability due to the early on-line warning capability that it produces. Damage can be caused by different reasons such as, impact loads, vibrations, overloading, thermal or environmental effects...etc [14]. The damage, represented by cracks or any similar agents, is the main cause for structural failure. This is the most dangerous case in civil structures due to its catastrophic consequences [15]. Hence, damage will negatively affect on durability of structures and reduces the designed service life if it is not early detected and controlled. The concept of damage detection or structural health monitoring is usually related with the non-destructive test methods, which are needed to keep the integrity of structures without more additional damages produced from the tests.

2.2 Theory of damage

In this article, a brief explanation is introduced on the damage theory, which represented here by the effect of cracks on structure, in general cases and the reasons that causes damage in structures. Moreover, the effect of damage on modal properties is highlighted due to the importance of this point in the present work.

2.2.1 Crack theory

Initiation and propagation of internal or external crack is the main reason that causes physical separation, or tearing, of the material. The crack is initiated when there are concentrations of stresses exist at weak regions in the material. The fracture could be either ductile or brittle depending on the material. If the releasing of strain energy, which is the stored energy inside the system when subjected to deformations, provides enough energy that exceeds resistance of material then crack will increase. This operation continues whenever the change in strain energy is equal to the change of material resistance. In general, crack propagation has three modes which describe the way that the forces act and affect on the cracks and the type of these cracks, as shown in *Figure 2.1*, [16].

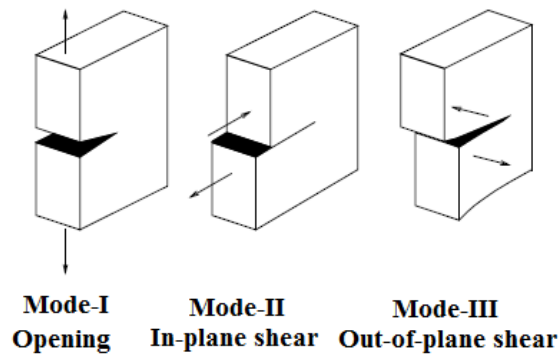


Figure 2.1: Crack modes [16]

It can be seen that from *Figure 2.1*, the forces act perpendicular on crack in the first case of mode (Mode I or tensile mode) and the crack tends to be pulled open. In the case of in-plane shear or sliding (Mode II), the forces act parallel to the crack and the crack tends to slide along itself. The last case (Mode III) represents out-of-plane shear or pushing (pulling) force action, where the forces are perpendicular to the crack and the crack tears

apart [16]. Among all types of failure modes, the dominant mode which has the most probability to occur under stresses should be identified for the design purposes [17].

2.2.2 Effect of damage on structural elements

In general, structural damage causes a reduction in the stiffness of the damaged element(s) that form the whole structure. It is assumed that the mass remains constant and there are no changes may occur, due to the low influence related with damage formation. Hence, stiffness matrix is the major part that influenced by the action of damage and exhibits sensitivity towards the resulted changes represented by perturbation of stiffness matrix for the damaged structure compared with the intact one [18], [19].

It is well known that the structure is either analyzed statically to calculate static parameters like displacements, forces, stresses....etc, or analyzed according to the modal analysis to extract structural modal properties such as natural frequencies, mode shapes and damping ratios. In the present work, the attention is given mainly to the modal properties which represented by natural frequencies and mode shapes. Hence, the effect of damage in the sense of these parameters is highlighted. Structural natural frequencies and mode shapes, the adopted parameters in the present work, are dependent on stiffness and mass distribution. Hence theoretically, modal parameters will affected by any changes that take place on the stiffness and mass matrix [20]. The eigenvalue equation describes modal characteristics of a structure as following [21]:

$$(K - \lambda_i M)\phi_i = 0 \quad (2.1)$$

where, $K (n \times n)$ and $M (n \times n)$ are structural stiffness and mass matrices, respectively, $\lambda_i = (2\pi f_i)^2$ is the i^{th} eigenvalue and f_i is the i^{th} natural frequency, ϕ_i is the i^{th} mode shape (eigenvector) of the intact structure and n is number of degree of freedom. According to the assumption that the damage causes changes in stiffness matrix only, the mass stiffness matrix remains constant before and after damage existence and the amount of change will be δK . As a result, eigenvector will be changed by $\delta\phi_i$ due to the changes

in stiffness matrix while the change in eigenvalue is $\delta\lambda_i$. Hence, the equation of eigenvalue for the damage state structure will be:

$$[K + \delta K - (\lambda_i + \delta\lambda_i)M](\phi_i + \delta\phi_i) = 0 \quad (2.2)$$

by expanding equation (2.2), leads to:

$$(K - \lambda_i M)\phi_i + (\delta K - \delta\lambda_i M)\phi_i + (K - \lambda_i M)\delta\phi_i + (\delta K - \delta\lambda_i M)\delta\phi_i = 0 \quad (2.3)$$

The first term in equation (2.3) represents eigenvalue equation, which is equal to zero according to equation (2.1). Now, by multiplying equation (2.3) by ϕ_i^T and applying the orthogonally condition of the mode shapes results:

$$\delta\lambda_i = \frac{(\phi_i^T \delta K \phi_i + \phi_i^T \delta K \delta\phi_i)}{1 + \phi_i^T M \delta\phi_i} \quad (2.4)$$

which is the sensitivity of eigenvalues to changes in the stiffness matrix due to damage in structure.

2.2.3 Damage sources

Structures, during their service life, exposed to different factors that effect on the integrity of these structures. These factors are represented by the internal and external loads applied on structures in addition to the environmental conditions, with chemical or physical effects, that participate in the process of damage formation in structures. Also, deterioration and/or aging of material properties, changes in boundary conditions, lack of integrity in connections, large deformations in geometry, overuse, overload, and absence of sufficient maintenance are all factors encourage the formation and propagation of damage. These factors may be influenced either individually or in combination which is then the worse case. Moreover, all the mentioned agents tend to cause damage gradually within relatively long period, while some other factors causes sudden damage like the unusual natural forces represented by earth quakes or explosions which effect within short time and high intensity [22]. It is evident that the last case considered as the more dangerous source of damage due to the high intensity generated forces which tend to initiate and propagate cracks severely.

2.3 Levels of damage detection

Generally, there are four levels of damage detection are taken into account during the implementation of health monitoring technique. Each level represents a result for the damage detection process which depends on the used method of damage detection. These levels could be summarized as [23], [24]:

- 1- Methods indicate that the damage is existing in the structure. In these methods an indication is given that the damage is generally exist somewhere in the structure regardless any other information concerns with the properties of damage. One of the techniques that used for this case is, for example, the change in structural modal properties before and after the presence of damage. This produces an indication that the damage is exist in the structure. Sinou, and Lees (2005) [25] presented in their work the changes in natural frequencies for a certain number of modes due to the presence of different cases of damaged shaft. They used a certain form represented by the percent of change in natural frequencies as an indication for the damage effects. Usually, such methods are referred to them as simple implemented procedures [25]. Hence, any similar form that compares between some of structural properties before and after damage occurrence could be considered as indicators for the presence of damage in structure.
- 2- Determination the geometric location of the damage in the structure. Here the detection level is more advanced than the previous. It is possible here to identify the location that the damage exist on, using special and more detailed methods compared with the previous level. Mosavi et al (2012) [26] used in their work a technique uses the context of statistical pattern recognition in the field of identifying damage position. The procedure adopts ambient vibration measurements that applied on steel bridge girder as a case study. The comparison with the intact model state was also taken into account in their work by evaluating the amount of variations in the damage features with respect to the intact state of the model. They declared that their procedure is able to detect the locations of different types of damages such as cracks or local buckling in real structures. Nahvi and Jabbari [27] used structural mode

shapes for the same purpose. A few number of modes could be able to localize the damage location by a certain error function that seeks for minimum error value, among many iterations, at which the location of damage could be detected. This result was also certified by experimental work applied using cantilever steel beam, in which, the location of the proposed damage was detected.

- 3- Quantification of damage severity, this is either implemented after the determination of the damage location or simultaneously within the same procedure, according to the adopted technique. Nahvi and Jabbari [27] applied another technique represented by plotting modal graphs for the first two modes in order to assess the severity of damage which has an already detected location using another technique explained earlier. On the other hand, Owolabi et al (2003) [28] used similar technique that depending on sketching the first three modes to localize and assess severity of damage in the same time using the intersection point of these three plotted modes. Almost methods of damage detection try to detect both, location and damage severity, numerically and/or experimentally in the same time which increases efficiency and reliability of the proposed method.
- 4- Assessing the remaining service life of the damaged structure. In most cases, this level is classified within the field of fracture mechanics, analysis of fatigue life or assessment of structural design, therefore, it is not addressed within the structural vibration or modal analysis [23].

2.4 Description of some damage detection methods

Due to the importance of damage detection process, several techniques were studied in literature in order to reach the proper way that implement the philosophy of damage detection. Each technique uses a certain physical principle that characterizes and gives this technique the importance in the field of damage detection. Those techniques are classified according to several ways, for example, based on vibration, guided wave, optical fiber, acoustic emission, differential pressure or electromagnetic field based methods [29]. On the other hand, some methods are classified according to the integrity of the tested specimens, whether they are destroyed or stay in use after the implementation of the test. More other

considerations are used in the philosophy of damage detection which are exist in literature. A review for some of those techniques are explained in this paragraph as following:

2.4.1 Damage detection according to the integrity of the tested model

In this classification, damage detection is implemented using either destructive or non-destructive tests [30], [31].

2.4.1.1 Destructive tests

In general, the destructive tests are represented by studying the behavior of a certain model when subjected to ultimate load capacity leading to the complete failure. Such kind of tests has several advantages with respect to the knowledge or economical considerations. Knowledge considerations include high amount of information that interpret the behavior of the tested model easily. While, economic considerations are exist in this kind of tests when the model is produced by large quantities and there is no matter if small number of specimens are destroyed. The usual way in applying these tests is using special equipments that monitor any change that may occur in the model during the test. The equipments are either widely marketed or still under development by researchers. For example, high speed camera is a proper tool that used in the procedure of crack detection according to some theories such as digital image correlation method [32]. Shih and Sung (2013) [33], used in their research advanced digital cameras (Camel NextShot 2C-2.1M) with high speed computers to develop techniques of digital image in the field of structural damage detection. Similar research was implemented by Chen et al (2014) [34] and used a special high speed camera that has 1500 frames per second and resolution of 1056x200. Other equipments, which are still under development, are also used to detect damage in models like the hybrid carbon fiber reinforced polymer (HCFRP) which is used to localize and measure crack formation in structural members. Yang et al (2008) [35] in their work used HCFRP as a sensors to monitor the structural health of an existing pre-stressed concrete box girder. Those sensors are glued to the investigated structural member to monitor and measure any initiation or propagation of cracks that happened in the destructive test [35].

Bakis et al [36], demonstrated in their work the self monitoring capability and pseudo-ductility of hybrid fiber reinforced polymer rods. The specimens were tensile tested in the quasi-static strength test until complete failure and the longitudinal strain was measured. They concluded that the pultruded specimens with fibers are able to sustain further loading after the failure. By this case, a warning of an impending failure was able to be obtained by simple electronic circuitry which can be a kind of warning for any excessive damage. Other researchers [37], [38] have also used the strategy of composite material under complete tensile failure test to investigate the ability of such material to produce warning against fractures.

2.4.1.2 Non-destructive tests

When the model is produced by few number of items, like building usually, it is not economical then to use destructive tests in such kind of models. In this case the need to the non-destructive tests is required as adequate methods which are necessary for locating and/or quantifying the severity of damage in damaged structures [39]. Non-destructive testing and evaluation methods which are used for damage detection can be divided, in general, into two approaches, conventional and modern. The first approach include: dye penetrate, magnetic particle induction, ultrasonic, eddy current, emission spectroscopy, fiber optic sensors, fiber-scope, hardness testing, isotope, magnetic perturbation, X-ray, noise measurements, pattern recognition, pulse-echo and radiography. These methods are practically applicable non-destructive and they have been developed, implemented and accepted by the industry [28], [40]. While, the modern methods are still under development, and have a limited use by some equipments and not fully accepted by the industry. Another kind of classification that could be applied on the non-destructive tests is that, local and global methods. The first method is suitable for small specimens which either be separated or connected with the main structure that has bigger size. This method requires prior knowledge about the location that likely to be damaged. Also, it is necessary that the explored specimen is able to be reached and handled by the testing staff during the detecting process. Both of these requirements make this kind of non-destructive test becomes limited in use and increase difficulties of the test. The more general methods

which have more generality in use with respect to the damage detection purposes are the global non-destructive methods. These methods depend on the assumption that the damage will produce changes in the global structural properties which leads to the damage detection [40]. In this approach, there is no need to the prior knowledge of the likely damaged location nor the ability to reach to the tested elements. This approach includes vibration-based damage detection method.

2.4.2 Damage detection based on static displacements

The use of static displacements, or static response, for the sake of damage detection without incorporating with other techniques is seldom [41]. Nevertheless, this technique is based on the assumption that the response which produced depending on some specific points in a system is more sensitive to damages than dynamic responses. He and Hwang (2006) [41] used static response incorporating with dynamic response to formulate an equation that has the ability to sense any change in static or dynamic parameters for the tested structure, and hence, to detect the damage. They used static displacements, in addition to dynamic responses, within a certain technique that used some optimization methods to achieve the ability of damage detection. Direct use of the static displacements without incorporating with dynamic responses was used by Chou and Ghaboussi (2001) [42]. With static displacements measurements of few degrees of freedom, the changes in physical properties of the structural members, like Young's modulus and cross-sectional area were identified by the difference of measured and computed displacements. They declared that their proposed method was able to detect damage even with small number of simulated measured static displacements and without use of finite element analysis.

The use of static displacement measurements in the field of damage detection is also related occasionally with a special technique called wavelet method. Wavelet is a function of time or spatial location that has a zero average, finite length, normalized norm is 1 and its centered lies at $x = 0$ [43], [44]. The wavelet transform technique is sensitive to any tiny perturbation that may happen in the signal that forming the function, which represented here by the function of static displacement line. In this case, the measured static displacements, which are represented by the deflected shape of the tested structure, are

treated as spatially distributed signal and the wavelet transform is computed for this signal. Any abnormal change or peak formation in the signal is an indication for the presence of damage and refers to its location. Damages, even they are not severe, can be sensed by wavelet transform due to their affection on the wavelet coefficients in the vicinity of damage [43]. Rucka and Wilde [43] (2006) used this technique for the sake of damage detection. With the aid of digital photographs of cantilever beams, they measured the displacements of spatially distributed points to be considered as the signal function for the wavelet technique. They used two sizes of cantilever beams that exposed to different types of damage severity. They concluded that the proposed method is effectively detecting the damage without knowledge of structure characteristics or mathematical model. Wang and Deng [45] (1999), have also used the static displacements, in addition to the dynamic properties, in the field of damage detection as a function for the wavelet transform technique. They considered that the use of static displacement has a special importance due to the ability of this method to be used in the case of full-field measurements which are suitable for the cases that have slowly varying signals. Based on the deflection response of the cracked beam, the wavelet transform (or wavelet coefficient [45]) are plotted according to different values of scales. They showed that according to high scale values (8 and above), the perturbation in the signal's function is clear and indicates to the damage location. While, low values of scale (7 and lower) may not be able to show any perturbation in the signal function, and hence, no damage is detected. Finally, the wavelet techniques have been used widely in literature and a review for researches which adopt this techniques is implemented by Kim and Melhem (2004) [46].

2.4.3 Vibration based damage detection

Vibration based damage detection method is according to the assumption that structural damage causes variation in structural parameters of the civil structure (Mass and Stiffness) which encourage the changes in the dynamic parameters of the structure (natural frequencies, mode shapes, damping ratio) [40]. On the other hand, the vibration based damage approach has more than one category, and the so called inverse approach is more appropriate one. The inverse approach is represented by determining damage parameters,

location and severity, from changes in the structural dynamic properties by using a procedure of comparisons between data obtained experimentally and numerically [11]. This approach has significant features, like, it does not need the tester to have access to component under analysis for crack detection. Also, this approach do not require the cleaning of local area compared to other locations, and it can detect the cracks which are existing far away from the sensors and locations that are not be able to be accessed [15]. Vibration based damage detection is a well-known technique and is a part of non-destructive inspection techniques which is generally used to investigate the critical changes in the structural parameters, so that an unexpected failure can be prevented. Vibration based damage detection technique is applied using one or more of the parameters like natural frequencies, mode shapes, damping ratios, strain energy, dynamic flexibility and the change in frequency response function (FRF) [23]. Using some of these parameters in damage detection is explained as following:

2.4.3.1 Damage detection according to strain energy

Damage detection method depending on strain energy has a wide use in literature. Theory of this method that derives a damage indicator for beam element can be explained as following [20]:

Strain energy according to Bernoulli-Euler beam, in the intact state, is given by

$$U = \frac{1}{2} \int_0^l EI \left(\frac{\partial^2 w}{\partial x^2} \right)^2 dx \quad (2.5)$$

where, EI is the beam flexural rigidity and $w(x)$ is the transversal displacement. The energy that associated with a certain modes shape, $\psi_i(x)$, is given by

$$U = \frac{1}{2} \int_0^l EI \left(\frac{\partial^2 \psi_i}{\partial x^2} \right)^2 dx \quad (2.6)$$

Now the beam is divided into N_d divisions, as in *Figure 2.2*, the energy of each sub-region

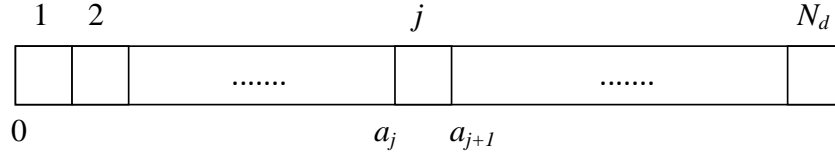


Figure 2.2: Sub-divisions of the beam [20]

the energy that associated with the region j due to i^{th} mode is given by:

$$U_{ij} = \frac{1}{2} \int_{a_j}^{a_{j+1}} (EI)_j \left(\frac{\partial^2 \psi_i}{\partial x^2} \right)^2 dx \quad (2.7)$$

the fractional energy will be:

$$F_{ij} = \frac{U_{ij}}{U_i} \quad (2.8)$$

the total fractional energy is then:

$$\sum_{j=1}^{N_d} F_{ij} = 1 \quad (2.9)$$

For the beam in the damaged state, all the previous quantities will be defined similarly as following:

$$U_i^* = \frac{1}{2} \int_0^l EI^* \left(\frac{\partial^2 \psi_i^*}{\partial x^2} \right)^2 dx \quad (2.10)$$

$$U_{ij}^* = \frac{1}{2} \int_{a_j}^{a_{j+1}} (EI)_j^* \left(\frac{\partial^2 \psi_i^*}{\partial x^2} \right)^2 dx \quad (2.11)$$

$$F_{ij}^* = \frac{U_{ij}^*}{U_i^*} \quad (2.12)$$

$$\sum_{j=1}^{N_d} F_{ij}^* = 1 \quad (2.13)$$

where the symbol $()^*$ refers that the quantity is measured according to the damaged mode shapes, ψ_i^* .

Assuming that for the small j^{th} sub-region, the flexural rigidity $(EI)_j$ remains constant and F_{ij}^* will be

$$F_{ij}^* = (EI)_j^* \frac{\frac{1}{2} (EI)_j^* \int_{a_j}^{a_{j+1}} \left(\frac{\partial^2 \psi_i^*}{\partial x^2} \right)^2 dx}{U_i^*} \quad (2.14)$$

If the damage is assumed to be located at one sub-region, then the fractional energy for other undamaged sub-regions will be relatively constant and $F_{ij}^* = F_{ij}$. For the damaged sub-region, with single damaged location $j = k$, it could be found that

$$\frac{(EI)_k \int_{a_k}^{a_{k+1}} \left(\frac{\partial^2 \psi_i}{\partial x^2} \right)^2 dx}{U_i} = \frac{(EI)_k^* \int_{a_k}^{a_{k+1}} \left(\frac{\partial^2 \psi_i^*}{\partial x^2} \right)^2 dx}{U_i^*} \quad (2.15)$$

In order to find the change in flexural rigidity due to damage in the beam, EI is assumed to be constant over the length of the beam for both intact and damaged sub-regions, and then the change in flexural rigidity of the sub-region can be expressed as:

$$\frac{(EI)_k}{(EI)_k^*} = \frac{\left[\int_{a_k}^{a_{k+1}} \left(\frac{\partial^2 \psi_i}{\partial x^2} \right)^2 dx \right]}{\left[\int_0^l \left(\frac{\partial^2 \psi_i}{\partial x^2} \right)^2 dx \right]} \bigg/ \frac{\left[\int_{a_k}^{a_{k+1}} \left(\frac{\partial^2 \psi_i^*}{\partial x^2} \right)^2 dx \right]}{\left[\int_0^l \left(\frac{\partial^2 \psi_i^*}{\partial x^2} \right)^2 dx \right]} \equiv \frac{f_{ik}^*}{f_{ik}} \quad (2.16)$$

Now, to use the effect of all modes that taken into account during the measurements, m , the damage index, β , for sub-region k is represented by:

$$\beta_k = \frac{\sum_{i=1}^m f_{ik}^*}{\sum_{i=1}^m f_{ik}} \quad (2.17)$$

The modes in the last two equations need not be normalized. Now the collection of damage indices, β_k , will assumed to be a sample of population that have normally distributed random variable, then a normalized damaged index is obtained as:

$$Z_k = \frac{(\beta_k - \bar{\beta}_k)}{\sigma_k} \quad (2.18)$$

where, $\bar{\beta}_k$ and σ_k represent the mean and standard deviation of the damage indices, respectively [20].

Cornwell et al. (1999) [20] used damage index to detect damage in a plate for different cases. They tested plate models with single and double damage locations with reduction in stiffness taken as 25% or 10%. Also, different amount of adopted modes were used during the test, ranging from 1 to 12 modes. They concluded that the change of strain energy (damage index) is able to detect all types of damage even within few modes and small damage percent of 10%.

Another theoretical basis of strain energy is represented by Kumar et al. (2009) [19]. They proposed the derivation of modal strain energy (MSE) which is defined as the product of the elemental stiffness matrix and second power of the mode shapes. They used in their work the summation of flexural strain energy and the shear strain energy as the total strain energy that produced in the beam. They used the changes in strain energy as a damage indicator with the aid of natural frequencies and mode shapes. Also, Shi et al. (1998) [18] used the sensitivity change of modal strain energy as an indicator to locate damage in structures but with the use of mode shapes and element stiffness matrix only as parameters for the damage identification process. This needs not a complete knowledge of stiffness or

mass matrices. They showed that this method is robust in detecting damage due to its sensitivity towards single or multiple locations of damage.

2.4.3.2 Damage detection using modal flexibility method

Modal flexibility, or the inverse of stiffness, method is a well known technique that has been accepted in the field of structural health monitoring. This method has several advantages related with the field of damage detection. For instance, this method depends only on the experimental data obtained from a structure to estimate the flexibility matrix, and hence, it does not require any analytical model for the tested structure for that purpose. Also, more other advantages for this methods like its simplicity and accuracy were mentioned in literature [47]. The flexibility matrix (the inverse of the stiffness matrix) is [48], [49]:

$$[F] = [\Phi] \text{diag} \left[\frac{1}{\omega_i^2} \right] [\Phi]^T = \sum_{i=1}^n \frac{1}{\omega_i^2} [\phi_i] [\phi_i]^T \quad (2.19)$$

where, $[\Phi]$ is mass normalized mode shape vectors ($[\Phi]$ modal matrix), $\text{diag} \left[\frac{1}{\omega^2} \right]$ is reciprocal of the square of natural frequencies and n is the number of degree of freedom.

The presence of damage will cause flexibility change with respect to the intact state as:

$$\Delta[F] = [F_d] - [F_u] \quad (2.20)$$

where, the subscripts, d and u refer to the damaged and undamaged states, respectively. Finally, the damage index can be represented by the following equation for n modes :

$$DI = \frac{\sum_{i=1}^n (F_{di} - F_{ui})}{\sum_{i=1}^n F_{ui}} \quad (2.21)$$

The complete derivation of the damage index DI according to flexibility matrix is explained in reference [50].

Wickramasinghe et al. (2013) [50] used in their work the method of modal flexibility to localize damage in suspension bridge under different damage scenarios implemented on the main cables and hangers with the aid of numerical simulation techniques. A finite element model of a suspension bridge is used to obtain mass normalized mode shape vectors and natural frequencies for both intact and damage states of structure. Their results indicated that modal flexibility based damage detection technique is able to detect damage in the cables and hangers of suspension bridge model. Pandey et al. (1994) [47] used this technique in their work to detect damage with few numbers of modes. They applied damage on steel I-section as a cantilever beam with different amounts of damage depths. Results showed that the damage was able to be detected for 50% damage severity close to the beam fixed end, even when using just the first mode only. Also, using the first two modes give an indication very close to the use of seven modes when sketching the results. They declared that this method has practical applicability on real-life structures.

2.4.3.3 Damage detection using frequency response function (FRF)

The use of FRF is one of the important and famous method in the vibration based damage detection techniques [23]. The definition of the FRF for a viscous damping system has n degree of freedom can be expressed as following [51]:

The equation of motion is:

$$[M]\{\ddot{x}(t)\} + [D]\{\dot{x}(t)\} + [K]\{x(t)\} = \{f(t)\} \quad (2.22)$$

where $[M]$, $[D]$ and $[K]$ represent $(n \times n)$ mass, damping and stiffness matrix, respectively. For a harmonic input system, external force and displacement can be expressed in the forms $\{f(t)\} = \{F(\omega)\}e^{j\omega t}$ and $\{x(t)\} = \{X(\omega)\}e^{j\omega t}$, respectively, and after substituting, equation (2.22) could be rewritten as following:

$$(-\omega^2[M] + j\omega[D] + [K])\{X(\omega)\}e^{j\omega t} = \{F(\omega)\}e^{j\omega t} \quad (2.23)$$

The Frequency Response Function (FRF) matrix $[H(\omega)]$, is define as:

$$[H(\omega)] = (-\omega^2[M] + j\omega[D] + [K])^{-1} \quad (2.24)$$

Then, the solution of equation of motion is given by

$$\{X(\omega)\} = [H(\omega)]\{F(\omega)\} \quad (2.25)$$

Hwang and Kim (2004) [31], used FRF to localize and predict the severity of damage in structures. The main point in their work is that the use of just few FRFs as a subset from a full set of FRFs, with repeating them for different frequency values, was enough to identify the location and extent of damage. This was proved according to two models that have been exposed to different damage scenarios numerically. In their work the dependence was only on FRFs to identify the damage, while Nozarian and Esfandiari [52] used in their work the change in FRF and the measured natural frequencies in addition to the change of mode shapes. The changes in structural parameters, represented by axial stiffness EA for truss model, were calculated using least square method. They applied their procedure for damage detection on a 2D truss model that performed numerically, from which, the damage location and severity was identified. They declared that this method could be an alternative for the conventional damage detection method. Bandara et al. (2014) [53], used FRF with the aid of an optimization method to identify the severity of damage. An experimental model represented by three-storey bookshelf structure was adopted in their work in addition to the numerical calculations to validate their procedure. They concluded that the use of an optimization method with summation of FRFs exhibits high accuracy of damage detection results compared with the use of an optimization method with individual FRFs. Therefore, authors [53] produced their procedure as a reliable technique that has the ability to be applied on real structures with good results in the field of damage detection.

2.4.3.4 Damage detection using natural frequencies and mode shapes

The direct use of modal properties is one of the features that the present work takes into account. Natural frequencies and mode shapes are the main parameters that used to formulate and improve certain procedures in the field of damage detection. In general, it is

known that vibration based damage detection technique faces some challenges during the application. These challenges could be summarized by the need for an accurate modeling of structure in a way that gives results close to the real case and the development of a powerful algorithm to detect the damage [55]. Nevertheless, those parameters are adopted in this work and the use of natural frequencies and mode shapes during the procedure of damage detection is highlighted as following:

2.4.3.4.1 Change in natural frequencies

Damage causes loss in stiffness for structural elements and this leads to decrease values of natural frequencies of the system. There are several advantages related with the use of this parameter in damage detection technique and can be summarized as following [23]:

1. The measurements of natural frequencies are easy to be obtained without time consuming.
2. There is no need for special complicated equipments rather than those traditional ones usually used for extracting measurements, from which, it is able to obtain great number of measurement points with minimum cost available.
3. The accuracy of the extracted measurements is relatively high and the errors can be controlled and assessed if enhanced experimental conditions are taken into account during the test. Nevertheless, results of the extracted information of natural frequencies are less contaminated by experimental noise [49].
4. It is able to get sufficient information about the intact state of the system by using finite element method FEM in the analysis which allows to select adequate certain points for measurements instead of whole points in the system. This produces the advantage of time and effort saving with a good level of accuracy.

Several researches [23], [49], [55], [56] focused on this subject in literature, making a general review of using natural frequencies in damage detection. It is usually required, when using the technique of natural frequencies, to implement a comparison between values of natural frequencies in the intact state and the values in the damaged state in the procedure of damage detection. But there are also another procedures need not prior knowledge of the intact state, but rather for example, the knowledge of the structural

material properties (Density and modulus of elasticity of the model) which are estimated using the intact natural frequencies [23]. Nevertheless, although of the several advantages explained earlier, this technique has several limitations should be taken into account when using in the field of damage detection. The most important limitation is that this approach is insensitive to the damage unless for the cases when severe damage exists [49].

2.4.3.4.2 Changes in mode shapes

Mode shape is a feature that describes the amplitude of the vibrated system spatially for each mode of resonant frequency value. In this way, it is suitable to use mode shapes in combination with the behavior of natural frequencies in the procedures of structural damage detection [23]. There is a priority for using mode shapes in the field of damage detection relatively to the use of natural frequencies based damage detection due to several advantages that can be summarized as following [49]:

1. The mode shapes are more sensitive to local damages due to the local information that contained in mode shapes, which in turns, makes it possible to determine the location of single or multiple existed damage.
2. The sensitivity of mode shapes towards the environmental effects is little, which makes it suitable to use for the in-situ tests.

Also, the use of this parameter as a base damage detection requires multi sets of sensors that extract data during the test, which is the same requirement that needed for using natural frequencies based damage detection.

According to the mode shapes based damage detection method, it is adequate also to use another criteria based on mode shape called the modal assurance criteria (MAC), which uses the orthogonality of mode shapes for the comparison between different modes that obtained from the tests [57]. The MAC form is represented as:

$$MAC_{ii} = \frac{\left(\Phi_{ij}^{N^T} \cdot \Phi_{ij}^E\right)^2}{\left(\Phi_{ij}^{N^T} \cdot \Phi_{ij}^N\right)\left(\Phi_{ij}^{E^T} \cdot \Phi_{ij}^E\right)} \quad (2.26)$$

where, Φ_{ij}^E and Φ_{ij}^N represent the normalized mode shape vector components in vertical and horizontal directions at measurement points, which are estimated from experimental measurements and numerical computations, respectively.

Natural frequencies, mode shapes and MAC are adopted in the present work to be used in the procedure of damage detection.

3. CIVIL STRUCTURE MODAL PROPERTIES IDENTIFICATION BASED ON AMBIENT VIBRATION MEASUREMENTS

3.1 Introduction

Ambient vibration response analysis or ambient vibration identification is often used technique for determination the dynamic properties of structures in civil engineering, [58], [59]. When the dynamic properties for any structure within ambient excitation are extracted under normal operating conditions, the measurements then will be more reliable and close to reality. It is mentioned earlier in chapter one that the structures are subjected to different types of natural loads that cause the structures to be vibrated. Hence, it is more desirable if the structural dynamic properties are measured by the ambient vibration identification methods [57]. The main advantage of the ambient vibration test is the ability of executing and analyzing the measurements without needing to know the amount of excitation forces. Moreover advantages are, the requirements of the test of small, light, and portable instrumentations. Also, the tests can be carried out without deactivating the service of the structure. Another advantage is that, through very small strain deformations which occur in the vibrated structures, the used equipments that represented by low noise accelerometers can sense the vibrations of the structures which have low amplitude ranges of the ambient vibration measurements (AVM). This feature is not applicable in other tests like stepped and sweep sine test, the release test or vibration test that caused by blast loading, in which, the tests of dynamic behavior require the structure to be under higher amplitude vibration [60]. Finally, this kind of testing is fast and cheap and can be implemented within short time [61].

3.2 Applications of Ambient Vibration Measurements (AVM) technique

As it was mentioned earlier that the ambient vibration measurements (AVM) describe the linear behavior of the structures, they can be also used to describe the linear behavior of damaged structures. Hence, knowledge of behavior of structural systems that are time-

amplitude dependant models will be useful for improving their analysis algorithms in the field of structural damage detection and control studies [5]. As a consequence, this subject was an attractive for researchers and got a considerable interest for developing experimental methods for in-situ measurements of full-scale partially damaged structures [5], [61]. Mišković et al. (2014) [61], used ambient vibration technique to extract the dynamic structural properties applied on real in-situ tested model. They considered a part of the Gazela bridge model as a case study, which is a main highway bridge in Belgrade-Serbia crossing the river of Sava in the capital city, *Figure 3.1*.



Figure 3.1: Tested part of GAZELA Bridge for AVM

They declared that it is easily to control the test of AVM and dealing with the equipments that are needed in the test if a certain strategy is considered. The strategy is represented by the way of testing which is making the test starts from the edges and finishes toward the centre of the bridge model. As a significant feature for the ambient vibration measurement test, few sets of data recording measurements devices were used in their test, from which, sufficient information they obtained as a result. The well-known data recording measurements devices in this field are the transducers (accelerometers), which are explained in the next sections of this chapter. These devices need to be handled and installed with care during the test for the sake of accuracy, as implemented by Mišković et al. (2014) [61], *Figure 3.2*. On the other hand, the number and locations of points that required for installing these data recording measurements devices (accelerometers) are also should be adequately selected on the model. They considered that, it is adequate for the case of small structural models to use just up to 10 points of measurements to produce sufficient information about the dynamic parameters of the tested model, while for large

structural models, it is required around 60 or more test points for representation relevant modal properties [61], [4].



Figure 3.2: Accelerometers handling and installation in test of structure of GAZELA bridge

In all cases, there are no clear guidelines of number of test points, and it depends on structural type, design, and other factors [61]. A proper layout should be implemented for the distribution of selected locations of the measurements points in any tested model. The aim of this layout is to make measurements points cover the whole tested model as much as possible during the test, in order to represent the best configuration of this model. Hence logically, the distribution of measuring points for the one dimensional structural models (like beams or columns) need to be with a line distribution, while for the case of two dimensional models (like wide bridges or surfaces) it is required to be as a two dimensional mesh distribution, *Figure 3.3*. For the three dimensional models, such as high buildings, it is better if three dimensional mesh distribution is adopted, although line distribution is possible for the narrow high structures. In the case of the work implemented by Mišković et al. (2014) [61], the distributed shape of the measuring points can be shown in *Figure 3.3*. The mesh shown in figure 3.3 represents the whole tested segment, from the bridge model, which represents the best distribution for the measuring points. The use of similar technique of vibration based damage detection method was implemented by Al-Wazni et al. (2014) [62], to extract structural modal properties represented by natural frequencies and mode shapes for the first few modes.

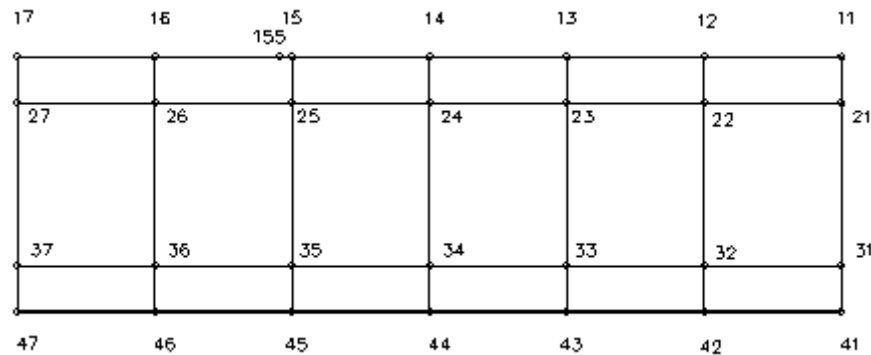


Figure 3.3: Layout of GAZELA bridge test points for AVM of the tested approach [61].

Zenunovic et al. (2015) [63] used AVM applied on three case studies, bridge models, to compare values of dynamic properties that extracted by AVM and those extracted by mathematical models. For each model, the accelerometers during the experimental test were installed in two rows that cover the whole length of the model. They found that there are some differences in the results between the two modal extracting methods, AVM and mathematical method. They declared that the reasons are due to, the real nature of the boundary conditions and the changes in the material properties of the structural elements after long time of model service life. Another reasons belong to the assumptions of the mathematical model were suggested like, the low strain levels, definition of the modulus of elasticity according to the used code which is based on different strain values than those imposed by AVM, concrete aging, friction mechanisms and the construction practice during concrete casting. They concluded that the AVM could produce a lot of useful information about dynamic properties and the comparison with mathematical analysis.

All of the previously mentioned studies used two dimensional structures as case studies to apply the concept of AVM for the sake of modal properties extraction. A three dimensional case study represented by 48 story building model was adopted by Lord et al. (2003) [64] to extract modal properties by the AVM technique. In this case, the measurements points were distributed in certain floors as a mesh to form, after assembling, three dimensional mesh represents the whole tested structure as much as possible. Each floor mesh has dimensions of (23.4 by 48.8) m as an elliptical shape and three transducers were used to monitor the translational, longitudinal and torsional modes of the building.

Results of their work exhibited good representation for the first six adopted modal properties specially the mode shapes.

It should be mentioned that, the use of AVM could be implemented in combination with different techniques that process the data obtained by AVM to predict the modal parameters. For example, all the previously mentioned researches used special software, which is called ARTeMIS software, that processes the obtained AVM spatial data by certain approaches provided within the software and produce the modal information. This software and the approaches that deal with the spatial data to extract modal properties will be extensively explained in the next paragraphs. In literature, researches used another approaches, for example, Mahmoud et al. (2001) [65] used in their work AVM to extract modal properties for a suspension bridge by a special techniques called the Random Decrement Vibration Analysis and Ibrahim Time Domain to find the high frequency mode vectors. By this technique, they showed that they can eliminate the influence of randomness of the aerodynamic force, hence, this force can be filtered and used without noise to be studied as an excited force without randomness. They concluded that the AVM can be considered as an adequate method to produce the structural dynamic properties under the real conditions. Another approach to collect and analyze ambient vibration data to extract structural modal properties was adopted by Lu et al (2006) [66] and called a MEMS (Micro Electro Mechanical Systems)-based wireless sensor system. They used as a case study a real pre-stressed concrete cable-stayed bridge divided into nine points for sensors (transducers) measuring in the vertical direction. They concluded that the use of new wireless sensors in AVM is better than the traditional wire sensors with respect to the test simplicity.

In the present study, the principle of AVM is adopted because, in addition to the several advantages that mentioned previously, it is output-only modal identification. In this identification procedure, dynamic properties are extracted depending on just the measured responses regardless the information about the exciting forces. Such forces are difficult to be controlled and predicted due to the nature of these forces that acted on structures, thus, dispensing with these forces is a feature that characterizes the AVM in civil engineering.

Hence, all these advantages encourage to use the AVM technique in the present work as a base for extracting modal properties of civil structures.

3.3 Adopted techniques of extraction dynamic properties from AVM recorded data

According to their analysis domains, output-only modal parameter estimation techniques are categorized into two distinct groups: frequency domain methods and time domain methods. The first method, which is adopted in the present work, deals with power spectral density while the second one deals with the correlation of past and future output. A well-known frequency domain technique is called Frequency Domain Decomposition (FDD) is adopted in the present work as an estimator for the structural modal parameters [67]. In addition to the FDD approach, Enhanced Frequency Domain Decomposition (EFDD) and the Stochastic Subspace Identification (SSI) are also highlighted for comparison purposes in this work. All of these approaches are provided within the software ARTeMIS which makes the dealing with the AVM data easier and efficient to extract the dynamic properties.

3.3.1 ARTeMIS software capabilities

ARTeMIS extractor software is a tool used in the field of modal identification when the vibrated systems have only known output responses. Modal identification can be accurately performed by the software for the structures under operational conditions without needing for the excited forces [4].

To give better understanding for the abilities of ARTeMIS software, it is important to highlight the main requirements that needed to perform analysis with the software. Firstly, a suitable structure and measurement configuration input file, should be written (as a script file) that contains the commands of geometry and measurements layout of the tested structure. The geometry consists of nodes, lines connect between nodes and plates connect between lines. This system is connected properly together in one configuration script file within special commands. As usual, there are certain instructions for each command used in the written program should be followed carefully in order to avoid any objection. The

configuration script file contains also, after the geometry commands, the measurement sets commands. This part of the configuration script file consists of data set names that followed by numbers and directions of each channel existed in this set. The channel refers to accelerometers that supply the acceleration data from the vibrated structure to the signal processing system or (data acquisition system). The accelerometer measures the acceleration depending on the direction that the accelerometer installed on. This usually applied depending on the direction that the structure is likely to be vibrated towards, for instance, vertically or horizontally or both. Each set of measurement consists of number of accelerometers (channels). One of these channels, at least, should be allocated to represent the so-called reference accelerometer which stays in the same location and direction for all other available sets. In this case a reference accelerometer is required and obligatory allocated for each direction of motion required to take its motion into account during the test of structure. The last paragraph in the configuration program is the equation commands, which contain the equations that connect the relations between the accelerometers according to their locations (nodes) and direction (way of vibration). For more details, an example for *Configuration input file (CFG)* is explained in the APPENDIX A of this dissertation.

The second main requirement is the data that needed to be analyzed by the software. It is represented by a number of sets, each of them contains readings of acceleration that recorded by the accelerometers during the test. Each accelerometer produces information of acceleration readings that recorded and arranged in the form of column data that assembled with other columns (from other sensors) of one set to form the whole file of ASC extension. The symbol ASC represents the extension of the file that contains readings of all accelerometers in one set which should be written in a certain name within the configuration program. A sample for *The acceleration data file (ASC file)* is listed in the APPENDIX B of the dissertation for further understanding.

Several features characterize the ARTeMIS software (in addition to the main features represented by providing FDD, EFDD and SSI approaches for modal identification) could be summarized as following [4]:

1. The software has ability of direct transfer for the recorded data with guided measurement procedure.
2. Processing huge amount of data which are obtained through multiple data sets and multiple reference points.
3. Produces fast identification for the modal properties represented by, natural frequencies, mode shapes and damping ratios.
4. Exhibits easy handling wizards to process the signals effectively.
5. Ability to animate mode shapes which gives better imagine for the vibrated shapes.
6. Calculations and comparisons between the extracted mode shapes from different projects using the orthogonality parameter between mode shapes which is the Modal Assurance Criteria (MAC) in different ways of displays.
7. Simplicity in transferring the final resulted information from the software to any file in order to be saved and used for further applications.

Many other features provided in the software which give the priority of using this software among other traditional methods for modal identification [4].

3.3.2 Frequency Domain Decomposition (FDD)

To realize the philosophy of FDD, the basis of *Spectral Density Matrix* (SDM) should be highlighted first. Power spectrum or spectral density of a time series $x(t)$ is a function that describes how the variance of the data $x(t)$ is distributed over the frequency domain. The distribution occurs for the spectral components when the series $x(t)$ decomposes. Units of spectral density is then considered as the square unit of x over a frequency unit, which is commonly expressed in watts per hertz [68]. On the other hand, the estimation of spectral density function at discrete equally spaced *frequency lines* in a range between zero frequency and the *Nyquist frequency* (which is the half of the rang of sampling frequency) produces the spectral density matrices (SDMs) [4]. The term *frequency lines* refers to the number of divisions that the range of frequency domain is equally divided, which has the values of (2, 4, 8, 16,, 262144) and the number corresponds to the number of samples in the inverse of Fourier transformation of the spectral densities. Hence, adequate number of frequency lines could help in appearing and then estimating the requested modes.

The approach of FDD is based on the signal processing using Discrete Fourier Transform to estimate the SDMs under the assumption that the excitation is pure white noise (random process) and all natural modes are lightly damped [58], [69]. For each Power SDM, a singular value decomposition (SVD) is carried out and all modes, at a certain frequency, are separated into principal values and orthogonal vectors. The first vector obtained by the SVD constitutes an estimate of the mode shape when the selected single mode is a dominant mode [69]. The separated modes can be estimated easily according to the peaks of the normalized singular values of SDMs [58]. Each singular value of the SDMs is normalized with respect to the area under the first singular value curve. The first singular value curve is the top curve that exists in the diagram of SDMs, *Figure 3.4*, which contains the most significant candidate modes that are likely to be selected as the structural modes. The significant modes (dominant modes) appears as peaks in the first singular value curve, from which, the selection by picking of each peak produces one estimated candidate mode (each mode is a candidate until certain confirmations are implemented to verify the mode stability). *Figure 3.4* shows the diagram of SDMs assigning the details mentioned previously.

The normalization process prevents weak modes from appearing and leads them to be in just one or few matrices [4]. The number of singular values of SDMs is represented by number of degree of freedom that adopted during the test. Each spectral density function corresponds to single degree of freedom which is represented by the readings of one accelerometer in each set of measurements. In the case of system that tested and represented by *Figure 3.4*, it has seven degree of freedom that produced seven singular values of SDMs as shown.

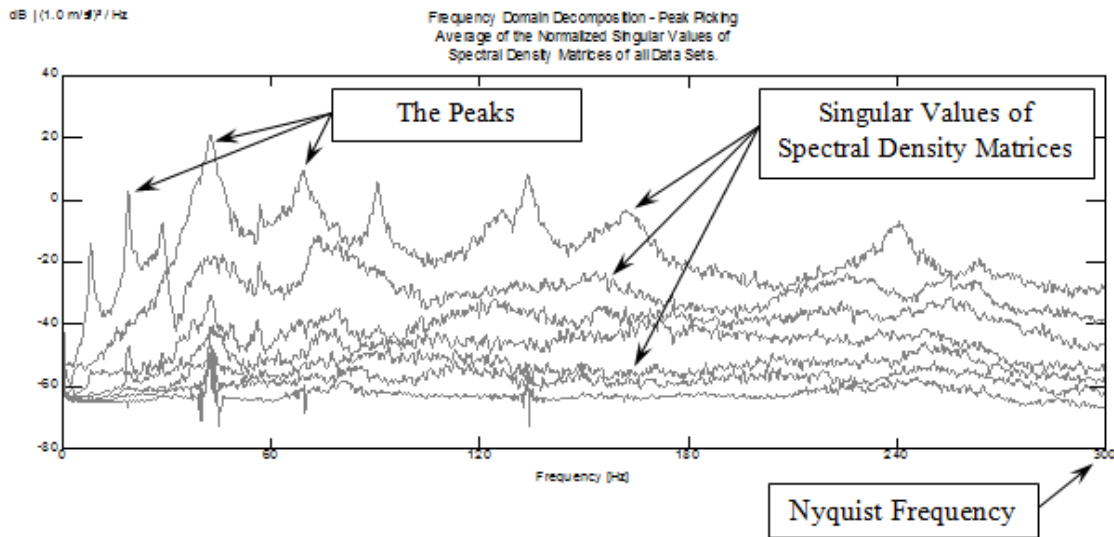


Figure 3.4: Average of the normalized singular values of spectral density matrices (SDMs) (for simple overhang model)

The mechanism of FDD approach in modal identification is represented by decomposing each of the estimated SDMs, and the singular values represent the estimates of the auto spectral density of the single degree of freedom systems, while the singular vectors are estimates of the mode shapes. If the modes are obviously separated, then the mode selection is implemented by picking the first singular value. Otherwise, for the repeated or closed modes, the picking is implemented on the second, third, ..., etc. singular value [58], [62].

Based on the white noise assumption, as can be observed in figures of APPENDIX C, a simplified explanation for the relationship between the system input, u , and the measured output, y , is expressed in continuous-time frequency domain as follows:

$$G_{yy}(j\omega) = H(j\omega)G_{uu}(j\omega)H^H(j\omega) \quad (3.1)$$

where, $G_{yy}(j\omega)$ is the PSD matrix of the output; $G_{uu}(j\omega)$ is the PSD matrix of the input, $H(j\omega)$ is the frequency response function (FRF) matrix; $H^H(j\omega)$ is its complex transpose conjugate. For the white noise excited system, the assumption, the term $G_{uu}(j\omega)$ will simply be a constant matrix in frequency axis; hence; $G_{yy}(j\omega)$ is directly proportional

to the product of FRFs, $H(j\omega) H^H(j\omega)$. By applying singular value decomposition (SVD) to equation (3.1), the output matrix can be decomposed into singular vectors (mode shapes) and singular values of dominant frequencies [67].

In literature, several researchers [69] - [72] used FDD in the modal identification. The approach of FDD is very easy to be used and gives a satisfactory level of accuracy for the identified modes, thus, present study adopts mainly this technique in modal identification.

3.3.3 Enhanced Frequency Domain Decomposition (EFDD)

The modal estimation in the case of Enhanced Frequency Domain Decomposition (EFDD) approach is implemented by two steps, the first step includes performing of FDD approach as same as it was explained previously by peak picking. The second step uses the previously identified mode shapes by FDD approach to identify what is called Single Degree Of Freedom (SDOF) Spectral Bell functions, which in turn, estimate all modal parameter. The comparison between modes (correlation analysis) using the modal assurance criterion (MAC) is the base for identifying SDOF Spectral Bell. In the comparison process, the identified mode shapes in the FDD stage are considered as reference vector. A MAC vector is calculated, on both sides of FDD picked frequency, between the reference vector (FDD mode shapes) and the singular vectors corresponding to a certain frequency. The aim of this step is to discover the highest MAC value which is existed in the MAC vector. The highest value is then compared with a certain value called (MAC Rejection Level) which is used to decide whether the singular value is included within the description of SDOF Spectral Bell or not. In this case the highest values of MAC that exist in the MAC vector either higher than the MAC rejection level or lower. Values above the rejection level refer to the ability of including the corresponding singular value (at which the MAC value exceeds the MAC rejection level) in the description of the SDOF Spectral Bell, and vice versa. The comparison process between the highest MAC value and other singular values that lie on both sides of the reference frequency is continued until no MAC values above the rejection level still exist. Hence, if the MAC rejection level is reduced, then there will be more singular values included in the SDOF Spectral Bell, and vice versa. Next, the corresponding singular values are averaged together to get the

improved mode shape. The natural frequency and the damping ratio of the mode are estimated by transforming the SDOF Spectral Bell to time domain. This leads to SDOF correlation function, from which, applying the regression analysis will lead to estimate natural frequency and the damping ratio [4].

Researchers [73], [74] used this approach for the modal identification in order to be compared with other available approaches and to obtain the best results of dynamic properties that could be applied in the structural purposes.

3.3.4 Stochastic Subspace Identification (SSI)

A technique was presented by Van Overschee and De Moor for modal identification of naturally excited systems, which identifies a stochastic state space model from output-only measurements [72]. One of the typical parametric structural model, uses in output-only modal analysis of linear and time-invariant physical systems, is the stochastic state space system defined as following [4], [62], [72], [74]:

$$x_{t+1} = Ax_t + Bw_t \quad (3.2)$$

$$y_t = Cx_t + Dv_t \quad (3.3)$$

where, x_t and x_{t+1} are the state space vectors, respectively at step t and $t+1$, y_t is the output vector while A and C are the state and the output matrices, respectively. The input terms Bw_t and Dv_t are assumed to be a process vector, the stochastic components w_t and v_t are noise of the process and noise of the measurements, respectively. Finally, B and D represent the input matrix.

Both equations (3.2) and (3.3) consist the parametric structural model, in which, the first equation represents the so-called State Equation that constitutes dynamic behaviour of the physical system and the matrix A contains the physical information. On the other hand, equation (3.3) represents the so-called Observation or Output Equation, which controls which part of the dynamic system can be observed in the output of the model, hence, the matrix C extracts the information that can be observed in the system response. Freitas and

Pereira [72] declared that the input terms represented by Bw_t and Dv_t are not measured, because of the naturally excited system that the responses only are measured and only the terms of noise w_t and v_t are separately affecting. It is assumed that the sequences of these terms are independent to each other, hence, equations (3.2) and (3.3) will be:

$$x_{t+1} = Ax_t + w_t \quad (3.4)$$

$$y_t = Cx_t + v_t \quad (3.5)$$

Equations (3.4) and (3.5) represents the basis for system identification in the time domain using natural excitation conditions. The SSI approach uses some numerical techniques like Singular Value Decomposition (SVD) and Least Square methods to identify the state matrix based on measurement data. After decomposing process, the system matrices A and C are determined from the state sequence through the solution of a Least Square problem, and hence, modal parameters are directly extracted from the estimated matrix [72].

With respect to the ARTeMIS software, three types of estimated modes are obtained by the SSI approach: Structural, Harmonic and Noise modes. The attention is given to the structural modes which are needed to be identified in order to be used for the dynamic structural purposes. According to the main assumption that adopted for the modal identification process, the system is linear and the excited forces are white noise. It is important to avoid noise modes during the modal identification which could be implemented by following of some instructions during the identification process. The base that structural mode in SSI approach (or in general) follows, is the value of damping ratio. It is usually for the structural modes, which belong to structures that behave as viscous damping systems, to be with damping ratio less than 5% [4], [75]. So, any mode has a value of damping ratio more than 5% should be avoided. Thus, only the stable modes (structural modes) remain to be used in the assembling process. The assembling process refers to the selection of each structural mode (stable mode) that extracted from the corresponding data set. It is important to mention that, according to modal identification procedure that

followed in SSI approach, several candidate modes are obtained from each set of measurements. Those modes are already recognized and assigned as either Stable (structural), Unstable, or Noise modes by the analysis implemented by SSI technique. Neither the unstable modes nor the noise modes are needed in the identification process, hence, the selection process should confine to the stable modes only. The selection process is implemented by selecting (picking) the structural mode that exists in each set of measurement in a way that forms a *Linked line*, *Figure 3.5*.

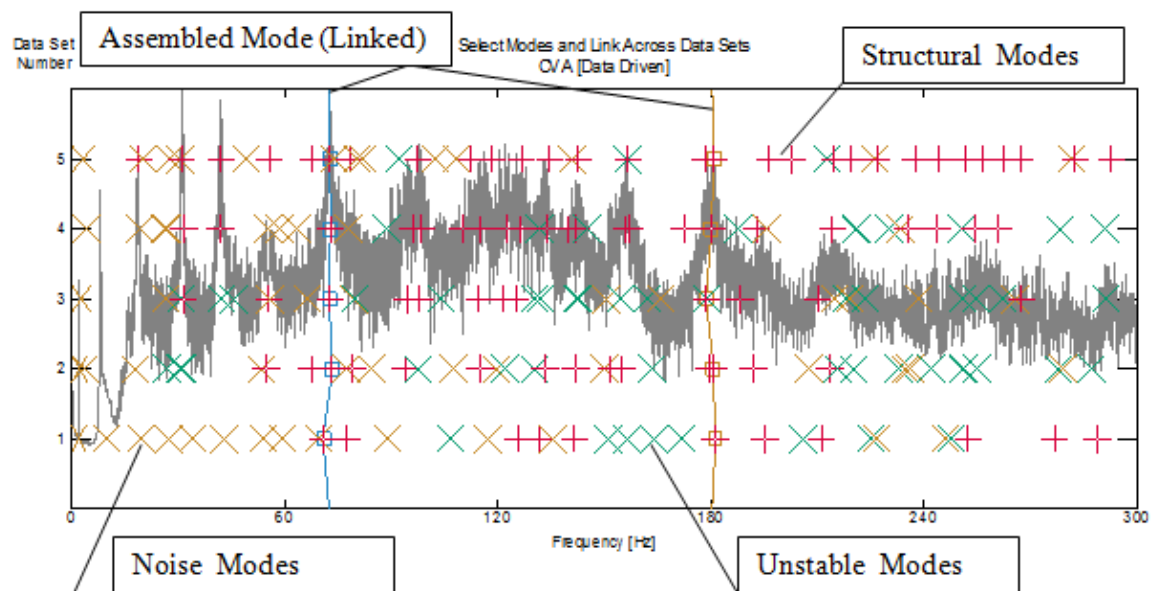


Figure 3.5: Selection and linking process for the structural modes exist in each data measurement (Intact Pedestrian bridge model)

The *Linked line* is close to a vertical line shape that linking the modes in each data set, which includes and links all stable modes that exist in all sets at a certain value of frequency.

The stable modes appear as red crosses in the widow of mode Selection and Link, while other modes appears as x-signs with green and brown colors to represent the unstable and noise modes, respectively. *Figure 3.5* shows the details of the selection and linking process which implemented according to the so-called Canonical Variate Analysis (CVA), which is a special way of modal identification belongs to the SSI technique.

Modal identification by SSI approach in ARTeMIS software is implemented according to three techniques of estimation, Unweighted Principal Component (UPC), Principle Component (PC) and Canonical Variate Analysis (CVA). The data that entered as input data to the subroutine of estimation (procedure or engine of SSI estimation) of state space model is weighted to be a weighted version of SSI Input matrix that consists of compressed time series data. The way that the matrix is weighted with, governs the type of technique among UPC, PC or CVA within the SSI approach.

References [72], [74] had used the SSI approach for modal identification in the case of output-only time domain based technique which include intensive explanation about this method and CVA technique, hence, it is recommended for these references and other [4] to be reviewed for further information.

In the present study, among all approaches of FDD, EFDD and SSI mentioned earlier, the mainly adopted method for modal identification is the FDD, and uses other approaches only in the first stage to verify the obtained results by FDD. ARTeMIS software provides all the mentioned techniques for the sake of modal identification and usually one of these methods is enough to estimate the results. The obtained results by any technique are not completely accurate, and because of that the expression of "estimated modes" is used frequently in any of procedures. Any estimated mode should be investigated under certain procedures which verify the identified mode as a stable (structural) mode or not. For example, according to FDD approach, the estimated mode should be picked (selected) within the peaks regions of the Singular Values of SDM to produce the more precise mode, otherwise, the resulted mode is inaccurate. Moreover, each estimated mode is considered as a structural mode if it has low value of MAC in comparison with other different estimated mode, and high value of MAC refers to the rejection of the estimated mode, *Figure 3.6*. Until this stage, it is enough to obtain sufficiently accurate structural modes according to FDD approach, and it is possible to use other EFDD and SSI techniques for more investigations about the analyzed data measurements to verify the results. Hence, the use of FDD approach in the present study, as modal identification method, is reasonable and could be adopted for sufficiently accurate results.

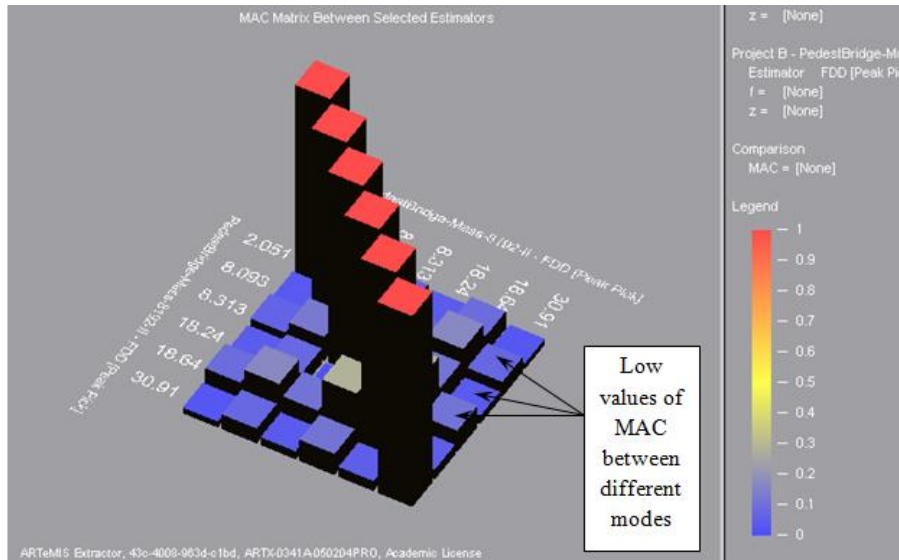


Figure 3.6: MAC comparison between different modes estimated by FDD approach

3.4 Equipments needed for AVM tests

AVM requires certain equipments to implement the tests and record acceleration data, which in turn, need to be analyzed and then to extract modal properties by any of the modal identification techniques mentioned earlier. The equipments are mainly as following:

3.4.1 Accelerometers

Generally, the accelerometers, or "sensor" / "transducer", refer to the device that used to convert one form of energy to another [76], [77], as shown in *Figure 3.7*.

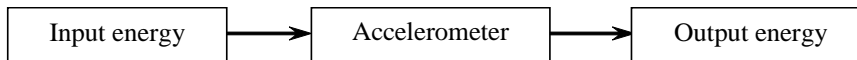


Figure 3.7: Converting energy by the accelerometer

Usually, there are certain differences among each precise term of the accelerometer, sensor and transducer which characterize each device with a certain function. In the field of engineering, the required device for this field application is usually the accelerometer. This device consists of a certain damped mass fabricated on spring to sense any exposed acceleration that causes the mass to be displaced on the spring. This will subject an acceleration within the same rate as the applied acceleration, hence, the output signal is

produced. For the case of vibrated systems, the accelerometers are used to convert the mechanical motion into an electric signal which is analyzed later by another device to produce the requested data. The accelerometers that used in the present work are from the type Low noise, high sensitivity and low frequency accelerometers, Silicon Designs Model 2400 with the range of DC-600 Hz, as shown in *Figure 3.8*.



Figure 3.8: Installed accelerometers in two perpendicular directions of measurements

Depending on the required direction of motion that needed to be discovered, the accelerometer should be installed, in order to sense the generated acceleration of the vibrated system. For instance, if the vibrated system tends to vibrate vertically, then the accelerometer should be installed either towards the top or bottom, which different in the sign only. By this way the motion is sensed to reflect the behavior of the vibrated system vertically regardless any existing motion in horizontal direction. Hence, another accelerometer is needed to sense the motion in the horizontal direction (if needed) to produce complete information about the behavior of vibrated system. The output of the accelerometer is represented by a signal that transmitted to another important device within the requirement of AVM procedure which is called the "Data Acquisition System".

3.4.2 Data Acquisition System

The sampling signals that received from the accelerometers are processed and the resulting samples are converted into digital numeric values that can be manipulated by a

computer. Data acquisition system, usually refers to which as DAS or DAQ, implements the converting process upon the signals that received from the accelerometers. The converting process represents converting the analog voltages, that received from the accelerometers, into digital signals to be able for processing by the host computer. This operation is called the analog-to-digital converting process and it is symbolized to as (A/D) [78]. Usually the data acquisition applications are controlled by software programs which are provided with the data acquisition system parts. In the present study, the used data acquisition system is from the type Data acquisition conducted by 24-bits 8 channel HBM - Hottinger Baldwin Messtechnik, QuantumX measuring amplifier, *Figure 3.9*.



Figure 3.9: QuantumX measuring amplifier

It can be clearly seen in *Figure 3.9*, there are 8-channel connections receive signals from 8 accelerometers which are used during the present work.

3.4.3 PC computer

The data that are processed and analyzed by DAS device is converted to digital values, as mentioned previously, which have to be displayed within a suitable device that produces the results in proper way. The suitable device in this case is the PC computer which is connected by the DAS unite to allow handling and displaying the output results. The output results could be in different categories such as, tables, chains of data saved in a matrix form, graphs, and other details, as shown in *Figure 3.10*.

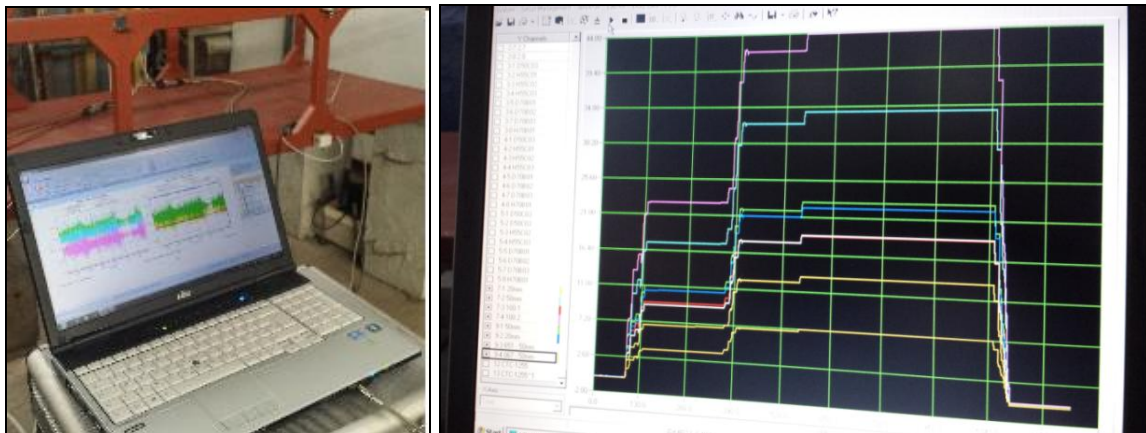


Figure 3.10: Various output graphs via PC computer during the AVM test

The most interesting output results that used in the modal identification processes are the acceleration data which appear as numbers in forms of columns and rows that are saved in special files. This file contains values of recorded acceleration for the AVM test that applied on the tested model during the test period which is recorded also. Other information are included in this file about the test and the parameters, such as sampling frequency, filtering frequency, date and many other else which are adopted in the test. During the AVM test the information that produced by PC computer should be monitored with care by the tester, as shown in *Figure 3.11*.



Figure 3.11: Monitoring of results during the test

The graphs that are displayed during the AVM test, *Figure 3.10*, produce important information with respect to the consistency of results during the progress of AVM test

procedure. When the results are consistent and there are no abnormal sudden changes along the test period, then the test could be considerable. Otherwise, the results should be ignored and the test must be repeated due to the influence of abnormal conditions, such as excessive excitations from other sources, which contaminate the results. Another information are displayed by the PC computer during the test, for instance, the status of the accelerometers and their options which are very important to be checked before and during the test. For example, if the accelerometer is installed to sense the motion in vertical direction, then the acceleration value of about $\pm 9.81 \text{ m/s}^2$ should be corresponded with the output acceleration results that produced by the accelerometer. This is called static calibration of the accelerometer. On the other hand, if the accelerometer is needed to sense the horizontal motion then values of acceleration close to 0.00 m/s^2 should be recorded for the output acceleration results. More other information are obtained and displayed by the PC computer which refers to the important role of this device during the AVM application.

3.4.4 Simulation of ambient vibrations - Low frequency and low level shaker excitation

The shaker is a tool that required to simulate the vibrations generated by the ambient natural conditions inside the laboratory. These vibrations, generated by the shaker, needed to affect on the tested structural system in a proper way that reflect the real behaviour of ambient conditions as much as possible.

Ivanović et al (2000) [5] declared that it is not accurate to supply shaker as an excitation force device for the tested ambient vibration based model if it is installed on the upper parts of that model to generate vibration. This case produces the forced vibration test which is not represents the ambient vibration simulation and the generated amplitudes due to shaker will not be similar to those obtained from real excitation forces. Usually, for the in-situ excitation, the real excitation forces affect on the sub-structural parts of the structure and the waves are transmitted through ground and affect on the sub-structural part towards the upper parts of the structure. Hence, the forced vibration should be avoided because it is not accurate representation for the in-situ excitation forces and not represents the ambient

vibration simulation. This consideration is taken into account in the present work and an attention is paid to install the shaker in the lower parts of all the tested models.

The used shaker, in the present work, is from the type low frequency 4 ohm impedance ButtKicker, as shown in *Figure 3.12*.



Figure 3.12: Electric shaking device

This device is a music device, bass shaker, which produces low vibrations in the range from 5 Hz to 200 Hz. It can be installed in different ways and several directions of vibrations can be achieved depending on the way of shaker installation, as shown in *Figure 3.12*.

3.4.5 Other complementary devices

Several other devices are required to accomplish the AVM procedure, such as the frequency intensity level device which controls the intensity level of the sampling frequency and is connected directly with the shaker. Another equipments are needed such as connectors, cables and batteries which are important to act as a one unit system during the implementing of AVM test.

As the AVM is completed, and the resulted data are analyzed by the FDD technique through ARTeMIS software to obtain modal parameters, the use of these parameters in the damage detection process is adopted, as in the next paragraphs.

3.5 Adopted damage detection procedure of civil structures based on ambient vibration measurements

As the extraction process of structural modal parameters is completed, the extracted parameters are used then in the procedure of damage detection. In the present study, the adopted parameters are the natural frequencies and mode shapes for the first few modes of the structural model.

3.5.1 Adopted procedure of damage detection

The common damages of a structure produce changes of its natural frequencies and mode shapes. Since the necessary measurements and extraction of natural frequencies and mode shapes require less human efforts, damage could be detected easier using dynamic analysis. As mentioned earlier, this kind of technique belongs to the global methods of non-destructive tests for damage detection. Damage assessment technique using analysis of recorded vibration data could be quite effective when implemented periodically during the service life of the structure [79]. The basis of the present assessment method is the observation of the changes of the structural natural frequencies and mode shapes which are evaluated through experimental modal analysis compared to their corresponding values of a known reference condition. The values of natural frequencies and mode shapes for the reference condition are represented by the original state of the structure, which reflects the behavior of the structure when it is intact and there are no damages occurred. In this way, any changes in the periodically measured values of modal parameters, natural frequencies and mode shapes, represent an indication for the presence of damages.

In the present work, the procedure of damage detection can be summarized in few steps which represent the main operations that implemented simultaneously to complete the procedure, as following:

1. Extracting modal properties of the tested model experimentally. This operation was explained previously, in which, the obtained AVM are processed in ARTeMIS software to estimate and extract the experimental modal parameters for the tested

real model. Usually in this process, modal parameters for both the intact and damaged model are extracted.

2. Extracting modal properties of the tested model numerically. This process is accomplished by creating a finite element (FE) structural model, as a simulation for the real experimental model, using certain software. In the present study the adopted finite element method (FEM) modeling software is the well-known ANSYS software which has a wide ability in this field. ANSYS software is used for modal computations and determination of structural dynamic properties (natural frequencies and mode shapes) which are implemented on the created FE model. This process is repeated several times (iterations) in order to simulate different locations and different severities of damage in each time. Hence, from each analysis, different values of modal parameters are produced for a certain damage location and severity. This procedure is so-called numerical FE model updating technique [30].
3. From each FE modal analysis that applied during the numerical model updating procedure, the obtained results of modal parameters (numerical modal parameters) are compared with the experimental modal parameters (resulted in step 1). Hence, each iteration (numerical model updating or application of modal analysis under certain damaged location and severity) produces different values of errors between experimentally extracted modal parameters and their corresponding numerically computed modal parameters. These values of errors are considered as indications for the presence of damage within a certain location and severity.

The process of comparison between experimentally and numerically modal parameters is implemented by using a certain form called the *Objective Function* or *Target Function*, which has an important role in the procedure of damage detection. It contains the parameters, represented by the modal parameters, which are taken into account in the comparison process. It produces values of errors in each iteration which are either high or low values. The high error value indicates that the proposed dynamic parameters in the numerical FE model updating procedure, which are selected in the recent iteration, are not the values that correspond to the actual values of the experimental modal parameters. Hence, this solution and the corresponded

values of parameter should be ignored. On the other hand, if the value of error is relatively within the lowest value, then the proposed dynamic parameters in the numerical FE model updating procedure, in this iteration, are close to the experimental modal parameters in real condition. Thus, result (solution) of this iteration is adopted. Further explanation and reviewing of the objective function will be in the next paragraph.

4. The last part in the procedure of damage detection is related with the use of certain optimization procedure that helps in selecting the optimum result (solution) among all candidate solutions within relatively short time. As mentioned in step 3, all the solutions are obtained across the application of objective function which contains the adopted variables (modal parameters) for the comparison. The optimization procedure seeks for the minimum value of error among all values that resulted from all iterations within short period. This approach will be intensively explained in the next chapter of this work.

The general procedure of damage detection can be summarized in the form of flow chart shown in *Figure 3.13*.

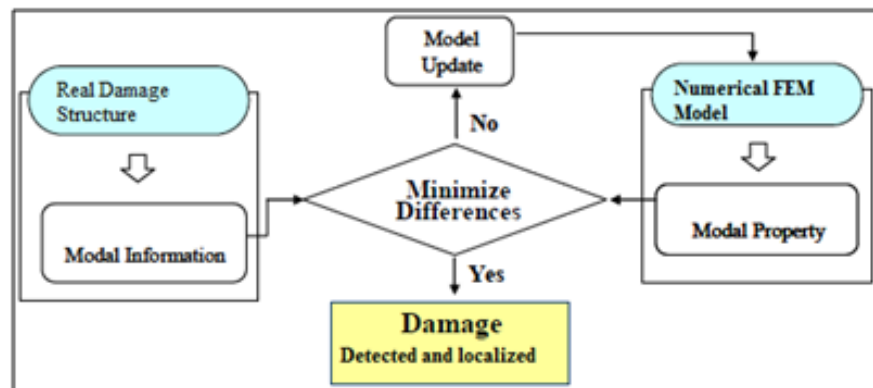


Figure 3.13: Damage detection general procedure [30]

In the present study, the procedure of damage detection which contains the optimization process is executed as a script routine (program) written in MATLAB environment. By this software, the written script routine connects all operations that are needed to be implemented simultaneously during the procedure of damage detection. For

instance, the experimental modal parameters are compared periodically with their corresponding parameters that computed numerically in each iteration. This requires the FEM analysis by ANSYS software to be preformed continuously as the comparison process still works according to the number of iterations. Thus, it can be imagined now the required number of analysis (iterations) by the ANSYS software are needed to be performed during the whole procedure of damage detection, which could be in several thousands in some cases. This usually impossible to be executed manually, and hence, the role of MATLAB software is aimed to control this process automatically. On the other hand, the optimization process should also be connected with the same procedure, and implementation of the optimization technique requires another script routine (program) to be written. In this case the program is written in MATLAB also which complements the program that used previously for controlling of modal parameter results. Hence, all operations of damage detection are implemented as one unit simultaneously by the role of MATLAB software.

3.5.2 Objective function

Due to the important role of the objective function in the procedure of damage detection in any optimization process, a review for the use of objective function in literature and the adopted forms in the present study are discussed as following:

3.5.2.1 General

Objective function, Error function or Target function is an extremely important segment of any optimization procedure, as it has to enable exploring the global solution of the problem. It has to take into consideration the most important parameters, according to the structure of the problem. Generally, in the case of vibration-based damage detection task, an objective function has to represent the difference between the experimentally estimated and numerically simulated modal parameters. The objective function in vibration based damage detection process usually takes into the account different parameters as a measure of compatibility of the results, such as modal frequencies, mode shape vectors, MAC (Modal Assurance Criterion) values, strain energy residuals and flexibility matrices [80].

Researchers used different combinations of these fundamental parameters, Nahvi and Jabbari (2005) [27] used in their work, as an objective function, the following form:

$$\varepsilon_i^{X^h} = \left[\sum_{j=1}^J (\phi_{ij}^e - \phi_{ij}^m)^2 \right]^{1/2} \quad (3.6)$$

where, $\varepsilon_i^{X^h}$ is the error function, X^h is the crack position, ϕ_{ij}^e and ϕ_{ij}^m represent the j^{th} component of the i^{th} mode shape which are obtained experimentally and numerically, respectively. They declared that the use of mode shapes parameter only was sufficient to achieve the value of error that indicates damage location. Meruane and Heylen (2010) [81] used the participations of natural frequencies and mode shapes as parts of their main form of objective function which includes other participations not mentioned here. The participation of the MAC is also considered which is depending on the mode shapes. Hence the three participations are respectively as following:

$$F1 = \sum_i \left(\frac{\omega_{A,i}^2(\{\beta\})}{\omega_{E,i}^2} - 1 \right)^2 \quad (3.7)$$

$$F2 = \sum_i \|\{\phi_{A,i}\} - \{\phi_{E,i}\}\|^2 \quad (3.8)$$

$$F3 = \sum_i (1 - MAC(\{\phi_{A,i}\}, \{\phi_{E,i}\}))^2 \quad (3.9)$$

where, ω_i^2 is the i^{th} natural frequency and ϕ_i is i^{th} mode shape. They observed during the detection procedure, in the cases of using the participations of just MAC and natural frequencies as objectives, the process was able to detect all studied scenarios of damage through the desired number of iterations in a certain method of optimization. This reflects the importance of properly selecting each part in the form of objective function to produce the best results. Also, this observation gives a conclusion that the use of some participations, alone or together, of modal parameters as well as MAC, could be enough to represent the whole objective function successfully. Nabeel and Aveen (2012) [82], also

used two forms of objective functions including differences in natural frequencies and MAC values. Their results show that the objective function based just on differences in natural frequencies produces better results than the objective function just with the MAC as an objective function. This also confirms the conclusion that observed from the study of Meruane and Heylen (2010) [81].

3.5.2.2 Adopted objective functions

In the present study, several forms of objective functions are considered depending on which one is suitable for each case of study. The participations of changes in natural frequencies, normalized mode shapes and MAC were the main parts that form any adopted objective function in combination or independently. These parts can be formulated as following:

1. The participation of changes in natural frequencies are adopted according either to the square of relative differences (F_r) in natural frequencies as following:

$$F_r = \sum_{i=1}^n \left(\frac{f_i^E - f_i^N}{f_i^E} \right)^2 \quad (3.10)$$

or according to the square of direct differences (F_d) in natural frequencies as following:

$$F_d = \sum_{i=1}^n (f_i^E - f_i^N)^2 \quad (3.11)$$

where, the symbols f_i^E and f_i^N represent the experimental and numerical values of natural frequencies for the tested model, respectively and n is the number of adopted modes.

2. The participation of the normalized mode shapes according to the form:

$$D = \sum_{i=1}^n \left[\sqrt{\sum_{j=1}^m (|\Phi_{ij}^E| - |\Phi_{ij}^N|)^2} \right] \quad (3.12)$$

where, symbols Φ_{ij}^E and Φ_{ij}^N in equation (3.12), represent the normalized reduced mode shape vector, obtained from experimental and numerically computed data, respectively. The measure of mode shape vector difference is based on the assumption that there are slight differences between the same sign of mode shape vector components. The m is the total number of measuring points that located at particular nodes of the FE structural model.

3. Orthogonality between mode shapes is represented by the parameter MAC. The participation of the diagonal MAC_{ii} values, the significant indication of mode shapes compatibility, are taken into the account as following:

$$M = \sum_{i=1}^n (1 - MAC_{ii}) = \sum_{i=1}^n \left(1 - \frac{\left(|\Phi_{ij}^N|^T \cdot |\Phi_{ij}^E| \right)^2}{\left(\Phi_{ij}^{NT} \cdot \Phi_{ij}^N \right) \left(\Phi_{ij}^{ET} \cdot \Phi_{ij}^E \right)} \right) \quad (3.13)$$

4. APPLICATION OF OPTIMIZATION PROCEDURES IN DAMAGE DETECTION OF CIVIL STRUCTURES

4.1 Introduction

Most methods of damage detection include optimization procedure in order to explore the optimum solution represented by the location and severity of structural damage. Nevertheless, the optimization problem may involve complexities such as discrete, continuous or mixed variables, multiple conflicting objectives, non-linearity, discontinuity and non-convex search region. The search space (design space or the domain that required to be searched) may be so large and the *Global optimum* cannot be found in a reasonable time. The *Global optimum* or *Global minimum* is the target which represents the minimum existed value of error between experimental and numerical parameters among all available values in the searching space. Hence, for the large space problems, the existing linear or nonlinear optimization methods may not be efficient or they are computationally expensive in determining the global minimum [83]. On the other hand, the high dependence on the initial searching point of conventional optimization methods is another important problem in damage detection that should be taken into account. It causes a decrease in the ability of wide exploring for the searching space. This encourages to implement more investigations that can lead to a robust optimization approach, which in turn, could solve this problem [84]. Several parameters exist in the process of comparison between measured and computed modal properties which are the base of vibration based damage detection procedure. Increasing of these parameters will make the whole process more complicated by increasing the probable solutions in the searching space. In this case, there could be no clear unique solution represents the target value of, in the field of damage detection, location and severity of damage that could be achieved. In contrast, several candidate solutions represented by the low values of errors resulted from the comparison process mentioned earlier will be available in the searching space called as *Local Minimum* values. Hence, the robust optimization technique is aimed to seek for the unique optimum solution as accurate as possible and avoids values of local minima [85].

Optimization procedures that involved in damage detection usually include a set of variables (such as the location and severity of damage), which have to be updated in order to obtain the minimum difference between the numerical and experimental results for damage state. Optimization procedures require construction of objective function that has to include all representative parameters that used in the comparison process. Convergence in the optimization procedure is influenced by the best selection of the objective function which is the most important part in the whole procedure [86].

Several optimization procedures are already available in literature which are used in the field of damage detection. Hence, an explanation for the main categories that characterized some selected well-known methods, is highlighted in the following paragraph.

4.2 Optimization techniques

In the recent years, there has been a great deal of interest in developing methods for solving global optimization problems. Such problems usually have functions with global and local minima and the so-called global optimization methods are required to prevent stagnation of the search into local minima [87], [88]. Local minima (or maxima) are not the target values in the searching space, hence, robustness of any optimization technique is the ability of avoiding local minimum values, *Figure 4.1*.

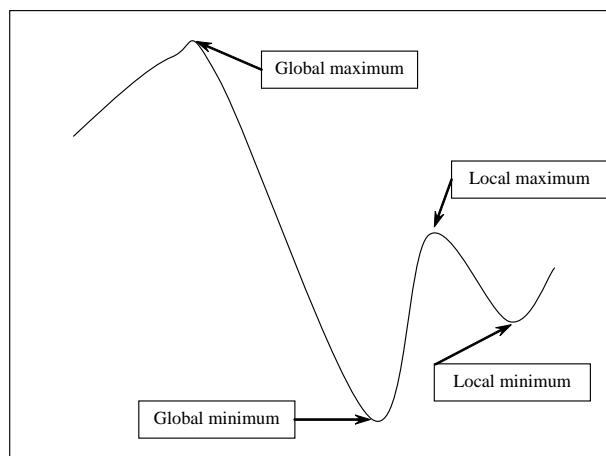


Figure 4.1: Global and local (maximum or minimum) values in the function.

When the optimization technique is able to check most of the searching space within relatively short time, it could be considered then as a global minimum technique. Otherwise, when just part of the search space is explored, the optimum results in this case are almost refer to local minima. Hill climbing technique is one of the most well-known mathematical optimization techniques which belongs to the family of local search. It starts the searching algorithm by arbitrary initial solution which is iteratively compared with other neighboring solutions of the current iterations. The first better neighboring solution is replaced with the initial (or current) solution and it is adopted as the best chosen solution with respect to the Simple or First Improvement Hill-Climbing procedure [89]. Simple Hill climbing method is suitable to find local optimum solution rather than global optimum solution which is not guaranteed to be found in this method. In this paragraph, some of the global minimum techniques are identified which have the ability to avoid the stagnation in local minima and lead to the best solution represented by global minimum value.

4.2.1 Genetic Algorithm (GA) technique

Genetic algorithms technique is a kind of the artificial intelligence based optimization tools which depends on the mechanism of natural selection and natural genetics (application of biological principles). It adopts the concept of survival of the fittest solution according to certain strings exposed to some modifications. GA algorithms have been extensively applied in structural damage detection applications [80], [90]. Unlike the classical optimization, GA are also able to deal with discrete optimum design problem and provide much stronger global optimization performance than traditional mathematical algorithms such as hill climbing method [80], [91].

Three operations usually consists the GA operation: *reproduction* (selection), *crossover* (recombination) and *mutation* (rarely random change). The first stage in the application of GA procedure is the *initial population*, which may, for example, corresponds to initial numerical values of a variable set. One of the most important characteristics in this stage is the size of the *population* which may vary, and generally relates to the problem under consideration. The population consists of members which are either strings of zeros and ones, i.e. binary strings, or strings of real parameters (real numbers). Each string of

population corresponds to a *chromosome* and each binary (or real [92]) element of the string to a *gene*. Population size refers to the number of *individuals* (*chromosomes*) consisting that population during one generation. The term *chromosome* refers to a possible solution of the problem and it consists of number of genes, while each gene represents a problem variable. A *new population* must be developed from initial population [93].

The *reproduction* or (selection) stage means that the selection of a set of chromosomes, based on natural selection, to be as *parents*. Thus, members of the population chosen for reproduction, based on their fitness, are defined according to some specified criteria. *Crossover* is a genetic operator that combines (mates) two chromosomes (parents) to produce a new chromosome (*offspring*). Behind the crossover lies the main idea that the new chromosome may be better than both of the parents, because it takes the best characteristics from the parents. The final process is *mutation* which randomly changes a particular gene in a particular chromosome. Thus, 0 may be changed to 1 or vice versa. The process of mutation in a genetic algorithm occurs very rarely and hence probability of a change in a string should be kept in very low levels [94]. The three main operations of GA procedure are shown in *Figure 4.2* [96].

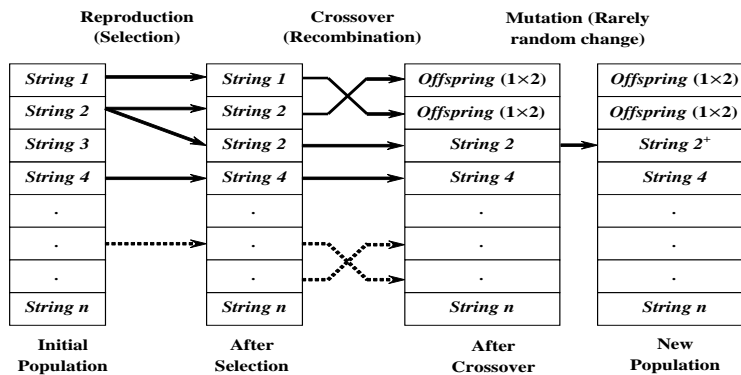


Figure 4.2: Selection, crossover and mutation processes in GA procedure

Arrows in *Figure 4.2* refers to the changes that occur in the genes of each string, which in turn, causes changes in the properties of the whole string. On the other hand, the operation of GA optimization is controlled by a certain *stopping criteria* which governs the continuity of the whole process until finish. Usually the *number of generation* is the most

well-known criteria that governs the optimization process from the start until the end. The role of stopping criteria within GA optimization procedure can be illustrated by the flow chart shown in *Figure 4.3* [95].

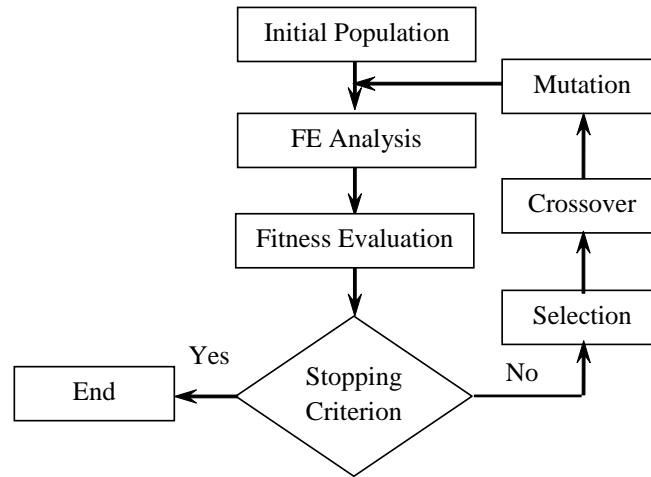


Figure 4.3: Flow chart of GA optimization procedure with stopping criteria

The stopping criteria should satisfy suitable continuity for the whole optimization process by allowing the improvement of objective function (fitness evaluation) to be in the best convergence (minimum error). Hence, the optimization process should continue until no significant convergence appears [95]. GA exhibits good performance in optimization procedure and can be implemented for complex systems effectively [96].

4.2.2 Simulated Annealing (SA) technique

A heuristic optimization probabilistic method well-known as Simulated Annealing (SA) was proposed by Kirkpatrick, Gelett and Vecchi (1983) [97] to find the global minimum of an objective function that may possess several local minima. It is an emulating for the physical process represented by slowly cooling of solids which is at the end, and at the "frozen" state, minimum energy configuration is reached [98]. Two main types of SA techniques are existed usually, the *classical simulated annealing* (CSA) or *Boltzmann machine* and the *fast simulated annealing* (FSA) or *Cauchy machine* [99]. The most significant feature that characterizes SA is its ability to avoid local optima by allowing moves to lower quality solutions with a pre-specified probability. This category is

implemented according to certain probability called *acceptance probability*, by which, the new solution is accepted according to the probability defined in Metropolis algorithm as following [100]:

$$P_1\left(\vec{x}_t \rightarrow \vec{x}_{t+1}\right) = \begin{cases} 1 & \text{Otherwise} \\ e^{-\frac{[E(\vec{x}_t) - E(\vec{x}_{t+1})]}{C_B T_1}} & \text{if } [E(\vec{x}_t) - E(\vec{x}_{t+1})] < 0 \end{cases} \quad (4.1)$$

where, P_1 is the acceptance probability, \vec{x}_t and \vec{x}_{t+1} are the recent and new solution, respectively, t is the discrete time, $E(\vec{x}_t)$ and $E(\vec{x}_{t+1})$ are the energy (function) at the recent and the new solution, respectively, C_B and T_1 are Boltzmann's constant and the temperature of the system at recent solution, respectively. Another big plus of SA is its ease of implementation. At each iteration of SA, the objective function value of the current solution and a new generated solution are compared. Improving moves are always accepted (as the acceptance probability is 1 in equation (4.1)) while only a fraction of non-improving moves are performed with the aim to escape local optimal solutions. The probability of accepting a non-improving move depends on the non increasing parameter of temperature. The cooling of the system has several procedures such as [101]:

$$T_{\text{new}} = T_{\text{initial}} \times 0.95^k \quad (4.2)$$

$$T_{\text{new}} = T_{\text{initial}} / k \quad (4.3)$$

$$T_{\text{new}} = T_{\text{initial}} / \log(k) \quad (4.4)$$

where T_{new} and T_{initial} are the new and initial temperature at the start of the algorithm, and k is the *annealing parameter*, which could refer to the iteration number in the algorithm [101]. Generally, this technique comes from annealing in metallurgy. In this process, a metal is heated and slowly cooled off, in order to increase the size of its crystals. The heating dissolves out atoms from their initial positions which can be seen as a local

minimum with respect to energy level. Such atoms can then freely move around. Slowly cooling off has the effect that the free atoms can end up in positions with lower energy level than the initial positions. The crucial factor is to choose the cooling procedure appropriately, because fast cooling off will not enable atoms to find better energy levels while slow cooling off causes very time consuming [100]. The SA optimization procedure is terminated according to the stopping criteria which depends on the temperature or on a certain level of convergence is achieved for the adopted parameters.

4.2.3 Artificial Neural Network (ANN) technique

Artificial neural network (ANN) are computational models established by McCulloch and Pitts in 1943, depend on the concept of neuron architecture and operation of the human brain. As the brain is composed of neurons, the ANN is also assembly of large number of neurons or nodes which are highly connected processing units. Unidirectional communication channels, so-called *connections* connect the nodes, as shown in *Figure 4.4* whereby the circles and arrows represent the nodes and connections, respectively [85], [102].

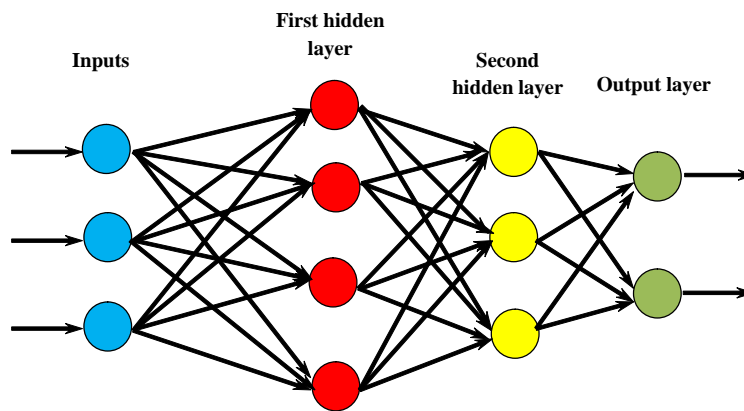


Figure 4.4: Structure of multi-layer neural network

Each column of nodes represents a layer and the intermediate layers are called the hidden layer. In fact, there is no precise method for selecting the appropriate numbers of hidden layers and nodes, and the trial and error method is most frequently used for that purpose in practical applications [85]. The strengths of the connections between the nodes

are represented by numerical values, so-called *weights*. Knowledge is stored in the form of a *collection of weights*. Each *node* has an activation value, which is a function of the sum of inputs received from other nodes through the *weighted connections*.

The neural networks are capable of self-organization and knowledge acquisition, i.e. learning. ANN has the ability of producing correct or close to correct outputs even when the inputs are incomplete. Most neural networks have some sort of "training" rule whereby the weights of connections are adjusted based on presented *patterns*. In other words, neural networks "learn" from examples and exhibit some structural capability for generalization. Training provides a set of known input-output pairs, *patterns*, to the network [102]. The number of hidden layers and number of nodes govern the learning capability of the ANN. The extremely small size of ANN causes slow convergence or makes the ANN fall into a local minimum. In contrast, if the size is relatively large then the training time increased significantly and the output will be very accurate depending on the input of training only but large errors are produced for the data of new input [85]. Error is defined as a measure of the difference between the computed pattern and the expected output pattern. The network iteratively adjusts the weights of each node to obtain the desired output (for each input set) within a desired level of accuracy. Typically, each node in lower level is connected to every node in the next higher level and should not skip any intermediate level exist. By this route, the signal is transmitted from the input layer through intermediate layer until the output layer, hence, output layer cannot receive signal directly from the input layer [102]. According to training process, the ANN obtain some knowledge about the data, and any new input leads the ANN to sense the changes which are needed as indications in the general optimization process. Training ANN with simulated data gives good capability to perform ANN in optimization field with good accuracy [102].

4.2.4 Tabu Search (TS) technique

Word *tabu* (*taboo*) comes from Polynesian Tongan language, where aborigines of Tonga Island used by to indicate things that cannot be touched because they are sacred. Tabu Search (TS) is a higher-level method for solving combinatorial optimization problems. *Tabu Search (TS)* technique is a meta-heuristic iterative procedure classified as

practical optimization tool and could be considered as an improvement of hill-climbing optimization method with short-term memories. The mechanism starts from some initial feasible solution and attempts to determine a better solution by exploring several neighbourhood *hyper-points* (position), and selects the new point (move) producing the best solution among all candidate points (moves) for current iteration. Selection of the best move (which may or may not improve the current solution) is based on the supposition that good moves are more likely to reach the optimal or near-optimal solutions. The set of admissible solutions attempted at a particular iteration, forms a candidate list. TS selects the best solution from the candidate list. Definition of searching space and neighbourhood around the trials are important basic steps of any TS heuristic which govern the distribution of checked solutions [103].

TS procedure is developed and proposed in the present work, and hence, extensive explanation for this technique is highlighted later.

4.3 Review of application of optimization methods in damage detection

In literature, wide use of different optimization procedures as complementary requirements were used for the sake of damage detection. The objective function, on the other hand, is the essential part in any optimization procedure which governs the convergence or divergence of errors that produced according to the compared parameters (or variables). Hence, in this paragraph, a brief overview for each optimization procedure mentioned previously that used for damage detection is explained as following.

4.3.1 GA procedure in damage detection

As mentioned earlier, GA procedure consists of strings that are being either real coded or binary coded numbers. Both types are usable in the algorithm and could satisfy the requirements of GA procedure. Xia and Hao (2011) [92] used in their work the real coded numbers to consist the strings of the adopted GA method for the sake of damage detection based on vibration data. They focused in their work on the preference of either use the combined participation of natural frequencies and mode shapes together or separately on the behavior of objective function within the GA procedure. Their observations were

applied on cantilever beam and portal frame as study cases. Their study led to the ability of use real coded number in the procedure of damage detection and the combined action of both modal parameters in the objective function as the better case. The use of real coded strings is relatively newer than the use of traditional binary coded strings in GA procedure which were the first GA methods to be applied in damage detection [84]. Meruane and Heylen (2008) [89] had adopted the real coded strings GA procedure due to its recency and ability to be performed faster than the binary coded GAs [41]. This is usually due to the effect of neglecting the decoding process that needed to be applied in the binary-coded GA which, in turn, enhances the accuracy of GA results [89]. They used GA procedure to detect damage in real space truss model according to the assumption that GA is a robust technique and can work even with high levels of noise. Classical procedure of GA is modified according to their work by adding a complementary routine that performs a local search algorithm to improve the results. Hence, a hybrid GA is referred to their modified procedure. On the other hand, the objective function consists of, mainly, the participations of natural frequencies and MAC and it was necessary to incorporate their influence, as what was declared previously by Xia and Hao (2011) [92]. Meruane and Heylen (2008) [84] declared that the use of additional term called damage penalization term can improve the performance of objective function. The improvement is represented by the ability of avoiding false damage detection resulted due to experimental noise or numerical errors. For instance, reducing the participation of the penalization term leads to three locations of damage for the case of single actual damage, while a unique single location is achieved for high participation of penalty term. They compared their results with another results obtained through conventional methods and they noticed that GA can reach more precise solution in the presence of noise [84]. On the other hand, Hui et al. (2011) [80] used traditional GA and, moreover, traditional objective function represented by the participation of natural frequencies and MAC only. As a comparison with the previous work implemented by Meruane and Heylen (2008) [84], the traditional GA and objective function can provide enough indication for damage detection in the study of Hui et al. (2011) [80]. A similar study was implemented by Au et al. (2003) [90] which uses the same terms in the objective function of Hui et al. (2011) [80] but with the norm of mode shapes

instead of MAC. This objective function was used to minimize difference between the experimental and numerical modal parameters within the procedure of micro GA. Unlike the conclusions of all the previously mentioned studies, Au et al. (2003) [90] declared that the use of mode shapes together with the natural frequencies in the objective function may have favorable or unfavorable effects on the accuracy of damage detection.

Hence, according to the previous observations, the use of real or binary coded strings in GAs, traditional or modified GAs, and combined or separated influence of natural frequencies and mode shapes within the adopted objective function, could all be used acceptably in the procedure of damage detection.

4.3.2 SA procedure in damage detection

Due to the long implementing period of simple GAs procedure, researchers seek for more better effective optimization procedures that could tackle drawbacks of GAs [41]. He and Huang (2006) [41] used SA procedure as an enhancer for the influence of GAs. They used SA procedure in addition to real coded GA procedure for damage detection within the same algorithm. The used objective function in their work represented by the participations of both static displacements and the natural frequencies which is implemented on a curved beam, cantilever beam and a clamped beam as study cases. The authors also accomplished the same proposed procedure under the same objective function using spherical composite shell as a case study [39]. In both studies, they declared that the proposed procedure improved the convergence speed to the desired solution during the optimization procedure for damage detection process. In literature, no sufficient information and extensive research about the use of SA procedure in the field of damage detection are available. It is probably due to the novelty of this method compared with others. Hence, it is recommended to make further investigations about SA procedure with damage detection.

4.3.3 ANN procedure in damage detection

The procedure of ANN technique is widely applied in the field of vibration damage detection in literature. One of the important characteristics of ANN technique is the ability to model nonlinear and complex relationship, which in turn, represents the relationship

between structural parameters and the modal parameters [85]. Aghabarati and Tehranizadeh (2011) [90] used three of ANN procedures to identify the locations of damage zones in a steel truss case study. They declared that all the adopted procedure were able to detect damaged zones properly with the analytical solution for the low value of damage. Kirkegaard and Rytter (1994) [102] studied the possibility of using multilayer neural network for the purpose of damage detection. The behavior of intact and damaged structure was trained to the network through the simulation of modal parameters values for each case to be recognized by the network. Hence, the information about damage states and locations are provided according to the information that obtained during the training process which implemented with the aid of FEM of the model. The next step after the training process is represented by considering the estimates of the changes in modal parameters due to damage as inputs for the network. Sensing of the changes in modal parameters by the ANN leads to the damage detection. Kirkegaard and Rytter (1994) [102] extensively explained the procedure of damage detection using ANN and how does the training process represents the main part in the whole procedure which leads to indicate damages. They used two steel columns to verify their work as hollow section and mast structures. They concluded that ANN is able to detect location of damages through experimental data even when it trained with simulated data. They considered that this conclusion is a base for periodically structural health monitoring [102]. Other researches [104], [105] also used the modal parameters as inputs for the ANN procedure in application of damage detection which refers to the wide use of ANN procedures in this field.

4.3.4 TS procedure in damage detection

Due to the absence of TS application in the field of damage detection, at least according to the exploration that is implemented by the author in the available space, this subject will be explained only according to the work that is implemented in the present thesis, as explained in the next paragraph.

4.4 Tabu Search - Adopted optimization technique in the study

4.4.1 General

Classical optimization algorithms are suitable for functions of local optima. Such functions contain only one convex that it is guaranteed to be reached by application of the classical algorithms. They are not guaranteed in case of global minimum optimization when there are more than one convex in the optimized function. Hence, these techniques, such as Hill-Climbing method, are not suitable in the cases where complex functions are used such as the functions of the present work which are characterized by being multi-convex objective function. Such functions, which contain more than one concavity in the produced shapes, require advance optimization techniques to achieve the global minimum in the presence of several local minima. Method such as TS is appropriate meta-strategy techniques for combinatorial optimization problems like the case of the present work, [107]. Classical optimization algorithms (like Hill-Climbing method) can be tackled by repeating the search procedure more times, which is usually a time consuming problem, and probably leads to the same local solutions. Also, using another optimization techniques rather than Hill-Climbing method is recommended as an alternative way to overcome the drawbacks of Hill-Climbing method. The stagnation in local minimum is the main drawback of Hill-Climbing method which indicates the current solution as better than all of its neighbours, but not better than some other solutions far away. The global optimization methods avoid all the existed local minima in the searching space and achieve the exact or close to exact target value represented by the global minimum.

4.4.2 Objectives of selecting TS technique in the present work

Two main reasons, whereby, this work uses TS as an optimization technique in addition to the reasons that mentioned previously in the last paragraph. The first and the most important one is the novelty of using this technique in the field of, generally, civil structural engineering and, precisely, damage detection applications. During the preparing of the present work, hard efforts being made for seeking the most novelty optimization method which is unused earlier in the field of structural damage detection. This technique is

required to be a part of the studied aspects in this work which leads to satisfy state-of-the-art. By this way, present work introduces a new participation for the global science. The second reason concerns with the ability of TS technique in the field of optimization which provides solution very close to the optimum. Among several optimization methods, TS is the most effective, if not the best, to tackle the difficult problems at hand. These successes have made TS extremely popular among those interested in finding good solutions to the large combinatorial problems encountered in many practical settings [106].

4.4.3 Characteristics of the adopted TS algorithm

In the present study, the simple form of TS procedure is proposed. It is sufficiently to use such technique to produce accurate results within reasonable time. The simple form of the TS procedure consists of the following elements:

4.4.3.1 Tabu list

The forbidden movements (or solutions) represented by the already visited solutions are recorded in the so-called tabu list. Each obtained solution that recorded in the tabu list is saved temporarily or permanently throughout the optimization process in order to avoid the repetition and stagnation in the same searching zone (local minimum). According to the used memory in TS procedure, checked solutions are saved temporarily in the short term memory and permanently in the long term memory, *Figure 4.5*.

4.4.3.2 Candidate list

TS make use of a candidate list that provides a list of candidate moves (solutions) that are needed to be checked. One solution or more can be selected from the candidate list to be investigated. The candidate solutions could be represented by either the neighbor solutions, some of the better solutions or only the best solution from each iteration. The candidate list has an important role in the performance of TS procedure. In the present work, the candidate list includes the neighbor solutions which represent a part from the whole search space, as shown in *Figure 4.5*.

4.4.3.3 Termination criterion

Termination criterion is an important part in the TS procedure which governs the continuity of the whole process according to certain criteria. It could be according to different considerations, for instance, according to a certain minimum value of objective function that the optimization process is stopped when reaching to this value at any iteration. Another stopping criteria represented by adopting a certain number of iterations that not produces any enhancements (reduction) in the value of objective function during the procedure, which allows to finish the whole process. The most frequent criterion is according to a certain number of iterations required to implement the optimization process. In this case, when the total proposed number of iterations is executed, the optimization process is terminated [106]. Therefore, if the number of iterations is increased then the probability of achieving the global minimum value will increase also. This feature, for TS technique, is useful to tune the optimization process when the low values of number of iterations are insufficient. This criterion is adopted in the present work, *Figure 4.5*.

4.4.4 Adopted TS procedure

The adopted TS optimization procedure can be explained, for all studied cases or models that are taken into account in the present work, according to the flow chart shown in *Figure 4.5*. In order to avoid repeated solutions in the search process, recent solutions are memorized in the so-called short-term memory. The Improvement of the algorithm could be achieved by adding the long-term memory for the same purpose, which enhances the performance simultaneously within iterations. Both types of memories contain lists of forbidden solutions memorized in so-called Tabu-lists. The adopted TS procedure with advanced long-term memory performance is summarized in *Figure 4.5*. The algorithm starts with the definition of iterations termination criterion. It has to be defined based on the nature of the problem, maximum number of iterations according to allowable computing, as well as to the satisfactory level of the objective function improvement during a certain number of subsequent iterations. It is assumed that the termination (stopping) criterion is part of the total number of possible solutions in the searching space. The maximum number of iterations for TS application is symbolized as N_T^{TS} , which represents a percent of the

total number of solutions. In order to investigate the whole searching space (set of all possible solutions), it is useful to initially divide it into a certain number of subsets, R .

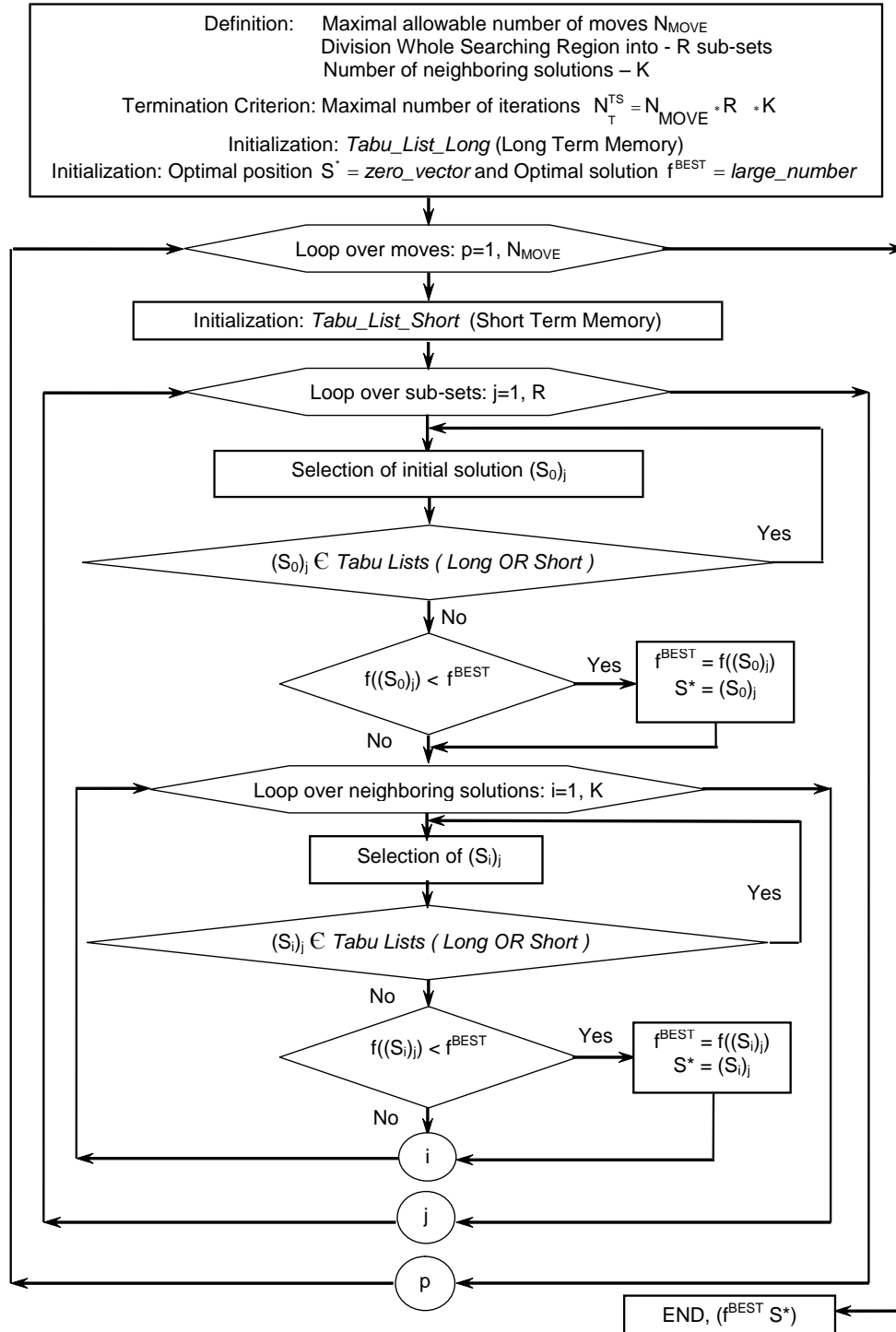


Figure 4.5: Flow chart of damage detection by Tabu Search optimization procedure

The long-term memory for storage of all checked solutions during the iteration process has to be initialised prior to the process. Also, the initial value of best approximation of objective function optimal value, f^{BEST} , has to be assumed, as a large number for the case of objective function minimization, as well as the solutions which corresponds to the optimal value of the objective function as a best solution, S^* . Iteration process is performed in three loops: the main loop, loop over subsets and loop over chosen solutions. The main (outer) loop over iterations corresponds to the total allowable moves, N_{MOVE} , in each of created subsets. The short-term memory memorizes (storage) just checked (visited) points in the actual move, and has to be initialised as zero vector at each move. The searching process in actual move begins randomly choosing the initial solution, over all subsets, $(S_0)_j$, $j=1,2,\dots,R$. Also, a certain number of K neighbouring solutions (trials), $N(S_i)_j$, $i=1,2,\dots,K$, has also been randomly selected around the initial solution of each set. Neighbouring solutions (points) form the so-called candidate lists, $N(S_i)_j$, of each set $j=1,2,\dots,R$. For all randomly-generated solutions of each set, either initial or neighbouring, it is necessary to determine their existence in the short and long-term memory. If better approximation of the objective function value appears at some point, the best approximation, f^{BEST} , as well as optimal solution S^* , have to be updated. The iteration process terminates when the maximum number of iterations is reached, which is represented by the number of checked solutions, $N_T^{\text{TS}} = R \cdot K \cdot N_{\text{MOVE}}$, in the adopted TS method. The termination (stopping) criterion plays an important role during the optimization process which governs the accuracy of final optimum value and the required time for implementing the whole process. The number of iteration is a part of the total number of possible solutions in the searching space; hence, it governs the percent of explored actual search space to the total available search space. The aim of any optimization process is to capture the optimum solution by exploring a percent of the whole search space. If this percent is relatively small and the optimized solution is accurate, then the optimization procedure is robust, otherwise, the optimization procedure is aimless.

5. EXPERIMENTAL RESEARCH ON STRUCTURAL MODELS OF DIFFERENT CONFIGURATIONS - RESEARCH PROGRAM AND RESULTS

5.1 Introduction

In order to achieve reliable results in the present work, four experimental models are adopted to execute AVM based damage detection concept. All the adopted models are made of steel and prepared in laboratory of the Faculty of Civil Engineering-University of Belgrade. Each model is needed to represent a certain structural behaviour under dynamic excitation according to degree of complexity. The first adopted model is a simply supported overhang beam model which is the simple case study that represents the behaviour of one dimensional 1D structural model. The second one is a grid-bridge model, which represents a pedestrian bridge deck model that has a plate action or two dimensional 2D structural model. The first model represents the influence of flexural action only while the second model represents the influence of both flexural and torsional structural action. More complicated models are adopted with general structural behaviour that include flexural, torsional and truss action simultaneously. The herein complex models are the third and fourth adopted models which represent three dimensional 3D structural behaviour models. The third model is a pedestrian bridge model that so-called Vierendeel bridge which behaves under the flexural and truss structural actions. The last model is the most complex one which represents a multi-storey building consists of 10 floors carrying various masses. Handling, erection, preparing and experimental testing of each model are extensively discussed in the next paragraphs.

5.2 Simply supported overhang beam model

Starting with the simple model of structures, a one sided overhang simply supported steel beam is considered and prepared for AVM test. All details concerning with the experimental test and results of this model are explained as following:

5.2.1 Experimental program - model erection

The adopted model is erected on two supports, the first is hinge and the second is roller with 1100 mm c/c distance between them. The hinged support is installed at 20 mm for the first (left) end of the model to insure the stability of the support. On the other hand, the roller support is executed at 380 mm from the second (right) end of the model which allows the performance of overhanging to be influenced. Hence, the total length of the over-hanged beam model is then 1500 mm, as shown in *Figure 5.1*.

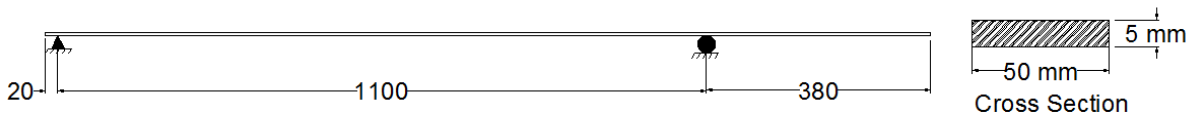


Figure 5.1: Simple overhang beam model

The model has a solid cross section of (5x50) mm dimensions rests on the long side, *Figure 5.1*. During the testing process, the model carries seven cubes made of plastic which are needed to fix the accelerometers in the AVM tests. The mass of each cube and accelerometer is listed in *Table 5.1*.

Table 5.1: Total masses of cubes and accelerometers on the overhang beam model

Cube	1	2	3	4	5	6	7	Average
Mass (gm)	33.1	37.4	33.4	35.7	33.8	35.2	33.1	34.53

In the next stage, the average value of the seven cubes and accelerometers is 34.53 gm (34.53×10^{-3} kg) is considered during the process of data analysing.

5.2.2 Preparing the requirements of AVM and experimental analysis

Configuration and installation of the model, cubes and accelerometers during the AVM tests are shown in *Figure 5.2* and *Figure 5.3*. The beam model is excited by the shaker, as mentioned in chapter 3, to simulate the ambient excitation. The shaker is installed on a center of timber beam which is tightly connected by two C-clamps (bench vice). By the same way, the timber beam is connected with two stands that holding the tested model. The two stands are connected tightly by the wall through bolts and provide a

stable base under the beam supports. In this way, it is guaranteed that the waves which are generated due to the excitation device (shaker) is transmitted from the shaker towards the tested model simultaneously across both of stands. Also in this case, the influence of these waves is exposed on the lower part (sub-structure) of the model and, hence, it is guaranteed that the ambient vibration is simulated not the forced vibration.

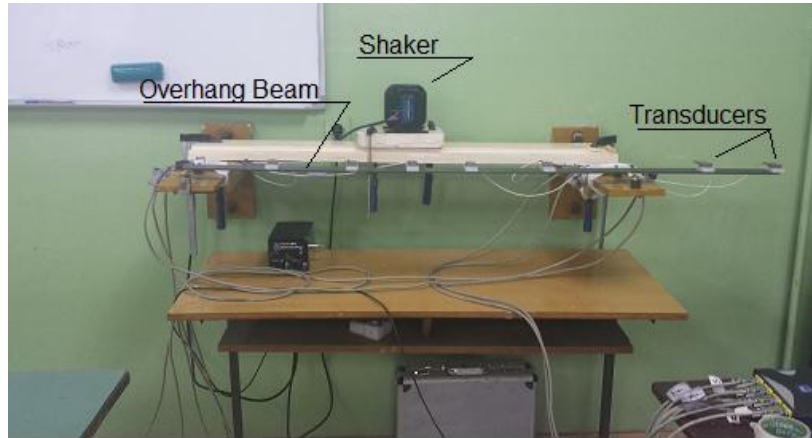


Figure 5.2: Overhang beam model during AVM test

It can be seen from *Figure 5.3* that accelerometers are installed with separating distances of 200, 200, 150, 150, 200, 400 and 180 mm to be as a single set of measurement and avoiding more sets for the sake of more accuracy.

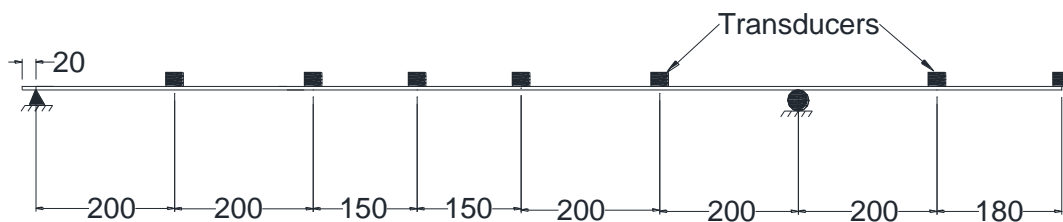


Figure 5.3: Locations of the installed accelerometers

All the necessary devices that needed to accomplish the AVM are prepared and connected, *Figure 5.2*. Seven accelerometers are fixed on their positions, *Figure 5.3*, and connected with the data acquisition device that described in chapter 3 through cables. On the other hand, the data acquisition device is connected with the PC computer, which in turn, connected by the shaker through the intensity level device, as in *Figure 5.4*. The PC

computer (or laptop as in *Figure 5.4*) transmits random signals that is amplified five times (i.e. the intensity level is 5) produced by white noise. *Figure 5.4* shows the whole assembly that prepared for AVM testing.



Figure 5.4: Complete assembly for AVM test

The previous descriptions and details of the test requirements and the beam model are applied for both cases of model integrity, intact and damage cases.

5.2.3 Implementing of AVM upon the overhang beam model

The prepared model represents the overhang beam model in the intact state but the following procedure is applied for both adopted structural health cases, intact and damaged overhang beam model. Experimental AVM test is accomplished using one set of measurement that consists of 7 accelerometers installed to sense the vertical motion only. In this case, only the vertical motion is taken into account for measurements which produces bending modes only. The test is started by trial measurements to investigate the reliability of test conditions and intermediate information that exhibited by the PC computer during the test, as described earlier in chapter 3. When it becomes clear that suitable test

conditions are available during the test, the adoptable tests are started and measurements are recorded carefully. The adopted sampling frequency in all tests is 600 Hz, filtering frequency is 200 Hz and intensity level is 5. The selected value of intensity level is adopted after some trials accomplished using intensity level equal 2 and 5, which adopted finally. The test is repeated to insure accuracy of final results and 30 min is the duration for each measurement. Hence, according to sampling frequency and duration of each measurement, around 1080000 values of acceleration are recorded by each accelerometer along the test.

5.2.4 Processing the configuration input file and AVM data by ARTeMIS software

In order to process the recorded data obtained by the AVM tests upon the overhang beam model, a special configuration input file (as a script file) is written to be performed in ARTeMIS software extractor, as mentioned earlier in chapter 3. The following procedure is applied for both adopted health cases of the model, intact and damage cases and the obtained data by AVM are only the change between the two procedures. The configuration input file contains certain commands to formulate the geometry of the model and describes the status of accelerometers (positions and directions). Flow chart of the implemented configuration file for the overhang beam model is shown in *Figure 5.5*.

The configuration input file starts with definition of sampling interval, which depends on the sampling frequency as following:

$$T = \frac{1}{f} \quad (5.1)$$

where f is the natural frequency (Hz) and the unit of T is in seconds. Also, the configuration input file contains the commands to process the information of data sets which represented by 1080000 rows and 7 columns of recorded acceleration values. To process these values, the ARTeMIS software according to the flow chart of *Figure 5.5* requires around 40 seconds through a computer has the properties of: Processor Core i7 CPU @ 2.1 GHz and RAM 6.0 GB, which reflects the huge data included.

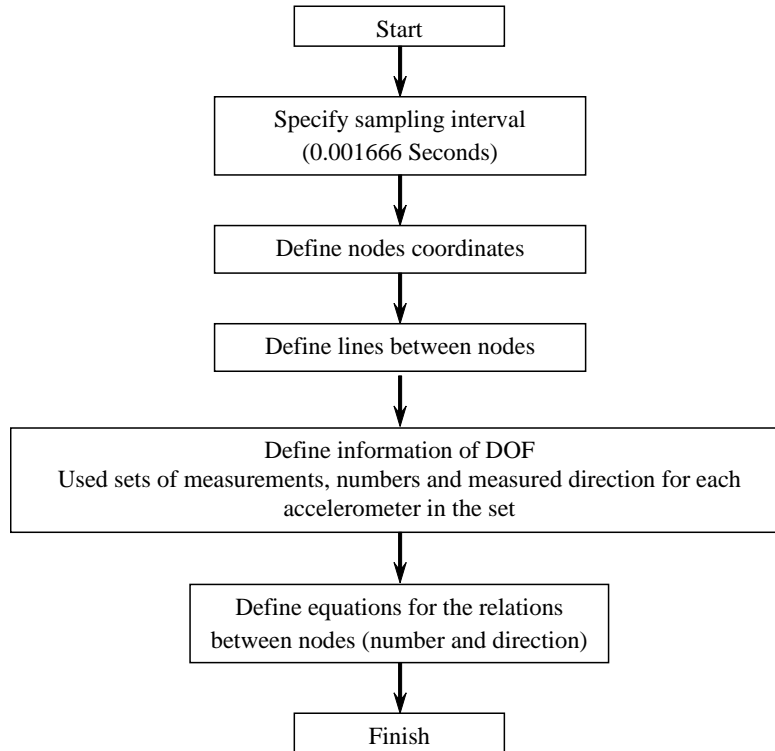


Figure 5.5: Flow chart of the configuration input file of the overhang beam model

The configuration input file depends on the size of model with all available nodes, distribution of accelerometers throughout the model length and direction of each accelerometer measurements. The distribution of accelerometers over the overhang beam model is considered as a line distribution due to the one dimensional behavior of the model. Hence, torsional modes are not taken into account in the case of overhang beam model. The distribution and directions of accelerometers over the overhang beam model is shown in *Figure 5.6* that performed by ARTeMIS software.

It can be seen that from *Figure 5.6*, only one set of measurement consists of seven accelerometers is able to represent behaviour of the whole beam and there is no need to divide the measurements into more than of one set. This can reduce the required time and efforts of measurements and decreases the errors resulted by removing and re-gluing the accelerometers.

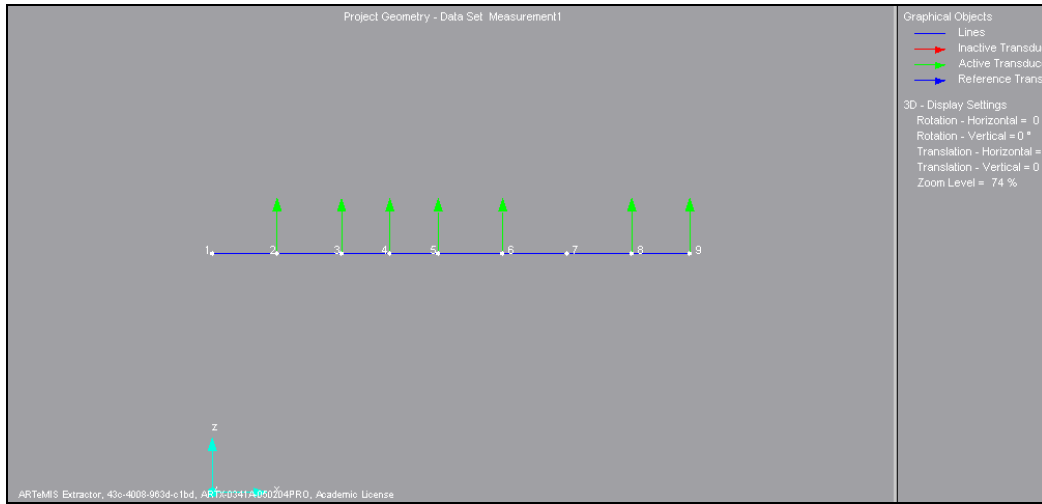


Figure 5.6: Geometry, distribution and measured directions of accelerometers throughout the overhang beam model

5.2.5 Intact case of the overhang beam model

5.2.5.1 Results of the extracted modal parameters using FDD technique

Analysing the adopted AVM data using FDD technique produces average of the normalized singular values of spectral density matrices of the data set that used in the overhang beam model, as shown in *Figure 5.7* which obtained by ARTEMIS software. The adopted results are according to frequency lines of 1024 and low pass filter. Due to the well separation between modes, the value of frequency lines of 1024 produces enough accuracy to indicate the peaks, from which, each candidate mode can be selected, as shown in *Figure 5.7*. Also from *Figure 5.7*, the value of Nyquist frequency of 300 Hz clearly consists the graph x-axis which is the half value of sampling frequency 600 Hz. Peaks appear referring to the locations of candidate modes throughout frequency range. In the present work, it is sufficient to use only first few modes to accomplish the required procedure of damage detection for the final stage. Hence, starting from the first four peaks existed in *Figure 5.7*, the selection process is implemented by FDD peak-picking to estimate candidate modes. The next stage is to check the selected modes. This is executed by comparison of modes using MAC, the indicator of modes orthogonality, which is available as validation process in ARTEMIS software editor.

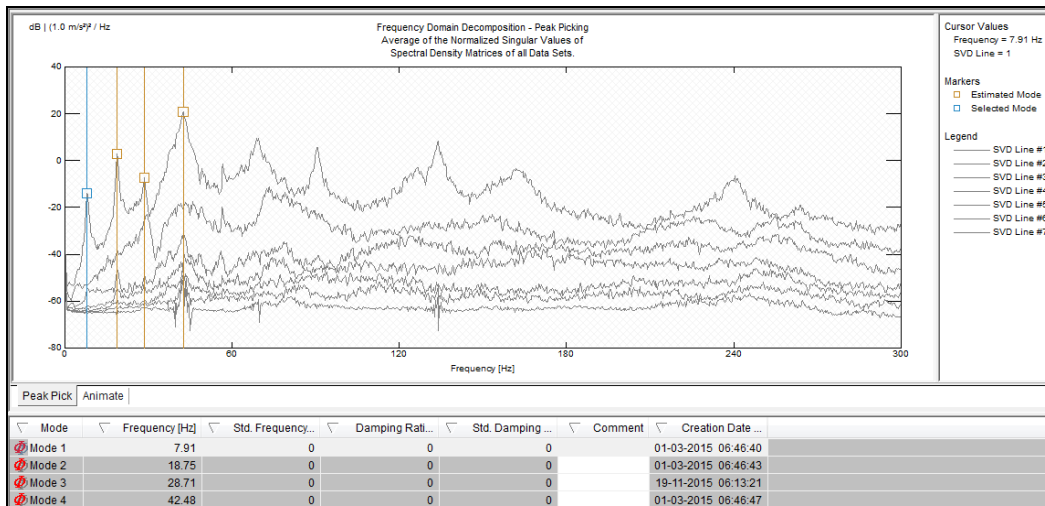


Figure 5.7: Normalized singular values of spectral density matrices of the overhang beam model data set using FDD peak-picking

Values of the estimated candidate natural frequencies and their mode shapes are listed in Table 5.2.

Table 5.2: Estimated candidate values of natural frequencies and their mode shapes

Mode No.	Natural frequency (Hz)	Mode shape
1	7.910	
2	18.750	
3	28.710	
4	42.480	

The blue lines in the figures of mode shapes refer to the non-deformed overhang beam, while the red lines indicate the deformed shapes during vibrations. The validation process exams each candidate mode according to the MAC matrix (or bar chart) to verify the high MAC values for diagonal modes and low values for others. Any existing high value between any non-diagonal modes indicates that the mode is not stable nor structural mode. *Figure 5.8* shows MAC bar chart for the estimated candidate first four modes of the overhang beam model.

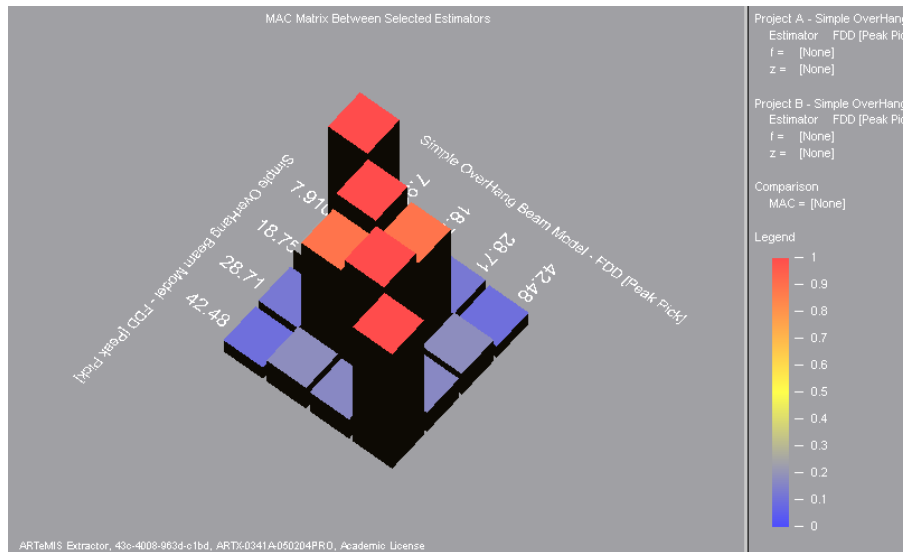


Figure 5.8: Comparison of the first four extracted modes using MAC bar chart

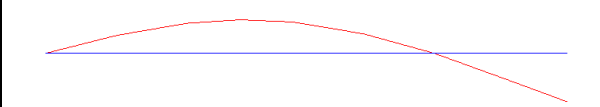
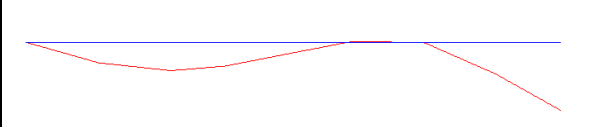
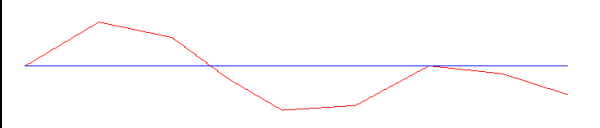
Obviously from *Figure 5.8*, the third estimated modes has high value of MAC which refers that the mode is not stable nor structural mode and should be neglected. Values of MAC for all modes are summarized in the MAC matrix, as shown in *Table 5.3*.

Table 5.3: MAC matrix for the extracted candidate modes

Modes	$f1=7.91$	$f2=18.75$	$f3=28.71$	$f4=42.48$
$f1=7.91$	1	0.248	0.122	0.098
$f2=18.75$	0.248	1	0.889	0.182
$f3=28.71$	0.122	0.889	1	0.167
$f4=42.48$	0.098	0.182	0.167	1

The MAC value of 0.889 which corresponds to the third mode is high for non-diagonal mode, hence, the third picked mode is not correct and should be avoided and not taken into account in the next stages. The final adopted accurate mode values (natural frequencies and mode shapes) which are considered as stable modes, are listed in *Table 5.4*.

Table 5.4: Adopted modes by FDD peak-picking for the intact overhang beam model

Mode No.	Natural frequency (Hz)	Mode shape	Mode shape char.
1	7.910		First bending
2	18.750		Second bending
4	42.480		Third bending

The comparison process between the three estimated modes using MAC bar chart is shown in *Figure 5.9*.

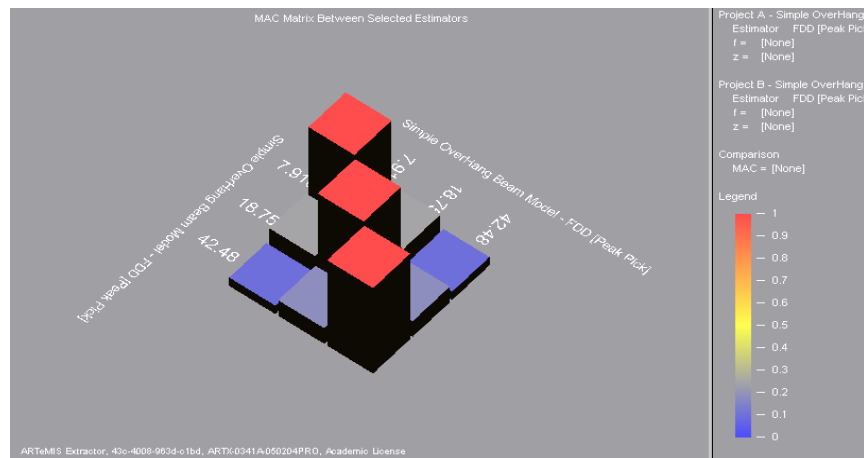


Figure 5.9: Comparison of the first three extracted modes using MAC bar chart

In Figure 5.9, there is no high values of MAC for the non-diagonal modes which gives an indication to the reality of the selected modes and their ability to be adopted as stable modes.

5.2.5.2 Verifying the extracted modal parameters using EFDD technique

To accomplish another investigation about validity of the extracted modal parameters obtained earlier by FDD technique, the modes are estimated again using EFDD technique in ARTeMIS software. In this case, the same parameters of frequency lines 1024 and low pass filter are adopted. Also, by picking the peaks of the normalized singular values of spectral density matrices, the modes are estimated, as shown in Figure 5.10.

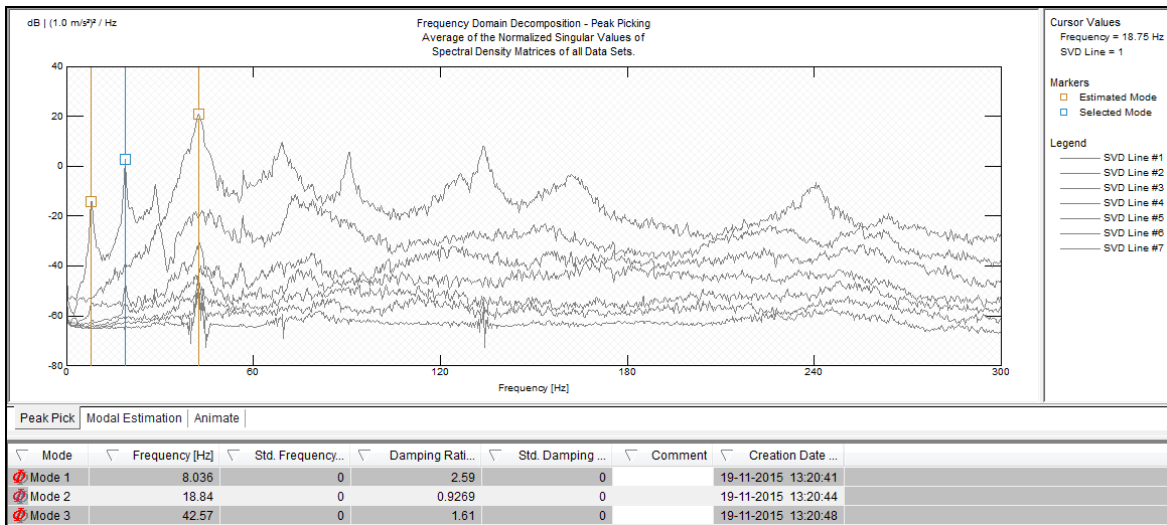


Figure 5.10: Normalized singular values of spectral density matrices of the overhang beam model data set using EFDD peak-picking

In Figure 5.10, the third peak is already neglected because it refers to a non-stable mode during the past stage. The EFDD technique is characterized by the ability of producing values of damping ratios. Hence, it is another indication for the validity of estimated modes. As mentioned earlier, the modes that have 5% or less damping ratio can be considered as stable modes, otherwise, modes should be rejected. Results of the estimated mode using EFDD technique are listed in Table 5.5.

Table 5.5: Estimated values of natural frequencies and damping ratios by EFDD technique

Mode No.	Values of natural frequencies (Hz)	Damping ratios (%)	Mode shape character
1	8.036	2.590	First bending
2	18.840	0.927	Second bending
3	42.570	1.610	Third bending

It can be noticed that from *Table 5.5*, the values of natural frequencies are close to the corresponding values obtained by FDD technique earlier. Also, values of damping ratio are below the value of 5%, which means that the estimated modes in the FDD technique are adoptable and can be used as stable modes in the next stages of this work.

5.2.5.3 Verifying the extracted modal parameters using SSI technique

The use of SSI technique as a modal identification process is relatively more complicated than the two previous techniques of FDD and EFDD. Nevertheless, the procedure of modal identification is produced here for the comparison with other techniques.

The procedure is started by selecting the modes according to Canonical Variate Analysis (CVA) method that belongs to the SSI technique. The modes are displayed by the stabilization diagram in ARTeMIS extractor as three types, red crosses, green x-s and brown x-s to represent stable, unstable and noise modes, respectively, as shown in *Figure 5.11*. All candidate modes are displayed as clusters and the target are the red crosses only which are being inspected for the selection of stable modes. The diagram in *Figure 5.11* depends on the matrix size that represents the *State Space* which is explored. Usually the matrix size includes all type of modes, stable, unstable and noise according to the so-called *Common SSI Input Matrix Estimation* which is an option that governs the *State Space Dimension*. As shown in *Figure 5.11*, the state space dimension is 120, and this value is obtained according to the initial proposed *number of structural modes* of 30 modes.

According to this value, the maximum number of all available modes is estimated in CVA of SSI technique.

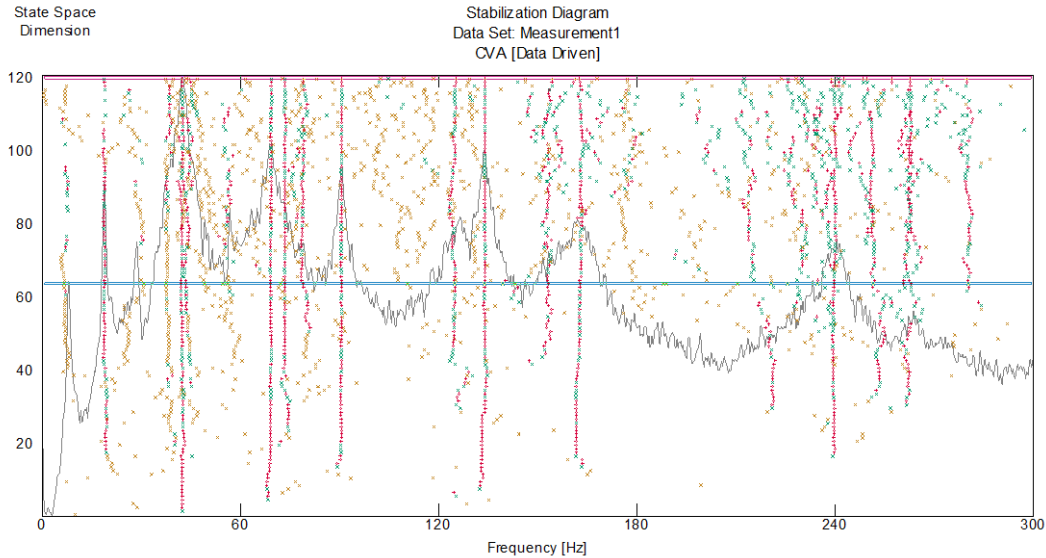


Figure 5.11: Stability diagram of CVA

Another value should be defined which is the *number of noise modes* in the options of SSI input matrix, and it is selected here as 30 modes. Now, both values of structural modes and noise modes forms 60 modes and it is duplicated to be 120 modes automatically by the ARTEMIS extractor software, as shown in the y- axis of *Figure 5.11*. Increasing of this value leads to increase the modal searching space, and nevertheless, all types of modes still appear at any values of the selected stable modes and with or without noise modes.

The mode selection is accomplished by searching on the cluster that contains significant numbers of red crosses. When this mode is selected, using ARTEMIS commands of *Mode Selection and Linkage*, the candidate modes throughout frequency range for the present set of AVM are appeared on the so-called *Select and Link Mode* editor, as shown in *Figure 5.12*. In this figure, due to the use of only one set of measurement in the overhang beam model test, only one row of candidate modes is appear. If, for example, more than one set of measurement are used, then another rows will appear above the first row of modes.

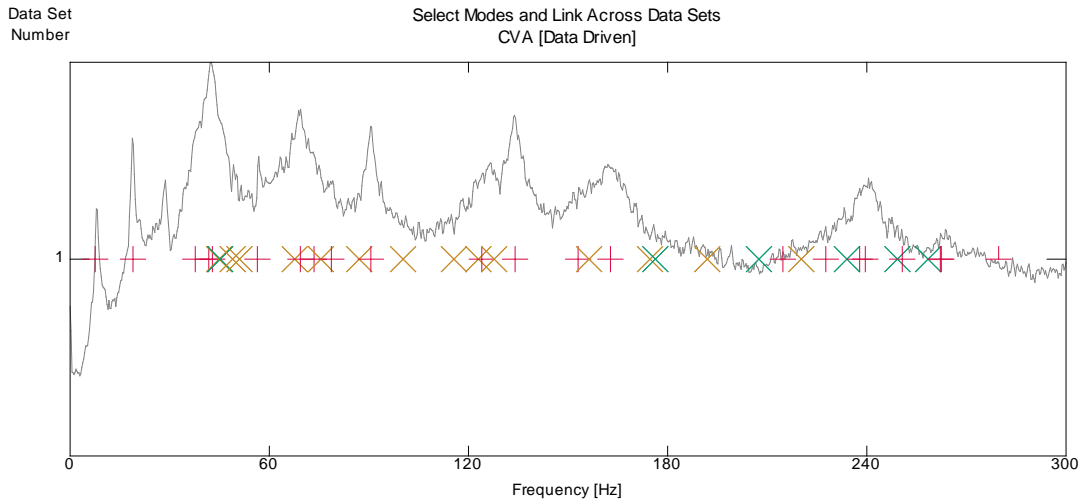


Figure 5.12: Candidate stable, unstable and noise modes throughout the frequency domain

The next step is the selection of stable (real) modes which represented by red crosses that rest in the expected locations of stable modes, *Figure 5.12* and *Figure 5.13*. As usual, the peaks indicate the locations of candidate modes that could be stable which are clearly shown in *Figure 5.11* as clusters under each peak in the diagram.

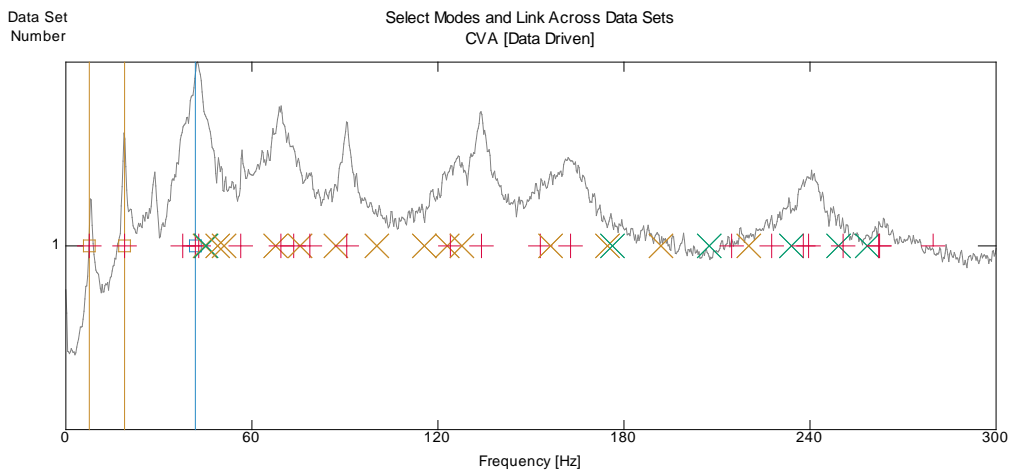


Figure 5.13: Complete selection of the first three modes by SSI technique

From *Figure 5.12*, the first red cross under the first peak is selected as a first mode by picking directly. Then, the other red crosses under the second and fourth peaks are selected to represent the second and third mode, respectively, as shown in *Figure 5.13*. As the mode

is selected, a vertical line is drawn passing through the selected crosses as shown in *Figure 5.13*. Values of each natural frequency, damping ratio and mode shapes characters are listed in *Table 5.6*.

Table 5.6: Estimated modal parameters of the overhang beam model using SSI technique

Mode No.	Natural frequencies (Hz)	Damping ratios (%)	Mode shape character
1	7.567	2.032	First bending
2	18.930	0.772	Second bending
3	41.770	2.223	Third bending

Also here, the estimated modes have values of natural frequencies close to the corresponding values obtained by FDD technique within damping ratios below 5% which indicate to the validity of the estimated modes obtained by FDD technique. The comparison between FDD results and each of EFDD and SSI, can be summarized in *Table 5.7* and *Figure 5.14*. *Table 5.7* shows that values of estimated natural frequencies by FDD technique represent approximately intermediate values between the corresponding values of natural frequencies obtained by EFDD and SSI methods, respectively.

Table 5.7: Differences of values of natural frequencies extracted by FDD, EFDD and SSI techniques

Mode No.	Values of natural frequencies (Hz)				
	FDD	EFDD	FDD-EFDD	SSI	FDD-SSI
1	7.910	8.036	-0.126	7.567	0.343
2	18.750	18.840	-0.090	18.930	-0.180
3	42.480	42.570	-0.090	41.770	0.710

Very close values of natural frequencies that extracted by the three techniques are shown in *Figure 5.14*, which verify the stability of the extracted modes.

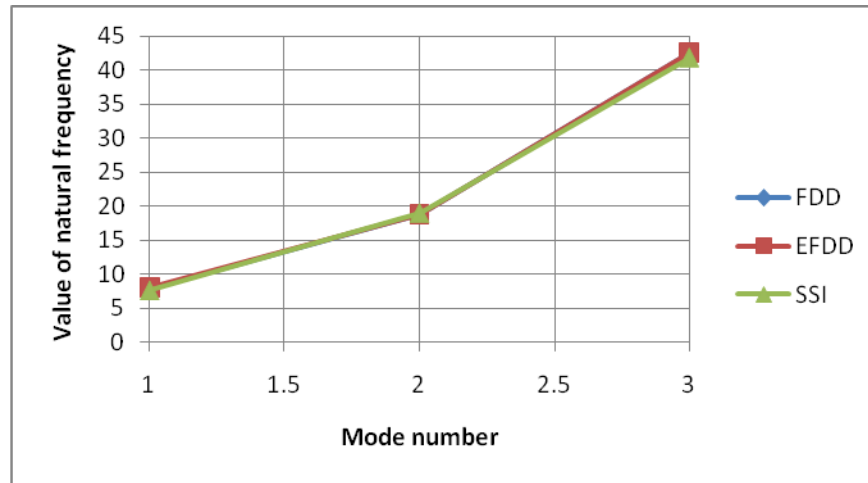


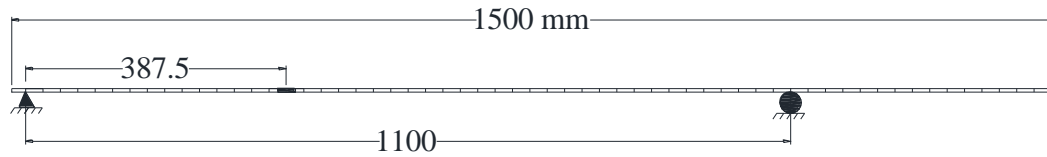
Figure 5.14: Values of natural frequencies extracted by FDD, EFDD and SSI techniques

5.2.6 Damaged case of the overhang beam model

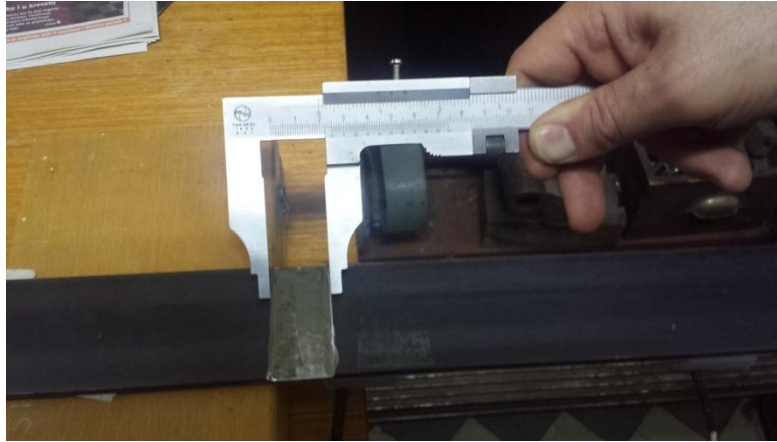
As the values of natural frequencies and mode shapes are extracted for the overhang beam model in the intact case, damage cases upon the model is implemented as the next step in the experimental program. The experimental program for the overhang beam model in damage state starts with low value of damage severity represented by certain length and depth of crack. After that, the severity of damage is increased to form the next more significant damage case in the model.

5.2.6.1 First adopted overhang damage case AODC-1

The first adopted scenario represents a damage that has a centreline position located at 387.5 mm from the left hinged support of the beam model, as shown in *Figure 5.15 (a)*. The damage is implemented by crack formation with dimensions of (25x1.9) mm for length and depth, respectively, as shown in *Figure 5.15 (b)*. All damages are formulated using hand grinding machine in the laboratory and the crack dimensions are checked periodically. The crack rests in the lower face of the overhang beam model, while accelerometers are in the upper face. Then, the model is tested under the same procedure and conditions that adopted in the tests of intact state model. AVM data are recorded and processed later by ARTEMIS software to extract modal parameters according to FDD peak-picking technique.



(a)



(b)

Figure 5.15: (a) Damage location, (b) Formation of damage case AODC-1

The procedure of modal identification by FDD peak-picking is used for the same frequency lines of 1024 and the extracted natural frequencies are listed in *Table 5.8*.

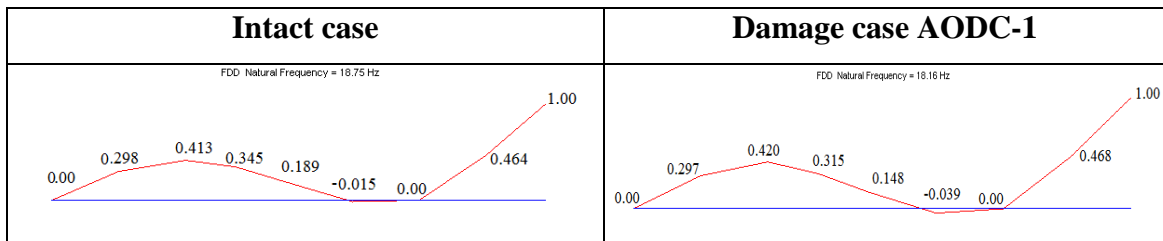
Table 5.8: Values of extracted natural frequencies for damage case AODC-1

Mode No.	Values of natural frequencies (Hz)	Mode shape character
1	7.910	First bending
2	18.160	Second bending
3	41.310	Third bending

Obviously from *Table 5.8*, there are changes in values of natural frequencies for the second and third mode in this damage case, AODC-1, compared with the corresponding values of the intact state. This indicates that the presence of damage causes changes in the dynamic behaviour of the overhang beam model which include natural frequencies and mode shapes. Although the changes in mode shapes are exist, but they could not be

recognized by the graph of these modes due to their small amounts. Nevertheless, the changes could be recognized by the normalized displacements values of each mode shape compared with intact state. For instance, *Table 5.9* shows a comparison between values of normalized displacements of the intact state with their corresponding values of damage state for the second mode shape.

Table 5.9: Normalized displacements for the second mode shapes of the intact and damage cases of the overhang beam model



The numbers shown on each shape represent values of normalized displacement in the measuring point (position of one accelerometer), in addition to the two supports. The changes are exist in each point of measurement, approximately, which indicates the changes in mode shapes due to the presence of damage. For instance, value of the normalized displacement of the first point of measurement (from the left side of the model) is 0.298 for the intact case which correspond to the value of 0.297 for the same point in the damage case. Also, the value of 0.413 for the second point of measurement in the intact case corresponds to the value of 0.420 for the same point in the damage case of model and so on. These differences refer to the changes in values of normalized displacements due to the presence of damage. Other values of normalized mode shapes for the three modes of the intact and damage case AODC-1 of the overhang beam model are listed in *Table 5.10*.

The normalization process is implemented automatically by ARTeMIS extractor software and the results in *Table 5.10* are ready obtained in normalized form. The concept of normalization represents dividing all existed values of *relative displacement* in the mode (according to the measuring points) by the highest value of relative displacement existed in the vector. For instance, the highest value in the vector of displacement of the first mode is the point of extreme right end of the overhang beam model which has value of 1.0 as

normalized displacement. These values are considered later in the participation of mode shapes for the objective function when applied in the optimization process.

Table 5.10: Normalized displacements for the three mode shapes of the intact and damage cases

Position	Mode-1		Mode-2		Mode-3	
	Intact	Damage	Intact	Damage	Intact	Damage
Hinge support	0.000	0.000	0.000	0.000	0.000	0.000
Accelerometer 1	-0.363	-0.400	0.298	0.297	-0.990	-0.899
Accelerometer 2	-0.612	-0.687	0.413	0.420	-0.640	-0.668
Accelerometer 3	-0.682	-0.732	0.345	0.315	0.278	0.301
Accelerometer 4	-0.637	-0.667	0.289	0.148	1.000	1.000
Accelerometer 5	-0.395	-0.406	-0.015	-0.039	0.898	0.867
Roller support	0.000	0.000	0.000	0.000	0.000	0.000
Accelerometer 6	0.521	0.522	0.464	0.468	0.176	0.191
Accelerometer 7	1.000	1.000	1.000	1.000	0.655	0.690

5.2.6.2 Second adopted overhang damage case AODC-2

The crack size that formulated in the previous case is increased to be the second damage scenario. The new crack size is (25x3) mm length by depth, hence, 1.1 millimetres deeper is implemented, as shown in *Figure 5.16* and *Figure 5.17*.

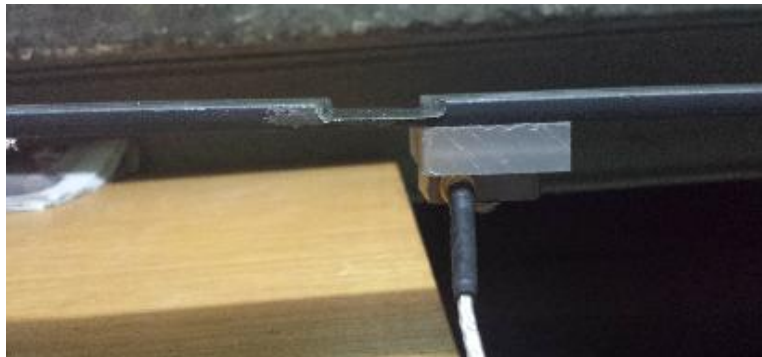


Figure 5.16: Increasing the crack depth of the model (overturned model position)



Figure 5.17: Reinstalling model for the test of second damage scenario

AVMs are executed for second damage scenario AODC-2 under the same test conditions of the previous intact and damage cases. Also, the same FDD peak-picking procedure is performed to extract modal properties of the overhang beam model according to damage scenario of AODC-2. Logically, it is expected that, due to the more severity of damage in this case, the changes in values of natural frequencies are increased compared with their original values in the intact state, as well as changes in mode shapes. *Table 5.11* shows values of natural frequencies of the modes that extracted under the second damage scenario AODC-2.

Table 5.11: Values of extracted natural frequencies for damage case AODC-2

Mode No.	Values of natural frequencies (Hz)	Mode shape character
1	7.031	First bending
2	17.580	Second bending
3	39.840	Third bending

Compared with values of natural frequencies of the intact state (*Table 5.4*), all modes in *Table 5.11* have changed due to damage. While, compared with values of natural frequencies in damage scenario AODC-1 (*Table 5.8*), the first mode has changed also in *Table 5.11* due to damage case AODC-2, as expected.

5.3 Grid-bridge model

The second adopted model as a case study in the present work is a steel grid bridge deck model, which is a part of another complete steel pedestrian bridge model explained later. Due to the 2-dimensional geometry of the bridge deck model, the structural behaviour of such models has plate action. This case study is more complicated than previous case of overhang beam model which focused on the behaviour of one dimensional structure under vibrations. The grid-bridge model represents a case study which simulate the dynamic structural behaviour of part of an existing model under ambient vibrations. The existing model is a pedestrian bridge crossing a certain road near the city of Belgrade-Republic of Serbia, and the grid-bridge model is a simulation for its deck. The experimental program of this case study is explained in the next paragraphs.

5.3.1 Experimental program

5.3.1.1 Scale considerations

The first step in the experimental program represents the process of scaling which implemented upon the selected real existed structure. As the model is selected to be as a case study, suitable scale values should be used to minimize real size of the case study. Here, it is also related with some specifications that mentioned in some references [108]. From these references and with the aid of multi trial analysis performed on case study, suitable scale values can be reached and adopted. For example, according to the case of grid-bridge model, the real dimensions of model are 1.9 m wide and 18 m long with 9 bays have 2 m long for each. These dimensions and whole structure are modified in order to be suitable for the case study. The first modification was upon dimensions of each part of the structure by scaling them according mainly to some values of scaling factors. For instance, width of the real structure is 1.9 m is scaled to be 0.8 m in the simulated experimental model, hence, scale factor is 0.421 ($0.8/1.9$). The original length of bridge is 18 m becomes 6.72 m after scaling with 0.373 ($6.72/18$) scale factor. These values are determined based on results of multi trial analysis and specifications [108]. Also availability of sections in the markets governs the selection of the adopted sections that consist the scaled model. For

example, in the real existing model, the two main hollow beams have I-cross section for each beam with (160x160) mm for the web and flange dimensions, respectively. Also, for the web and flange, the thicknesses are 7 mm and 10 mm, respectively. This cross section of the beam becomes, in the simulated experimental model, rectangular hollow cross section with (30x50x2.8) mm for width, depth and thickness dimensions, respectively. The second modification includes the geometry of the model itself, this happened by adding an additional grid to the whole model in order to provide a centreline rests in the middle length of the bridge. Such line is useful for the sake of modal analysis test which provides a points that serve in installing testing equipments (like accelerometers), from which, the central deflected point can be obtained.

5.3.1.2 Model erection

After the application of scaling process, the grid-bridge model becomes with total length of 6720 mm that consists of 10-grids (in longitudinal direction) at 672 mm c/c for each. The total width of model is 800 mm c/c containing 8 spaces (sub-grids in transverse direction) of 100 mm c/c. The model is firstly erected by preparing the required steel sections inside the laboratory, as shown in *Figure 5.18*.



Figure 5.18: Preparing the main steel sections of the grid-bridge model

Two main longitudinal hollow steel beams represent the main girders that hold other parts of the model with a cross section of (30x50x2.8) mm dimensions for each beam. The

two beams are located at the extreme edges of the model representing the width of the model, *Figure 5.19*.

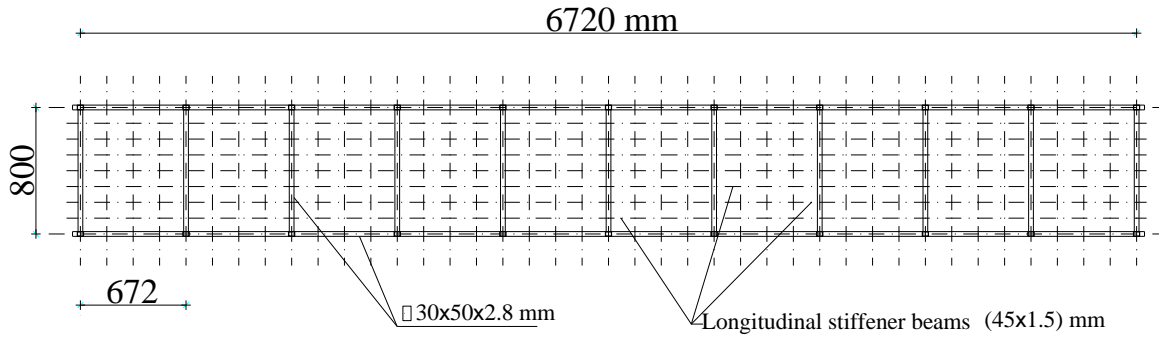


Figure 5.19: Top view sketch of the grid-bridge model with dimensions

Using the same cross sections of the main longitudinal beams, 11 main transverse beams are welded with the main longitudinal beam at 672 mm c/c to formulate the 10-grids of the model. Hence, the main frame of the grid-bridge model is completed until this stage. Additional longitudinal beams act as stiffeners welded in their ends by the main transverse beams. The longitudinal stiffeners are equally spaced and distributed throughout the model width at 100 mm c/c. Each stiffener has a plate section of (45x1.5) mm dimensions welded in their top sides by a plate that covers the whole bridge deck. The covering plate is welded with the main frame on the top side at 50 mm welding for each 150mm spacing. The erected grid-bridge model is shown in *Figure 5.20* as an overturned position.

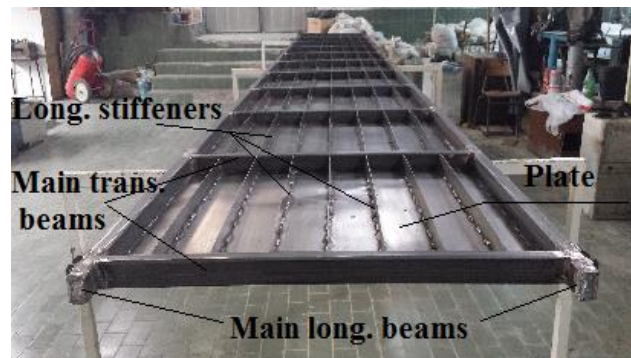


Figure 5.20: The complete manufactured model of the grid-bridge (overturned position)

Supports are implemented by welding cylinders on the extreme corners of the bridge model, as shown in *Figure 5.21*. The structural behaviours of these supports, according to the hinged or roller behaviour, are controlled by restricting movements in the corresponding directions by friction between cylinders and the base. Operations of filing and painting are accomplished after completing the process of manufacturing and *Figure 5.21* shows the model after painting.



Figure 5.21: Supports and the painted model (overturned position)

The final stage, after completing the manufacturing process of the model, is the model installation. Four concrete long cubes are fixed vertically under the model to provide a stable base under each support cylinder of the bridge model, *Figure 5.22*.



Figure 5.22: Grid-bridge model on concrete supports

Also, each two concrete support cubes that rest on the far ends of the bridge model are stiffened together by gluing additional concrete struts to prevent any longitudinal movement that likely to be occurred upon the supports, *Figure 5.22*. The concrete strut also serves as a base for the shaker that required to be installed in a position so that the vibration waves affect on the supports of the model. The model is properly installed on concrete cubes and further checks are considered to insure horizontality of the bridge model, as in *Figure 5.22*.

5.3.2 States of mass applications

In order to explore a wide range of frequencies, the grid-bridge model is exposed to two states of mass applications, without and with additional mass states. the first state investigates the behaviour of the bridge model when exposed to vibrations under its own mass only. While the second state highlights the effect of additional masses that applied on the bridge under vibrations. *Figure 5.23* shows the bridge model in the additional mass state.

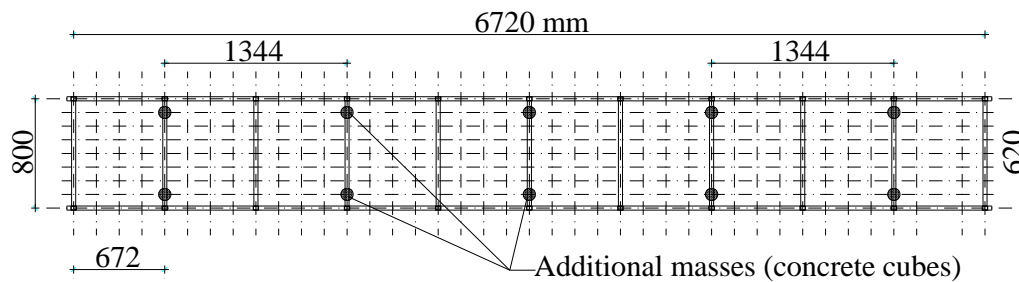


Figure 5.23: Grid-bridge model in the additional mass state

The additional mass state is represented by 10 concrete cubes of (150x150x150) mm dimensions, distributed in two rows along the length of the bridge deck. Hence, the distance between each two masses is 1344 mm in the longitudinal direction and 620 mm in the transverse direction of the bridge model, as shown in *Figure 5.23*. The average mass of the cubes is 7.925 kg, which is adopted in the calculations.

5.3.3 Preparing requirements of AVM and experimental analysis

As it has been done in the previous overhang beam model, the grid-bridge model is prepared for AVM test by installing all the required devices in their places, as shown in *Figure 5.24*. The same procedure is applied for all adopted cases: intact or damage and without or with additional mass states of the bridge model. The shaker is tightly connected by four C-clamps with the lower concrete strut which in turn connects the two vertical concrete cubes that carry the bridge model. In this way, it is guaranteed that the vibrations are transmitted from the substructure towards the structure, *Figure 5.24*.

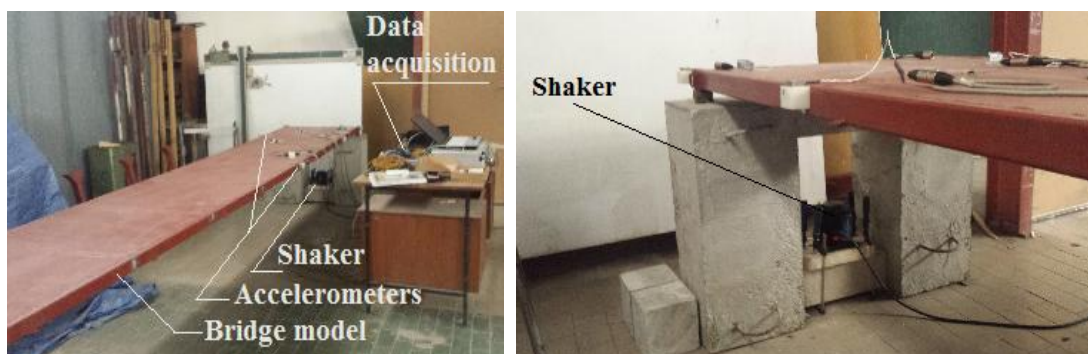


Figure 5.24: Preparing the devices of AVM tests

Eight accelerometers are used to sense the vertical and horizontal motions that exposed on the bridge model. The accelerometers are distributed in a way that form a two dimensional mesh of measurement which coincide with the structural behaviour of the tested model, as shown in *Figure 5.25*. Therefore, it is expected that two structural modes are obtained, bending and torsional modes. Numbers that appeared in *Figure 5.25* represent the measuring points (nodes) where the accelerometers are installed on. On the other hand, each arrow represents a certain accelerometer that senses the motion either in vertical or

horizontal direction. The green arrows represent the accelerometers in each one set of measurement which is transported periodically grid-after-grid when the testing time for each set is over. The blue arrows represent the reference accelerometers which are fixed in their position along the whole test, as described earlier in chapter 3. Therefore, five sets of measurements are sufficient to cover the whole model which consists of 10 spaces. In this case, all the requirements of AVM are prepared and the model is ready to be tested, as in the next paragraph.

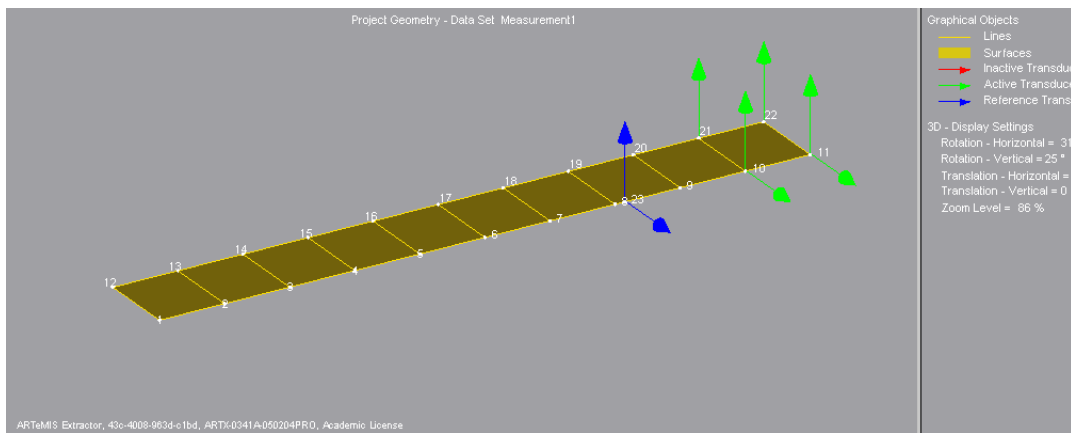


Figure 5.25: Accelerometers mesh of measurements for the grid-bridge model

5.3.4 Implementing AVM upon the grid-bridge model

The procedure of AVM is repeated for all adopted cases of intact or damage cases without or with additional mass states of the grid-bridge model. The test conditions are checked inside the laboratory such that the vibrations are generated due to the shaker only without any additional unwanted excitations. In all tests, sampling frequency is 600 Hz, filtering frequency is 200 Hz and intensity level is 7. Each set of measurement lasts 30 minutes duration, so that the resulted acceleration data has 1080000 rows for each one of the 8 accelerometers.

5.3.5 Processing the configuration input file and AVM data by ARTEMIS software

Each adopted case within the grid-bridge model, intact or damage, without or with additional mass states, has a special configuration input file that required to analyze the

obtained AVM data by the ARTeMIS software. Nevertheless, the configuration input file has similar steps in all cases except the sets of data measurements which characterize each case alone. Hence, the procedure is the same for all cases and can be summarized by the flow chart shown in *Figure 5.26*. In this figure, the same steps are used in the present model as in the model of overhang beam except the additional command which defines the surfaces that are used in the grid-bridge model. Obviously, this belongs to the absence of any surfaces (plate) in the overhang model and using them in the grid-bridge model only. The required time to process the configuration input file, using the procedure shown in *Figure 5.26*, is 200 seconds through a computer has the properties of: Processor Core i7 CPU @ 2.1 GHz and RAM 6.0 GB. This means that processing of the grid-bridge model is five times the processing of the overhang beam model and this also reflects the huge information that included in this case study.

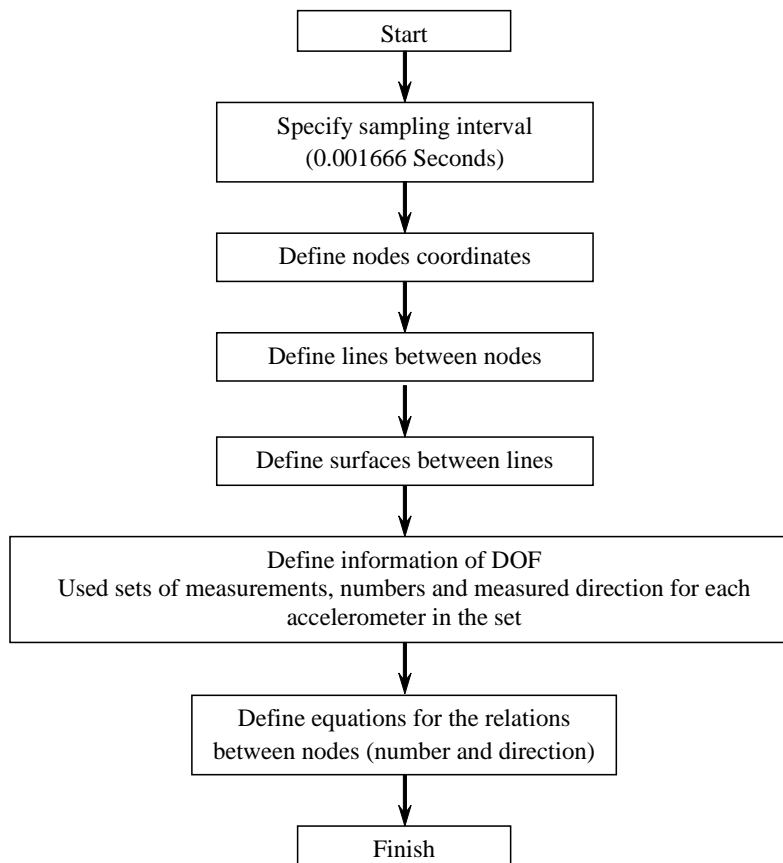


Figure 5.26: Flow chart of the configuration input file of the grid-bridge model

Unlike the case of overhang beam model, five sets of measurements are required to complete AVM upon the whole model of grid-bridge. It depends, therefore, on the size of the tested model which governs the amount of the required sets of measurements when there is limited number of accelerometers available. Also, the required accuracy for the obtained parameters, mode shape for instance, plays an important role in determining the suitable number of measurements sets.

5.3.6 Intact case of the grid-bridge model

In this paragraph, the intact case of the grid-bridge model is highlighted. Model under its own mass only and with additional mass states are considered as following:

5.3.6.1 State of model without additional mass

5.3.6.1.1 Results of the extracted modal parameters using FDD technique

Using ARTeMIS software, analysing the adopted AVM data using FDD technique produces average of the normalized singular values of spectral density matrices of the five data sets. These values are obtained according to grid-bridge model without additional mass state, as shown in *Figure 5.27*.

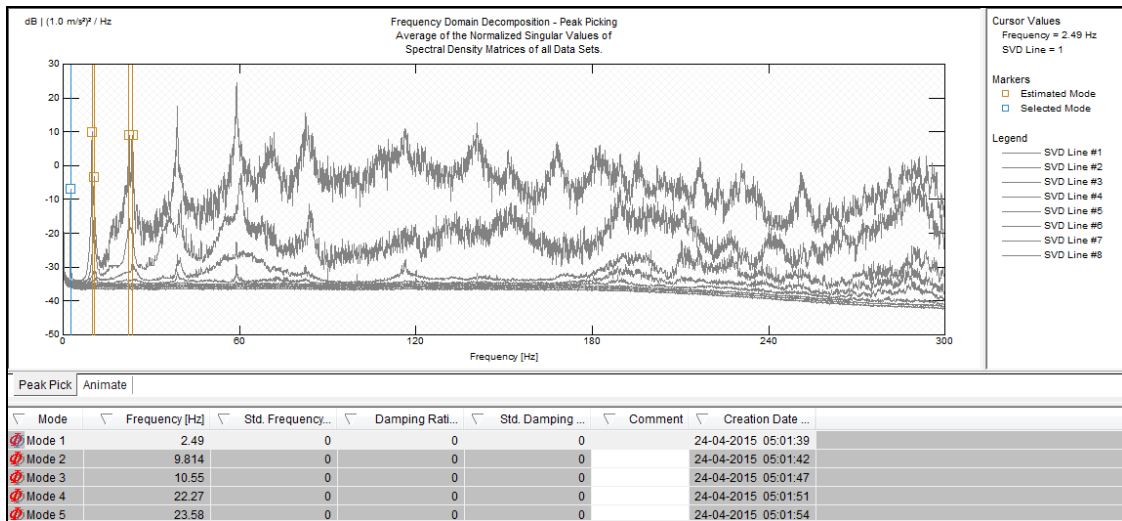


Figure 5.27: Normalized singular values of spectral density matrices of the grid-bridge model without additional mass state using FDD peak-picking

In *Figure 5.27*, the resulted normalized singular values of spectral density matrices are according to frequency lines of 4096. Other values of frequency lines of 1024, 2048 and 8192 are also used to explore the difference between results. *Table 5.12* exhibits the extracted values of natural frequencies by FDD peak-picking for values of frequency lines of 1024, 2048, 4096 and 8192.

Table 5.12: Values of natural frequencies of the grid-bridge model without additional mass extracted by FDD technique based on different values of frequency lines

Mode No.	Values of natural frequencies (Hz)			
	Freq. Lines 1024	Freq. Lines 2048	Freq. Lines 4096	Freq. Lines 8192
1	2.637	2.490	2.490	2.490
2	9.961	9.814	9.814	9.814
3	10.550	10.550	10.550	10.550
4	22.270	22.270	22.270	22.270
5	23.440	23.580	23.580	23.580

It can be seen that from *Table 5.12* for all values of frequency lines, the estimated values of natural frequencies for the first five modes are the same except for the value of frequency lines of 1024 which produces different estimations. This value of frequency line of 1024 could be suitable for simple models and the well-separated and clear modes that appear in the normalized singular values of spectral density matrices, as in the case of overhang beam model. But, for more complicated structures, it is required to use frequency lines that produce more accuracy for displaying the candidate modes. Henceforth, the adopted values of frequency lines are 2048 and higher for all adopted models in the present work. On the other hand, it is adequate and accurately enough to use any of the frequency lines value of 2048, 4096 or 8192 in the modal estimation procedure implemented by FDD peak-picking to extract stable modes.

In the grid-bridge model, the first five modes are extracted to accomplish the required procedure of damage detection in the next final stage of the present work. Validity of the estimated five modes should be checked according to MAC matrix (or MAC bar chart) as shown in *Figure 5.28*.

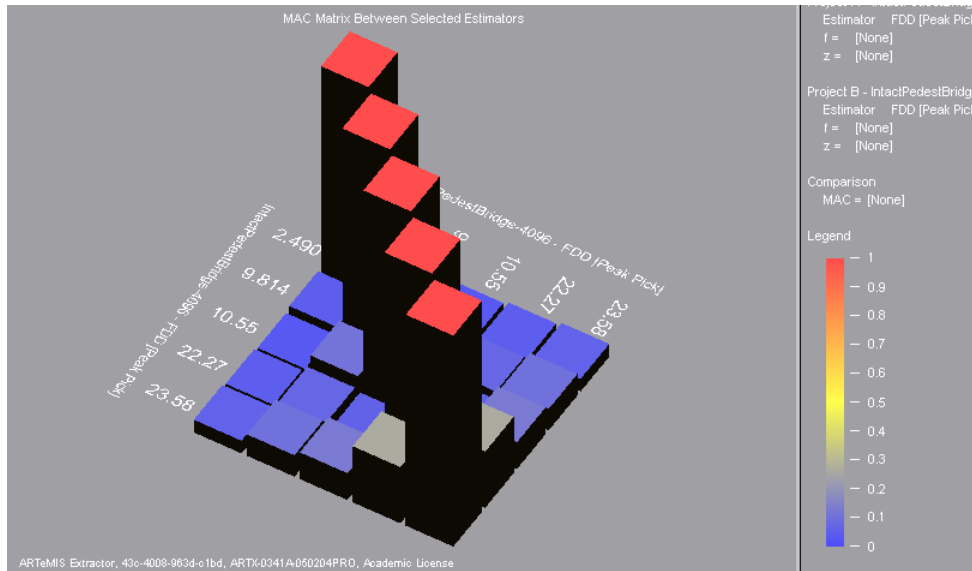


Figure 5.28: Comparison of the first five extracted modes of the grid-bridge model without additional mass using MAC bar chart

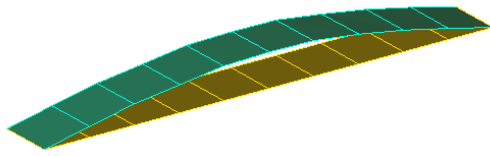
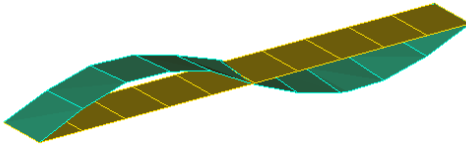
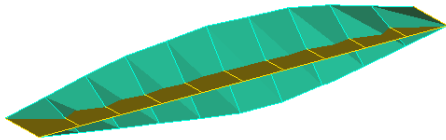
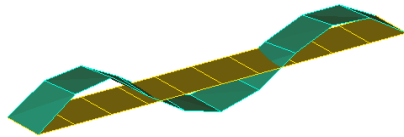
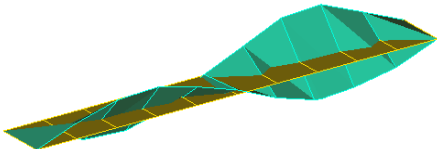
Values of MAC matrix for the first five modes of the grid-bridge model without additional mass are listed in Table 5.13.

Table 5.13: MAC matrix for the extracted modes of the grid-bridge model without additional mass

Modes	First mode	Second mode	Third mode	Fourth mode	Fifth mode
First mode	1	0.047	0.033	0.046	0.059
Second mode	0.047	1	0.107	0.073	0.101
Third mode	0.033	0.107	1	0.060	0.126
Fourth mode	0.046	0.073	0.060	1	0.266
Fifth mode	0.059	0.101	0.126	0.266	1

According to Figure 5.28 and Table 5.13, all values MAC for the non-diagonal modes are in the low level which indicates the stability of estimated modes. Hence, all the five estimated modes can be considered in the grid-bridge model and the adopted values of natural frequencies with their mode shapes are shown in Table 5.14.

Table 5.14: Values of natural frequencies and mode shapes of the intact grid-bridge model without additional mass

Mode No.	Value of natural frequency (Hz)	Mode Shape	Mode shape character
1	2.490		First bending
2	9.814		Second bending
3	10.550		First torsion
4	22.270		Third bending
5	23.580		Second torsion

5.3.6.1.2 Verifying the extracted modal parameters using EFDD technique

Another verification of the estimated values of natural frequencies that extracted by FDD peak-picking technique is implemented by estimating natural frequencies using EFDD technique for the first modes. Based on different values of frequency lines, values of extracted natural frequencies and damping ratios for the first five modes of the grid-bridge model without additional mass are listed in *Table 5.15*.

Table 5.15: Values of natural frequencies of the grid-bridge model without additional mass extracted by EFDD technique based on different values of frequency lines

Mode No.	Frequency Lines 2048		Frequency Lines 4096		Frequency Lines 8192	
	Frequency (Hz)	Damping ratio (%)	Frequency (Hz)	Damping ratio (%)	Frequency (Hz)	Damping ratio (%)
1	2.493	2.857	2.493	1.509	2.495	0.805
2	9.832	0.864	9.835	0.478	9.835	0.295
3	10.500	0.933	10.490	0.563	10.500	0.379
4	22.340	0.502	22.340	0.367	22.340	0.299
5	23.530	0.528	23.530	0.410	23.530	0.375

All values of damping ratios for the five modes are lower than 5%, which verify the stability of the estimated modes, as listed in *Table 5.15*. On the other hand, values of natural frequencies are so close to each other with respect to, firstly, the corresponding values of natural frequencies extracted by FDD technique, and secondly, the different used values of frequency lines within the same EFDD technique. Results give a conclusion that the FDD peak-picking technique and any value of frequency lines of 2048, 4096 or 8192 are suitable to estimate stable modes that can be used in structural purposes.

The mode shapes characters of the modes that extracted by EFDD technique are the same as mode shapes characters of the extracted modes by FDD technique which are listed in *Table 5.14*.

5.3.6.1.3 Verifying the extracted modal parameters using SSI technique

The procedure of SSI technique that applied in the overhang beam model is repeated for the grid-bridge model. Hence, the *Mode Selection and Linkage* diagram for the five data sets after estimating the modes is shown in *Figure 5.29*. It can be seen that in *Figure 5.29* there are no any red crosses align to the first, second and third peaks and the existence of red crosses are only close to the fourth peak and above. This means that there are no any stable mode could be estimated for these values of frequencies.

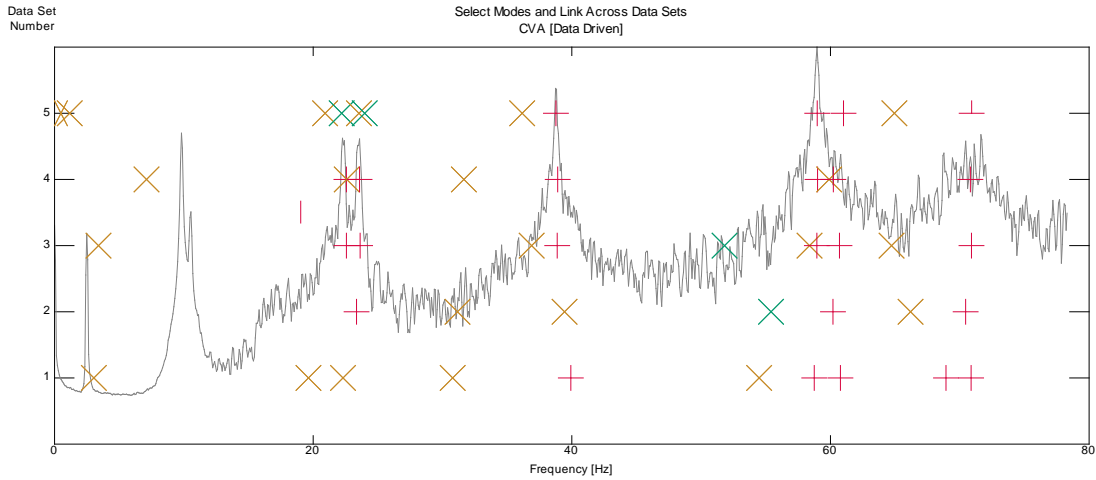


Figure 5.29: Candidate stable, unstable and noise modes throughout the frequency domain

Therefore, it could be stated that the SSI technique is relatively a complicated method for modal identification and perhaps no mode could be estimated even in the locations of candidate modes (peaks) on the frequency domain. Henceforth, FDD peak-picking is the adopted technique in modal identification according to the verification that accomplished earlier by EFDD technique and for all adopted models in the present work.

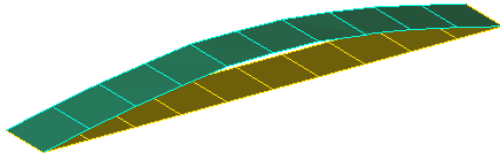
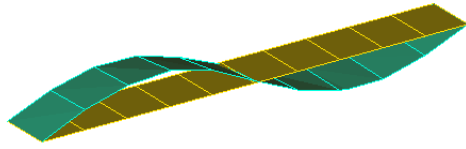
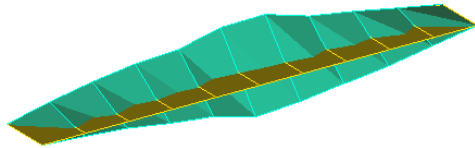
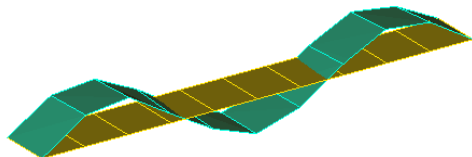
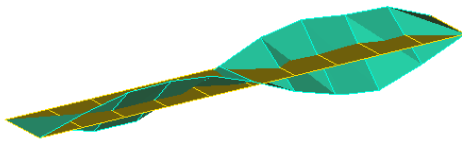
5.3.6.2 Results of the extracted modal parameters using FDD technique for the model with additional mass state

Similar procedure of FDD peak-picking is implemented for the grid-bridge model with additional mass state. The estimated values of natural frequencies and mode shapes for the first five modes are listed in *Table 5.16*.

Usually, due to the applied masses on the grid-bridge model, values of natural frequencies are decreased compared with the model without additional mass state, as shown in *Table 5.16*.

On the other hand, the mode shape characters are still the same, compared with the state of additional mass, except of some changes in the third and fifth modes (torsional modes). These values of natural frequencies are adopted in the present work for the state of intact grid-bridge model with additional mass state.

Table 5.16: Values of natural frequencies, mode shapes and mode shape characters for the first five modes of the intact grid-bridge model with additional mass state

Mode No.	Value of natural frequency (Hz)	Mode Shape	Mode shape character
1	2.051		First bending
2	8.093		Second bending
3	8.313		First torsion
4	18.240		Third bending
5	18.640		Second torsion

5.3.7 Damaged case of the grid-bridge model

Damage cases upon the grid-bridge model is implemented as the next step in the experimental program. The cases that effectively influenced by the damage existence are adopted in next paragraphs for both without and with additional mass states of the model.

5.3.7.1 State of the model without additional mass

Starting with the state of model under its own mass only, the influence of damage on the adopted model is highlighted. The program starts with low severities of damage which

are increased later to study the influence of damage on the structural dynamic behaviour of the model as explained in the next paragraph.

5.3.7.1.1 First adopted right side damage case RAGDC-1

On the right side of the model, *Figure 5.30*, the first adopted damage scenario of the grid-bridge model without additional mass is characterised as Right Adopted Grid bridge Damage Case (RAGDC-1). Damage represented by crack size of (21×11.5) mm length by depth, respectively, is executed by hand grinding machine on the lower face of the main hollow beam that rests on the right side of the grid-bridge model, as shown in *Figure 5.30*. The damage centreline is located at 2247 mm from the nearest support, which is increased gradually to represent scenarios of damage on the right side of the bridge model, *Figure 5.30*.

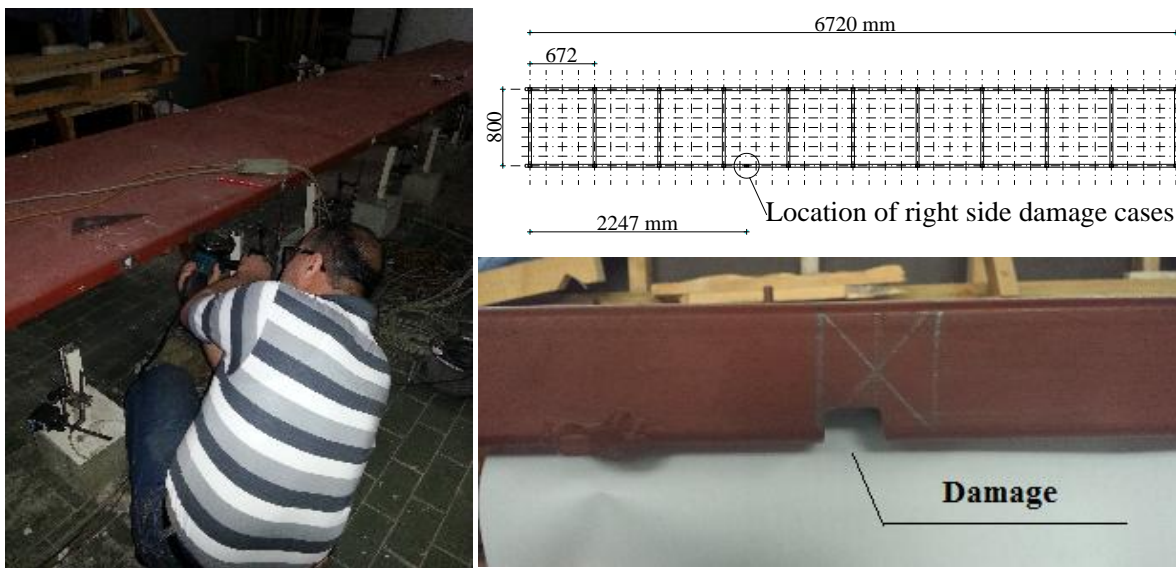


Figure 5.30: Formation of damage case RAGDC-1

AVMs are implemented upon this case of damage and the recorded data are analysed by ARTeMIS software to extract modal parameters using FDD technique. Extracted values of natural frequencies and their mode shape character are listed in *Table 5.17*. In *Table 5.17*, changes in values of natural frequencies are appeared in modes 2-5 compared with the corresponding values of *Table 5.14*. These changes, in addition to the changes in values of

normalized displacements of each mode shape as explained earlier in the overhang beam model, are able to indicate damage in the present case study for the final stage.

Table 5.17: Extracted values of natural frequencies for damage case RAGDC-1

Mode No.	Values of natural frequencies (Hz)	Mode shape character
1	2.490	First bending
2	9.777	Second bending
3	10.437	First torsion
4	22.412	Third bending
5	23.400	Second torsion

5.3.7.1.2 Second adopted right side damage case RAGDC-2

The crack in the previous case is increased more to represent the second scenario. The size of crack in this damage case RAGDC-2 has (42x20) mm dimensions length by depth, respectively. By the same procedure that implemented in the previous damage case, values of natural frequencies and mode shapes are extracted for RAGDC-2 and listed in *Table 5.18*.

Table 5.18: Extracted values of natural frequencies for damage case RAGDC-2

Mode No.	Values of natural frequencies (Hz)	Mode shape character
1	2.453	First bending
2	9.704	Second bending
3	10.363	First torsion
4	22.412	Third bending
5	23.400	Second torsion

Compared with *Table 5.14* for the values of natural frequencies of the intact model without additional mass state, all five modes in *Table 5.18* have some changes in values of natural frequencies due to the presence of damage. These changes are expected due to the increasing of damage severity which affects on both modal parameters, natural frequencies and mode shapes, of the tested model.

When the tests in the right side are completed, the model is repaired and the AVM test is repeated again to insure that the same modal parameters for the intact model state are obtained.

5.3.7.1.3 Adopted left side damage case LAGDC-1

Another scenarios are implemented on the lower face of the main hollow beam of the left side of the model, *Figure 5.31*, by the same procedure that implemented for the right side. The crack is located at 1659 mm from the hinged support on the left side of bridge model (nearest end of the bridge model). In this case, the adopted damage scenario has a crack size of (42x20) mm dimensions length by depth, respectively. It is important to mention that, damage in the left side of bridge model is implemented after completing all tests on the right model side.

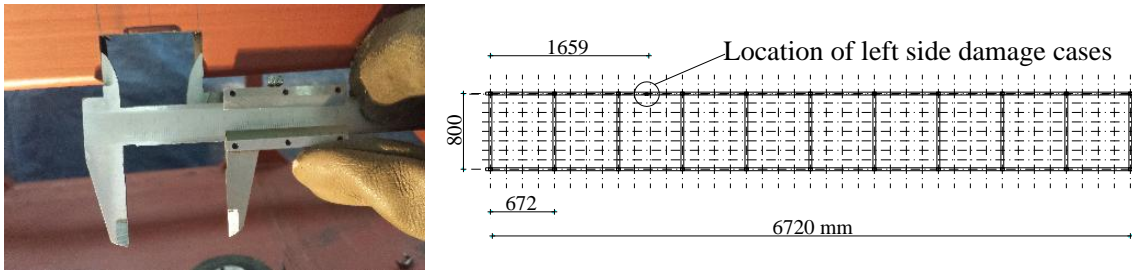


Figure 5.31: Formation of damage case LAGDC-2

Extracted values of natural frequency and mode shape characters for the damage case LAGDC-1 are listed in *Table 5.19*.

Table 5.19: Extracted values of natural frequencies for damage case LAGDC-1

Mode No.	Values of natural frequencies (Hz)	Mode shape character
1	2.453	First bending
2	9.631	Second bending
3	10.327	First torsion
4	22.119	Third bending
5	23.401	Second torsion

Although the crack size in this damage case is the same as the most severity damage case on the right side (RAGDC-1), values of natural frequencies are not the same between the two damage cases, *Table 5.18* and *Table 5.19*. This reflects the influence of damage

location on the modal parameters of the model similarly as the influence of damage severity.

5.3.7.2 State of the model with additional mass

Ten masses of concrete cubes are distributed on the grid-bridge model to implement additional damage scenarios upon the bridge model with additional mass state. Usually, each AVM test of the model with additional mass state is implemented after the AVM test of the model without additional mass state and for all damage scenarios. Results of the extracted modal parameters for each scenario are as following:

5.3.7.2.1 Adopted right side damage case with mass RAGDC-1M

The scenario of damage with crack size of (42x20) mm dimensions length by depth, respectively, is considered as the first significant damage case in the right side of the bridge model with additional mass state (RAGDC-1M). AVM test is implemented and the extracted values of natural frequencies and mode shape characters are listed in *Table 5.20*.

Table 5.20: Extracted values of natural frequencies for damage case RAGDC-1M

Mode No.	Values of natural frequencies (Hz)	Mode shape character
1	2.050	First bending
2	7.946	Second bending
3	8.239	First torsion
4	18.090	Third bending
5	18.420	Second torsion

Compared with values of natural frequencies of the intact bridge model with additional mass state that listed in *Table 5.16*, all values of natural frequencies are changed and minimum change is upon the first mode as shown in *Table 5.20*.

5.3.7.2.2 First adopted left side damage case with mass LAGDC-1M

A damage severity of (21x20) mm dimensions length by depth, respectively, is implemented on the left side of the bridge model under the influence of masses to represent the first damage scenario for the state with additional mass. AVMs are accomplished and the analysis of recorded data is performed to extract modal parameters for this case. Values of extracted natural frequencies and characters of mode shapes are listed in *Table 5.21*.

Table 5.21: Extracted values of natural frequencies for damage case LAGDC-1M

Mode No.	Values of natural frequencies (Hz)	Mode shape character
1	2.050	First bending
2	7.983	Second bending
3	8.203	First torsion
4	18.090	Third bending
5	18.530	Second torsion

In Table 5.21, all values of natural frequencies are changed compared with Table 5.16 and the minimum change is in the first mode.

5.3.7.2.3 Second adopted left side damage case with mass LAGDC-2M

The most severe damage scenario on the left side of the state of bridge model with additional mass is at crack size of (42x20) mm dimensions length by depth, respectively. The tests of AVMs are implemented here to record the acceleration data which are analysed to extract modal parameters of the grid-bridge model. Results of the extracted natural frequency values are listed in Table 5.22.

Compared with Table 5.16, all modes have got changes in their values of natural frequencies due to damage, while compared with Table 5.21, torsional modes are still without changing when the damage is increased.

Table 5.22: Extracted values of natural frequencies for damage case LAGDC-2M

Mode No.	Values of natural frequencies (Hz)	Mode shape character
1	2.014	First bending
2	7.910	Second bending
3	8.203	First torsion
4	18.054	Third bending
5	18.530	Second torsion

5.3.8 Repairing the damaged model

The grid-bridge model is repaired immediately after completing all tests of AVM for all damage cases. The AVM is implemented again on the repaired model to insure that the modal parameters of the repaired model are the same as for the original intact model. This

verification is achieved in the present work which indicates the validity of the previously adopted results.

5.4 Vierendeel bridge model

The third case study that adopted in the present work is the so-called Vierendeel bridge model. The naming Vierendeel refers to the civil engineer Arthur Vierendeel (1852-1940) who invents the idea of Vierendeel bridges around 1896 [109]. This kind of bridges has the truss mechanism, although, it is designed without the usual triangular voids seen in the usual trusses models. Instead of that, the bridge consists of rectangular opening and rigid connections in the elements. Unlike the conventional trusses, the connections in the bridge joints should resist substantial bending forces in addition to the axial forces [109]. Hence, this kind of bridge models has both structural actions, flexural and truss actions. In literature, almost of researchers use models with either flexural behaviour or truss behaviour, which does not give the generality for the study. On the other hand, almost of the models that adopted in literature deals with repeated models that are probably explored earlier. Therefore, present work select the Vierendeel bridge model to be as a case study in order to give the research more generality and paucity. The grid-bridge model explained earlier is the main complementary part which represents the bridge deck of the present Vierendeel bridge model. So, this case study is the final complete structure that adopted according to a real structure which constructed near the city of Belgrade, as mentioned earlier. This case study represents 3D structural behaviour, so that, it is more complicated than the previous two models of the overhang beam and the grid-bridge which represent 1D and 2D structural behaviour, respectively.

5.4.1 Experimental program

5.4.1.1 Scale considerations

The adopted case study of the Vierendeel bridge is a scaled model of an actual structure in site. The actual structure is scaled according to some specifications that mentioned in some references [108] in order to be suitable as a case study and workable within the available space in the laboratory. The bridge deck was explained earlier which

represents the grid-bridge model. Hence, just two fences are required to be added to the bridge deck to produce the complete Vierendeel bridge. These fences are scaled to be with height of 394 mm c/c instead of the real height of 1160 mm c/c, i.e., scale is 1/3 approximately. Also, the upper two main beams are scaled to be with hollow cross section of (30x50x2.8) mm for width, depth and thickness, respectively instead of the hollow cross section (150x200x6) mm dimensions. Therefore, the scale factors for each width, depth and thickness of the cross section are respectively 0.2, 0.25 and 0.467 which are according to the availability of sections in the markets. By the same way, the cross section of the columns are scaled. The original dimensions are (140x180x6) mm which are scaled to be (30x40x2.2) mm, respectively.

5.4.1.2 Model erection

As the bridge deck is already completed from the previous case study, the two fences are only the required parts that should be added and connected with the bridge deck to produce the whole Vierendeel model. The fence in each bridge side consists of 11 columns with section of (30x40x2.2) mm dimension, connect the main lower beam of the bridge deck with similar main upper beam, as shown in *Figure 5.32*.



Figure 5.32: Fences of the Vierendeel bridge model

Each of the upper main beam is a rectangular hollow steel section of (30x50x2.8) mm dimensions placed longitudinally parallel to the lower main beam. Each column is stiffened

by two triangular steel parts have dimensions of (70x70x100x2.8) mm for three side lengths and thickness, respectively, on the top and bottom. The completed Vierendeel bridge model after erection is shown in *Figure 5.33* and it has been supported as same as the way of supporting the case of grid-bridge model, *Figure 5.33*. Dimensions of the Vierendeel's main parts are shown in *Figure 5.34*.



Figure 5.33: Vierendeel bridge model

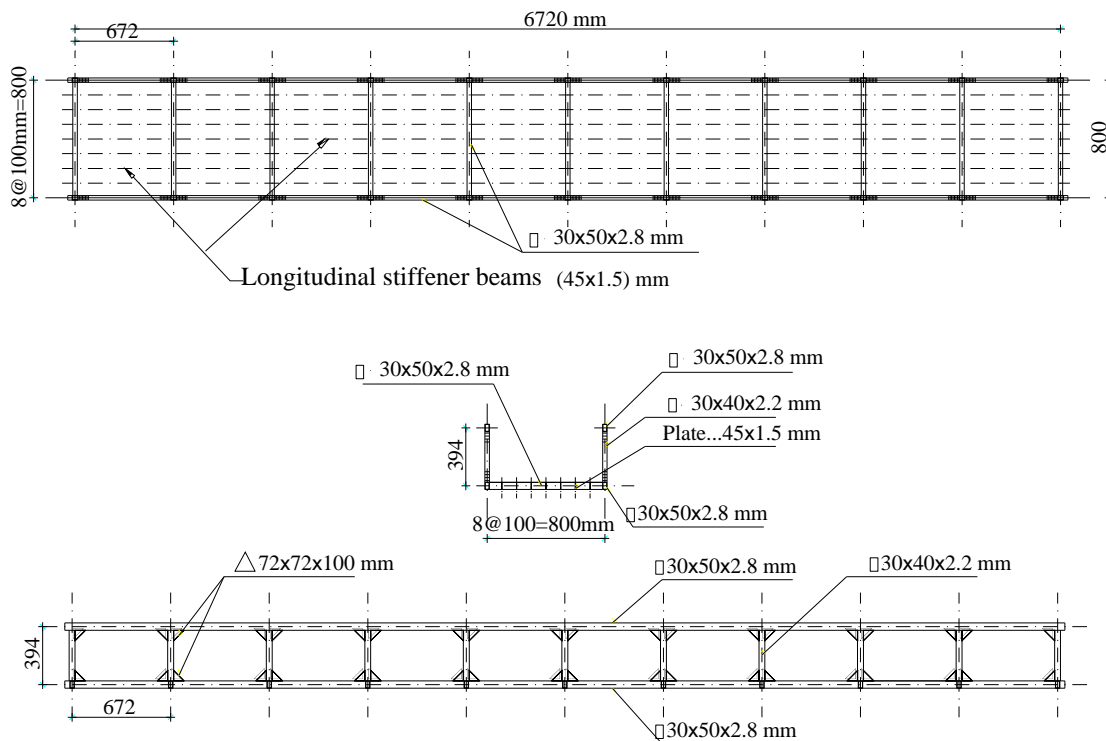


Figure 5.34: Details of the experimental Vierendeel bridge model

5.4.2 States of mass applications

Vierendeel bridge model is prepared to implement AVM upon two states of mass applications, without masses and with ten concrete cubes as additional masses to increase the range of explored values of natural frequencies, as the procedure of the previous case study. The masses, within the additional mass state, are distributed along the bridge deck as same as the distribution that adopted in the grid-bridge model, *Figure 5.23* and *Figure 5.35*, with the same mass average of 7.925 kg for each concrete cube.



Figure 5.35: Masses distribution along the bridge deck for the model with additional mass state

5.4.3 Preparing requirements of AVM and experimental analysis

The Vierendeel bridge model is prepared for AVMs tests by installing all the required devices by the same way that implemented during the tests of grid-bridge model explained earlier. The most important difference in this case is the distribution of sets of measurements. Due to the complexity of the Vierendeel bridge model, it needs special attention given to the selected mesh of measurement points (accelerometers positions). The Vierendeel bridge model represents 3D structural behaviour, hence, it is required to sense the motion in the horizontal and vertical direction for the both levels of the bridge: deck level and upper beam level. By this way, it is possible to extract bending and torsional

modes of vibration for 3D structure properly. Thus, each set of measurement in this case study, which also has 8 accelerometers, consists of 3 accelerometers for each upper and lower levels of the bridge model. Three of the accelerometers are installed to sense the motion of the vertical direction and three for the horizontal direction of motion. The reference accelerometers are the same as in the case of grid-bridge model with respect to the location and position, as shown in *Figure 5.36*.

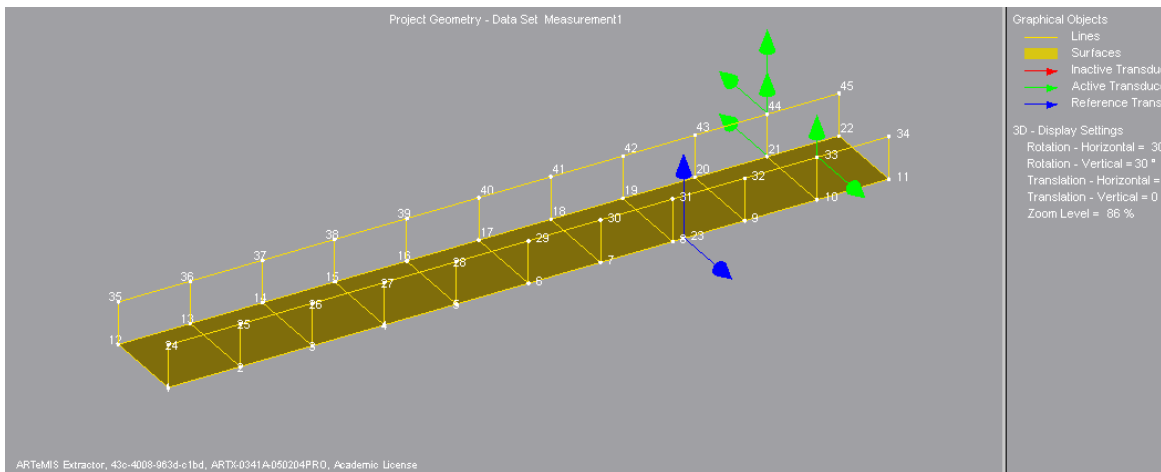


Figure 5.36: Accelerometers mesh of measurements for the Vierendeel bridge model

In order to extract more accurate results of modal parameters, 10 sets of measurements are adopted in the Vierendeel bridge model case study. Each set of measurements represents installation of the accelerometers group on each pairs of inner columns throughout the bridge model, while one set of measurement includes the upper points of both outer pairs of columns. In this way, the accelerometers forms a 3D mesh of measurements that covers the whole tested model properly as shown in *Figure 5.36*.

5.4.4 Implementing of AVM upon the Vierendeel bridge model

The same procedure of AVM tests that adopted previously for overhang and grid-bridge models is adopted also for the Vierendeel bridge model under the same conditions and verifications, *Figure 5.37*. The test adopts, sampling frequency of 600 Hz, filtering frequency of 200 Hz and intensity level of 7. Each set of measurements lasts 20 minutes

duration, hence, the resulted data of acceleration consist of 720000 rows for each one of the 8 accelerometers.



Figure 5.37: Vierendeel bridge model during AVM

5.4.5 Processing the configuration input file and AVM data by ARTeMIS software

The configuration input file for each adopted case, intact, damaged, without or with additional mass states of the Vierendeel bridge model is performed in ARTeMIS software according to special acceleration measurements data for each case. The procedure of implementing the configuration input file by ARTeMIS software in this case study is similar to the procedure that implemented in the grid-bridge model, as described by the flow chart shown in *Figure 5.26*. The elapsed time for analysing the configuration input file of the Vierendeel bridge model is 260 second using a computer has the properties of: Processor Core i7 CPU @ 2.1 GHz and RAM 6.0 GB. It can be seen that, although there are 10 sets of measurements used in AVM test of this model, the analysing time has no big difference compared with the analysing time of the configuration input file of the grid-bridge model which includes 5 sets of measurements. This is due to the test duration time of each set of measurements in the Vierendeel bridge model which lasts for 20 minutes only instead of 30 minutes in the case of grid-bridge model.

5.4.6 Intact case of the Vierendeel bridge model

The intact case of the Vierendeel bridge model is considered in this paragraph to extract the modal parameters for both without and with additional mass states, as following:

5.4.6.1 State of the model without additional mass

The behaviour of Vierendeel bridge model under its own mass only is considered here to estimate modal properties of the model based on AVM. In this paragraph, only FDD technique is adopted to extract modal parameters and EFDD is used for the sake of comparison only.

5.4.6.1.1 Results of the extracted modal parameters using FDD technique

The acceleration measurements data that recorded from AVM tests upon the Vierendeel bridge model are analyzed in ARTeMIS software and the normalized singular values of spectral density matrices are obtained based on frequency lines of 4096, *Figure 5.38*.

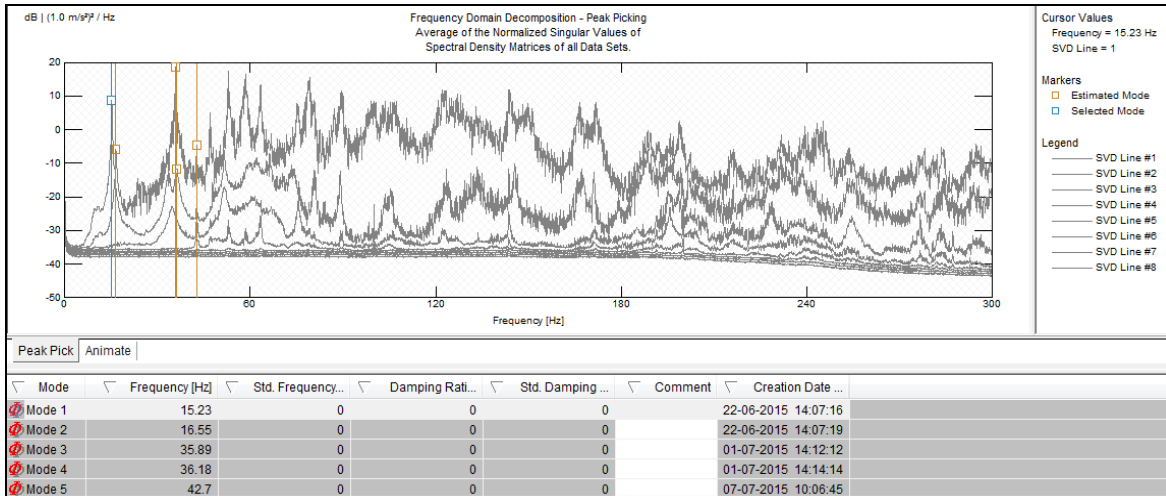
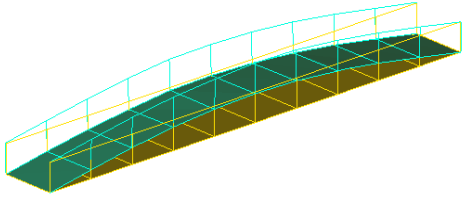
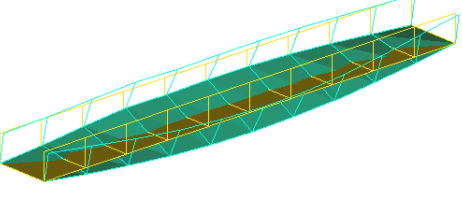
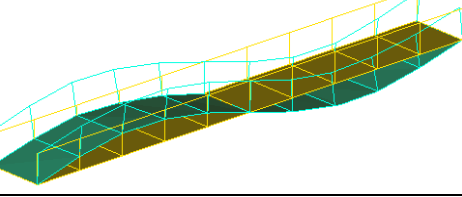
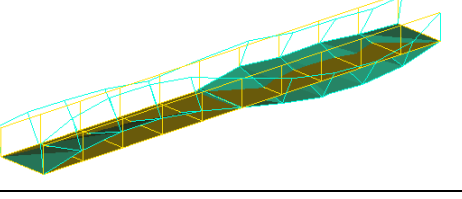
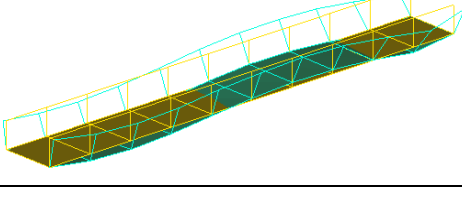


Figure 5.38: Normalized singular values of spectral density matrices of the Vierendeel bridge model without additional mass state using FDD peak-picking

According to FDD peak-picking technique, the extracted values of natural frequencies, mode shapes and mode shapes characters for the intact Vierendeel bridge model without additional mass are listed in *Table 5.23*.

Table 5.23: Values of natural frequencies, mode shapes and mode shapes characters for the first five modes of the intact Vierendeel bridge model without additional mass

Mode No.	Value of natural frequency (Hz)	Mode Shape	Mode shape character
1	15.230		First bending
2	16.550		First torsion
3	35.890		Second bending
4	36.180		Second torsion
5	42.700		Third bending

Validity of the estimated five modes of the intact Vierendeel bridge model without additional mass are checked using MAC matrix as shown in the MAC bar chart of *Figure 5.39*. According to *Figure 5.39*, all the non-diagonal modes have low values of MAC which indicate the stability of the five modes. The fifth mode has MAC values of around 0.1 and 0.2 compared with the first and third modes, respectively.

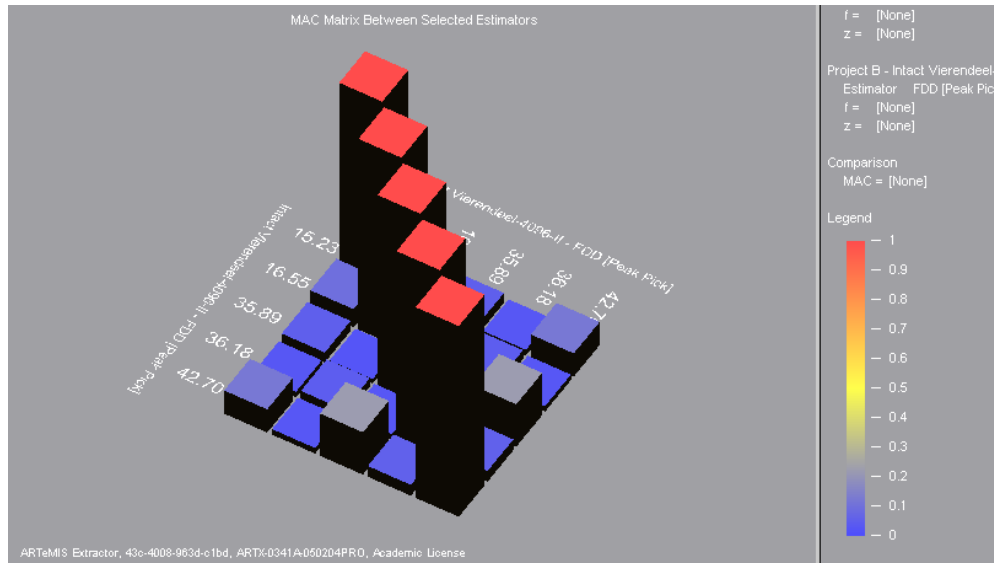


Figure 5.39: Comparison of the first five extracted modes of the intact Vierendeel bridge model without additional mass using MAC matrix bar chart

5.4.6.1.2 Verifying the extracted modal parameters using EFDD technique

The estimated values of natural frequencies that extracted by FDD peak-picking technique are verified by EFDD technique (based on frequency lines of 4096) to insure the convergence between the corresponding modes. The values of natural frequencies, mode shapes characters and damping ratios are listed in Table 5.24.

Table 5.24: Values of natural frequencies for the first five modes of the intact Vierendeel bridge model without additional mass extracted by EFDD technique

Mode No.	Natural frequency (Hz)	Damping ratio (%)	Mode shape character
1	15.250	0.485	First bending
2	16.560	1.043	First torsion
3	35.840	0.207	Second bending
4	35.900	1.478	Second torsion
5	42.730	0.185	Third bending

Results in *Table 5.24* exhibit high convergence between values of natural frequencies extracted by EFDD technique compared with the corresponding values of natural frequencies extracted by FDD technique in *Table 5.23*. Also, damping ratios are lower than 5% which indicate that the extracted modal parameters by FDD technique are stable (structural) modes and could be used in this work.

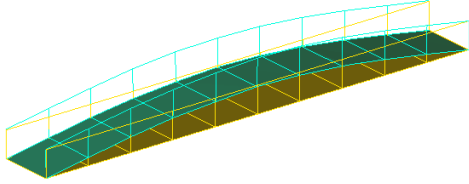
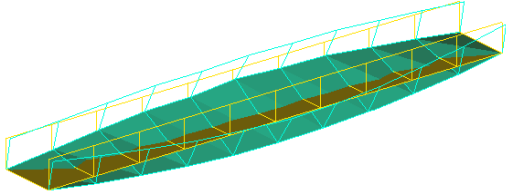
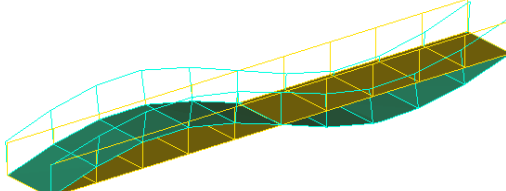
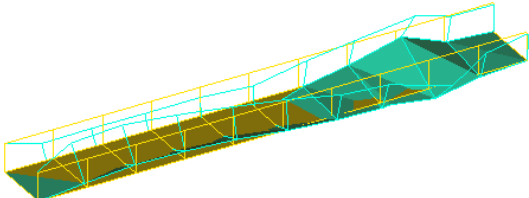
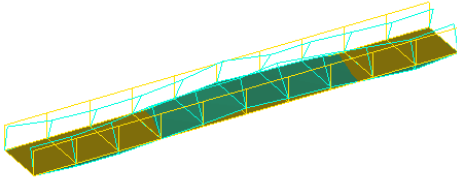
5.4.6.2 Results of the extracted modal parameters using FDD technique for the state of model with additional mass

Procedure of extracting modal parameters using FDD peak-picking technique is implemented for the state of the Vierendeel bridge model with additional mass, and the extracted values of natural frequencies, mode shapes and mode shapes characters are listed in *Table 5.25*.

In addition to the usual changes in values of natural frequencies due to the application of masses, two significant observations could be seen from *Table 5.25* in comparison with *Table 5.23* with respect to the changes in mode shapes. The first observation is that, the fourth mode becomes unclear double torsion under the presence of additional mass, while it was clear double torsion in the state without additional mass. The second observation is the change of fifth mode which is not completely similar to the fifth mode during the state of model without additional mass.

The MAC bar chart for the extracted values of natural frequencies are shown in *Figure 5.40*.

Table 5.25: Values of natural frequencies, mode shapes and mode shapes characters for the first five modes of the intact Vierendeel bridge model with additional mass

Mode No.	Value of natural frequency (Hz)	Mode Shape	Mode shape character
1	13.220		First bending
2	14.900		First torsion
3	30.910		Second bending
4	32.630		Second torsion
5	42.630		Third bending

In *Figure 5.40*, the highest MAC value between non-diagonal modes is between the third and the fourth modes which is about 0.3.

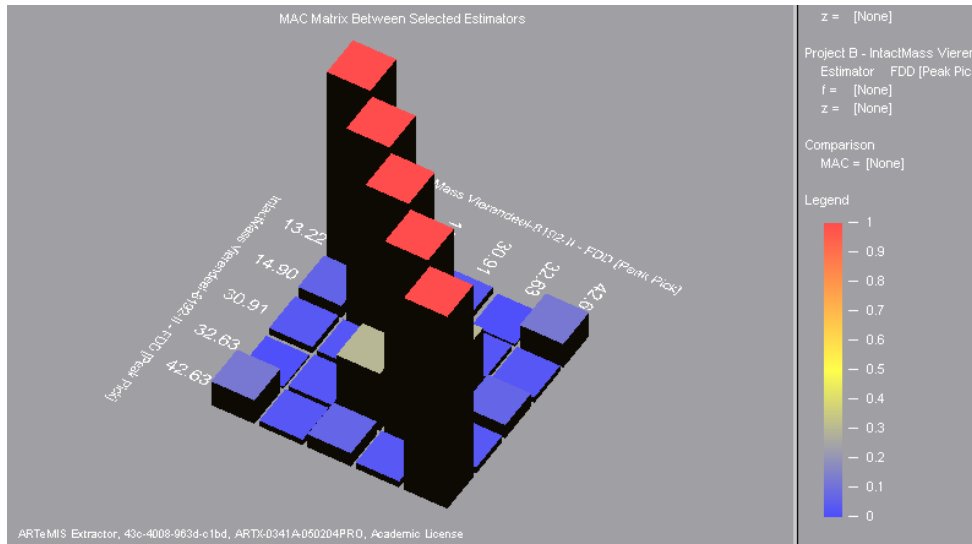


Figure 5.40: Comparison of the first five extracted modes of the intact Vierendeel bridge model with additional mass using MAC matrix bar chart

5.4.7 Damaged case of the Vierendeel bridge model

Procedures of damage scenarios of the Vierendeel bridge model include damage in beam or in column. One scenario of damaged beam is adopted when the model behaves under its own mass only while the masses are added during the adopted scenario of damaged column.

5.4.7.1 State of the model without additional mass AVDC-1

The first Adopted Vierendeel damage case is denoted as AVDC-1 (Adopted Vierendeel Damage Case-1) which is accomplished by creating a damage on the upper main beam that rests at 483 mm from the left support of the Vierendeel bridge model, *Figure 5.41 (a)*. Hand grinding machine is used to create the damage which is created with a size of (42x20) mm length by depth, respectively, as shown in *Figure 5.41 (b)*.

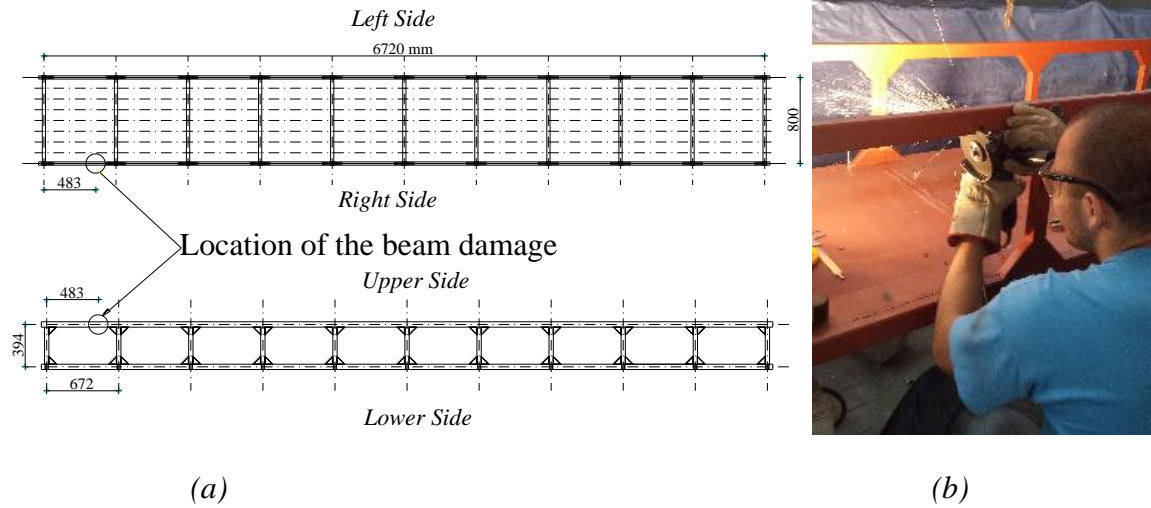


Figure 5.41: (a) Beam damage location, (b) formation process of the scenario AVDC-1

The model is tested for AVMs during this case of damage and the recorded data of acceleration are analyzed in ARTeMIS software. Values of natural frequencies that extracted by FDD technique are listed in Table 5.26.

Table 5.26: Extracted values of natural frequencies for damage case AVDC-1

Mode No.	Values of natural frequencies (Hz)	Mode shape character
1	15.197	First bending
2	16.552	First torsion
3	35.778	Second bending
4	36.181	Second torsion
5	42.626	Third bending

Compared with Table 5.23, all modes in Table 5.26 have got changes in values of natural frequencies due to the presence of damage. The changes in value of natural frequencies of the flexural modes (mode 1, 3 and 5) are more than the corresponding changes that happened in the torsional modes (mode 2 and 4). The first mode usually is the most significant among all other modes and it has a change in value of natural frequency.

5.4.7.2 State of the model with additional mass AVDC-1M

The distribution of masses shown in *Figure 5.35* is used to represent the model with additional mass state of the Vierendeel bridge model under damage. This damage scenario represents damaged columns instead of beam and characterized as AVDC-1M where the symbol M refers to the mass. The crack is created in the column to study the influence of damaged column on the modal properties of the model. The third column on the right side of the model, *Figure 5.42*, is selected to be damaged by a crack that located in the lower part of the column with a centre line rests at 63 mm from the bottom.

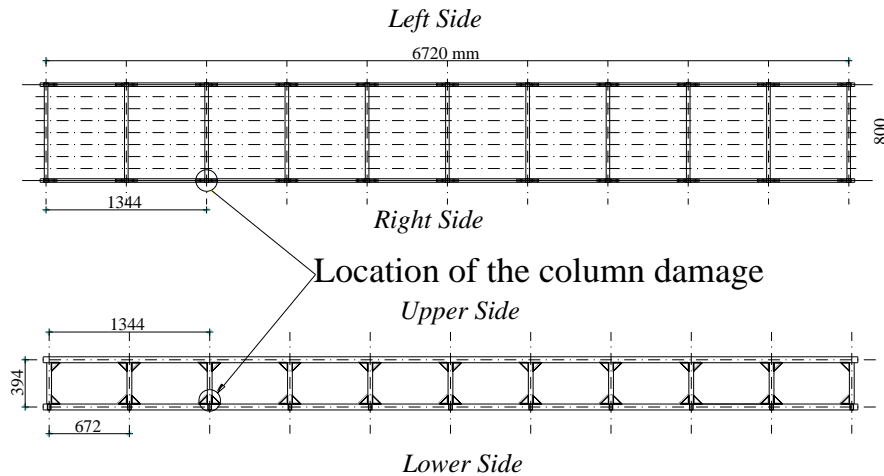


Figure 5.42: Damage in the lower part of column AVDC-1M

This part contains stiffener, hence, the crack in this case is not regular because it crosses through the stiffener until reaches the column, as shown in *Figure 5.43*. The lower side of the crack has 57 mm because it has to pass through the stiffener until it reaches to the column. On the other hand, the upper side of the crack has only 5 mm because it influences directly on the column. The total length of the crack is 58 mm which represents a segment with (5x58) mm dimensions that removed from the column shorter side. *Figure 5.43* shows the dimensions of the adopted crack (in millimetre) which affected on the beam-column joint that has the highest stress values in the column. AVMs are accomplished for the damaged model with additional mass state and the recorded acceleration data are analysed in ARTeMIS software to extract modal parameters. Using

FDD technique, the extracted values of natural frequencies and mode shapes characters for this damage case are listed in *Table 5.27*.

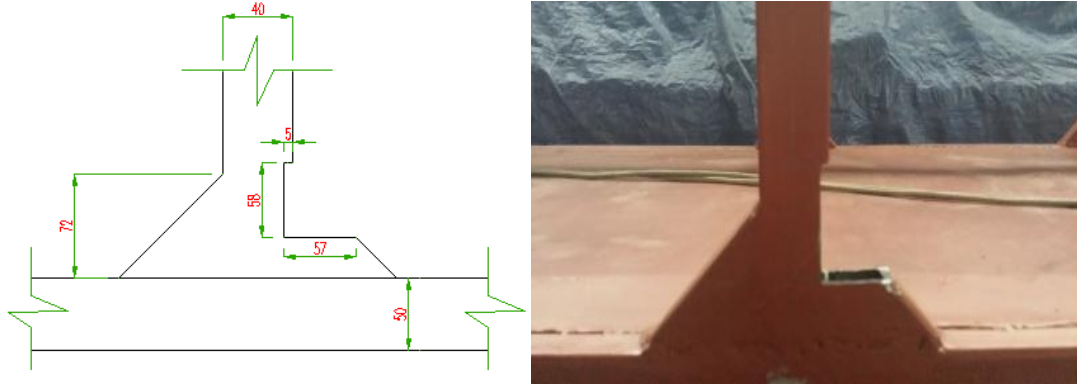


Figure 5.43: Dimensions of damage scenario AVDC-1M

Table 5.27: Extracted values of natural frequencies for damage case AVDC-1M

Mode No.	Values of natural frequencies (Hz)	Mode shape character
1	13.150	First bending
2	14.870	First torsion
3	30.910	Second bending
4	32.630	Second torsion
5	42.630	Third bending

Changes in values of natural frequencies in *Table 5.27* compared with the intact case of *Table 5.25* are the first and second mode only. On the other hand, the changes in values of normalized displacements in each mode, which are usually exist in each damage case, are taken into account as an indicator of the damage. In other words, sometimes there are no significant changes in values of natural frequencies due to damage but there are usual changes in values of normalized displacements. In this case, the changes in values of normalized displacements have the dominant influence to indicate the changes in structural dynamic behaviour under damage. Hence, the significant role of the changes in values of normalized displacements could be, sometimes, a sufficient parameter in the objective function to perform the damage detection optimization procedure.

5.4.8 Repairing the damaged model

After completing all tests of AVM for all damage cases, the Vierendeel bridge model is repaired immediately and the AVM is implemented again on the repaired model to verify the values of natural frequencies in the intact case. The same results are obtained which verify the validity of the previously adopted results.

5.5 Multi-storey building model

The fourth case study that adopted in the present work is the model of steel multi-storey building. The behaviour of 10-storey steel building under ambient vibrations is studied to explore the ability of application of damage detection procedure. This model represents, also, the 3D structural behaviour which is the second most complicated case in addition to the previous Vierendeel bridge model case. Description and handling of the structure are illustrated in the next paragraphs.

5.5.1 Experimental program

The multi-storey building (MSB) model consists of 10-storeies represents the z-direction with 3000 mm total height, as shown in *Figure 5.44*. Three bays in each x and y directions of the ground floor which becomes 3 and 2 bays in x and y directions, respectively, for the first floor of the building. In the third and fourth floors, there are 1 and 2 bays in the x and y directions, respectively, and still fixed as one bay in both directions for the remaining other floors. Each bay has 300 mm height and (300x300) mm dimensions in x and y directions, as shown in *Figure 5.44*.

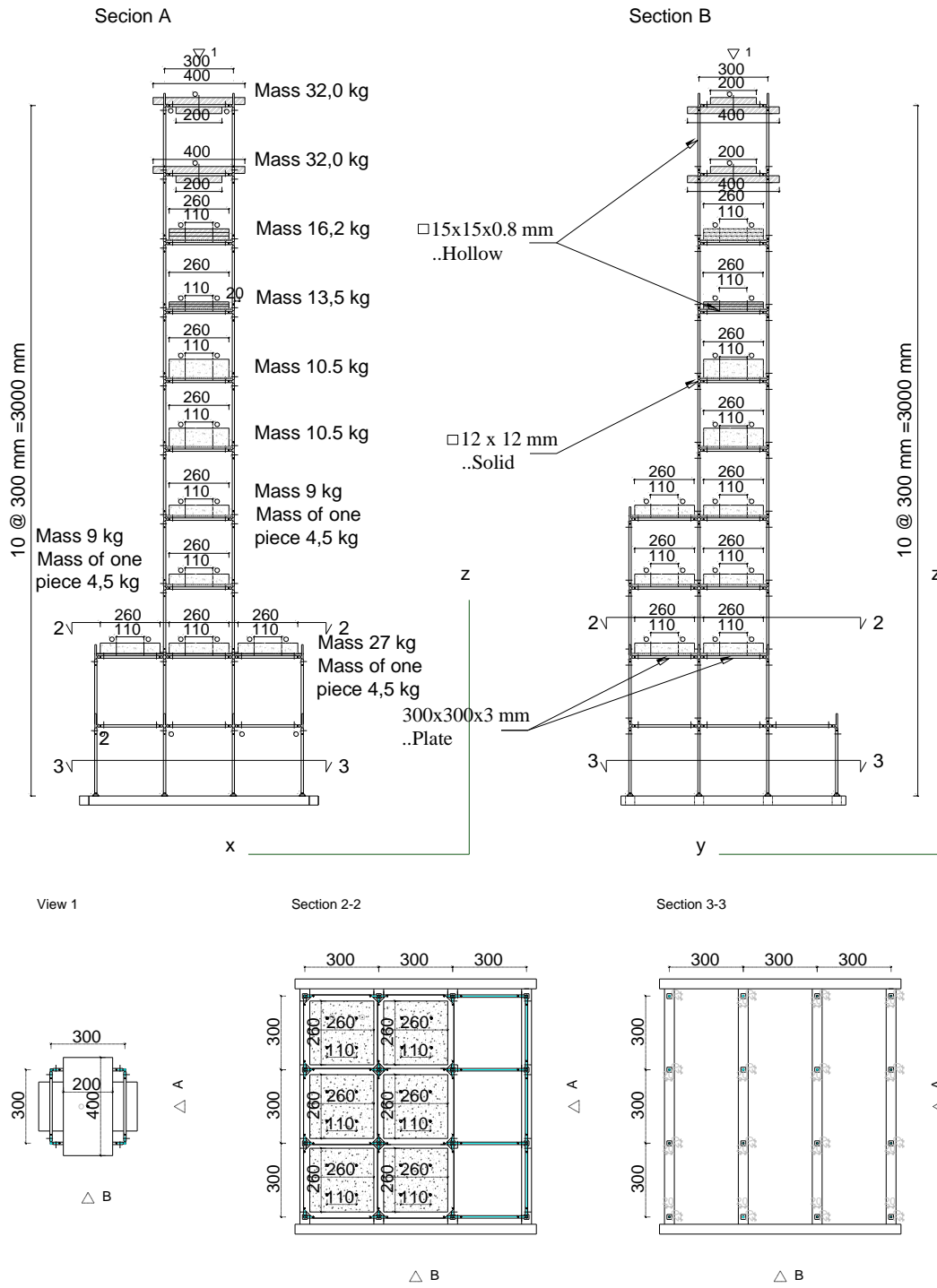


Figure 5.44: Details of the multi-storey building MSB model

The zero level of the building contains a rigid steel base that acts as a fixed support for the columns of the ground floor which are connected with the base by welding, as shown in *Figure 5.45*.



Figure 5.45: MSB model fixed on rigid support

In the level of 300 mm, there are no plates to act as roofs for the ground floor, while six steel plates are provided for the level of 600 mm to carry six of 4.5 kg concrete blocks as additional mass on the roofs. Each steel plate, wherever found, has 3 mm thick and connected by eight bolts by the perpendicular beams in the x and y directions. For the levels of 900 mm and 1200 mm, two of the steel plates carry two of 4.5 kg concrete blocks for each level which are connected by 4 bolts with the steel plate. For both levels of 1500 mm and 1800 mm, one concrete block has 10.5 kg is used as additional mass while a steel block has 13.5 kg is used in level 2100 mm to represent the mass. Another steel mass of 16.2 kg is used for the level 2400 mm which is also connected by the steel plate in this level. For the last two levels, 2700 mm and 3000 mm, there are no steel plates used and

only two masses of brick are used for each level that have 32 kg total mass in each level as shown in *Figure 5.44*.

Beams and columns of the MSB model are represented by square hollow steel sections have (15x15x0.8) mm as the first type of used sections, *Figure 5.44*. The second adopted type of sections in MSB model are solid square steel sections have (12x12) mm that used in the locations of beam-column joints only. Each hollow beam or column is connected with the solid section by two perpendicular bolts in each end, as shown in *Figure 5.46*.

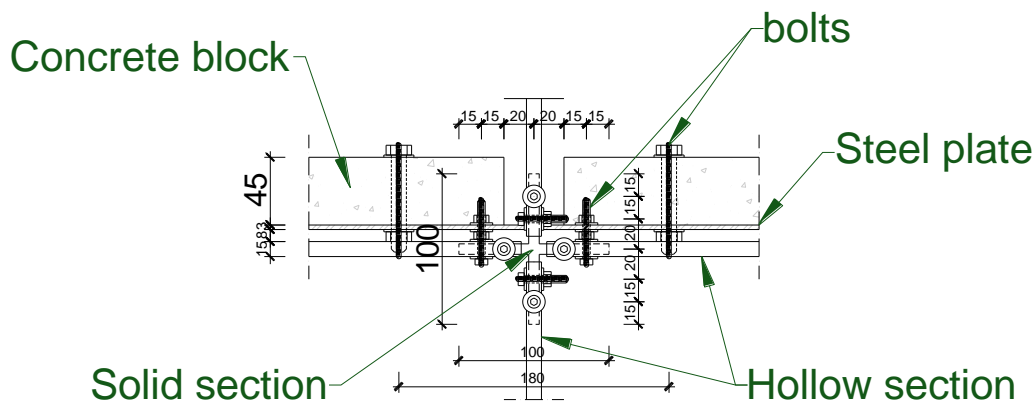


Figure 5.46: Details of beam-column joint

A rigid steel base is used to fix the shaker, *Figure 5.45*, which is welded by the main steel base of the structure to allow waves of vibrations to influence on the base of the model. In this way the excitation is insured to be from the foundation towards the structure, as adopted in each model earlier.

5.5.2 Preparing the requirements of AVM and experimental analysis

The MSB is a complex 3D structure has unsymmetrical geometry about central y-axis and unsymmetrical mass distribution about central x-axis. In this case, a special attention should be paid to the distribution of the limited number of accelerometers to be able to cover the whole structure properly. The local distribution of each set of accelerometers governs the global mesh of accelerometers (measurement), which should be in 3D form.

The most important part in the whole MSB which exhibits enough representation for the whole frame if it is taken into account, is the tower of the MSB frame. The highest part, which represents the intermediate tower that extended 10-floors, is adopted to install all sets of measurements to monitor all expected modes, bending-x, bending-y and torsional modes, as shown in *Figure 5.47*.



Figure 5.47: Installing of accelerometers on the tower part of the MSB model

The face of tower, *Figure 5.47*, that consists x - z plane is selected to install accelerometers according to 5 sets of measurements, while the rear side of the tower is handled by equations that governs its motions according to the face side motions. Six accelerometers represent each movable set of accelerometers that installed on each pair of floors from the face side simultaneously. Also, two fixed reference accelerometers are installed on the rear face to complete each one set of measurement, as shown in *Figure 5.47* and *Figure 5.48*.

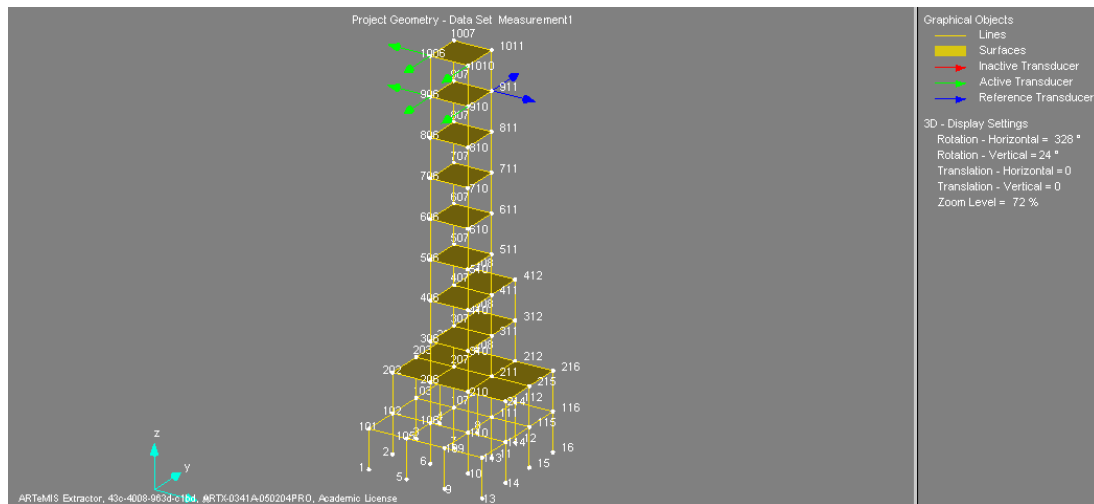


Figure 5.48: Accelerometers, locations and directions on the 3D mesh of measurement for MSB

The shaker is installed in the located position on the rigid steel base, as shown in Figure 5.49.



Figure 5.49: Installed shaker on the rigid steel base of the MSB model

All other devices that required for implementing AVM tests are prepared and installed to execute the tests.

5.5.3 Implementing of AVM upon the MSB model

The procedure of implementing the AVMs is adopted to record acceleration data upon the MSB model under the same conditions and verifications that mentioned earlier. The adopted sampling frequency is 600 Hz, filtering frequency 200 Hz and intensity level is 7. Each set of measurements lasts 20 minutes duration, hence, the resulted acceleration data has a dimensions of 720000 rows for each one of the 8 accelerometers.

5.5.4 Processing the configuration input file and AVM data by ARTeMIS software

The configuration input file for the MSB model is processed in ARTeMIS software which has similar procedure for each of the intact or damaged cases except for the included acceleration data, as usual. The time needed for analysing the configuration input file of the MSB model is 130 second using a computer has the properties of: Processor Core i7 CPU @ 2.1 GHz and RAM 6.0 GB. This is exactly the half of the time that was required for the Vierendeel model which is also reflects the huge amount of included data in this model.

5.5.5 Intact case of the MSB model

ARTeMIS extractor software processes the data of acceleration that recorded during AVM tests, and produces the normalized singular values of spectral density matrices for the intact state of MSB model, as shown in *Figure 5.50*.

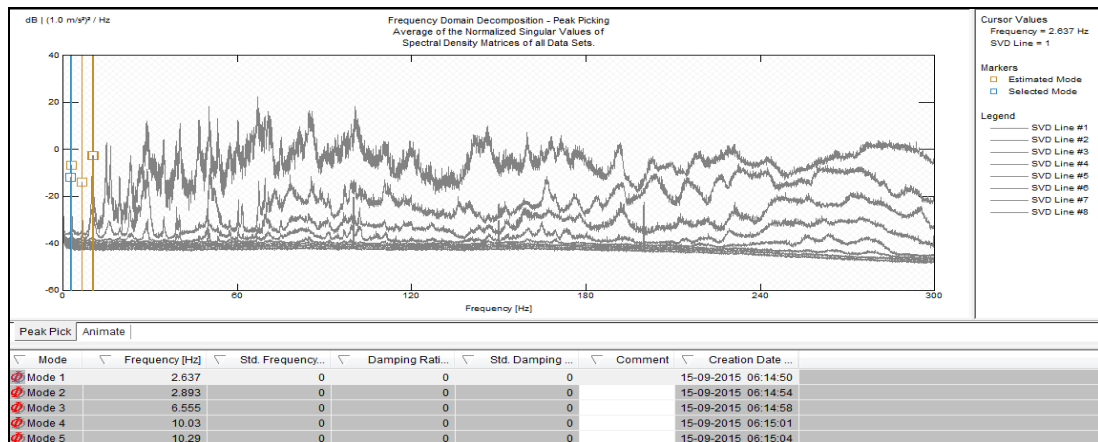
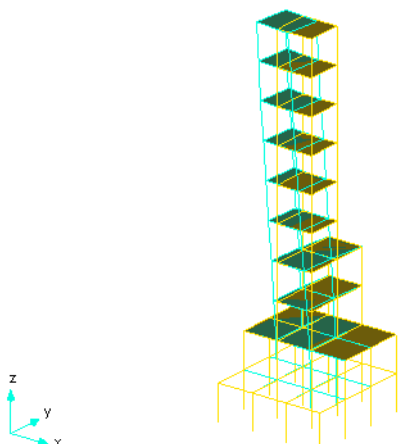
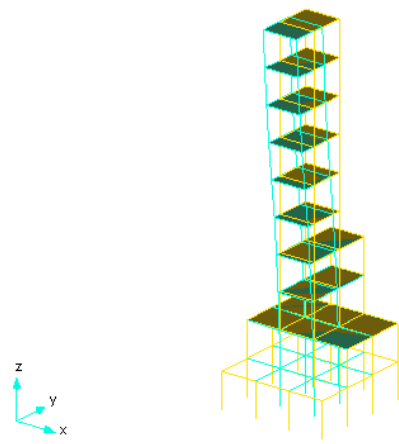


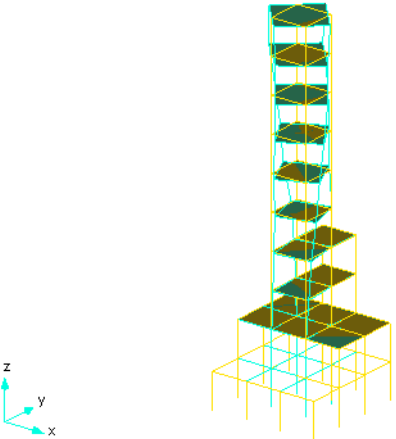
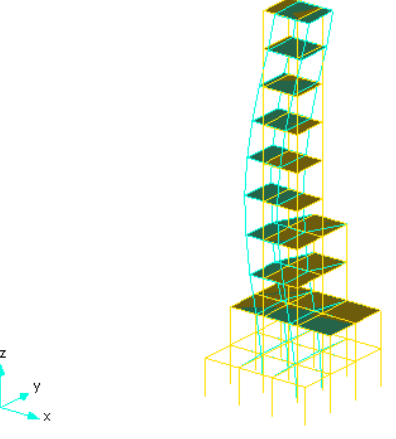
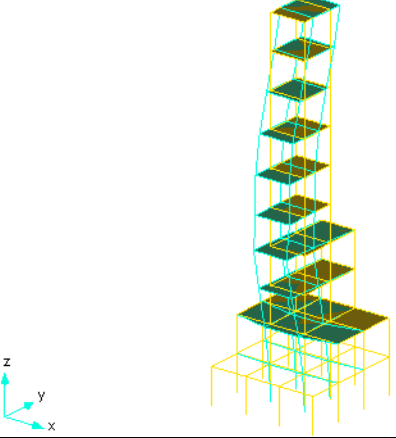
Figure 5.50: Normalized singular values of spectral density matrices of the intact MSB model data sets using FDD peak-picking

Using FDD peak-picking technique, the extracted values of natural frequencies, mode shapes and mode shapes characters for the intact MSB model are listed in *Table 5.28*.

Table 5.28: Values of natural frequencies, mode shapes and mode shapes characters for the first five modes of the intact MSB model

First and second modes		
Mode No.	1	2
Frequency (Hz)	2.637	2.893
Mode shape	<p>FDD Natural Frequency = 2.637 Hz</p> 	<p>FDD Natural Frequency = 2.893 Hz</p> 
Mode shape character	First bending about y-axis	First bending about x-axis
Third and fourth modes		
Mode No.	3	4
Frequency (Hz)	6.555	10.030

Experimental research on structural models of different configurations - Research program and results

Mode shape	<p align="center">FDD Natural Frequency = 6.555 Hz</p> 	<p align="center">FDD Natural Frequency = 10.03 Hz</p> 
Mode shape character	First torsion	Second bending about y-axis
Fifth mode		
Mode No.	5	
Frequency (Hz)	10.290	
Mode shape	<p align="center">FDD Natural Frequency = 10.29 Hz</p> 	
Mode shape character	Second bending about x-axis	

Validity of the estimated five modes of the intact MSB model are checked using values of MAC matrix as listed in *Table 5.29*.

Table 5.29: MAC matrix for the extracted modes of the intact MSB model

Modes	First mode	Second mode	Third mode	Fourth mode	Fifth mode
First mode	1	0.016	0.110	0.313	0.033
Second mode	0.016	1	0.022	0.017	0.268
Third mode	0.110	0.022	1	0.094	0.018
Fourth mode	0.313	0.017	0.094	1	0.108
Fifth mode	0.033	0.268	0.018	0.108	1

In Table 5.29, the highest values of non-diagonal MAC are 0.313 and 0.268 for the comparison between (first and fourth) and (second and fifth) modes, respectively. These values are not so high, hence, the five modes could be considered as acceptable modes to be used in the next stages.

5.5.6 Damaged case of the MSB model ABDC-1

The adopted damage scenario in the MSB model is the damaged column due to the special importance of the column members in any civil structure. It is known that the damage in columns has more dangerous effect than damage in beams with respect to the integrity of structures. Hence, this paragraph highlights the experimental program of MSB model when exposed to damage in the column.

The selected damaged column is located between the levels 1500 mm and 1800 mm, on the left face side of the MSB model, and the crack centre is at 1575 mm from the base, as shown in Figure 5.51. The crack size has dimensions of (60x7.5) mm length by depth, respectively, to represent damage scenario ABDC-1 (Adopted Building Damage Case-1), as shown in Figure 5.51.

Tests of AVM are performed and the acceleration data are recorded to be analyzed in ARTeMIS software. Using FDD peak-picking technique, the extracted values of natural frequencies are listed in Table 5.30.

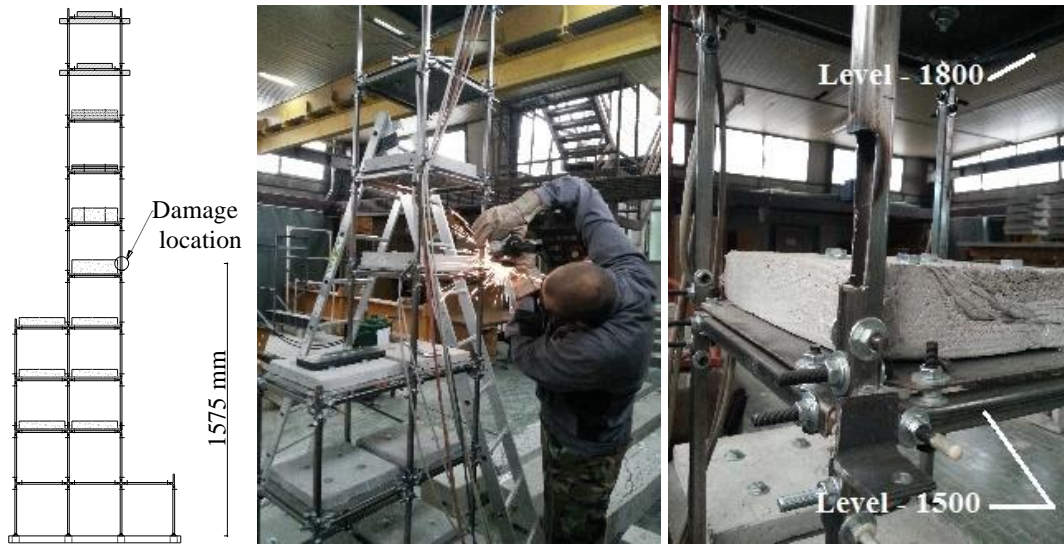


Figure 5.51: Column damage scenario ABDC-1

Table 5.30: Extracted values of natural frequencies for damage case ABDC-1

Mode No.	Values of natural frequencies (Hz)	Mode shape character
1	2.637	First bending about y-axis
2	2.893	First bending about x-axis
3	6.445	First torsion
4	9.997	Second bending about y-axis
5	10.290	Second bending about x-axis

In Table 5.30, values of natural frequencies of the third and fourth modes are changed compared with their corresponding values in the intact state of Table 5.28 with the same mode shape characters.

5.5.7 Repairing the damaged model

The MSB model is repaired immediately after completing all tests of AVM for all damage cases. As usual, AVM is implemented again on the repaired model to verify the values of natural frequencies in the intact case which leads to the same values of natural frequencies that obtained before creating of damages.

6. NUMERICAL MODELLING AND ADJUSTMENT OF NUMERICAL RESULTS OBTAINED BY FEM AND EXPERIMENTAL RESULTS

6.1 Introduction

Damage identification techniques include comparison of the experimental modal properties with those computed by finite element (FE) analysis of the same structure. Hence, the importance of performing the FE analysis for the structure under consideration is the same as the importance of experimental analysis that implemented earlier. Both analyses have crucial role in the results of damage identification technique. Often, this technique faces the disparity of modal properties due to the effect of various parameters that are included in the FE model, such as, material properties and geometry of the structure. Therefore, in order to make a convergence between the experimental and computed modal properties, calibration process for the FE model is required. The calibrated modal properties lead to facilitate the procedure of damage identification method by decreasing errors between experimental and calibrated responses. The calibration process could be performed in confidently predicting the structural behavior under various states of additional mass application of the model [110]. This chapter focuses on the FE analyses for each adopted model as a case study in addition to the procedure of calibration process.

6.2 Numerical modal analysis of FE model

The FE structural analysis for all adopted models in the present work is performed by the advanced well-known ANSYS software package, to extract modal parameters numerically. ANSYS software is used since ANSYS architecture provides quick batch process to integrate its process and postprocessor with other programs easily [41]. Routine script files are written using ANSYS language commands to describe and create each adopted model in the present work leading to perform modal analysis of FE model numerically. For all models, these steps are adopted and numerical analysis is carried out using *Beam4* element type and *linear elastic isotropic* material.

6.3 Calibration process by FE model updating

6.3.1 General

The term *numerical model updating* was mentioned earlier in the procedure of damage detection, Chapter 3, when FE structural analysis is repeated periodically to determine dynamic properties which are compared with the corresponding experimental results to find the errors. In that case, the analysis is repeated when changing of some parameters, location and severity of damage, that influence on the structural modal results such as natural frequencies and mode shapes. In this chapter, the term *FE model updating* is considered which represents the changing that is accomplished upon some structural parameters, such as modulus of elasticity, mass density, sections geometry... etc, to produce new approximate results. Hence, it should not be confused between the two terms and keeping each term with its suitable case.

Usually, computations of dynamic responses according to the initial FE model produce no complete accuracy compared with the dynamic responses that extracted from the experimental model. This leads to certain errors resulted due to some reasons, such as inaccurate values of material properties and difficulty in modeling complex real life shapes [111]. Hence, calibration process upon the FE model is needed which is implemented by updating the included physical parameters (structural parameters). This process will improve the initial FE modal properties, natural frequencies and mode shapes, to coincide with those obtained experimentally [112]. Calibration process is implemented in the present work according to the so-called *Iterative Technique* which is considered as a basic for FE model updating. The iterative technique computes the updated values of structural parameters of FE model in such a way that during each iteration will be a reduction in the mismatch between experimental and FE responses. This process will continue until the iterations stopped when the values of updating parameters stop converging or the error function is reduced to tolerable level. These techniques require a number of reasonable iterations before achieving the final result.

It is important to mention that, before applying any FE updating technique, the experimental and FE dynamic responses need to be compared so as to ensure existence of

some correlation between experimental and FE responses. Also, it is aimed to determine whether it is worth to update the proposed FE model or a completely new model is required. These techniques include comparison of FRFs, natural frequencies, mode shapes and Modal Assurance Criterion (MAC). The present study proposes the procedures including only natural frequencies for that purpose.

Generally, there are two proposed structural model updating techniques, classical approach and FE route. Both of these techniques are used in the present work by simply implementing the classical approach using hand calculations and the advanced performing of TS optimization proposed procedure for the FE route.

6.3.2 Structural parameters for FE model updating process

As mentioned earlier, before the application of FE model updating process, the existence of some correlation between experimental and FE responses should be insured to make the updating procedure worth. Hence, the increasing in values of structural parameter is limited to a certain maximum and minimum allowable limits, after which, it will be unreasonable procedure. In the present work, the allowable reasonable limits that permits modifying any value of included structural parameters is in the range [-5% to +5%] of the original value. Therefore, sometimes under this range, including of only one parameter in the FE model updating process is insufficient to achieve good convergence between the experimental and FE responses and the additional parameters are required. Trial and error could be suitable option to determine the sufficient number of included structural parameters in the FE model updating process, which is adopted in the present work.

Due to the significant influence of the material modulus of elasticity on the physical properties of the whole structure, it is wisely to use this parameter in the updating process. The higher the value of material modulus of elasticity, the higher the values of natural frequencies for structural model. Mass density of the model is another important structural parameter that is often used in the FE model updating process to act simultaneously with other parameters in the calibration process. The influence of mass density is obviously opposite of the influence of modulus of elasticity towards the values of natural frequencies. The third structural parameter that taken into account in the FE model updating process is

the geometry of sections that consists the structural members. Also, width, depth and thickness of sections could be, all or some, included in the process as needed. Finally, the geometry of the model itself could be modified in some parts to achieve the required convergence and reduce errors between results of experimentally and numerically extracted natural frequencies.

6.3.3 Adopted method for Calibration of FE model

According to the iterative technique, the minimizing of the proposed objective function is aimed to produce optimal values of updated parameters during the calibration process. The objective function is minimized according to the equation (6.1):

$$\text{Obj_Func} = \sum_{i=1}^n \left(\frac{f_i^T - f_i^U}{f_i^T} \right)^2 \quad (6.1)$$

where f_i^T and f_i^U are the tested and updated computed values of natural frequencies, respectively. Equation (6.1) is the objective function that used in the FE model updating process for all adopted cases in this work which is in the form of *relative error (difference)*. The allowable limits of changes that could be implemented for each parameter in each case study are:

$$[p_k - 0.05 \times p_k] \leq [p_k] \leq [p_k + 0.05 \times p_k] \quad (6.2)$$

where, p_k represents the updated parameters and k is the number of included parameters in the calibration.

ANSYS software is used to implement the calibration procedure of FE model updating with the aid of MATLAB software. A unified flow chart that summarizes the MATLAB routine to execute the procedure of FE model updating process can be shown in *Figure 6.1* [111]. Classical FE model updating using hand calculations is implemented upon the overhang beam model case study. While, the advanced iterative FE route updating technique is adopted for calibration process in all other models that used in this work.

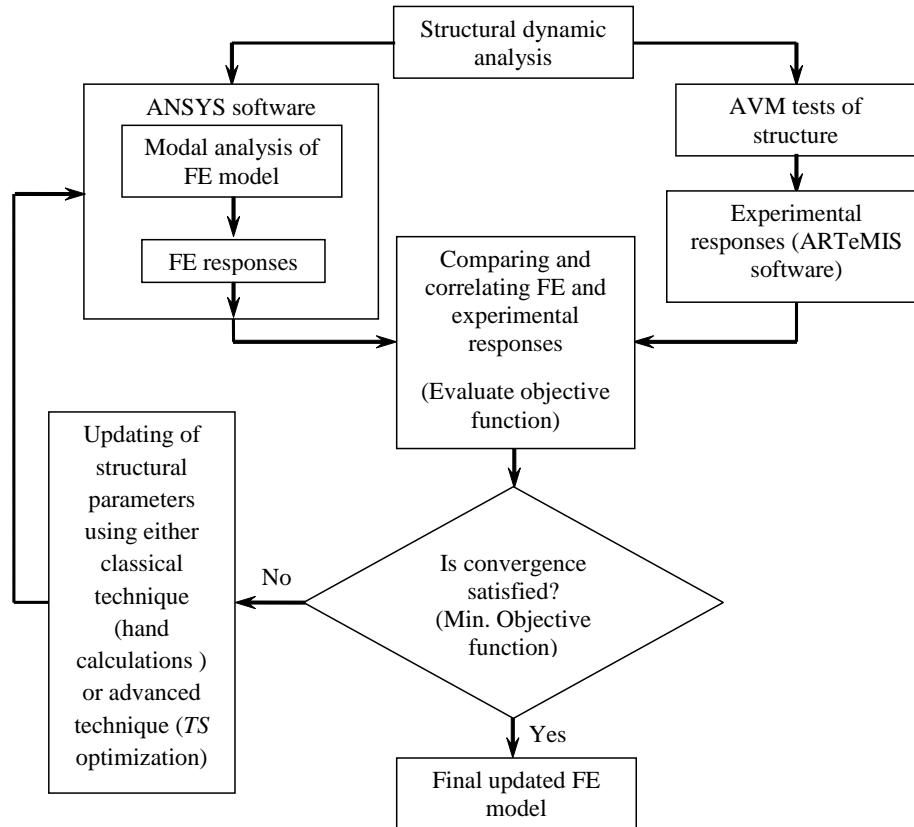


Figure 6.1: Flowchart of the proposed calibration procedure of FE model updating

The procedure is implemented with the aid of TS optimization proposed procedure to achieve the optimum values of structural parameters. The optimum parameters satisfy the convergence between the experimental values of natural frequencies and their corresponding values that computed numerically. The structural parameters are updated according to the proposed TS optimization procedure using objective function represented by equation (6.1). FE updating process with the aid of TS optimization procedure can be shown in *Figure 6.1*, where the TS optimization is a part that uses similar procedure as explained in *Figure 4.5*. This is implemented for all three models, grid-bridge, Vierendeel bridge and the multi-storey building that adopted in the present work and for both states, without and with additional mass, of these models.

6.4 Numerical calculations of the simply supported overhang beam model

The general procedure that adopted in any case study is to perform numerical modal analysis upon initial intact state of the model using ANSYS software. After that, calibration

process of the FE model is implemented to update the initial selected structural parameters. In this process, the best convergence between the experimental extracted and numerical computed values of natural frequencies is reached. The updated values of structural parameters are adopted in the next stages to apply numerical modal analysis of FE model under damage states for the case study.

6.4.1 FEM analysis of the initial intact model

Numerical FE model of the first adopted case study, overhang beam model, is created in ANSYS software which consists of 60 elements have length between (20-30) mm range, as shown in *Figure 6.2*. The initial adopted modulus of elasticity of the beam material is $E_{\text{initial}}=2 \times 10^5 \text{ N/mm}^2$, while the initial mass density is $D_{\text{initial}}=7.86 \times 10^3 \text{ kg/m}^3$ and Poisson's ratio is $\nu = 0.3$.

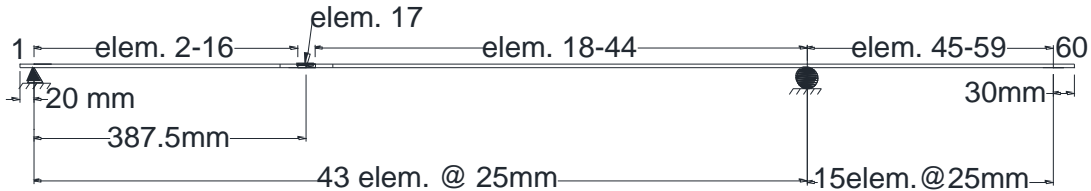


Figure 6.2: Overhang FE model

Masses are considered also in FE model, as described earlier in *Figure 5.3*, with their average mass value of $34.53 \times 10^{-3} \text{ kg}$ and moment of inertia of $5.395 \times 10^{-6} \text{ kg m}^2$. Moment of inertia is calculated according to the following form:

$$I_y = M \times d^2 \quad (6.3)$$

where, I_y is the mass moment of inertia about the y-axis with units of kg m^2 , y is the axis that perpendicular on the plane of paper, M is the mass with units of kg and d is the distance from the centre of mass to the center of beam thickness, as shown in *Figure 6.3*. The first three modal parameters of the initial intact FE model are computed in ANSYS software and compared with their corresponding modes that extracted experimentally in chapter-5.

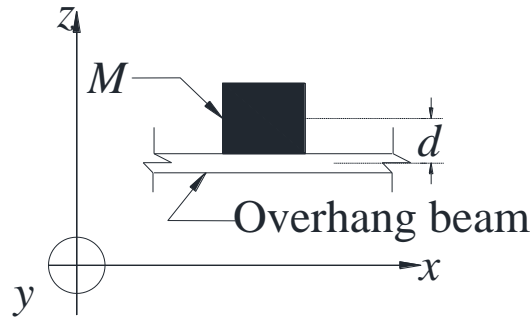


Figure 6.3: Parameters of mass moment of inertia

Results of comparison between experimental values of natural frequencies with their corresponding numerical values are listed in *Table 6.1*.

Table 6.1: Experimentally extracted and numerically computed values of natural frequencies of the intact overhang beam model

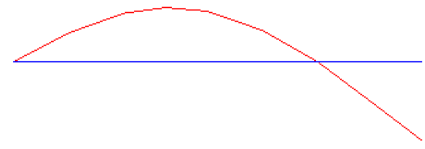
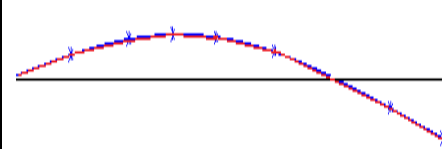
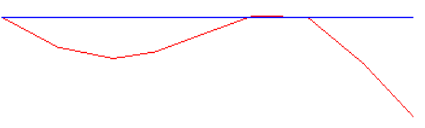
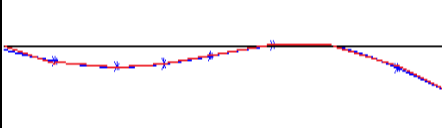
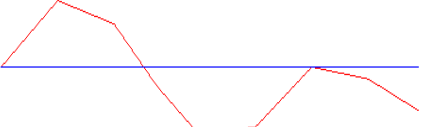
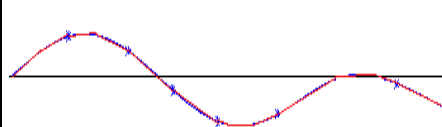
Mode No.	Experimental value of natural frequency (Hz) ARTeMIS software (Table 5.4)	Numerical value of natural frequency (Hz) ANSYS software	Err. (Hz)	(R. Err.) ²
1	7.910	7.720	+0.190	0.00058
2	18.750	18.380	+0.370	0.00039
3	42.480	42.510	-0.030	5.0x×10 ⁻⁷

Values of the column (Err. (Hz)) represent the *direct* difference between values of experimentally extracted and numerically computed natural frequencies, while the values in the last columns represent square of *relative* difference between the frequencies according to equation (6.4).

$$R_Error = \left(\frac{f_i^E - f_i^N}{f_i^E} \right)^2 \quad (6.4)$$

where, i , is the mode number. The experimentally extracted and numerically computed mode shapes, in addition to their mode shape characters, are shown in *Table 6.2*.

Table 6.2: Experimentally extracted and numerically computed mode shapes of the intact overhang beam model

Mode No.	Mode shape extracted experimentally ARTEMIS software (Table 5.4)	Mode shape computed numerically ANSYS software	Mode shape character
1			First bend.
2			Second bend.
3			Third bend.

It is found that, by trial and error method, the use of the first three modes is enough to produce indication for the sake of damage detection procedure in final stages of this work.

6.4.2 Calibration process by FE overhang model updating

Calibration process is implemented upon the intact FE model to update some of the structural parameters leading to the best convergence with the values of natural frequencies extracted experimentally. In this case study of overhang beam model, the classical calibration process is accomplished by hand calculations upon the structural parameters. The adopted structural parameter in this case is only the material modulus of elasticity, which exhibits enough ability to achieve convergence immediately after few trials. The hand calculations are implemented by using trial values, within the range mentioned in equation (6.2), of the modulus of elasticity and monitoring the convergence. Value of

modulus of elasticity that leads to the best convergence between the computed and experimentally estimated values of natural frequencies is the target value. *Table 6.3* shows the first three computed modal frequencies for varied values of modulus of elasticity in the proposed range.

Table 6.3: Modal frequencies computed based on different values of modulus of elasticity

Mode No.	Value of modulus of elasticity E (N/mm ²)							
	$E = 2.00 \times 10^5$		$E = 2.05 \times 10^5$		$E = 2.09 \times 10^5$		$E = 2.10 \times 10^5$	
	f (Hz)	(R. Err.) ²	f (Hz)	(R. Err.) ²	f (Hz)	(R. Err.) ²	f (Hz)	(R. Err.) ²
1	7.720	0.00057	7.820	0.00013	7.890	4×10^{-6}	7.910	1.4×10^{-7}
2	18.380	0.00039	18.600	0.00006	18.780	3×10^{-6}	18.830	1.7×10^{-5}
Error respect to experimental values according to equation (6.1) including first two modal frequencies								
$\sum(\text{Err.})$		0.00096		0.00019		7×10^{-6}		1.71×10^{-5}
3	42.510	5.0×10^{-7}	43.040	0.00017	43.460	0.00053	43.560	0.00065

The values in the columns (f (Hz)) of *Table 6.3* represent the computed updated values of natural frequencies based on different trial values of modulus of elasticity. The values in the columns ((R. Err.)²) of *Table 6.3* represent the square of relative difference between values of experimentally estimated and the updated computed natural frequencies due to the changes in values of modulus of elasticity. The values in the row (\sum (Err.)) represent summation of (R. Err.)² values that exist in each column, excluding the third mode values, according to the equation (6.1). Another form can be used as an objective function based on the direct difference between values of natural frequencies, given in equation (6.5).

$$\text{Error} = \sum_{i=1}^n |f_i^E - f_i^N| \quad (6.5)$$

The best agreement between computed and experimentally estimated values of natural frequencies is reached for the value of modulus of elasticity of $E_{\text{optim}} = 2.09 \times 10^5$ N/mm². This is achieved according to the sum of square relative

differences of equation (6.1), of the first two best tuned modal frequencies. It should be noticed that, in *Table 6.3*, the calibration and convergence is adopted according to results of only first two modes because of the divergent behavior of the third mode. For better illustration, the convergent and divergent behaviors for the first two and the third modes, respectively, can be explained according to the relation between modulus of elasticity and each mode, as shown in *Figure 6.4*.

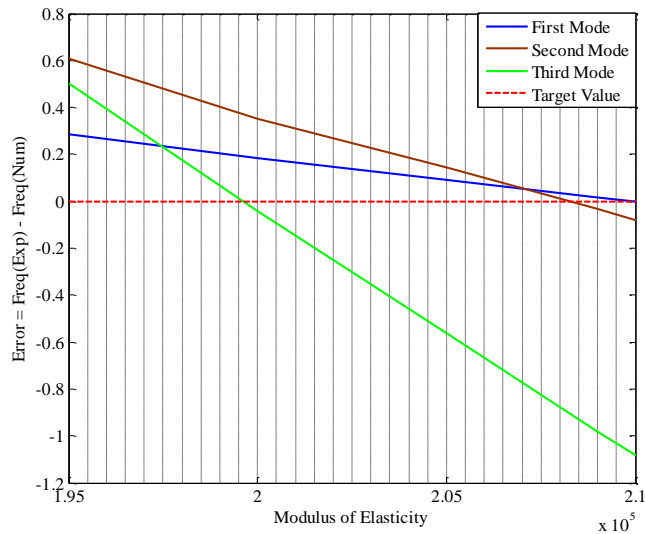


Figure 6.4: Differences between experimentally estimated and numerically computed natural frequencies for different values of modulus of elasticity

Obviously in *Figure 6.4*, there is no any single point that gathers the three modes in the same time close to the zero value (target value). Hence, the optimum modes close to the target value are the first and second modes and the optimum value of modulus of elasticity that keep them close to the zero is $E_{\text{optim}} = 2.09 \times 10^5 \text{ N/mm}^2$. Finally, there is big difference between results of experimentally estimated and numerically computed initial values of natural frequencies for the first two modes in *Table 6.1* and their corresponding updated values in *Table 6.3*. The changing from 7×10^{-6} to 9.4×10^{-4} of values of square relative difference of the first two modes refers to the convergence that produced due to E_{optim} value.

6.4.3 Simulation of damaged element in FE model

As mentioned previously in chapter-5, the centerline of the created crack position rests at 387.5 mm from the left support of the beam model which is the same location that simulated as a damaged element in the FE model, as shown in *Figure 6.2*. This element has number of 17 which is considered as a target element number during the final stage of damage detection optimization process.

6.5 Numerical calculations of the grid-bridge model

The same steps that previously adopted in the procedure of numerical calculations of the overhang beam model are implemented upon the grid-bridge model. These steps include performing numerical modal analysis upon the initial intact state of the model using ANSYS software and the implementing of calibration process.

6.5.1 FEM analysis of the initial intact model

A script configuration file contains routine of commands written in ANSYS language is used to create FE model of the grid-bridge without or with additional mass states. The script configuration file consists of about 300 steps. The two states of additional mass application are simulated as following.

6.5.1.1 Initial FE model without additional mass state

The initial adopted modulus of elasticity of the material of all used steel section is $E_{\text{initial}}=2 \times 10^9 \text{ N/m}^2$, the initial mass density is $D_{\text{initial}} = 7.86 \times 10^3 \text{ kg/m}^3$ and Poisson's ratio is $\nu = 0.3$. FE model is simulated to be similar to the experimental model except of some variations. The first variation is that, the numerical FE model is created without upper plate that covers the deck. Instead of that, the longitudinal stiffener beams are simulated to be with T-sections that have (45x50x1.5) mm dimensions of web, flange and thickness, respectively, *Figure 6.5*. Hence, the neighboring flanges of these T-sections provide the influence of the upper plate. The second variation includes providing additional transverse hidden stiffener beams to enhance the internal lateral supports for the bridge model.

Numerical modelling and adjustment of numerical results obtained by FEM and experimental results

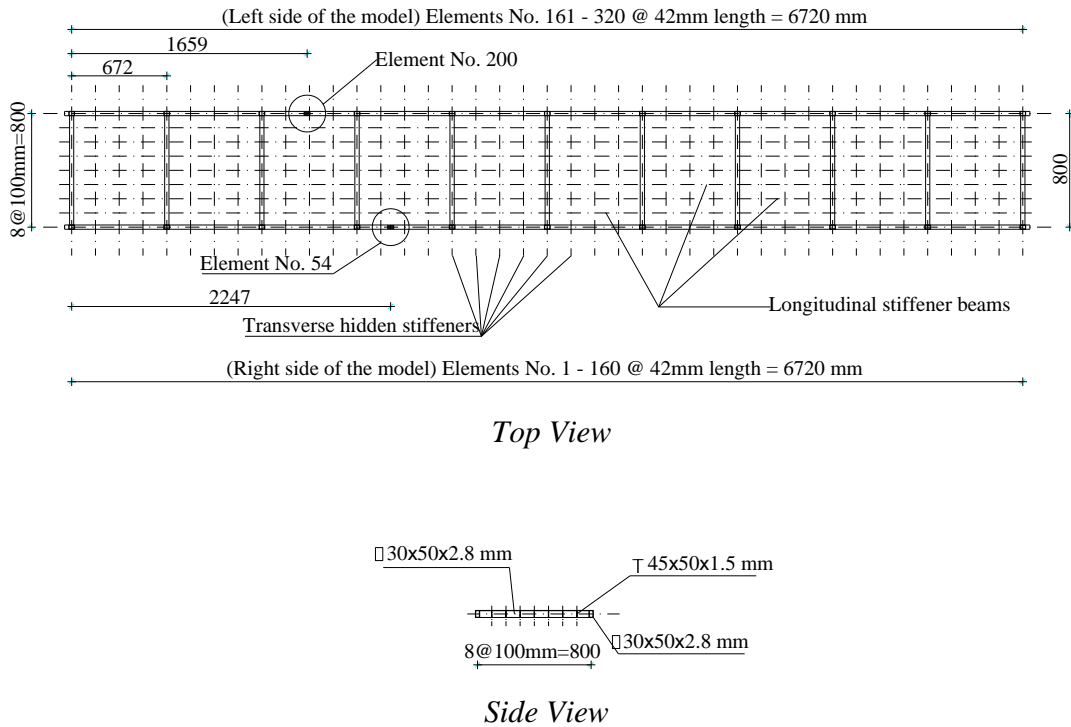


Figure 6.5: Details of initial FE grid-bridge model

The term *Hidden* refers to the zero mass density that characterizes the transverse stiffeners in order not to add any additional mass upon the FE model. These hidden transverse stiffeners are distributed laterally along the length of the FE model at each 168 mm c/c. Thus, 30 hidden transverse stiffeners, with (1.5x50) mm cross-section dimensions, are exist throughout the bridge length, as shown in *Figure 6.5*. Enhancing the internal lateral support of the FE model is aimed to prevent local modes in modal analysis. The FE model consists of 2424 elements with different lengths. The main elements that form the main two hollow beams have 42 mm length for each one, which are the candidate elements for the damage occurrence. Hence, there are 320 elements represent candidate elements to be damaged in the optimization process when the procedure seeks for the actual damaged element in the searching space, *Figure 6.5*. The same length of 42 mm is considered for the elements that forming the longitudinal stiffeners of the model. Other elements, that form the transverse main hollow beams and the transverse hidden stiffeners, have 100 mm length due to their minor role with respect to the damage occurrence. The state of the grid-bridge

model under its own mass only is simulated in ANSYS software to create and perform modal analysis of the FE model, as shown in *Figure 6.6*.

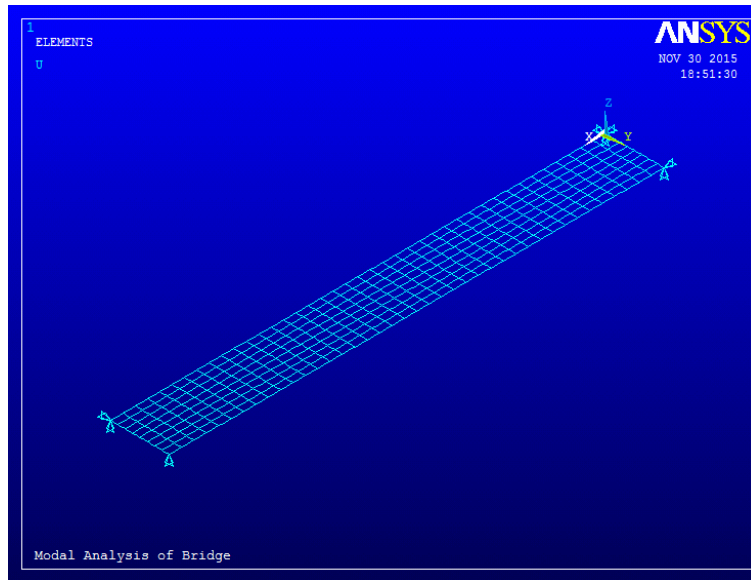


Figure 6.6: Grid-bridge FE model without additional mass created in ANSYS

Modal analysis is performed in ANSYS software upon the created initial intact FE model without additional mass state and the first five modes are computed and compared with their corresponding modes that extracted experimentally in chapter-5. Comparison of results between experimental values of natural frequencies with their corresponding numerical computed values are listed in *Table 6.4* based on the direct and square relative error (Err. (Hz)) and ((R.Err.)²), respectively.

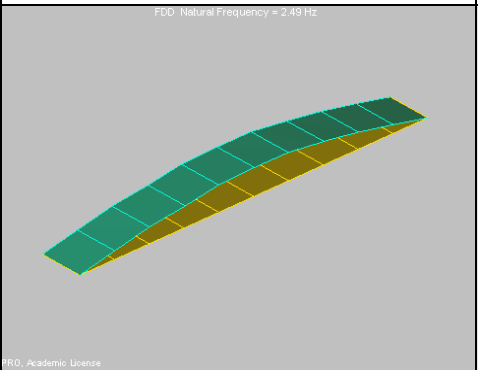
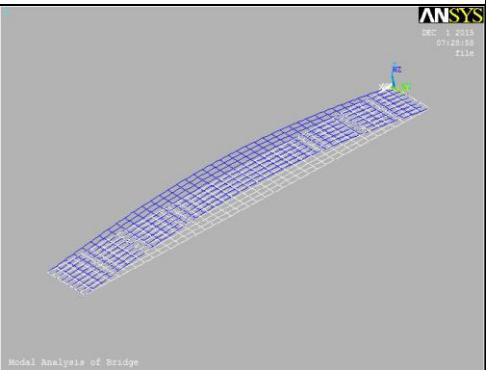
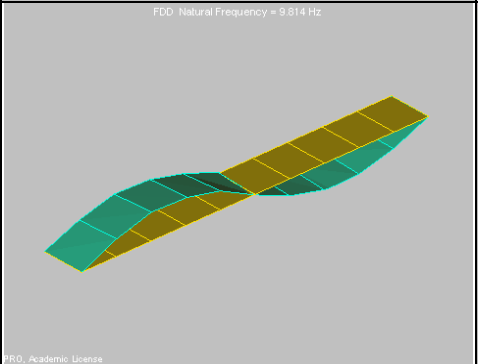
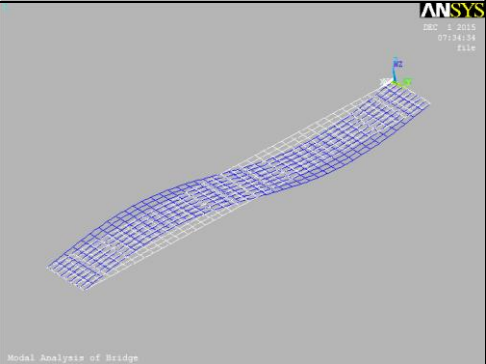
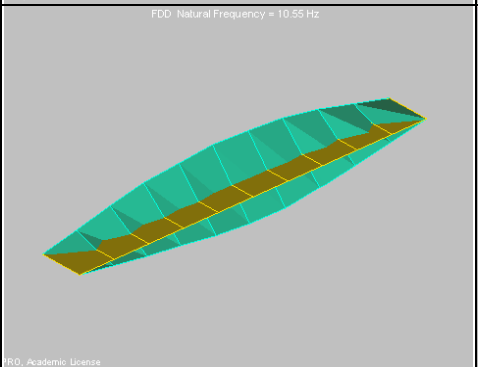
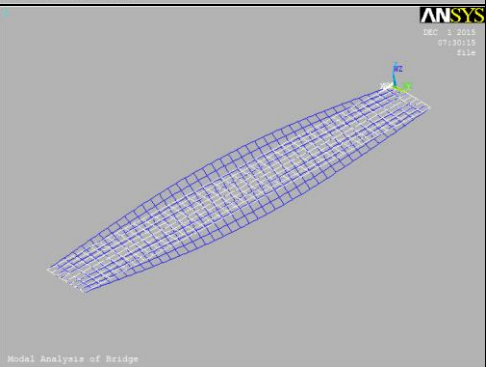
Table 6.4: Experimentally extracted and numerically computed values of natural frequencies of the intact initial FE grid-bridge model without additional mass state

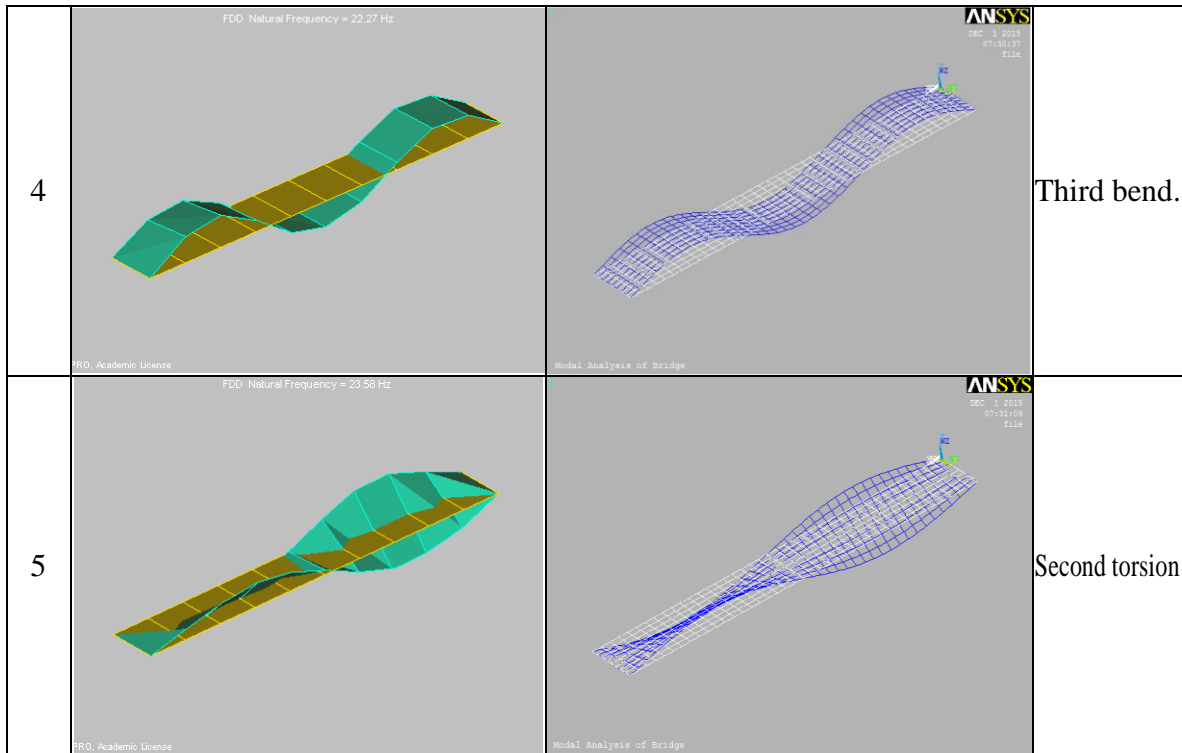
Mode No.	Values of natural frequencies (Hz)		Err. (Hz)	(R. Err.) ²
	Experimental/ Table 5.14	Numerical initial		
1	2.490	2.488	0.002	7.8 × 10 ⁻⁷
2	9.814	9.942	-0.128	0.00017
3	10.550	10.987	-0.437	0.00171
4	22.270	22.324	-0.054	5.9 × 10 ⁻⁶
5	23.580	23.766	-0.186	6.2 × 10 ⁻⁵
$\sum (R. Err.)^2$				0.00195

Numerical modelling and adjustment of numerical results obtained by FEM and experimental results

Experimentally extracted and numerically computed mode shapes, as well as the character of mode shapes, are shown in *Table 6.5*.

Table 6.5: Experimentally extracted and numerically computed mode shapes of the intact initial grid-bridge model without additional mass state

Mode No.	Mode shape extracted experimentally ARTeMIS software (Table 5.14)	Mode shape computed numerically ANSYS software	Mode shape character
1			First bend.
2			Second bend.
3			First torsion



6.5.1.2 Initial FE model with additional mass state

The same details that mentioned in the grid-bridge model without additional mass state are considered in the state of model with additional mass. The grid-bridge model that is exposed to 10 concrete cubes for the state of model with additional mass is simulated in ANSYS software. Another script configuration file is written in ANSYS language commands to create the FE model with additional mass state. All the used structural parameters are in their initial proposed values to produce the initial computed modal parameters. Analyzing the script configuration file in ANSYS software leads to the initial intact FE model with additional mass state, as shown in *Figure 6.7*. The same number, properties and lengths of elements that created in the FE model without additional mass state is created for the model with additional mass state. There are 10 additional elements represent the 10-masses of the FE model which are distributed along the deck as shown in *Figure 6.7*.

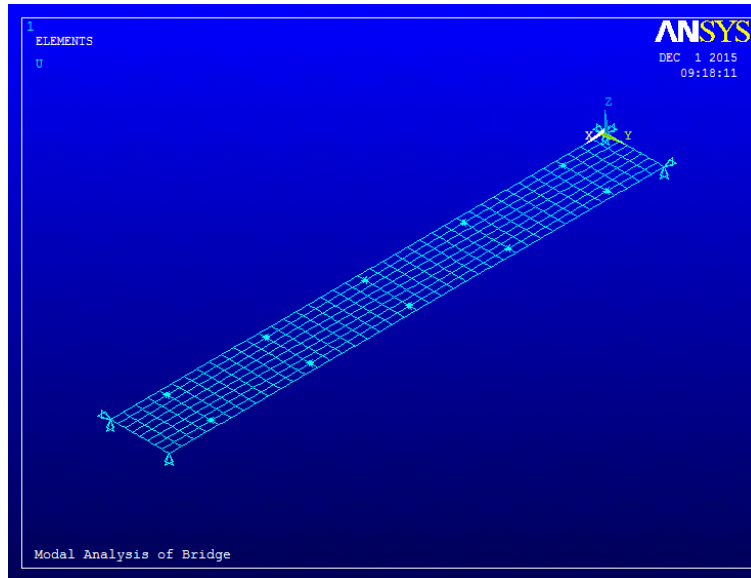


Figure 6.7: Grid-bridge FE model with additional mass state created in ANSYS

The masses are distributed along the bridge deck according to the dimensions that explained earlier in *Figure 5.23*. Masses are simulated to be distributed in the same locations that assigned in the experimental model described in chapter-5. According to the initial intact FE model with additional mass state, modal analysis is performed in ANSYS software and the first five modes are computed and compared with their corresponding modes that extracted experimentally in chapter-5.

Table 6.6: Experimentally extracted and numerically computed values of natural frequencies of the intact initial FE grid-bridge model with additional mass state

Mode No.	Values of natural frequencies (Hz)		Err. (Hz)	(R. Err.) ²
	Experimental/ARTeMIS Table 5.16	Numerical initial/ANSYS		
1	2.051	1.930	0.115	0.00313
2	8.093	7.720	0.369	0.00210
3	8.313	8.290	0.022	7.0x10 ⁻⁶
4	18.240	17.260	0.975	0.00286
5	18.640	17.870	0.762	0.00167
$\sum (R. Err.)^2$				0.00976

Characters of mode shapes that obtained numerically by ANSYS for the first five modes are the same as those obtained during the state of the FE model with additional mass. Hence, only values of the numerically computed natural frequencies of the FE model are considered in the comparison, as listed in *Table 6.6*.

6.5.2 Calibration process by updating of FE grid-bridge model

The advanced iterative FE route updating technique is adopted for calibration process upon the FE grid-bridge model, for both states of mass application, using the proposed TS optimization procedure. The dependence on just values of natural frequencies in the objective function as a convergence indicator is considered during the optimization procedure of calibration process. Hence, only the changes in values of natural frequencies are highlighted during this paragraph.

In the case of grid-bridge model, three structural parameters are adopted for the sake of FE model updating process. These include material modulus of elasticity, mass density and sides thickness of the main hollow rectangular beam of the model. Hence, the proposed TS optimization procedure consists of 3 variables in this case which are represented by the structural parameters. Usually, the allowable changes in structural parameters are relatively small (within $\pm 5\%$) and the corresponding mode shape character will be the same before and after the application of FE model updating process. The adopted updated structural parameters are used for each state of mass application, under the own mass and with additional mass state of the model. Under MATLAB environment, a script file is written for each state of mass application to implement FE model updating procedure according to the flow chart mentioned in *Figure 6.1* with about 300 steps. The routine is executed several times in order to find the sufficient number of iterations that could be adopted as termination criteria for the proposed TS procedure. Also, repetition of analysis is aimed to verify the optimum results of structural parameters that obtained in each analysis.

Table 6.7 exhibits total number of probable included values of each adopted structural parameter within the optimization process according to the minimum and maximum allowable limitations of equation (6.2).

Table 6.7: Total number of the included values of adopted structural parameters in the FE model updating procedure for the grid-bridge model

No. of variable	Type of included structural parameter	Minimum allowable value	Maximum allowable value	Total number of included values
1	E (N/mm ²)	1.90×10^5	2.10×10^5	41
2	D (Ns ² /mm ⁴)	7.46×10^{-9}	8.24×10^{-9}	40
3	t (mm)	2.66	2.94	29

where, E is the material modulus of elasticity, D is the mass density and t is the sides thickness of the main hollow rectangular beam of the model.

During the optimization process, each value inside the range of (Minimum allowable value and Maximum allowable value) is selected randomly. Hence, the total searching space contains 47560 (41x40x29) total probable solutions that could be obtained during the application of TS optimization procedure in the FE model updating process. In other words, the whole searching space is required to be searched for 47560 iterations in order to catch the accurate solution (best updated values of E , D and t) without using TS optimization procedure. Therefore, using of the proposed TS optimization procedure is aimed to achieve the optimum solution within reasonable number of iterations through checking a part of the total searching space. In the case of grid-bridge model, and due to several trial analyses, the proposed number of iterations is 1000 iterations which considered as the termination criterion for the proposed TS optimization procedure. Thus, the proposed TS optimization procedure checks only 2.1% (1000/47560) from the whole searching space to achieve the optimum solution.

6.5.2.1 Calibration of the grid-bridge model without additional mass state

The calibration process upon the FE grid-bridge model under its own mass only is implemented using the proposed TS optimization procedure. *Figure 6.8* shows the progress of the proposed TS optimization process during the FE model updating.

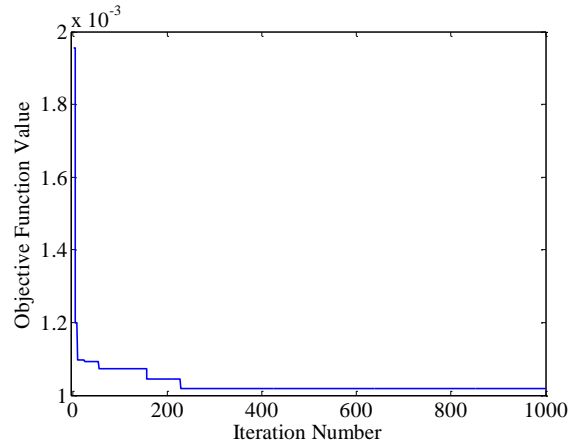


Figure 6.8: Improvement of FE model based on minimum objective function value by TS optimization procedure for grid-bridge model without additional mass state

It can be seen that in *Figure 6.8*, the optimum solution is achieved after 227 iterations which lead to the optimum updated structural parameters as following:

- 1- Optimum value of material modulus of elasticity $E = 2.035 \times 10^5 \text{ N/mm}^2$.
- 2- Optimum value of mass density $D = 8.22 \times 10^{-9} \text{ Ns}^2/\text{mm}^4$.
- 3- Optimum value of thickness $t = 2.66 \text{ mm}$.

The relative change in each value of structural parameters is within the range of (-5% to +5%) during the FE model updating process, as shown in *Figure 6.9*.

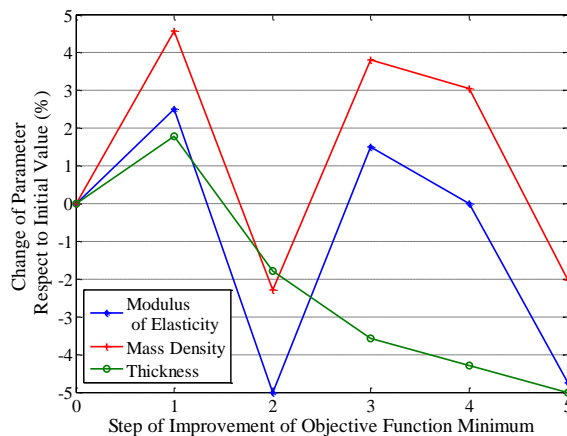


Figure 6.9: Change of structural parameters during the improvement of objective function minimum value of the model without additional mass state

The optimum (minimum) value of objective function, according to equation (6.4), after 227 iterations is 0.0010. This value refers to the summation of errors between values of natural frequencies that extracted experimentally and the corresponding values of natural frequencies that computed numerically for the first five modes of the grid-bridge model without additional mass state. The optimum values of structural parameters are applied in the modal analysis of the FE model using ANSYS software to compute values of natural frequencies for the first five modes of the updated FE grid-bridge model without additional mass state. A comparison with the values of natural frequencies of the initial FE grid-bridge model without additional mass state is produced in *Table 6.8*.

Table 6.8: Comparison between experimental, numerical initial and numerical updated values of natural frequencies of the grid-bridge model without additional mass state

Mode No.	Experimental values (Hz) (Table 5.14)	Numerical values (Hz) of the initial FE model	Error (Hz)	(R. Err.) ²	Numerical values (Hz) of the updated FE model	Error (Hz)	(R. Err.) ²
1	2.490	2.488	0.002	7.8×10^{-7}	2.458	0.032	0.00017
2	9.814	9.942	-0.128	0.00017	9.822	-0.008	6.9×10^{-7}
3	10.550	10.987	-0.437	0.00172	10.829	-0.279	0.00070
4	22.270	22.324	-0.054	5.8×10^{-6}	22.053	0.217	9.5×10^{-5}
5	23.580	23.766	-0.186	6.2×10^{-5}	23.431	0.149	3.9×10^{-5}
Objective function value (\sum (R. Err.) ²)				0.0019	\sum (R. Err.) ²		0.0010

According to *Table 6.8*, the calibration process leads to reduction in value of objective function of about 47% ($(0.0019-0.001)/0.0019$). This reduction reflects the amount of convergence between the experimentally extracted values of natural frequencies and their corresponding computed values of the updated FE model. With respect to values of natural frequencies of the experimental model, errors of natural frequency values of the updated FE model are lower than those existed in the original numerical model. The

amount of reduction in values of direct errors with respect to the natural frequency values of the experimental model are shown in *Figure 6.10*.

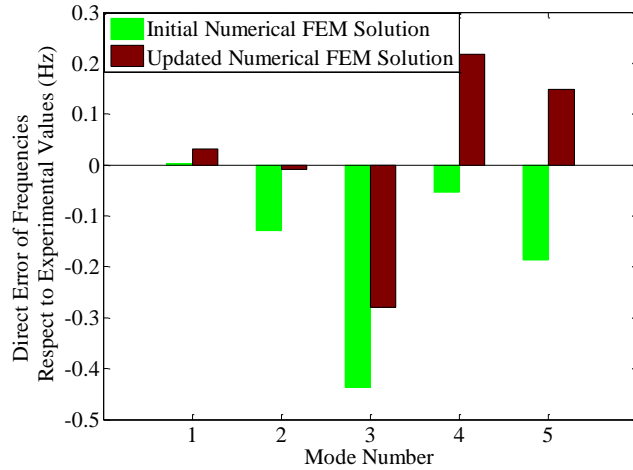


Figure 6.10: Errors of initial and calibrated FE modal frequencies respect to experimental values of the grid-bridge model without additional mass state

The degree of convergence between results of natural frequencies for the updated FE model and those for the initial FE model with respect to the corresponding experimentally extracted values are shown in *Figure 6.11*.

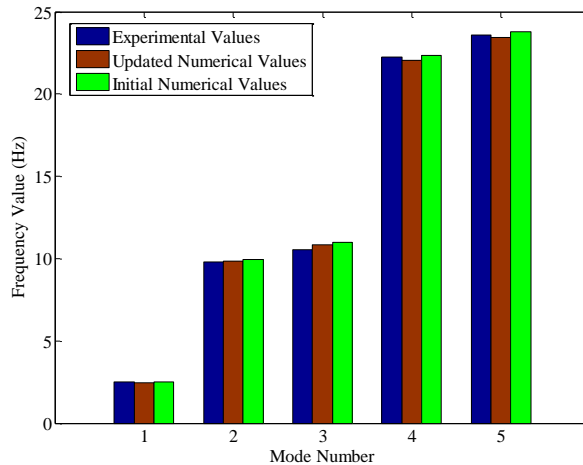


Figure 6.11: Convergence between experimental and numerical updated values of natural frequencies for the grid-bridge model without additional mass state using TS procedure

Although there are increasing in the errors with respect to the first and fourth modes, *Figure 6.10* and *Figure 6.11*, the convergence is achieved due to the significant reduction in errors with respect to the second, third and fifth modes which govern the final result.

6.5.2.2 Calibration of the grid-bridge model with additional mass state

The procedure of the advanced iterative FE route updating technique is performed to implement calibration process with respect to the grid-bridge model with additional mass state. Convergence progress during the proposed TS optimization procedure to update the structural parameters can be shown in *Figure 6.12*.

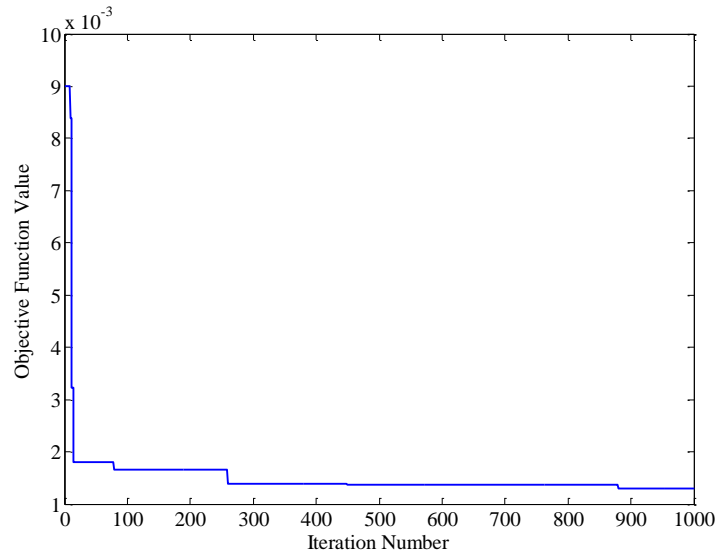


Figure 6.12: Improvement of FE model correlation based on minimum objective function value by TS optimization procedure for grid-bridge model with additional mass state

The optimum solution is achieved after 880 iterations which lead to the optimum updated structural parameters as following:

- 1- Optimum value of material modulus of elasticity $E = 2.1 \times 10^5 \text{ N/mm}^2$.
- 2- Optimum value of mass density $D = 7.46 \times 10^{-9} \text{ kg/mm}^3 \text{ (Ns}^2\text{/mm}^4\text{)}$.
- 3- Optimum value of thickness $t = 2.79 \text{ mm}$.

The relative change in each value of updated structural parameter during the optimization process can be shown in *Figure 6.13*.

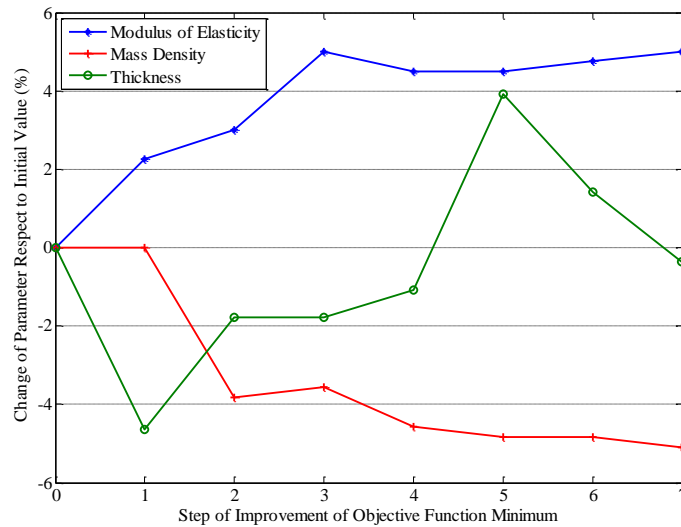


Figure 6.13: Change of structural parameters during the improvement of objective function minimum value of the model with additional mass state

According to *Figure 6.13*, the changes happened 7 times during the optimization process for the three adopted structural parameters which are still within the permissible limits of equation (6.2), as shown.

Performing modal analysis upon the FE model using the updated structural parameters, modulus of elasticity, mass density and thickness, leads to the updated FE grid-bridge model with additional mass state.

The comparisons between the experimental values of natural frequencies with their corresponding numerical initial values as well as the numerical updated values of FE grid-bridge model with additional masses, are listed in *Table 6.9*.

The value of objective function minimum of 0.00128 indicates to a reduction of about 86% $((0.00976-0.00128)/0.00976)$ in error with respect to the initial FE model before updating, as shown in *Figure 6.14*.

Table 6.9: Comparison between experimental, numerical initial and numerical updated values of natural frequencies of the grid-bridge model with additional mass state

Mode No.	Experimental values (Hz) (Table 5.16)	Numerical values (Hz) of the initial FE model	Error (Hz)	(R. Err.) ²	Numerical values (Hz) of the updated FE model	Error (Hz)	(R. Err.) ²
1	2.051	1.936	0.115	0.00313	2.015	0.036	0.00030
2	8.093	7.724	0.369	0.00210	8.039	0.054	4.4x10 ⁻⁵
3	8.313	8.291	0.022	7.0x10 ⁻⁶	8.502	-0.189	0.00052
4	18.240	17.262	0.975	0.00286	17.966	0.271	0.00022
5	18.640	17.878	0.762	0.00167	18.376	0.264	0.00020
Objective function value (\sum (R. Err.) ²)				0.00976	\sum (R. Err.) ²		0.00128

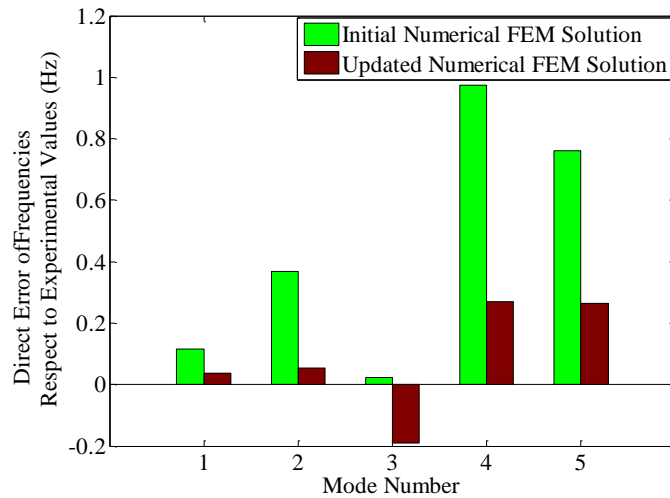


Figure 6.14: Errors of initial and calibrated FE modal frequencies respect to experimental values of the grid-bridge model with additional mass

Also, the degree of convergence between results of natural frequencies for the updated FE model and those for the initial FE model with respect to the experimentally extracted values of natural frequencies are shown in *Figure 6.15*.

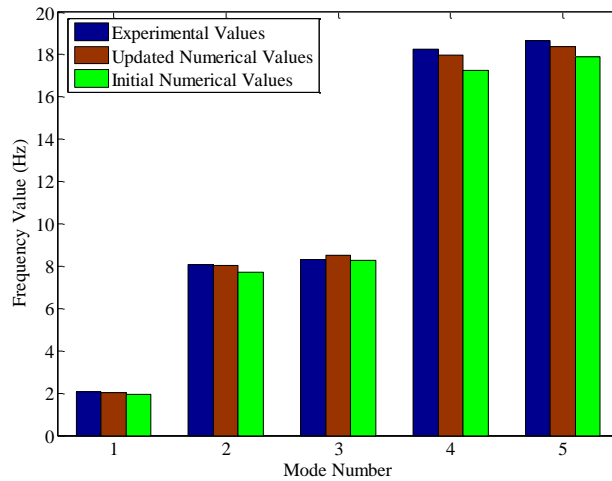


Figure 6.15: Convergence between experimental and numerical updated values of natural frequencies for the grid-bridge model with additional mass state using TS procedure

The updating process increases error only in the third mode while all other four modes have got decrease in errors values, as shown in *Figure 6.14* and *Figure 6.15*.

6.5.3 Equivalent of severity of damage with respect to the used length of element in FE model

As mentioned earlier in chapter-5, three different damage severities are applied upon the experimental grid-bridge model which are considered as significant damage cases. These severities are (21x11.5) mm, (21x20) mm and (42x20) mm, for damage length and depth, respectively. In the FE element model, the damaged element has 42 mm length and the whole length is simulated to be damaged during the analysis. It is clear that there is compatibility between damage length in both experimental and numerical FE models for the case of damage severity of (42x20) mm, but for other cases it is not. Hence, damage length in the simulation of FE model should be equivalent to the actual damaged length in the experimental model. During numerical simulation of the damage, stiffness of the whole element have to be reduced, despite of the crack length could be smaller than the element length in FE model. In order to treat this case, the amount of the displacement of deflected simulated cantilevered element which has 42 mm length is considered as an indication for the severity of applied damage with a certain length. The adopted element in the simulated

FE model is analyzed statically as a cantilever beam subjected to a certain fix value of bending moment in the free end to determine the highest value of displacement. When applying the first severity of damage (21x11.5) mm, length and depth respectively, on the cantilevered 42 mm element, there will be a certain displacement exists at the free end under the action of applied fixed bending moment. This value of displacement (or close to it) will be the target result that should be achieved when applying different values of depth of damage under the length of whole 42 mm element. By trial and error, the value of damaged depth of the whole 42 mm element which gives the same displacement as produced by applying the (21x11.5) mm damage dimensions on the same cantilevered element, will be the equivalent damage depth value.

The static structural analysis of the cantilevered element is performed by ANSYS software to compute the displacements under fixed concentrated moment value M with different depths of crack, as shown in *Figure 6.16*. *Figure 6.16* shows the simulated 42 mm cantilevered element under both case of damage, actual and equivalent. The results show that the value of damage of 42 mm width by 5.4 mm depth is the equivalent damage value that corresponds to the experimental (real) damage value of 21 mm length by 11.5 mm depth. The same procedure is applied for the second severity of damage which has a damage size of 21 mm length by 20 mm depth in the experimental model. In this case, the equivalent damage value is 42 mm length by 13.4 mm depth, as shown in *Figure 6.16*.

Table 6.10 summarizes results of actual applied damage on the model and their equivalent values that could be simulated in the FE model.

The last row in *Table 6.10* represent values of displacements of the extreme free edge point of the cantilevered 42 mm element shown in *Figure 6.16*.

The concept of damage equivalent value is considered as an approximate indication due to the dependence on higher displacement only during the comparison process. This concept is adopted for the prismatic damage only. If the damage has non-prismatic shapes then the concept of minimum value of objective function that obtained according a certain severity of damage value is considered and the optimum value of damage severity is adopted.

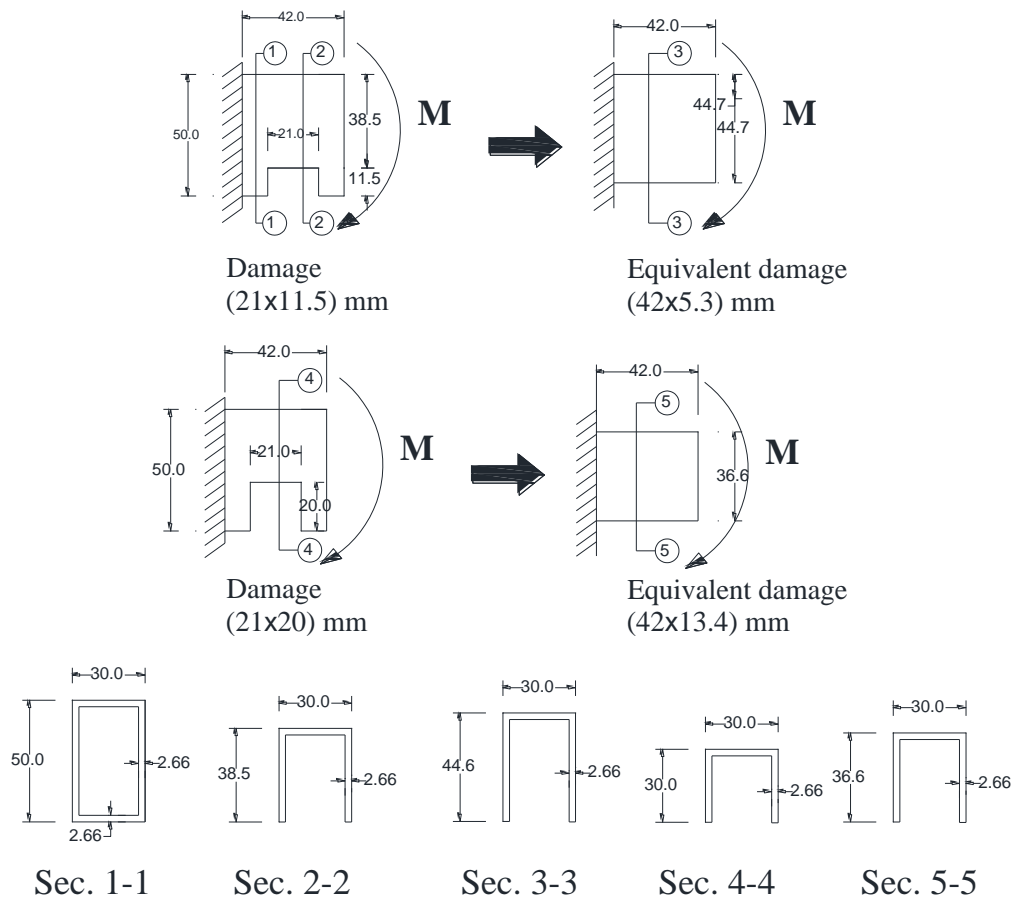


Figure 6.16: Equivalent damage value for the cantilevered 42mm element model

Table 6.10: Equivalent damage severity

Article	Implemented damage severities		
	First damage severity <i>RAGDC-1</i>	Second damage severity <i>LAGDC-1M</i>	Third damage severity <i>RAGDC-2, LAGDC-1, RAGDC-1M, LAGDC-2M</i>
	(length x depth) mm	(length x depth) mm	(length x depth) mm
Actual damage severity	21x11.5	21x20	42x20
Equivalent damage severity	42x5.3	42x13.4	42x20
Displacement value in the cantilevered element model (mm)	0.069	0.121	-----

6.5.4 Simulation of damaged elements in FE model

In the case of FE grid-bridge model, the simulated damaged element for the right side damage scenario has the rank of 54, which corresponds to the distance of 2247 mm from the nearest end of the bridge model, as shown in *Figure 6.5*. While, for the damage scenario in the left side of bridge, the damaged element in the FE model is located on element number 200 which corresponds to the distance of 1659 mm from the nearest end of the bridge model, *Figure 6.5*. Hence, the elements number 54 and 200 represent the target elements for the right and left side damage scenario, respectively, during the final stage of damage detection optimization process.

6.6 Numerical calculations of the Vierendeel bridge model

The procedures of numerical calculations are considered for the case study of Vierendeel bridge model. Performing of modal analysis upon the FE model using ANSYS software and applying the calibration process are the main subjects which are highlighted in this paragraph.

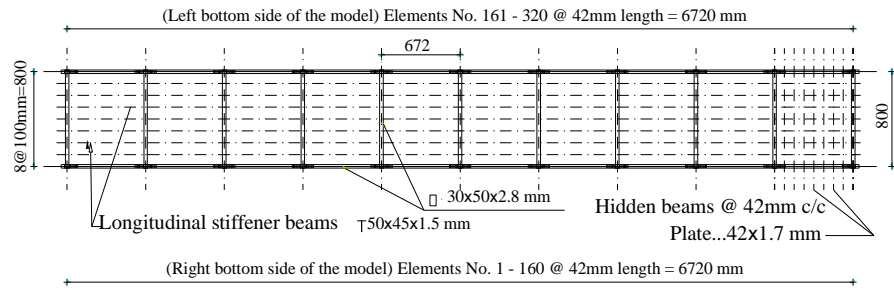
6.6.1 FEM analysis of the initial intact model

A special script configuration file contains routine of commands written in ANSYS language is adopted to create and analyze FE Vierendeel bridge model. The script configuration file consists of approximately 500 steps. This procedure is implemented separately for each states of mass application, without and with additional mass states.

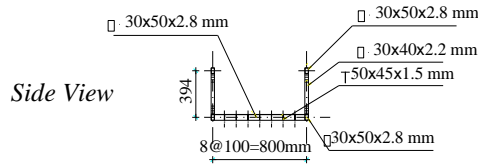
6.6.1.1 Initial FE model without additional mass state

The deck of the Vierendeel bridge model represents the grid-bridge model and two fences are added to form the whole Vierendeel bridge. Similar FE simulation of the grid-bridge model is considered in the simulation of FE Vierendeel bridge model except the distribution of hidden beams. They are distributed at 42 mm c/c instead of 168 mm c/c with cross section of (1.7x42) mm dimensions in this case study, *Figure 6.17 (a)*.

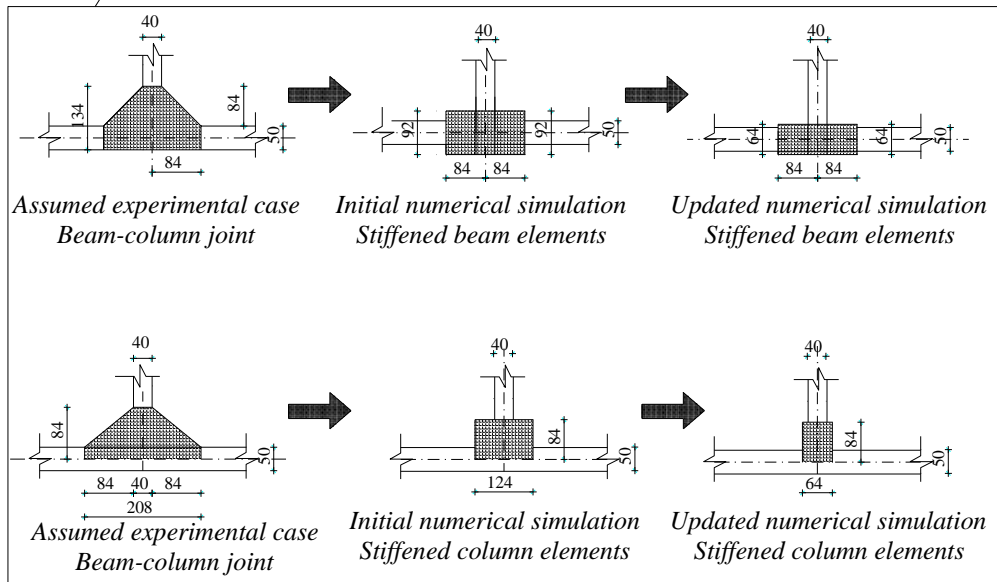
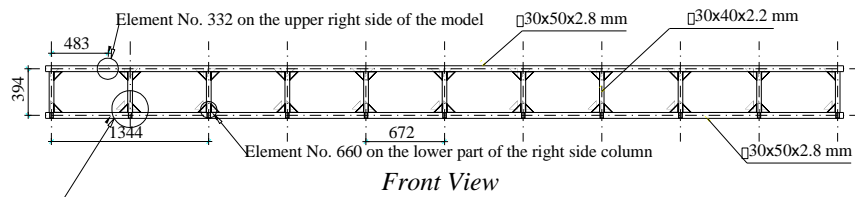
Numerical modelling and adjustment of numerical results obtained by FEM and experimental results



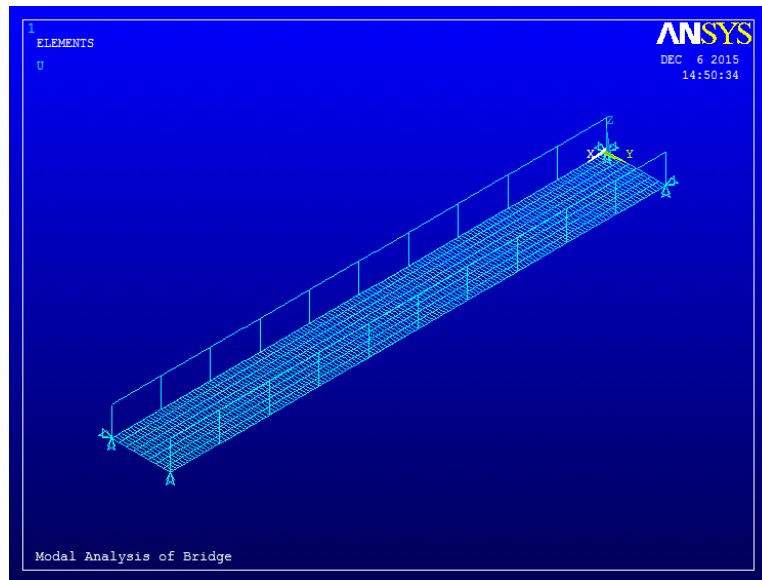
Top View



For the upper right side of the model: Elements No. 321 - 480. For the upper left side of the model: Elements No. 481 - 640.



(a)



(b)

Figure 6.17: (a) Details of the initial FE Viereendeel bridge model, (b) Viereendeel bridge FE model without additional mass created in ANSYS

The total number of elements is 5932 for the case of model without additional mass. The length of each element that consists the main longitudinal hollow beams is 42 mm. In this case, there are 640 elements consist the four upper and lower main beams which are candidates to be damaged in the optimization procedure. The elements that forming columns have 42 mm length for each one and the total elements in all columns are 198 elements. Other elements that rest on the transverse beams, main hollow and hidden beams, are still have the same length that adopted previously in the grid-bridge model. The initial adopted modulus of elasticity of the material of all used steel sections is $E_{\text{initial}}=200$ GPa, the initial mass density is $D_{\text{initial}} = 7.86 \times 10^3$ kg/m³ and Poisson's ratio is $\nu = 0.3$. Also, the initial proposed cross sectional dimensions of the stiffened beam elements which are existed in the lower and upper parts of the Viereendeel columns (locations of beam-column joints) are assumed to be (30x92x2.8) mm. The value of 92 mm represents the length of the longer side of the stiffened beam element cross section (L_{stif}), while the corresponding initial value of the stiffened column element is assumed to be 124 mm. The selection of

these values (92 mm and 124 mm) is assumed because the elements in these locations are tapered. The stiffened beam elements have 50 mm depth of cross section in one side and 134 mm (50+84) in the other, where the value of 84 mm is the double of 42 mm which is the length of elements in the FE model. Hence, the average value is assumed to be the approximately adopted value which is 92 mm $((134+50)/2)$ in the calculations of initial values of natural frequencies. The same concept is adopted for the stiffened column elements which have 208 mm (84+40+84) in one side and 40 mm in the other. Then, the average value is 124 mm $((208+40)/2)$ which is assumed to simulate the tapered shape of the stiffened elements in the FE model. All the previously mentioned details, *Figure 6.17 (a)*, are considered for both states of model: without and with additional mass states.

The designed script configuration file is implemented in ANSYS software to create and analyze the FE model of the intact Vierendeel bridge without additional mass state, as shown in *Figure 6.17 (b)*.

Modal analysis in ANSYS software is performed upon the FE model and the first five modes are computed and compared with their corresponding modes that extracted experimentally, as listed in *Table 6.11*.

Table 6.11: Experimentally extracted and numerically computed values of natural frequencies of the intact initial FE Vierendeel model without additional mass state

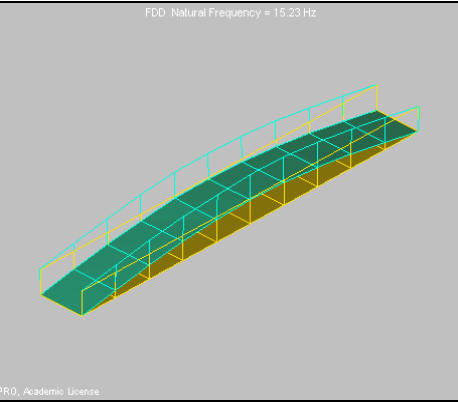
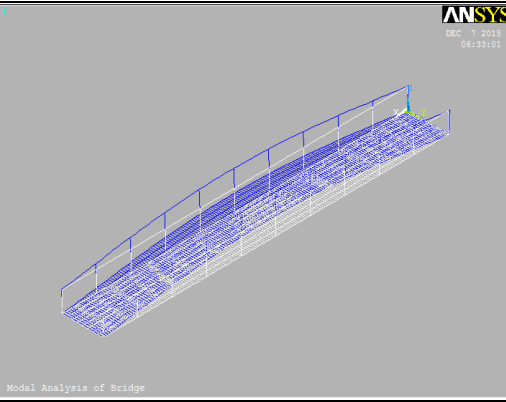
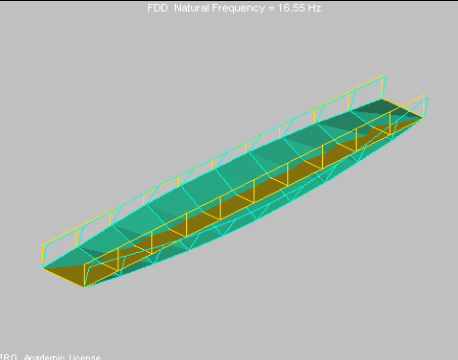
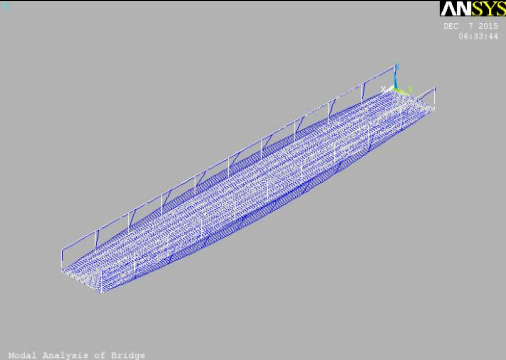
Mode No.	Values of natural frequencies (Hz)		Err. (Hz)	(R. Err.) ²
	Experimental/ARTeMIS (Table 5.23)	Numerical/ANSYS		
1	15.230	17.250	-2.020	0.01759
2	16.550	18.123	-1.573	0.00903
3	35.890	40.825	-4.935	0.01891
4	36.180	40.896	-4.716	0.01699
5	42.700	49.085	-6.385	0.02236
Value of objective function ($\sum (R. Err.)^2$) for the first 4 modes only				0.0625
Value of objective function ($\sum (R. Err.)^2$) for the first 5 modes				0.0849

Numerical modelling and adjustment of numerical results obtained by FEM and experimental results

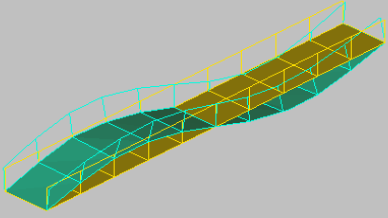
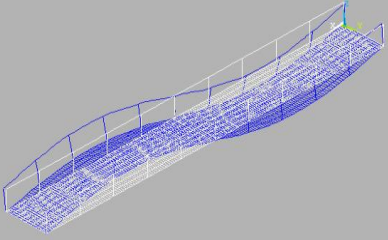
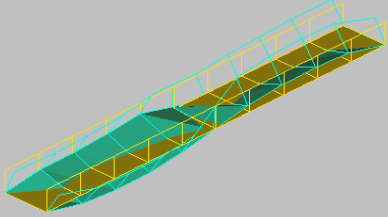
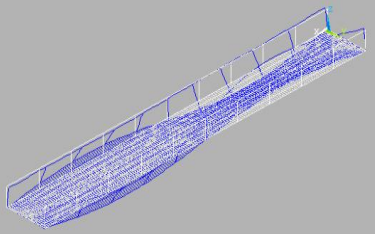
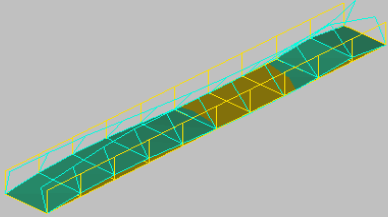
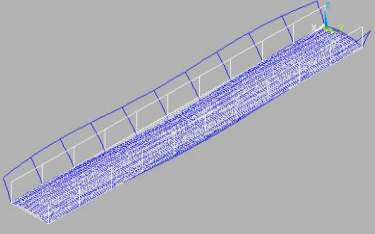
Due to the relatively high difference between value of the fifth mode of experimental natural frequency and the corresponding value of numerical natural frequency, *Table 6.11*, the inclusion of this mode in the procedures of calibration process is examined in the next stages. Thus, both values of objective function without or with inclusion of the fifth mode are listed in *Table 6.11*.

Also, a comparison between the experimentally extracted and numerically computed mode shapes, and their characters, are exhibited in *Table 6.12*.

Table 6.12: Experimentally extracted and numerically computed mode shapes of the intact initial Vierendeel bridge model without additional mass state

Mode No.	Mode shape extracted experimentally ARTeMIS software (Table 5.23)	Mode shape computed numerically ANSYS software	Mode shape charact.
1	 <p style="font-size: small;">FDD Natural Frequency = 15.23 Hz</p> <p style="font-size: x-small;">RO, Academic License</p>	 <p style="font-size: x-small;">ANSYS DEC 7 2015 06:33:01</p> <p style="font-size: x-small;">Modal Analysis of Bridge</p>	First bend.
2	 <p style="font-size: small;">FDD Natural Frequency = 16.55 Hz</p> <p style="font-size: x-small;">RO, Academic License</p>	 <p style="font-size: x-small;">ANSYS DEC 7 2015 06:33:44</p> <p style="font-size: x-small;">Modal Analysis of Bridge</p>	First torsion

Numerical modelling and adjustment of numerical results obtained by FEM and experimental results

3	<p style="text-align: center;">FDD Natural Frequency = 35.89 Hz</p>  <p style="text-align: center;">RO, Academic License</p>	<p style="text-align: center;">ANSYS DEC 7 2015 06:34:15</p>  <p style="text-align: center;">Modal Analysis of Bridge</p>	Second bend.
4	<p style="text-align: center;">FDD Natural Frequency = 36.10 Hz</p>  <p style="text-align: center;">RO, Academic License</p>	<p style="text-align: center;">ANSYS DEC 7 2015 06:34:45</p>  <p style="text-align: center;">Modal Analysis of Bridge</p>	Second torsion
5	<p style="text-align: center;">FDD Natural Frequency = 42.7 Hz</p>  <p style="text-align: center;">RO, Academic License</p>	<p style="text-align: center;">ANSYS DEC 7 2015 06:35:19</p>  <p style="text-align: center;">Modal Analysis of Bridge</p>	Third bend.

In *Table 6.12*, the similarity between mode shape characters of the experimentally extracted modes and their corresponding characters of the numerically estimated modes are clearly shown.

6.6.1.2 Initial FE model with additional mass state

FE model for the Vierendeel bridge with additional mass state is simulated by another script configuration file that written in ANSYS language commands and the created FE model is shown in *Figure 6.18*.

The mass distribution appears clearly in *Figure 6.18* which are located in the same positions as in the case study of grid-bridge model with additional mass state.

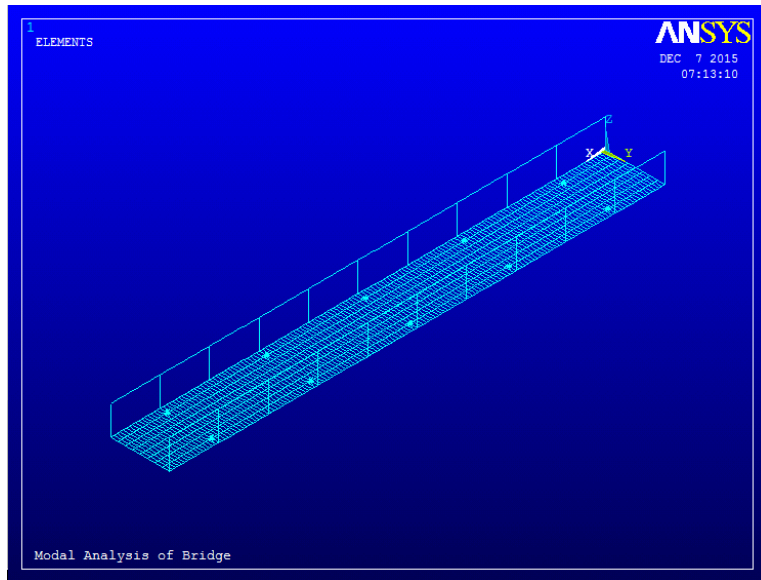


Figure 6.18: Vierendeel bridge FE model with additional mass state created in ANSYS

Modal analysis is performed upon the initial intact FE model of the Vierendeel bridge with additional mass state using ANSYS software to compute the first five modes under the initial proposed structural parameters values as listed in *Table 6.13*.

Table 6.13: Experimentally extracted and numerically computed values of natural frequencies of the intact initial FE Vierendeel model with additional mass state

Mode No.	Values of natural frequencies (Hz)		Err. (Hz)	(R. Err.) ²
	Experimental/ARTeMIS (Table 5.25)	Numerical/ANSYS		
1	13.220	14.688	-1.468	0.01233
2	14.900	16.532	-1.632	0.01199
3	30.910	34.647	-3.737	0.01462
4	32.630	37.736	-5.106	0.02449
5	42.630	47.960	-5.330	0.01563
Value of objective function ($\sum (R. Err.)^2$) for the first 4 modes only				0.06341
Value of objective function ($\sum (R. Err.)^2$) for the first 5 modes				0.07906

In *Table 6.13*, The computed values of natural frequencies for the first five modes are compared with their corresponding values that extracted experimentally. Similar mode shape characters are obtained in this analysis as those obtained earlier in the analysis of FE model without additional mass state, hence, only values of natural frequencies are listed in *Table 6.13* to show the comparison.

6.6.2 Calibration process by updating of FE Vierendeel bridge model

The advanced iterative procedure of calibration process by FE model updating is implemented upon the Vierendeel bridge model using the proposed TS optimization procedure. The same objective function that depends on error between the corresponding frequencies is adopted in the optimization process. For each state of mass application, a special routine is written according to MATLAB environment. The routine consists of about 480 steps to perform the procedure of calibration process using TS optimization procedure, based on *Figure 6.1*. For the proposed TS optimization procedure, the routine is executed several times in order to find the sufficient number of iterations that could be adopted as a termination criterion. Also, the analysis is repeated to insure the validity of the optimum updated structural parameter values that obtained by the proposed procedure. The allowable changes of the updated structural parameters are within the limits of $\pm 5\%$ (except of one parameter excluded represents the length of longest side of the column stiffener). Hence, the updated mode shape before and after the calibration process are the same and will not be redrawn during the next paragraph.

6.6.2.1 Calibration of the Vierendeel bridge model without additional mass state

The calibration process upon the FE Vierendeel bridge model under its own mass only is implemented using the proposed TS optimization procedure. In this state of model, the objective function that used in TS optimization procedure is adopted according to two cases of included modes, five modes in the first case and four modes in the other. The included number of modes is aimed to study the influence of including or excluding the last fifth mode which exhibits relatively high difference between experimental and numerical values of natural frequencies, as listed in *Table 6.11*.

6.6.2.1.1 Including of five modes in the objective function

Three structural parameters are included during the FE model updating process for the sake of calibration. They include material modulus of elasticity (E), the length of the longer side of the stiffened element cross section (L_{stif}) and sides thickness of the main hollow rectangular beam (t). The stiffened elements are assumed to have the same dimensions in all locations of their existence which are on the start and end of each column and main hollow longitudinal beam. The value of (L_{stif}) is excluded from the range $\pm 5\%$ and the ratio of $\pm 15\%$ is considered due to the high uncertainty between the original and simulated models. *Table 6.14* exhibits total number of probable included values of each adopted structural parameter within the optimization process according to the minimum and maximum allowable limitations of equation (6.2).

Table 6.14: Total number of the included values of adopted structural parameters in the FE model updating procedure for the Vierendeel bridge model using five modes

No. of variable	Type of included structural parameter	Minimum allowable value	Maximum allowable value	Total number of included values
1	E (N/mm ²)	1.9×10^5	2.1×10^5	41
2	L_{stif} (mm)	55	75	21
3	t (mm)	2.66	2.94	29

Values inside the range (Minimum allowable values and Maximum allowable values) are selected randomly during the optimization process. Therefore, the searching space contains 24969 ($41 \times 21 \times 29$) solutions that likely to be checked throughout the whole domain. The proposed TS optimization procedure checks only 4.00% ($1000/24969$) from the whole search space to achieve the optimum solution. The progress of the proposed TS optimization process with objective function that includes five modes during the FE model updating can be shown in *Figure 6.19*.

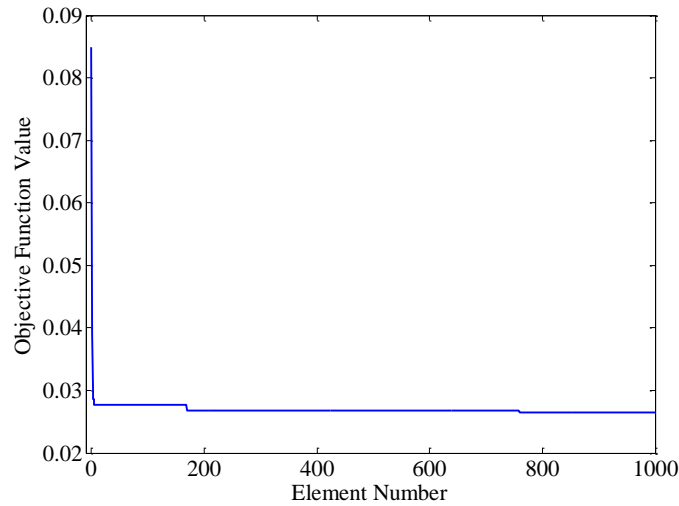


Figure 6.19: Improvement of FE model correlation based on minimum objective function value by TS optimization procedure for Vierendeel model without additional mass state using five modes

As shown in *Figure 6.19*, after 759 iterations, the optimum solution is achieved by reducing the objective function from initial value of 0.0849 to the updated value of 0.0265 including five modes. The optimization procedure leads to the optimum updated structural parameters as following:

- 1- Optimum value of material modulus of elasticity $E = 1.905 \times 10^5$ N/mm².
- 2- Optimum value of longer side of the stiffened element cross section $L_{\text{stif}} = 64$ mm.
- 3- Optimum value of thickness $t = 2.93$ mm.

6.6.2.1.2 Including of four modes in the objective function

Excluding of the fifth mode is considered in this case to insure the validity of optimum structural parameter values that obtained in the previous case. Moreover, an extensive study on the ability of using either three or four structural parameters is implemented. Using the same structural parameters of E , L_{stif} and t in the calibration process in the first trials and including the mass density (D) in the other trials. The total number of probable included values of each adopted structural parameter within the optimization process according to the minimum and maximum allowable limitations are the

same as in *Table 6.14* for the three included structural parameters. For the trials of four included structural parameters, the total number of probable included values of D are listed in *Table 6.15*.

Table 6.15: Total number of the included values of adopted mass density in the FE model updating procedure for the Vierendeel bridge model using four modes

No. of variable	Type of included structural parameter	Minimum allowable value	Maximum allowable value	Total number of included values
1	D (Ns ² /mm ⁴)	7.46×10^{-9}	8.24×10^{-9}	39

Therefore, the whole searching space in the trials of three included structural parameters is 24969 solutions (as in the case of 5 included modes) while for the trials of four included variables, it consists of 973791 (41x21x29x39) solutions. This means that TS optimization procedure explores only 0.10% (1000/973791) from the whole searching space. Calibration process by TS optimization procedure is implemented several times using either three or four included structural parameters. Results of the calibration process are listed in *Table 6.16* for both cases of using either three or four included updated structural parameters. According to *Table 6.16*, the values of updated structural parameters of $E = 1.905 \times 10^5$ (N/mm²), $L_{stif} = 64$ mm and $t = 2.93$ mm exhibit the minimum value of objective function. Hence, these values are adopted and considered as the optimum updated structural parameters. On the other hand, these values are exactly the same as those obtained previously in the case of using five modes in the objective function which verifies the validity of the updated values of structural parameters. Thus, obtaining exactly the same values of optimum structural parameters in both cases of using either 5 or 4 included modes in the objective function, with minimum value of objective function, indicates the ability of using any of them in the calibration procedure.

Table 6.16: Implementing TS optimization process using three and four included structural parameters upon FE Vierendeel without additional mass state using four modes only

Analysis No.	Including 3 structural variables				Including 4 structural variables				
	Type of variables			Value of objective function	Type of variables				Value of objective function
	E (N/mm ²)	L_{stif} (mm)	t (mm)		E (N/mm ²)	L_{stif} (mm)	t (mm)	D (Ns ² /mm ⁴)	
1	1.905x10 ⁵	64	2.90	0.00094	2.075x10 ⁵	74	2.86	7.46x10 ⁻⁹	0.0030
2	1.905x10 ⁵	64	2.93	0.00089	2.080x10 ⁵	75	2.75	7.56x10 ⁻⁹	0.0032

The progress of the proposed TS optimization procedure during the FE model updating which leads to the adopted optimum values of structural parameters is shown in *Figure 6.20*.

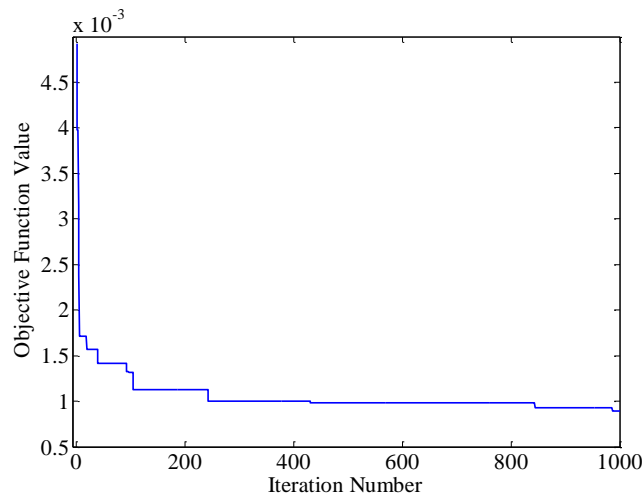


Figure 6.20: Improvement of FE model correlation based on minimum objective function value by TS optimization procedure for Vierendeel model without additional mass state using four modes

Although *Figure 6.20* should start from the initial value of objective function of 0.0625 (using only 4 modes, *Table 6.11*), it is started from the value of 0.005 to appear the convergence in values of objective function in the lower part of the graph obviously. Hence, *Figure 6.20* shows that after 987 iterations, the optimum solution is reached with

Numerical modelling and adjustment of numerical results obtained by FEM and experimental results

decreasing the objective function value from initial value 0.0625 to 0.00089, Table 6.16. The relative change upon each parameter during iterations is shown in Figure 6.21, which contains 13 successful iterations to reach optimum solution for the three updated structural parameters during the optimization process.

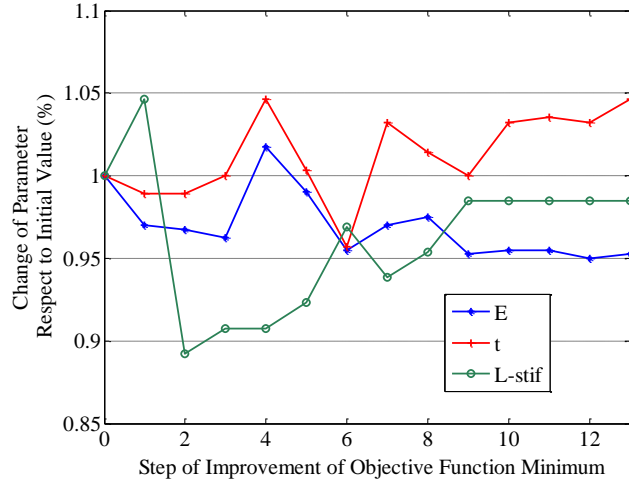


Figure 6.21: Change of structural parameters during the improvement of objective function minimum value of the Vierendeel model without additional mass state

Table 6.17: Comparison between experimental, numerical initial and numerical updated values of natural frequencies of the Vierendeel bridge model without additional mass state

Mode No.	Experimental values (Hz) (Table 5.23)	Numerical values (Hz) of the initial FE model	Error (Hz)	(R. Err.) ²	Numerical values (Hz) of the updated FE model	Error (Hz)	(R. Err.) ²
1	15.230	17.250	-2.020	0.01759	15.254	-0.024	2.5×10 ⁻⁶
2	16.550	18.123	-1.573	0.00903	16.691	-0.141	7.3×10 ⁻⁵
3	35.890	40.825	-4.935	0.01891	35.160	0.730	0.00041
4	36.180	40.896	-4.716	0.01699	36.906	-0.726	0.00040
5	42.700	49.085	-6.385	0.02236	49.533	-6.833	0.02561
Objective function value (∑ (R. Err.) ²)				0.0849	∑ (R. Err.) ²		0.0265

According to the optimum updated values of structural parameters, values of the computed updated natural frequencies are compared with their corresponding initial values with respect to their corresponding values that extracted experimentally as shown in *Table 6.17*. In *Table 6.17*, the reduction in value of objective function from value of 0.0849 to 0.0265 refers to the convergence between the experimental and computed values of natural frequencies due to the calibration process. The convergence behavior can be displayed according either to the values of direct difference between the experimental and computed (initial and updated) values of natural frequencies or each value of natural frequencies, as shown in *Figure 6.22* and *Figure 6.23*, respectively.

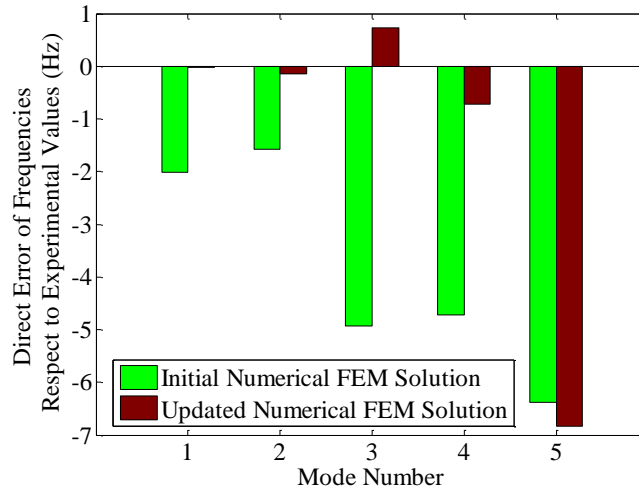


Figure 6.22: Errors of initial and calibrated FE modal frequencies respect to experimental values of the Vierendeel bridge model without additional mass state

Figure 6.22 and *Figure 6.23* show that only the fifth mode exhibits divergence between the initial and updated values of natural frequencies. While, for the other four modes the convergence behavior is clearly shown due to the calibration process.

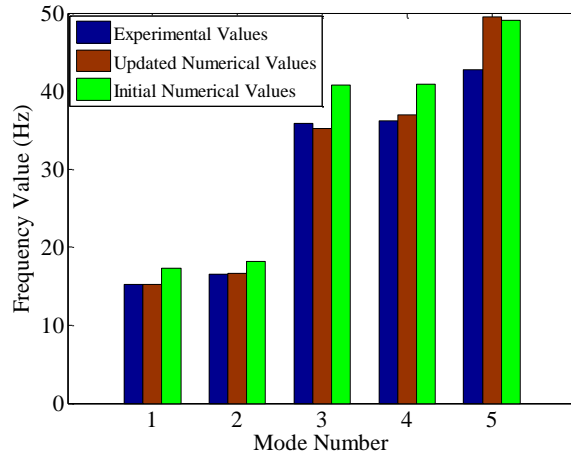


Figure 6.23: Convergence between experimental and numerical updated values of natural frequencies for the Vierendeel model without additional mass state using TS procedure

6.6.2.2 Calibration of the Vierendeel bridge model with additional mass state

Based on the conclusions that obtained earlier in the case of model under its own mass only, four mode shapes are sufficient to be considered in the present case of model with additional mass state during the calibration process. The number of included variables (structural parameters) in the optimization process is investigated also as implemented previously in the case of model under its own mass only. Two trials are listed in *Table 6.18* using either three variables (E , L_{stif} and t) or four variables (E , L_{stif} , t and D) in the optimization process.

Table 6.18: Implementing TS optimization process using three and four included structural parameters upon FE Vierendeel with additional mass state using four modes only

Analysis No.	Including of 3 structural variables				Including of 4 structural variables				
	Type of variables			Value of objective function	Type of variables				Value of objective function
	E (N/mm ²)	L_{stif} (mm)	t (mm)		E (N/mm ²)	L_{stif} (mm)	t (mm)	D (Ns ² /mm ⁴)	
1	1.910x10 ⁵	64	2.94	0.0030	1.905x10 ⁵	70	2.85	8.22x10 ⁻⁹	0.0023
2	1.925x10 ⁵	65	2.94	0.0029	1.915x10 ⁵	68	2.93	8.24x10 ⁻⁹	0.0023

Results in *Table 6.18* indicate that including of four structural parameters exhibits better values (minimum) of objective function (0.0023) during the proposed TS optimization process. This can give a conclusion that using three structural parameters is recommended in the calibration process of the model under its own mass only while four parameters is recommended in the case of model with additional mass state. Hence, the values of $E=1.915 \times 10^5 \text{ N/mm}^2$, $L_{\text{stif}}= 68 \text{ mm}$, $t= 2.93 \text{ mm}$ and $D=8.24 \times 10^{-9} \text{ N.s}^2/\text{mm}^4$ are adopted in the present Vierendeel with additional mass state to be used in the updated FE model. *Figure 6.24* shows the progress of the proposed TS optimization procedure during the FE model updating which leads to the adopted optimum values of structural parameters.

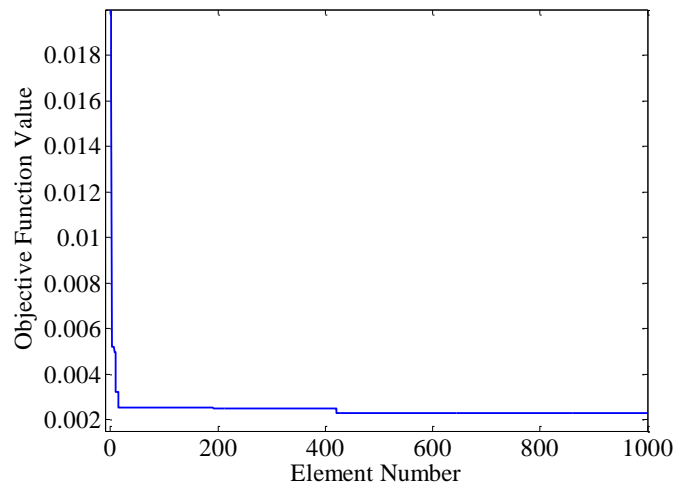


Figure 6.24: Improvement of FE model correlation based on minimum objective function value by TS optimization procedure for Vierendeel model with additional mass state using four modes

Figure 6.24 starts from the value of objective function of 0.02 instead of the initial value of 0.0634, *Table 6.13*, to appear the convergence in values of objective function in the lower parts of the graph obviously. After 421 iterations, the optimum solution is reached with decreasing of initial objective function value of 0.0634 to the updated value of 0.0023 as shown in *Figure 6.24*. The relative change upon each parameter during iterations is shown in *Figure 6.25*. The optimization process contains 8 successful iterations to

achieve the optimum solution for the three updated structural parameters as shown in *Figure 6.25*. The modulus of elasticity influences better when minimizing its value while other parameters influence better if they are increased during the optimization process.

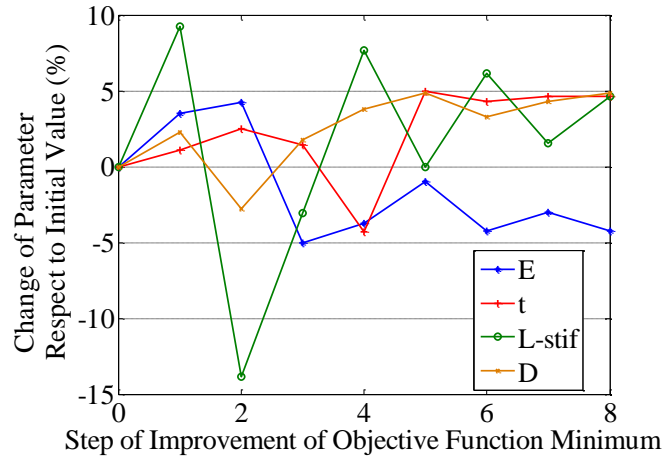


Figure 6.25: Change of structural parameters during the improvement of objective function minimum value of the Vierendeel model with additional mass state

Modal analysis is performed using the optimum updated values of structural parameters to compute natural frequencies and mode shapes by ANSYS software for the Vierendeel bridge model with additional mass state. The first five modes are computed in ANSYS software to investigate the results.

Values of the computed updated natural frequencies are compared with their corresponding values of initial computed natural frequencies with respect to the values of natural frequencies that extracted experimentally, as shown in *Table 6.19*.

It should be observed that the fifth mode is not taken into account during the calculation of objective function values (0.0634 and 0.0023) as it was the adopted option in this case, *Table 6.19*.

Table 6.19: Comparison between experimental, numerical initial and numerical updated values of natural frequencies of the Vierendeel bridge model with additional mass state

Mode No.	Experimental values (Hz) (Table 5.25)	Numerical values (Hz) of the initial FE model	Error (Hz)	(R. Err.) ²	Numerical values (Hz) of the updated FE model	Error (Hz)	(R. Err.) ²
1	13.220	14.688	-1.468	0.01233	12.972	0.248	0.00035
2	14.900	16.532	-1.632	0.01199	15.032	-0.132	7.9x10 ⁻⁵
3	30.910	34.647	-3.737	0.01462	29.904	1.006	0.00106
4	32.630	37.736	-5.106	0.02449	33.565	-0.935	0.00082
5	42.630	47.960	-5.330		45.252	-2.622	
Objective function value (\sum (R. Err.) ²)				0.0634	\sum (R. Err.) ²		0.0023

The convergence behavior according to the direct difference in values of natural frequencies between initial and updated values with respect to the experimental values are shown in *Figure 6.26*.

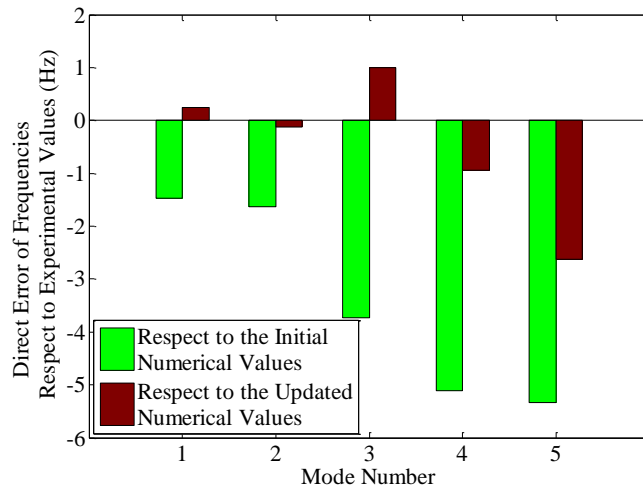


Figure 6.26: Errors of initial and calibrated FE modal frequencies respect to experimental values of the Vierendeel bridge model with additional mass state

The degree of convergence between results of natural frequencies for the updated FE model and those for the initial FE model with respect to the experimentally extracted values of natural frequencies, can be seen in *Figure 6.27*.

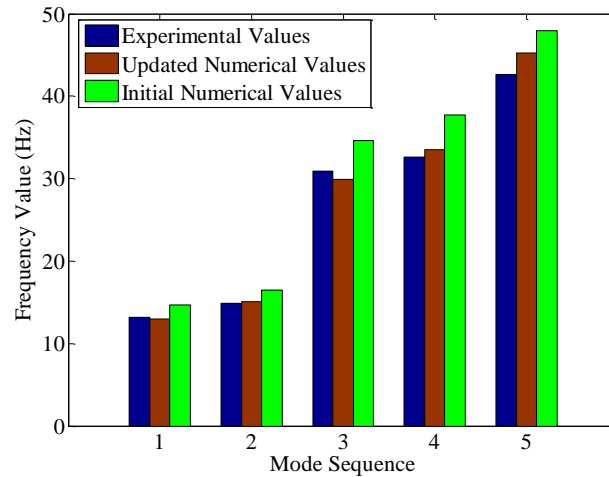


Figure 6.27: Convergence between experimental and numerical updated values of natural frequencies for the Vierendeel model with additional mass state using TS procedure

Finally, it is important to observe that during the proposed TS optimization process that adopted upon the previous models of grid-bridge and the recent Vierendeel bridge models, the searched space by the TS procedure was in the range of (0.11 - 4.25) %. This indicates that even if there is a sharp curtailment upon the designed termination criteria of TS optimization procedure, TS still able to achieve optimum solutions within acceptable accuracy.

6.6.3 Equivalent of severity of damage with respect to the used length of element in FE model

The adopted damaged beam scenario in the Vierendeel bridge model has damage severity of (42x20) mm, for damage length and depth, respectively. Hence, there is no need for the process of equivalent damage severity as the simulated damaged length is the same as the experimental damaged length.

Due to the complex damage shape that represents damaged column scenario, another consideration is adopted in this case represented by the minimum value of objective

function. The optimum damage severity that obtained during the procedure of damage detection optimization process is considered as the equivalent damage value. This value usually is represented by the length of damaged element of 42 mm which is constant value and an optimum depth represents the severity of damage. Hence, the non-prismatic damage shape of the damaged column is equivalent to the damage of (42×depth) mm damage severity that obtained by the optimization procedure of damage detection. This consideration is based on the assumption that the actual damage value is reached at the minimum difference between values of modal parameters that obtained experimentally and numerically. This method usually gives an approximate indication for the severity of damage that has unorganized shape.

6.6.4 Simulation of damaged elements in FE model

The significant damaged beam scenario of the Vierendeel bridge model is accomplished by implementing damage at 483 mm from the nearest support of the bridge model. It is located on the upper main hollow beam of the right side of the bridge model as shown in *Figure 6.17 (a)*. This location is equivalent to the element number 332 in the FE model of the Vierendeel bridge. On the other hand, the location of damaged column scenario, which described earlier in chapter 5, is equivalent to the element number 660 in the FE Vierendeel bridge model, *Figure 6.17 (a)*. These elements 332 and 660 represent the target elements that required to be detected during the procedure of damage detection in beams and columns, respectively, in the next chapter.

6.7 Numerical calculations of the Multi-storey building (MSB) model

The FE model of the fourth case study that adopted in the present work represented by the multi-storey building model is required to be created and analyzed by similar procedure that applied earlier for other models. ANSYS software is used to accomplish this mission as shown in the next paragraphs.

6.7.1 FEM analysis of the initial intact model

A special designed script configuration file with commands written according to ANSYS language is considered to create the FE model of the MSB, as shown in *Figure 6.28*.

Numerical modelling and adjustment of numerical results obtained by FEM and experimental results

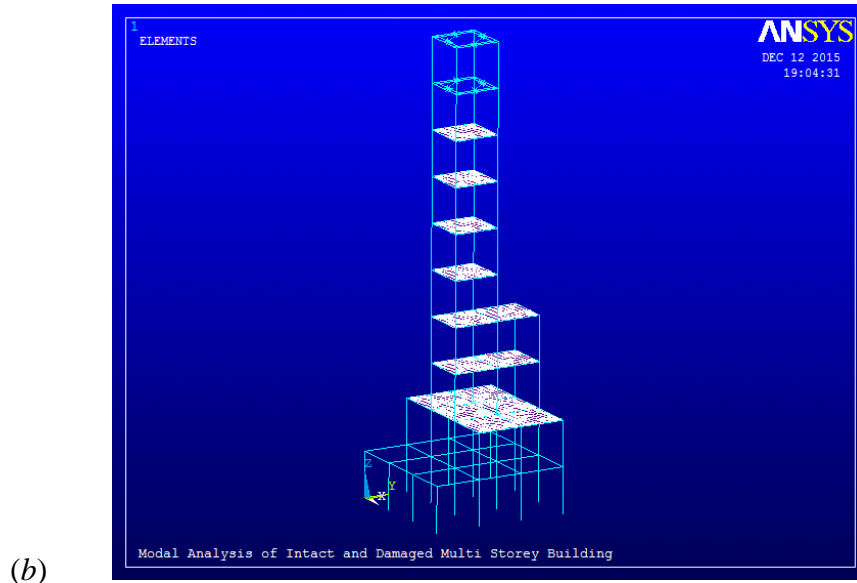
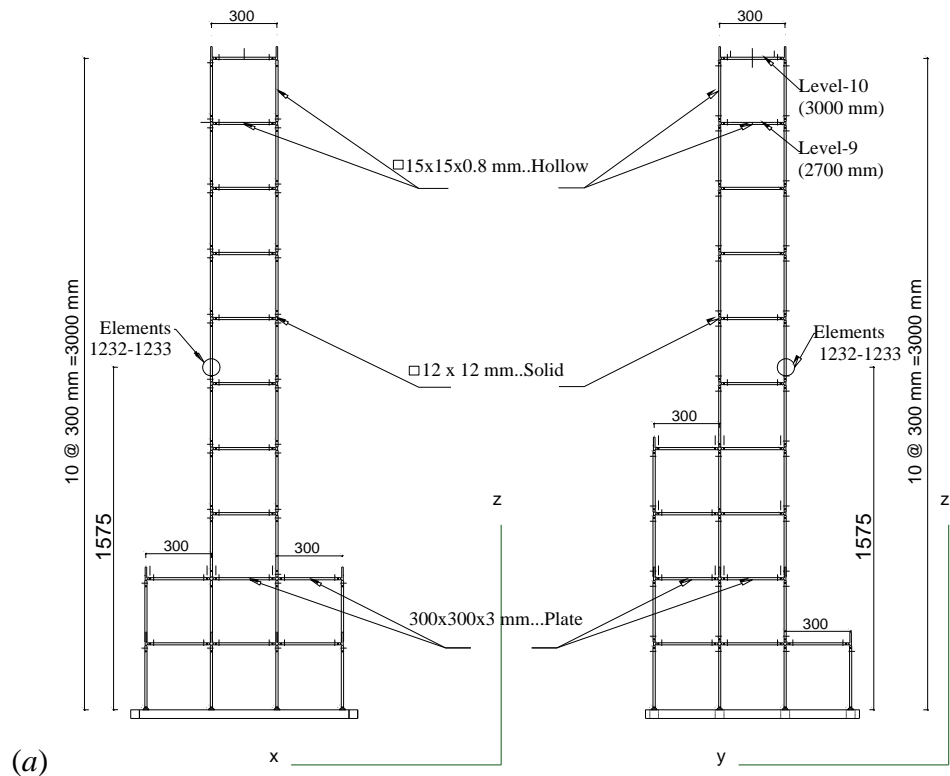


Figure 6.28: (a) Details of the initial FE Vierendeel bridge model, (b) MSB FE model created in ANSYS

The script configuration file consists of about 2100 steps, which is the longest configuration file in this study. In this case study, the model is studied under its own and additional masses as one state of mass application.

The FE model consists of 3112 elements represented by the types *Beam4*, *Shell63* and *Mass21* to simulate the elements of members, areas and applied masses respectively. The members include beams and columns and beam-column joints which are simulated with elements have 30 mm length for each one. All the adopted steel sections have initial adopted material modulus of elasticity $E_{\text{initial}} = 200$ GPa, the initial steel mass density is $D_{\text{initial}} = 7.86 \times 10^3$ kg/m³ and Poisson's ratio is $\nu = 0.3$. Surfaces that carry masses are simulated by *Areas* that are created and connected with the underneath beams by 8 surrounding points. All additional masses are applied on the surfaces (*Areas*) except for the levels 9 and 10 of the model which are simulated as concentrated masses distributed on four cross beams in each level, *Figure 6.28 (a)*. In the levels 9 and 10, the masses are initially distributed as 8 masses with 4 kg for each one that located at 120 mm from the edge of floor. In general, the additional masses are either concrete blocks (have 4.5 kg or 10.5 kg), steel blocks (have 13.5 kg or 16.2 kg) or brick blocks (have 32 kg). Except for the masses of brick blocks that applied on the levels 9 and 10, each block is fixed on the steel plate, *Figure 6.28 (a)*, in the lower levels. Hence, in the present work, the density of the steel plate and the applied mass are assembled to produce an equivalent density for both materials in order to be simulated in the FE model according to equation (6.6) as following:

$$D_N = \frac{M_{CS} + M_p}{V_p} \quad (6.6)$$

where, D_N (kg/mm³) is the new density of both steel plate and the applied mass, M_{CS} (kg) is the additional applied mass (concrete or steel block), M_p (kg) is the mass of steel plate and V_p (mm³) is the volume of the steel plate. It is assumed that both steel plate and the applied mass will be in the volume of steel plate which has the dimensions of (300x300x3) mm for length, width and thickness, respectively, but with the new density

Numerical modelling and adjustment of numerical results obtained by FEM and experimental results

D_N . The equivalent density for each applied mass is considered in the calibration process. Table 6.20 summarizes the calculations of the equivalent density for each mass applied on the steel plate.

Table 6.20: Equivalent values of densities for the applied masses and the steel plate

No. of level in MSB with included mass	Weight of the mass in the level M_{CS} (kg)	Weight of the steel plate M_P (kg)	Volume of the steel plate V_P (mm^3)	Equivalent Density (kg/mm^3) D_N
2 - 4	4.5	2.122	270000	2.4526×10^{-5}
5, 6	10.5	2.122	270000	4.6748×10^{-5}
7	13.5	2.122	270000	5.7859×10^{-5}
8	16.2	2.122	270000	6.7859×10^{-5}

The total elements during the procedure of damage detection in the whole MSB FE model are 1144 elements that are likely to be damaged. This number includes elements of beams and columns without including areas because the damage is simulated upon members only. Using ANSYS software, the modal analysis is performed upon the FE model of MSB to compute values of natural frequencies and mode shapes for the first five modes.

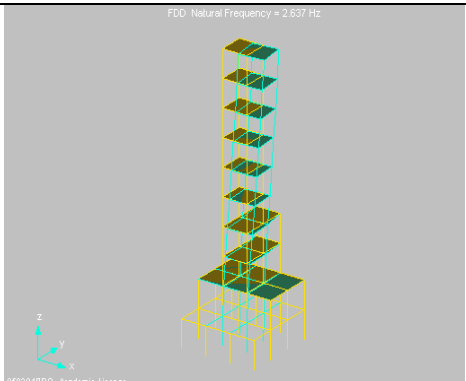
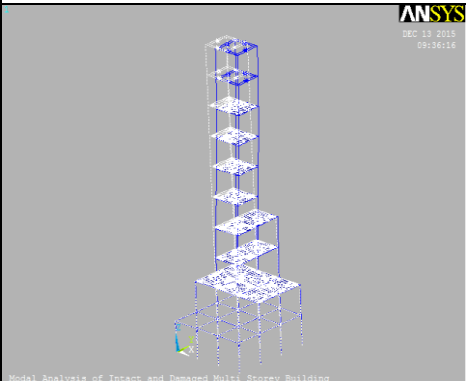
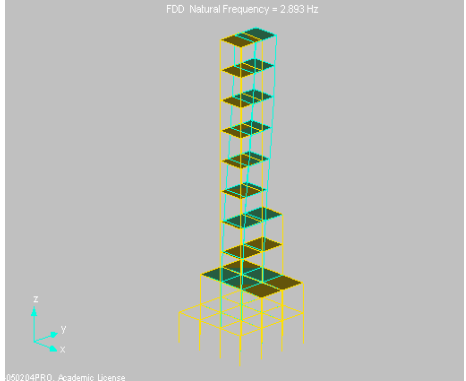
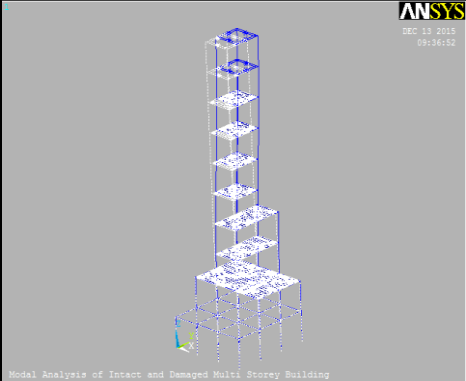
Table 6.21: Experimentally extracted and numerically computed values of natural frequencies of the intact initial FE MSB model

Mode No.	Values of natural frequencies (Hz)		Error (Hz)	(R. Err.) ²
	Experimental/ARTEMIS (Table 5.28)	Numerical/ANSYS		
1	2.637	2.558	0.079	0.00090
2	2.893	2.704	0.189	0.00427
3	6.555	5.997	0.558	0.00725
4	10.030	9.334	0.696	0.00482
5	10.290	9.433	0.857	0.00694
$\sum (R. Err.)^2$				0.02418

Numerical modelling and adjustment of numerical results obtained by FEM and experimental results

Table 6.21 lists values of natural frequencies of the intact initial MSB FE model for the first five modes as a comparison with the corresponding values that extracted experimentally in chapter 5. Another comparison includes the experimentally extracted mode shapes (chapter 5) with the numerically computed mode shapes is implemented and displayed in Table 6.22.

Table 6.22: Experimentally extracted and numerically computed mode shapes of the intact initial MSB model

Mode No.	Mode shape extracted experimentally ARTEMIS software (Table 5.28)	Mode shape computed numerically ANSYS software	Mode shape charac.
1			First bend. about y-axis
2			First bend. about x-axis

Numerical modelling and adjustment of numerical results obtained by FEM and experimental results

3	<p>FDD Natural Frequency = 6.555 Hz</p> <p>450204PRO, Academic License</p>	<p>ANSYS DEC 13 2015 09:37:59</p> <p>Model Analysis of Intact and Damaged Multi Storey Building</p>	First torsion
4	<p>FDD Natural Frequency = 10.03 Hz</p> <p>450204PRO, Academic License</p>	<p>ANSYS DEC 13 2015 09:38:24</p> <p>Model Analysis of Intact and Damaged Multi Storey Building</p>	Second bend. about y-axis
5	<p>FDD Natural Frequency = 10.29 Hz</p> <p>450204PRO, Academic License</p>	<p>ANSYS DEC 13 2015 09:38:50</p> <p>Model Analysis of Intact and Damaged Multi Storey Building</p>	Second bend. about x-axis

6.7.2 Calibration process by updating of FE MSB model

Calibration procedure using both classical and advanced iterative method for FE model updating are implemented upon the MSB model. The classical method focuses mainly on updating the locations of the distributed masses in the levels 9 and 10, while the advanced iterative method using TS optimization procedure is adopted to update other structural parameters. The same objective function represented by the difference between experimental and numerical values of natural frequencies is adopted in the present model.

A special script file is written in MATLAB environment consists of about 300 steps to perform the procedure of calibration process, under the main steps of *Figure 6.1*. The routine is performed several times to investigate the proper number of required iterations (termination criterion) of the optimization process and the validity of the results. The included structural parameters (variables) are modified according to the allowable percent of equation (6.2). Thus, the updated mode shapes are still similar before and after the calibration without needing to repeat their shapes. The first trials are implemented by the advanced iterative TS procedure which does not take into account the variation of the mass locations in levels 9 and 10 as an included structural parameter.

The structural parameters that adopted in the calibration process by the advanced iterative TS optimization are listed in *Table 6.23*.

Table 6.23: Total number of the included values of adopted structural parameters in the FE model updating procedure for the MSB model

No. of variable	Symbol of the structural parameter	Description of the structural parameter	Initial value	Total number of included values
1	E (N/mm ²)	Steel modulus of elasticity	2.000×10^5	5
2	$D1$ (Ns ² /mm ⁴)	Density of members and steel plates	7.860×10^{-9}	5
3	$D2$ (Ns ² /mm ⁴)	Density of steel plates and the 4.5 kg concrete block	24.526×10^{-9}	5
4	$D3$ (Ns ² /mm ⁴)	Density of steel plates and the 10.5 kg concrete block	46.748×10^{-9}	5
5	$D4$ (Ns ² /mm ⁴)	Density of steel plates and the 13.5 kg steel block	57.859×10^{-9}	5
6	$D5$ (Ns ² /mm ⁴)	Density of steel plates and the 16.2 kg steel block	67.859×10^{-9}	5
7	L_{hollow} (mm)	Side length of the hollow square cross section	15	5
8	L_{solid} (mm)	Side length of the solid square cross section	12	5
9	t (mm)	Thickness of the side of hollow section	0.8	5

Values in the column *Initial values* in Table 6.23, refer to the initial assumed values of each structural parameters. Each initial value is able to be increased or decreased by 5% as allowable limits and the updated values within this range are selected randomly. The searching space that is required to be checked consists of 1953125 (5^9) probable solutions exist in the domain. It is clearly that this space is very complicated and requires a robust optimization technique to be used. This can be considered as a good test for the efficiency of the proposed TS optimization procedure that is used to explore such space. By trial and error, using 8000 iteration is enough as termination criterion for the calibration process by TS optimization procedure. During the calibration process, TS optimization procedure explores only 0.41% (8000/1953125) from the whole searching space when using 8000 iterations as termination criterion. The convergence of the objective function during the progress of optimization process is shown in Figure 6.29 for the trial that exhibits the optimum updated values of the included structural parameters.

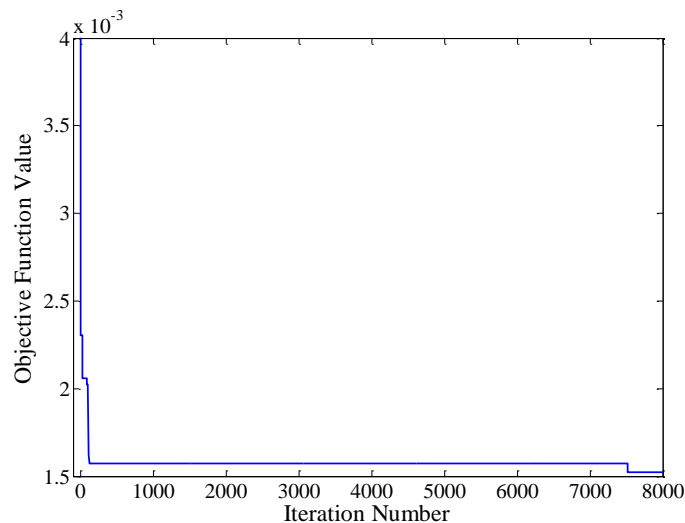


Figure 6.29: Improvement of FE model correlation based on minimum objective function value by TS optimization procedure for MSB model - Advanced iterative calibration method

Although Figure 6.29 should be started from the initial value of objective function 0.02418, but the y-axis is limited up to the value of 0.004 in order to display the improvements of the figure clearly during the progress of optimization. The optimization

process achieves the optimum solution after 7518 iterations, *Figure 6.29*, with the minimum value of objective function 0.00152. The optimum updated values of structural parameters are listed in *Table 6.24*.

Table 6.24: Optimum updated values of the included structural parameters during the proposed TS optimization process upon the FE model of MSB

Parameter	E	$D1$	$D2$	$D3$	$D4$
Optimum value	2.10×10^5	7.46×10^{-9}	23.30×10^{-9}	44.40×10^{-9}	59.30×10^{-9}
Parameter	$D5$	L_holow	L_solid	t	
Optimum value	67.85×10^{-9}	15.75	12.00	0.80	

Units of each parameter in *Table 6.24* are the same as mentioned in *Table 6.23* for each parameter. The relative change upon each parameter during iterations of the proposed TS optimization process is shown in *Figure 6.30*.

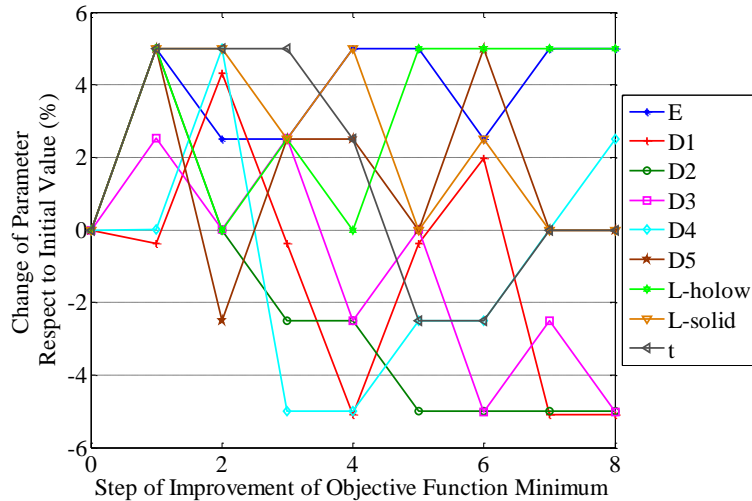


Figure 6.30: Change of structural parameters during the improvement of objective function minimum value of the MSB model

The next stage represents implementing of classical optimization process upon the FE model by changing the distribution masses in the levels 9 and 10 using the same values of optimum parameters in *Table 6.24*. As mentioned earlier, each of levels 9 and 10 contains

brick blocks have 32 kg total mass and are simulated to be distributed on 4 beams in each level as shown in *Figure 6.31*. The beams are assumed to represent the additional lateral support that is produced by the stiff brick blocks in the original experimental case of the model. During the iterations, the masses are distributed either at 4 kg on 8 surrounding locations, which is the distribution that adopted during the advanced iterative method, or vice versa. The best situation is reached when the masses are distributed as 8 kg at 4 points instead of 4 kg at 8 points in each level, as shown in *Figure 6.31*. The re-distribution of masses leads to the minimum value of objective function of 0.00121, as listed in *Table 6.25*, which is lower than the previous value of 0.00152 that obtained by the advanced iterative procedure.

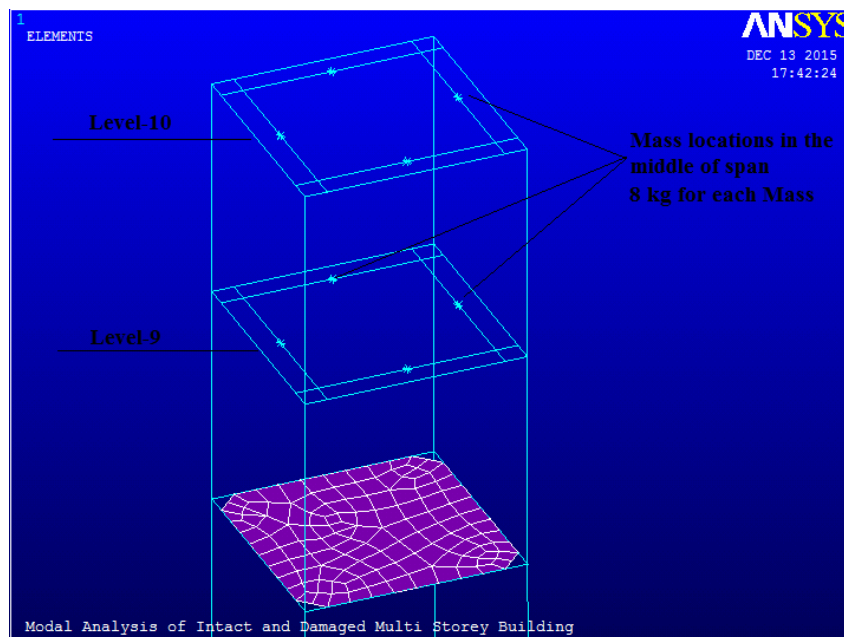


Figure 6.31: Optimum mass distribution in levels 9 and 10 of the FE MSB model during the classical method of calibration process

Hence, modal analysis is performed in ANSYS software to compute values of natural frequencies of the updated FE MSB model according to the optimum updated structural parameters, as listed in *Table 6.25*.

Table 6.25: Comparison between experimental, numerical initial and numerical updated values of natural frequencies of the MSB model

Mode No.	Experimental values (Hz) (Table 5.28)	Numerical values (Hz) of the initial FE model	Error (Hz)	(R. Err.) ²	Numerical values (Hz) of the updated FE model	Error (Hz)	(R. Err.) ²
1	2.637	2.558	0.079	0.00090	2.723	-0.086	0.00106
2	2.893	2.704	0.189	0.00427	2.877	0.016	3.1×10 ⁻⁵
3	6.555	5.997	0.558	0.00725	6.557	-0.002	9.3×10 ⁻⁸
4	10.030	9.334	0.696	0.00482	10.088	-0.058	3.3×10 ⁻⁵
5	10.290	9.433	0.857	0.00694	10.194	0.096	8.7×10 ⁻⁵
Objective function value (\sum (R. Err.) ²)				0.02418	\sum (R. Err.) ²		0.00121

The decreasing in the value of objective function between the initial and updated FE MSB model is obviously shown in *Table 6.25* which reflects the efficiency of calibration process.

The convergence of the results due to the application of the proposed TS optimization procedure gives a conclusion about the ability and efficiency of using this optimization technique in the problems of complex search space.

The convergence in values of natural frequencies between initial and updated values with respect to the experimental values, according to the direct difference of natural frequency values, are shown in *Figure 6.32*.

Also, the values of natural frequencies that experimentally extracted and numerically computed (for both initial and updated) corresponding values of the first five modes are summarized in *Figure 6.33*. Both of *Table 6.25* and the bar chart diagrams (*Figure 6.32* and *Figure 6.33*) are suitable for the comparison between the initial and updated values of natural frequencies which are estimated before and after the application of calibration process, respectively.

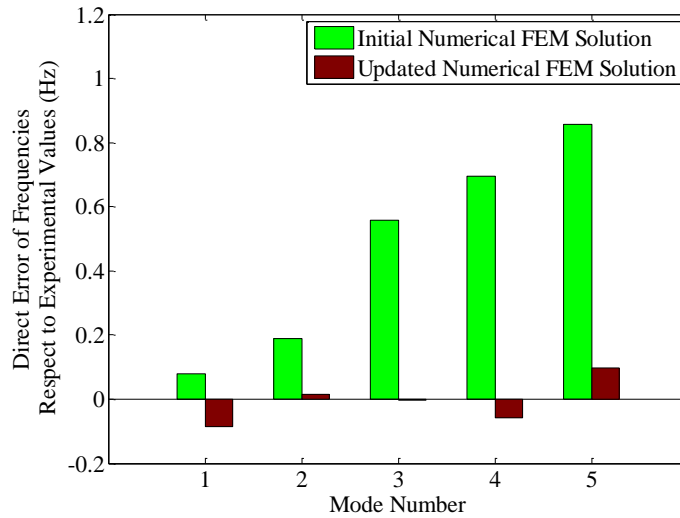


Figure 6.32: Errors of initial and calibrated FE modal frequencies respect to experimental values of the MSB model

According to *Table 6.25*, *Figure 6.32* and *Figure 6.33*, it is clearly shown that except of a small increase in the error occurred in the first mode, the errors in the all other four modes are significantly reduced due to the application of calibration process.

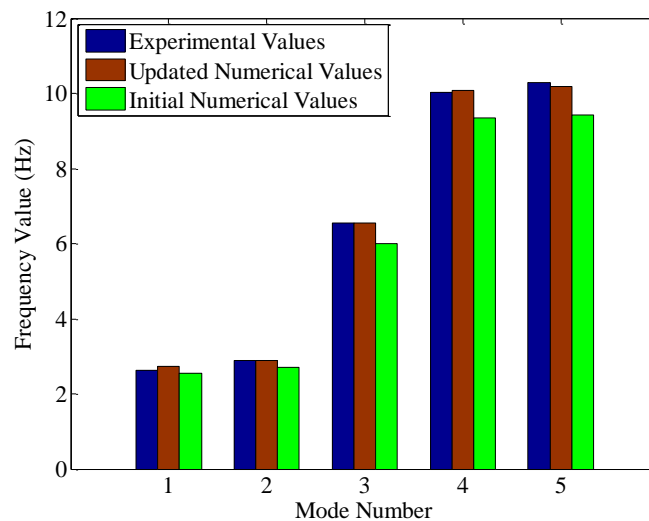


Figure 6.33: Modification of FE MSB model and the convergence between experimental and numerical values of natural frequencies, using TS procedure

6.7.3 Equivalent of severity of damage with respect to the used length of element in FE model

In the case of MSB model, the damaged element in the FE model has length of 30 mm which is the half value of the damaged length in the experimental model of 60 mm. Therefore, similar procedure as explained in *Figure 6.16* is considered here but for the case of MSB model as illustrated in *Figure 6.34*.

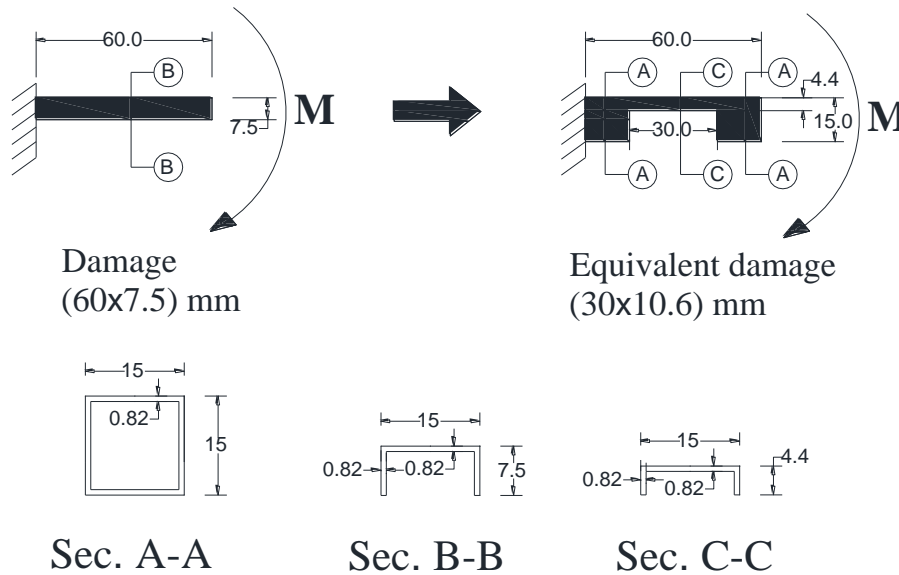


Figure 6.34: Equivalent damage value for the cantilevered 30 mm element model

A static structural analysis is implemented upon cantilevered element with 60 mm length subjected to an assumed concentrated fixed value of bending moment M , *Figure 6.34*. The displacement of the extreme point in the free end of the cantilevered element is measured upon the damage severity of (60x7.5) mm, length by depth, respectively. According to the same value of displacement, the value of the crack depth is examined by trial and error with different values until reaching to the proper value with the aid of interpolation.

In *Figure 6.34*, the real damage case in the experimental model has damage size of (60x7.5) mm, length by depth, respectively, which is equivalent to the damage size of (30x10.6) mm, length by depth, respectively, in the simulated damage of the FE model. The

obtained results can be used to give an approximate indication for the equivalent severity of damage between the real experimental model and the corresponding value in the numerical FE model.

6.7.4 Simulation of damaged elements in FE model

The damaged element in the FE MSB model is represented by elements number 1232 and 1233, as shown in *Figure 6.28 (a)*. These elements consider as the target which are required to be achieved as damaged elements during the damage detection optimization procedure.

7. VERIFICATION OF THE PROPOSED NUMERICAL MODEL, DETECTION AND LOCALIZATION OF DAMAGE USING TABU-SEARCH OPTIMIZATION METHOD

7.1 Introduction

The final stage of the present work is to use both of the experimental extracted and numerical updated values of natural frequencies and mode shapes in the procedure of damage detection with the aid of TS optimization procedure. The procedure of damage detection that explained earlier in chapter-3 is applied here to detect and localize the damage in each case study. The proper objective functions which are adequate for each case study are considered in this chapter. Hence, the applicable objective functions and application of the proposed TS optimization procedure are the main steps which are highlighted in each case study during the next paragraphs.

7.2 Damage detection in the overhang beam model

Creating the proper objective function which includes the adopted modal parameters and their weighting factors is the most important step in the procedure of damage detection. Usually, the sensitivity of the objective function for any changes in modal parameters due to damage is the adopted indicator for the damage location and severity. The changes in modal parameters are due to the periodically updating of FE model according to two variables, the simulated damaged location and its severity. These two variables are updated periodically during the optimization procedure until reaching the minimum value of objective function. When the minimum value of objective function is achieved, this means that the modal parameters in both of experimental case and numerical updated case are compatible. Hence, the updated variables (damage location and severity) at this point are the optimum requested values.

7.2.1 Creating the form of objective function

Several trials are performed according to each term of equations (3.10), (3.11), (3.12) and (3.13) which are included, separately or assembled, to create the proper objective function. Each term with its weighting factor is investigated alone or with other terms gradually by trial and error until reaching the best form. Trial and error method is represented by randomly assuming a certain fixed value of damage severity to be applied upon the whole elements that likely to be damaged in the model. Each simulated damaged element represents variable parameter to update the FE model under a certain damage severity. The term of *updating FE model* in this chapter refers to the modal analysis of the FE model under the damaged element and severity, therefore, it should not be confused with the term of *FE model updating* that used earlier in the calibration process of chapter-6. From each trial a new updated FE model is produced, from which, a certain value of objective function is obtained. The value of objective function represents the error which is produced due to the difference between values of modal parameters of the experimentally damaged model with their corresponding values of numerically computed damaged FE model. The resulted value of objective function is according to a trial number of included modes that are taken into account during the calculation of objective function value. Hence, the included number of modes is also a parameter that governs the creating process of the applicable objective function. The damaged element under the assumed value of damage severity produces a certain value of objective function which is recorded. This process is repeated for all available elements that are likely to be damaged in the FE model to record each new value of objective function. A graph is plotted for the relationship between all damaged elements in the range and the corresponding values of objective function. From this graph, the global minimum could be clearly observed in addition to all local minima that exist in the range. If the optimum location of damaged element is within the acceptable location (close to the actual damaged location in the experimental model) then the created objective function is accepted. Otherwise, the form of objective function should be updated by replacing the selection between the terms (equations (3.10) - (3.13)) and/or weighting factors. Hence, the acceptable location is the criterion that has the priority and governs the

acceptability of the behaviour of objective function in this work rather than damage severity. The optimum damage severity is considered according to the search that is implemented by the proposed TS optimization during the procedure of damage detection. The procedure of creating the proper objective function can be summarized by the flow chart shown in *Figure 7.1*.

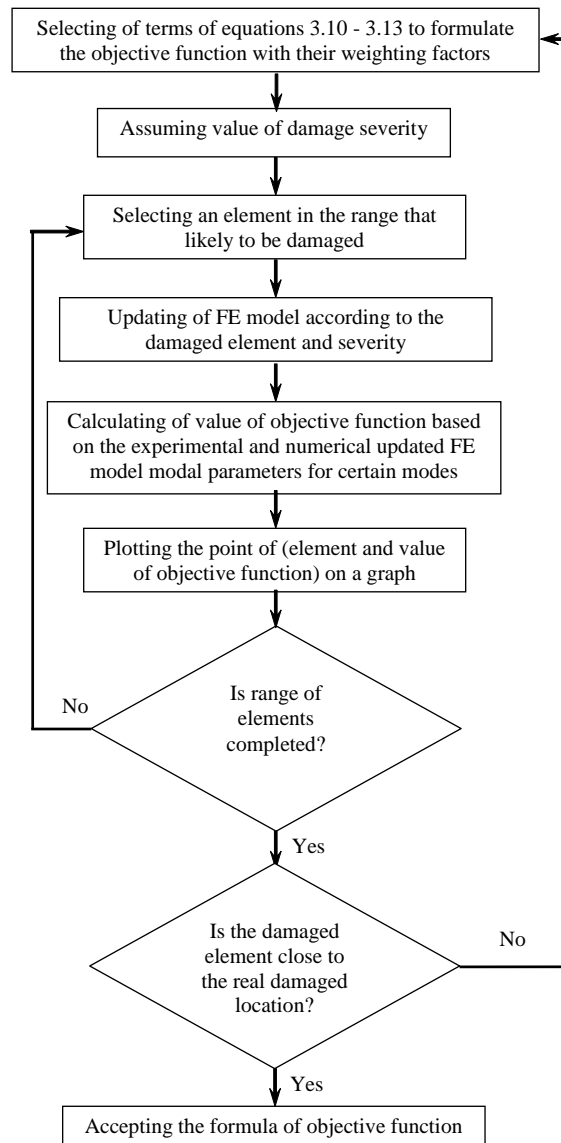


Figure 7.1: Flow chart of the creating process of the applicable objective function

In *Figure 7.1*, the *certain modes* represent the included modes during the calculation of objective function values which are usually taken between 3 and 5 included modes. In the case of overhang beam model, three modes exhibit the best behaviour to create the applicable objective function. Manual process in addition to special routine that written with about 150 steps in MATLAB environment perform the flow chart shown in *Figure 7.1*. Modal analysis upon the FE model using ANSYS software is simultaneously performed within the MATLAB routine to update the model according to both of element and damage severity. Applying the flow chart of *Figure 7.1* leads to the best applicable form of objective function for the overhang beam model as following:

$$\text{Obj_Func} = W_f F_r + W_d D + W_m M \quad (7.1)$$

where W_f , W_d and W_m are the weighting factors for the participations of relative difference in values of natural frequencies F_r (equation (3.10)), normalized mode shapes D (equation (3.12)) and the diagonal MAC M (equation (3.13)), respectively. Several trials are accomplished to find out the most adequate values of weighting factors that could be used. *Table 7.1* contains the tested values of weighting factors that used in the study.

Table 7.1: Studied values of weighting factors in objective function during the trial and error method according to equation (7.1)

	W_f	W_d	W_m
Values of the weighting factor	0 / 2 / 4 / 6 / 8 / 10	0 / 1	0 / 1

The proper designed values of W_f , W_d and W_m in equation (7.1) are proposed as 4, 1 and 1, respectively. The plot that used during the procedure of creating the objective function for the relationship between values of objective function and element numbers is shown in the next paragraph.

7.2.2 Application of the objective function

The created (designed) applicable form of objective function (equation (7.1)) is now applied on each damage case to observe the locations of global and local minima.

7.2.2.1 Objective function through damage case of AODC-1

The proposed objective function is applied according to the damage case of AODC-1. Values of objective function are plotted with model elements which have the same length of the applied damage, i.e., 25 mm element length. According to a randomly selected damage severity of 2 mm depth, values of objective function are calculated when each element is damaged periodically. *Figure 7.2* shows the relationship between values of objective function and damaged element numbers in the damage case AODC-1.

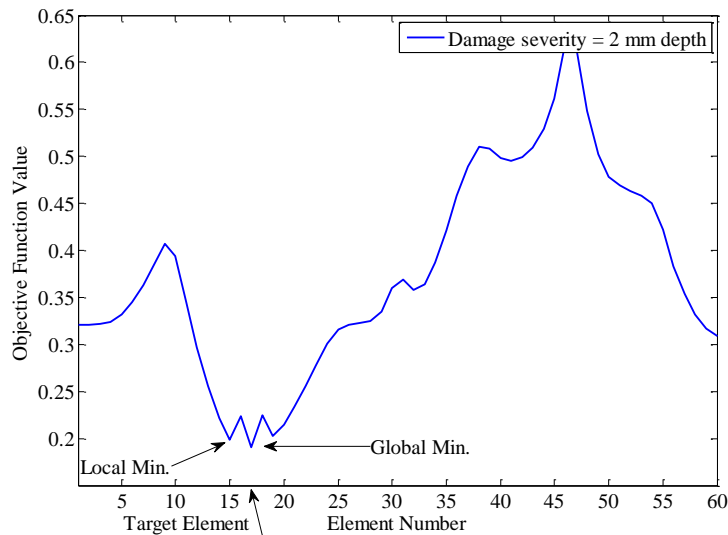


Figure 7.2: Behavior of the objective function for damage case AODC-1

It can be seen that from *Figure 7.2*, the global minimum is located at element number 17 which is exactly the same damaged location in the experimental model, *Figure 6.2*. This reflects the efficiency of the proposed form of objective function and verifies the ability of using this form in the TS optimization procedure for the sake of damage detection.

7.2.2.2 Objective function through damage case of AODC-2

The relationship between the damaged element at each trial and the value of objective function under assumed value of damage severity (2 mm depth) is investigated to find the location of global minimum for the damage case of AODC-2. *Figure 7.3* shows the locations of global and local minima existed on the graph of relationship between the damaged element at each trial with the corresponding value of the proposed objective function under damage severity of 2 mm.

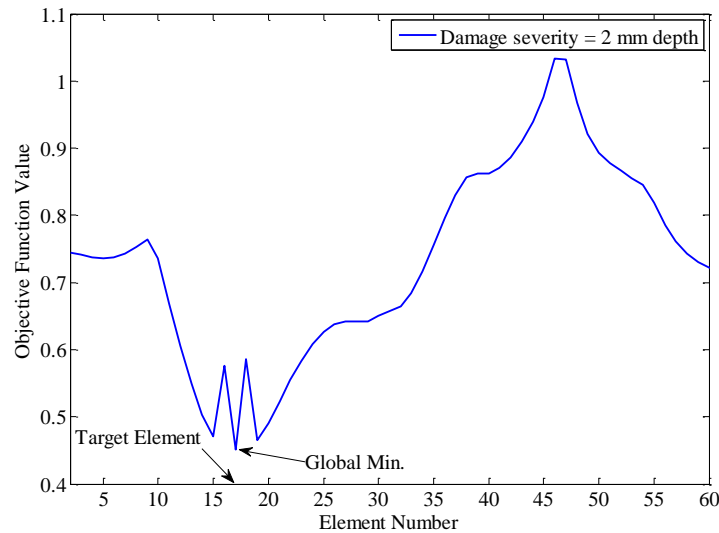


Figure 7.3: Behavior of the objective function for damage case AODC-2

The global minimum value is located on element number 17 which corresponds exactly to the same damaged location in the experimental model, *Figure 6.2*. Hence, this verifies the ability of using the proposed objective function in this damage case during the procedure of damage detection.

7.2.3 Damage detection using the proposed TS optimization procedure

The proposed procedure of TS optimization that explained in the flow chart of *Figure 4.5* (Chapter-4) is now applied upon each damage case to detect location and severity of damage. As any optimization technique, TS searches the optimum solution that is close to

the target value as much as possible. The proposed objective function is used in the procedure of TS optimization for damage detection. The adopted searching space has range of damage severities from [0.25 - 3.5] mm damage depth with increment of 0.25 mm between each two damage severities. Hence, there are 14 different discrete values in the whole range that are incorporated with the total number of elements of 60 in the FE model to produce the 840 possible solutions in the searching space. By trial and error, the maximum number of iteration is designed to be 120 iterations (as the termination criterion). This value limits the actual searching space by about 14% (120/840) from the whole possible solutions in the searching space. Usually, increasing the number of iterations increases the probability of achieving the optimal solution in the TS procedure. Searching only 20% or less from the whole possible solutions in the searching space represents a reasonable ratio that adopted by the optimization process [113] [114]. The ability of TS optimization procedure to detect damage and avoid local minima is investigated for each significant damage case, as following.

7.2.3.1 Application of TS procedure for damage detection of AODC-1

During the application of the proposed TS optimization procedure for damage detection, the improvement of the objective function values towards the global minimum value approximation is progressed with the sequence of iterations, as shown in *Figure 7.4*.

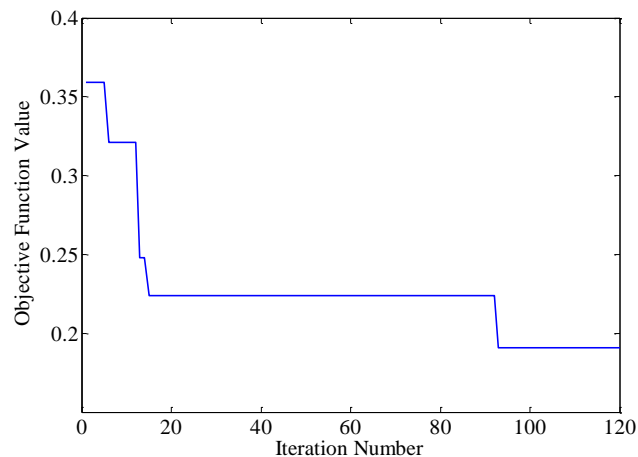


Figure 7.4: Improvement of objective function minimum value during iterations of the proposed TS based damage detection of the overhang model in AODC-1 damage case

After 93 iterations during the optimization process, *Figure 7.4*, the optimal solution is reached, which represents the optimal damaged element and severity of damage. The exact position of damaged element number 17 is achieved with damage severity of 2 mm depth which is the best approximation of the actual damage severity that implemented in damage case AODC-1. This result reflects the efficiency of the proposed TS optimization procedure in this damage case.

7.2.3.2 Application of TS procedure for damage detection of AODC-2

TS optimization procedure is implemented upon the most severity damage scenario AODC-2 to detect location and severity of damage. The progress of the optimization in this damage case is shown in *Figure 7.5*.

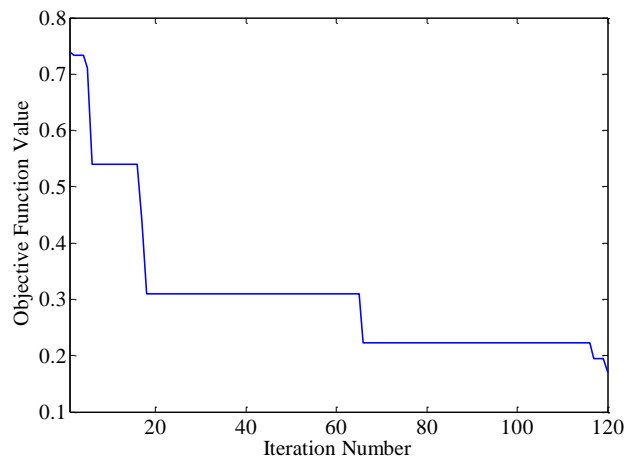


Figure 7.5: Improvement of objective function minimum value during iterations of the proposed TS based damage detection of the overhang model in AODC-2 damage case

For the damage case AODC-2, the optimal solution is reached after 120 iterations as shown in *Figure 7.5*. The optimization process produced element number 17 as the optimal solution which is the exact location as implemented in the experimental model. On the other hand, the damage severity of 2.75 mm is detected as an optimal damage severity

which is also the exact damage severity that implemented in the experimental model. Hence, the proposed TS optimization procedure, according to the proposed weighting factors and form of objective function, exhibits a robust behaviour in detecting the optimal solution for both adopted damage cases.

7.3 Damage detection in the grid-bridge model

The same procedure that explained by *Figure 7.1* to create and design proper form of objective function and weighting factors for the grid-bridge model is considered in this paragraph. Also, the procedure of damage detection that explained by the flow chart of *Figure 4.5* is implemented to detect and localize damage in the grid-bridge model under its own mass only and with additional mass states.

7.3.1 Creating the form of objective function

In addition to the procedure shown in *Figure 7.1*, creating the proper objective function in the case of grid-bridge model is accomplished by investigating the ability of using equation (7.1) which is created earlier in the overhang beam model. It is found that the proper form is obtained when applying two modifications upon equation (7.1). The first modification represents using the term of F_d (equation (3.11)) instead of F_r for the participation of natural frequencies values. While the second modification is implemented by updating values of weighting factors for each term in the form of objective function. *Table 7.2* lists the used weighting factors during the trial and error method to modify weighting factors of equation (7.1).

Table 7.2: Studied values of weighting factors in modifying of equation (7.1)

	W_f	W_d	W_m
Values of the weighting factor	0 / 1 / 4 / 10 / 100 / 10000	0.1 / 0 / 1	0 / 1

The proper designed values of weighting factors of W_f , W_d and W_m are 1, 0.1 and 1 respectively. Hence, the adopted form of objective function with its weighting factors is:

$$\text{Obj_Func} = W_f F_d + W_d D + W_m M \quad (7.2)$$

The created form of objective function is based on the information (modal parameters) of the first five modes which exhibit the proper behaviour of the objective function. The plot of the relationship between values of objective function and number of elements under a certain damage severity can be shown in the next paragraph. This plot is used during the procedure of creating the form of objective function.

7.3.2 Application of the objective function

The objective function is applied upon all scenarios of damage to plot the relationship between damaged elements and values of objective function under certain damage severity. Then, it is possible to see if the location of global minimum is close to the target element or not in each damage case.

7.3.2.1 Objective function through damage case of RAGDC-1

The proposed form of objective function (equation (7.2)) is applied on the FE model according to damage scenario RAGDC-1. An assumed value of damage severity of 20 mm depth is adopted to be exposed upon each damaged element. Value of objective function from each damaged element is recorded to plot the relationship with the corresponding damaged elements. From the plot, the global minimum is located on damaged element number 48, as shown in *Figure 7.6*.

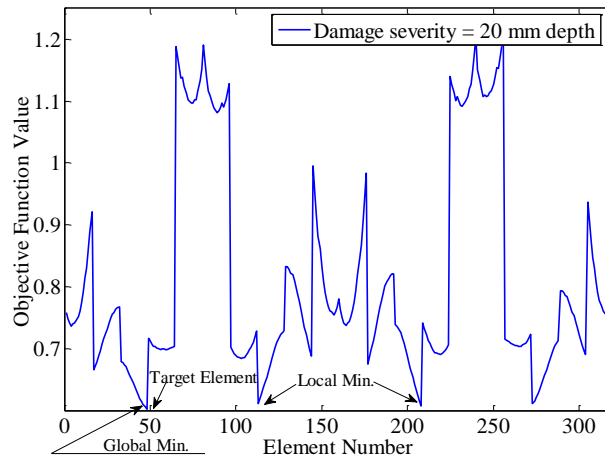


Figure 7.6: Behavior of the objective function for damage case RAGDC-1

It can be seen that from Figure 7.6, the global minimum (element number 48) is located close to the target element (element number 54), which exhibits the good behaviour for the proposed objective function. This also gives an indication that, in this case of damage, the proposed form of objective function could be used in the procedure of TS optimization for the sake of damage detection. The close values between global and local minima of objective function in the searching space increases the complexity of the optimization to reach the global minimum. This can be considered as a good test to the proposed TS optimization procedure for that purpose.

7.3.2.2 Objective function through damage case of RAGDC-2

Using experimental modal parameters of damage case RAGDC-2 as variables in the objective function form, values of the proposed objective function are computed according to a certain value of damage severity (20 mm depth). This value of damage severity is exposed on each element in the FE model that likely to be damaged. Then, resulted values of objective function are plotted with each rank of damaged element in the FE model, as shown in Figure 7.7.

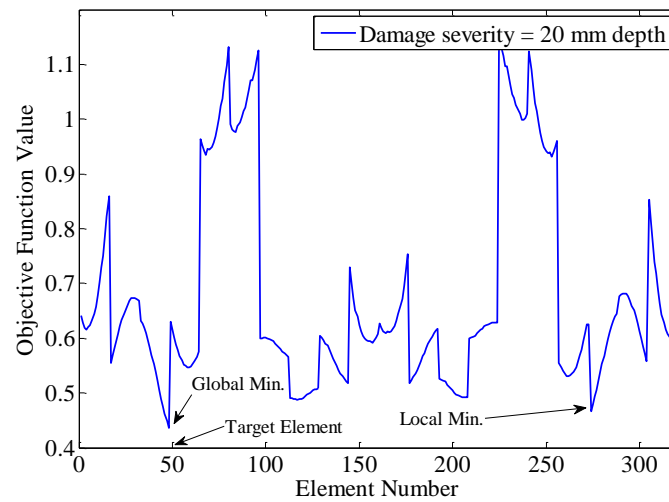


Figure 7.7: Behavior of the objective function for damage case RAGDC-2

Global minimum is located on element number 48 which is close to the target element number 54 as shown in Figure 7.7. This also indicates the ability of using this case of damage with the proposed objective function in the optimization procedure for damage detection.

7.3.2.3 Objective function through damage case of LAGDC-1

The same procedure of testing the behaviour of the proposed form of objective function is repeated upon the damage case LAGDC-1. It is found that the global minimum value of objective function is located on element number 203, as shown in Figure 7.8.

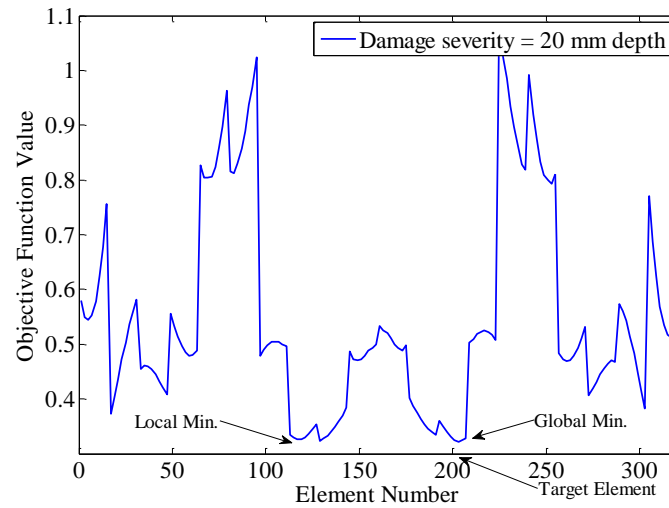


Figure 7.8: Behavior of the objective function for damage case LAGDC-1

Element number 203 is close to the target location represented by element number 200 in the FE model, (Chapter-6). Hence, this damage case is able to be used in the procedure of damage detection using the created objective function in the TS optimization procedure.

7.3.2.4 Objective function through damage case of RAGDC-1M

This damage case is the first scenario of significant damage that implemented on the right side of model with additional mass state. The proposed form of objective function is applied upon this damage case to explore the location of global minimum value when each element is damaged periodically within a certain damage severity. It is found that the global minimum value is located on element number 48 (right side damage scenario) which is close to the target element number 54, as shown in *Figure 7.9*.

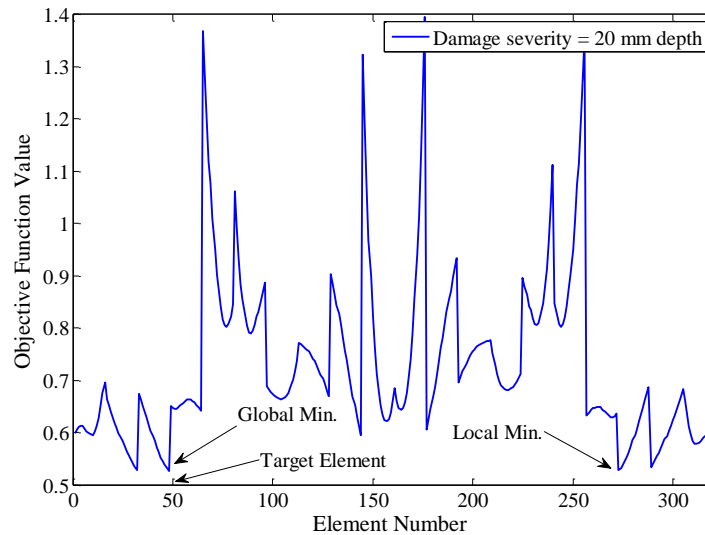


Figure 7.9: Behavior of the objective function for damage case RAGDC-1M

The minimum value of objective function is 0.526 which is very close to the local minimum value that existed on element number 273 which has value of objective function of 0.527. If the proposed TS optimization procedure is able to avoid the local minimum and indicate the global minimum as an optimum value, then it is a verification to the robustness and efficiency of this optimization procedure. Nevertheless, the location of global minimum shown in *Figure 7.9* refers to the ability of using this damage case with the proposed form of objective function in the procedure of damage detection.

7.3.2.5 Objective function through damage case of LAGDC-1M

In order to test the ability of applying damage scenario LAGDC-1M with the proposed form of objective function in the procedure of damage detection, objective function is applied on this damage case under the assumed value of damage severity (20 mm depth). The produced global minimum value of objective function is located on element number 201, as shown in *Figure 7.10*.

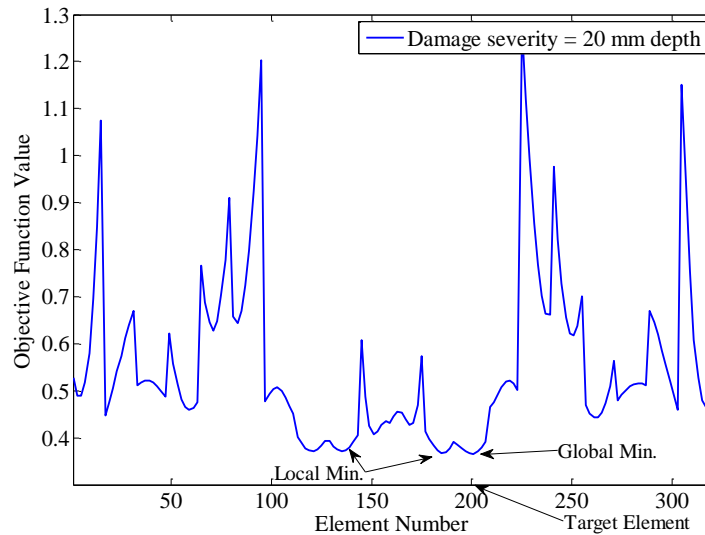


Figure 7.10: Behavior of the objective function for damage case LAGDC-1M

Figure 7.10, shows the close location of the global minimum value to the target location represented by element number 200. This verifies the ability of using this damage case in the procedure of damage detection under the proposed form of objective function. The location of global minimum has a value of objective function of 0.366 while in the location of local minimum (element number 185) it is 0.367. These values of objective functions are so close and reflect the need to an efficient optimization technique that is able to avoid trapping in the values of local minima. Hence, TS optimization is used to discover this ability.

7.3.2.6 Objective function through damage case of LAGDC-2M

The proposed form of objective function is applied on damage case LAGDC-2M under the assumed value of damage severity (20 mm) for each damaged element in the FE model. The global minimum value of objective function is located on element number 191, Figure 7.11. The global minimum value of objective function is 0.317 located at element number 191 while the local minimum value is 0.323 located at element number 129. Therefore, global minimum value is close to the target element (200) which refers to the

ability of adopting this damage case, with the proposed form of objective function, in the procedure of damage detection.

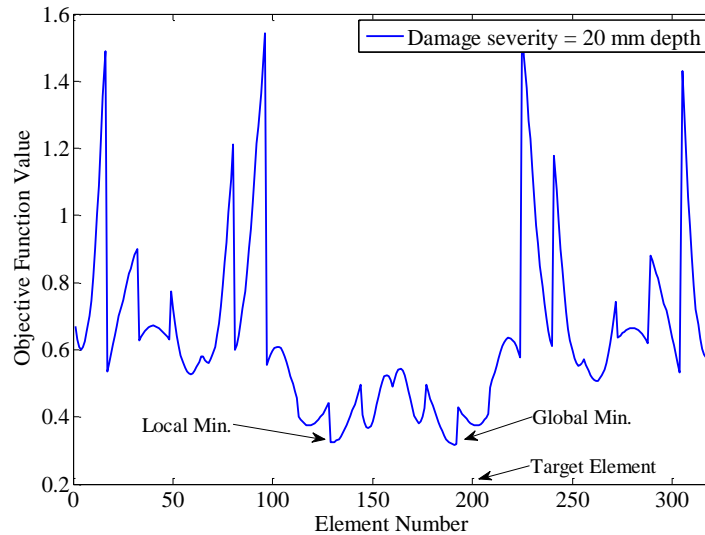


Figure 7.11: Behavior of the objective function for damage case LAPDC-2M

7.3.3 Damage detection in the grid-bridge model using the proposed TS optimization procedure

Each applicable damage case of the grid-bridge model is adopted in the procedure of damage detection using the proposed TS optimization technique to detect location and damage severity. The range of possible damage severities that used during the TS optimization procedure is [1 - 47] mm which represents the depths of damage for elements in the FE model. This range in addition to the total number of candidate elements that could be damaged (320 elements) form the total searching space of 15040 (47x320) solutions likely to be obtained. It is found that by trial and error method, the required number of iterations for the optimization process is 800 iterations suitable for all significant damage cases in the grid-bridge model. Hence, the actual searching space by the proposed TS optimization procedure is 5.3% (800/15040) from the whole existed searching space. The application of the proposed TS optimization procedure to detect damage in each applicable damage case is implemented as following.

7.3.3.1 Application of TS procedure for damage detection of RAGDC-1

Improvement of the objective function values during the application of TS optimization procedure is progressed towards the value of global minimum, as shown in *Figure 7.12*.

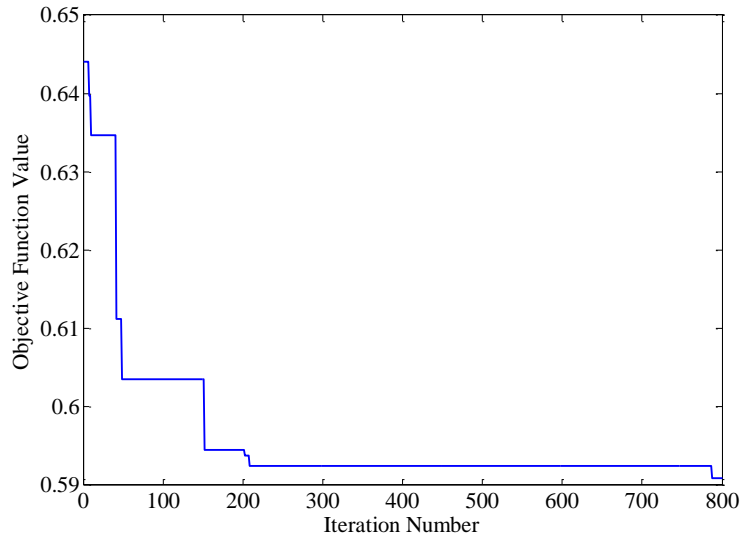


Figure 7.12: Improvement of objective function minimum value during iterations of the proposed TS based damage detection of the grid-bridge model in RAGDC-1 damage case

The optimum solution (damaged element and severity of damage) is achieved after 788 iterations which has value of objective function of 0.591. The optimum location is represented by element number 48 while optimum severity of damage is 7 mm depth. It is clear that element number 48 is close to the target damaged location in the experimental model which is represented by element number 54 in the FE model. On the other hand, the optimum severity of damage (7 mm) is close to the equivalent value of damage severity in the damage case (RAGDC-1) that mentioned in *Table 6.10* which is equal to 5.3 mm depth. Therefore it is concluded that the proposed TS optimization procedure successfully detected the optimum values of damaged element and its severity within consistent results.

The proposed procedure of TS optimization is able to avoid all locations of local minima and selects the global minimum only. This verifies the efficiency of the proposed

procedure of TS optimization in the case of complex functions. The distribution of the explored points in the searching space during the optimization procedure reflects the proper searching process that implemented by the proposed TS optimization procedure which covers the whole searching space within a limited number of iterations, as shown in *Figure 7.13*.

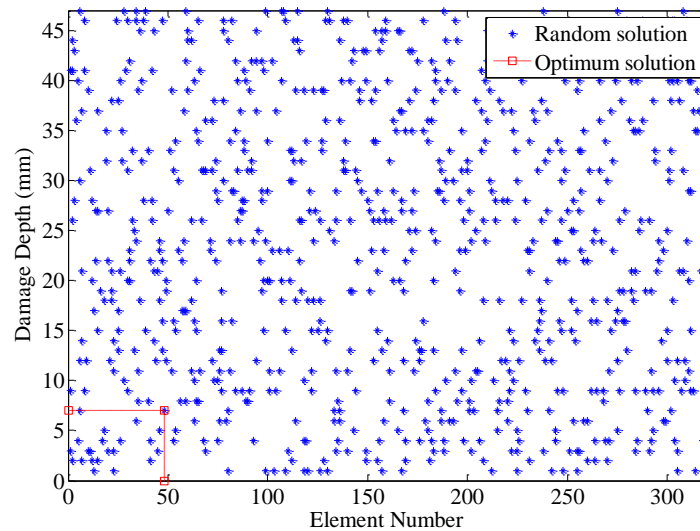


Figure 7.13: The distribution of the explored solutions in the tested space using TS optimization procedure for damage case RAGDC-1

7.3.3.2 Application of TS procedure for damage detection of RAGDC-2

According to the damage case RAGDC-2, TS optimization procedure is applied to detect the damage in this case. The progress of optimization with improvement of objective function value is plotted in *Figure 7.14*. After 240 iterations, the optimum solution is achieved that represented by element number 47 as the optimum location of damage and 20 mm depth as optimum damage severity. The optimum damage location (element 47) is close to the target damage location represented by element number 54. On the other hand, the optimum value of damage severity is exactly the same as the severity of damage that implemented in the experimental model which is (42x20) mm dimensions length by depth, respectively.

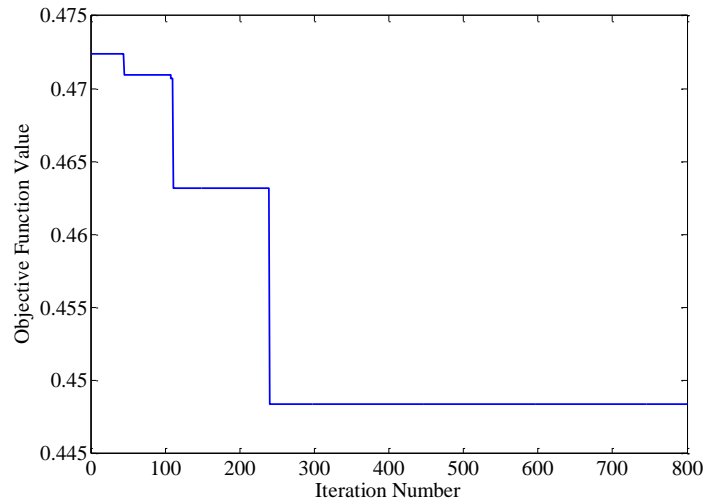


Figure 7.14: Improvement of objective function minimum value during iterations of the proposed TS based damage detection of the grid-bridge model in RAGDC-2 damage case

The damaged element in the FE model during the optimization process has the same length as experimental damage (42 mm). Therefore, process of equivalent damage severity (Table 6.10) is not required in this damage case. To observe the distribution of the explored points in the searching space during the optimization process, Figure 7.15 is considered.

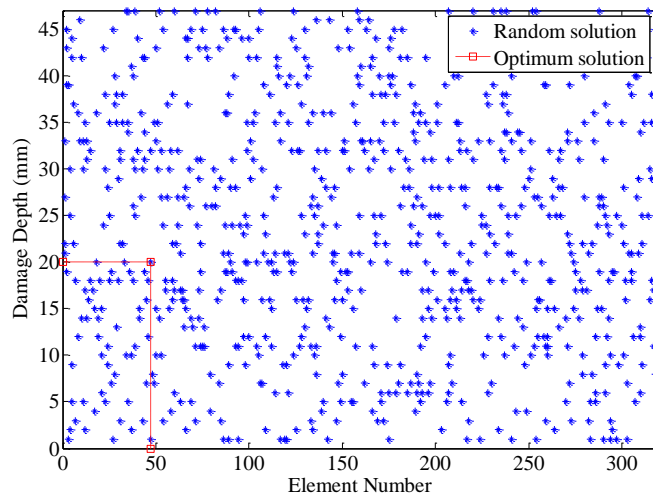


Figure 7.15: The distribution of the explored solutions in the tested space using TS optimization procedure for damage case RAGDC-2

The checked points shown in *Figure 7.15* are selected from the whole searching space which reflect the excellent behavior of the proposed TS procedure during the optimization process.

7.3.3.3 Application of TS procedure for damage detection of LAGDC-1

Improvement of the objective function value during the progress of TS optimization procedure that implemented upon the damage case LAGDC-1 is shown in *Figure 7.16*.

The optimum solution has a value of objective function of 0.302 which produces the optimum damage location of element number 203. This optimum location is very close to the actual damaged location in the experimental model that represented by element number 200. Also, the optimum solution represents the optimum severity of damage which is 29 mm as a depth of the damaged element in the FE model. This value has 9 mm difference from the actual damage severity in the experimental model which is 20 mm depth. In this case, there could be seen an overestimation in the result of damage severity during the optimization procedure. The distribution of the explored points during the optimization process is shown in *Figure 7.17*.

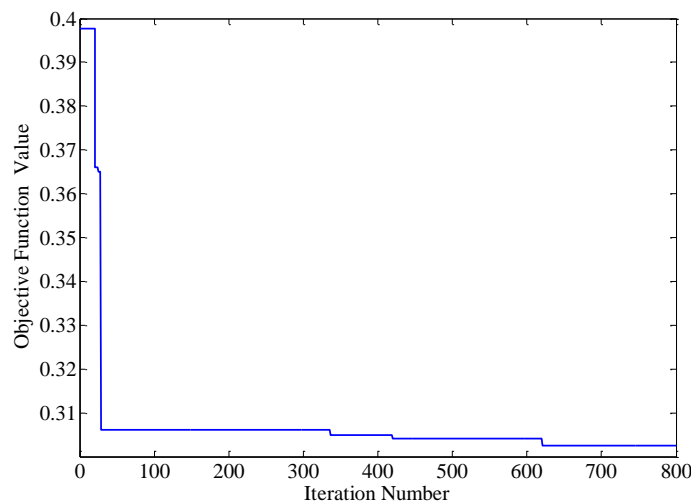


Figure 7.16: Improvement of objective function minimum value during iterations of the proposed TS based damage detection of the grid-bridge model in LAGDC-1 damage case

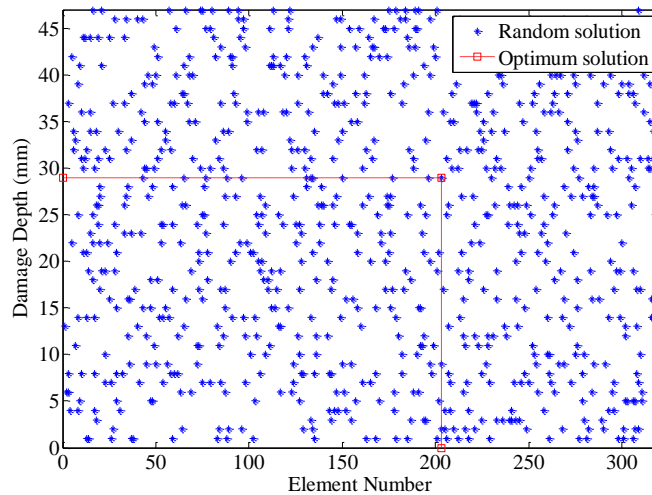


Figure 7.17: The distribution of the explored solutions in the tested space using TS optimization procedure for damage case LAGDC-1

Figure 7.17 shows that the whole searching space is approximately covered during the optimization process according to the limited number of iterations during the proposed TS optimization procedure.

7.3.3.4 Application of TS procedure for damage detection of RAGDC-1M

Damage detection process using the proposed TS optimization procedure is implemented upon the scenario of damage case RAGDC-1M for the model with additional mass state. The improvement progress of the objective function value during the optimization is plotted in Figure 7.18. The optimization process achieves the optimum solution after 172 iterations which corresponds to the value of objective function of 0.500. The optimum solution refers to element number 48 as the optimum damaged location while the optimum damage severity is 25 mm depth. Both of these values are close to the corresponding target values that implemented in the experimental model which are element number 54 and damage severity of 20 mm depth. Hence, TS optimization is successfully achieved to the optimum solution within a reasonable number of iterations.

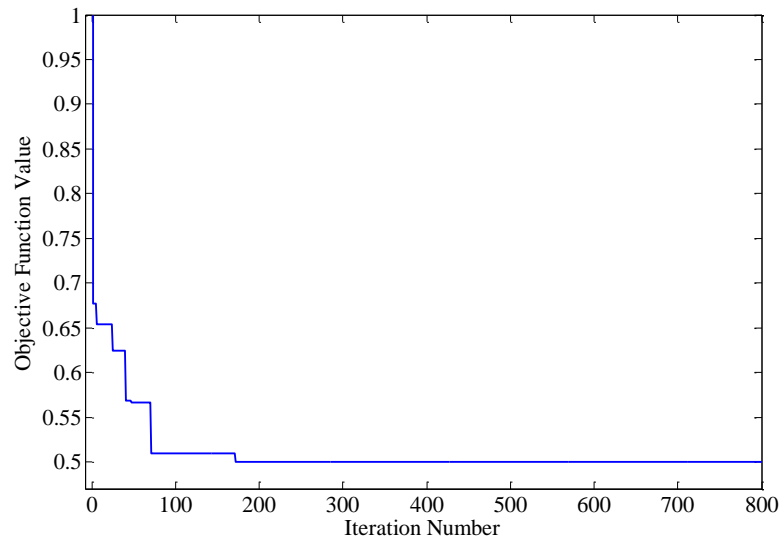


Figure 7.18: Improvement of objective function minimum value during iterations of the proposed TS based damage detection of the grid-bridge model in RAGDC-1M damage case

Figure 7.19 shows the distribution of the explored solutions in the searching domain during the optimization process.

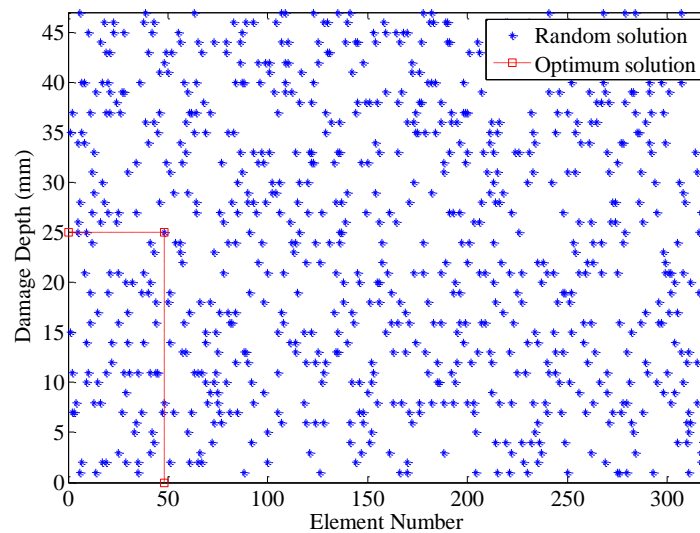


Figure 7.19: The distribution of the explored solutions in the tested space using TS optimization procedure for damage case RAGDC-1M

7.3.3.5 Application of TS procedure for damage detection of LAGDC-1M

TS optimization procedure is implemented upon the damage case LAGDC-1M to detect the damage that exist on the left side of bridge model. *Figure 7.20* shows the progress of convergence towards the minimum value of objective function during the optimization procedure. After 443 iterations, the optimum location of damaged element is explored which represented by element number 191 while the optimum severity of damage is 13 mm depth. There are only 9 elements difference between the actual damage location in the experimental model represented by element number 200 and the optimum solution. This difference is small if it is taken into account the total candidate damaged elements in the searching space which are 320 element. On the other hand, this damage case has length of damage equal to 21 mm in the experimental model, hence, an equivalent value of damage severity should be calculated based on element length of 42 mm in the FE model. According to *Table 6.10*, the equivalent damage value of the case LAGDC-1M is 13.4 mm depth. Thus, only 0.4 mm is the difference between the optimum value and the equivalent damage value. This result refers to good estimation which indicates the efficiency of the proposed TS optimization procedure.

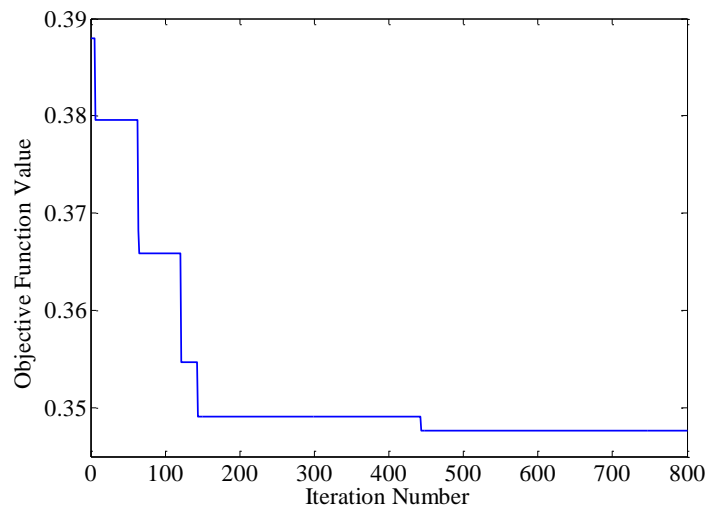


Figure 7.20: Improvement of objective function minimum value during iterations of the proposed TS based damage detection of the grid-bridge model in LAGDC-1M damage case

The checked solutions during the process of TS optimization can be shown in *Figure 7.21* for the checked points during the optimization process.

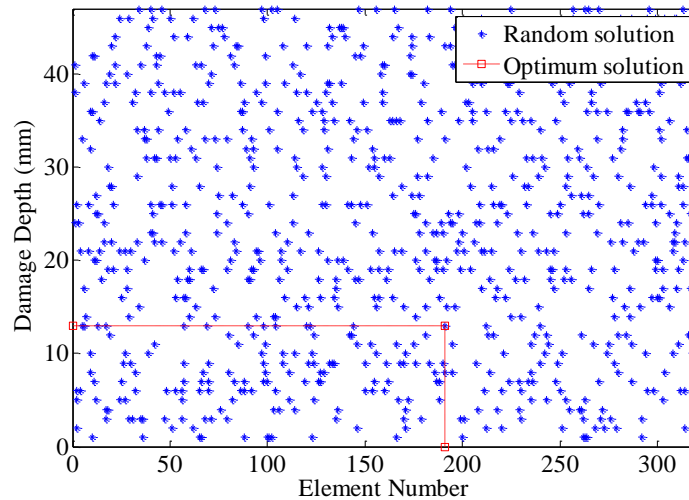


Figure 7.21: The distribution of the explored solutions in the tested space using TS optimization procedure for damage case LAGDC-1M

In *Figure 7.21*, the optimization process covers the whole searching space which encourages to find the optimum solution and avoids the local minima.

7.3.3.6 Application of TS procedure for damage detection of LAGDC-2M

The last damage case is examined under the proposed procedure of TS optimization to detect the location and severity of damage. The improvement of the objective function values is represented by *Figure 7.22*. The optimum solution is reached after 723 iterations, at which, the minimum value of objective function is 0.319. The optimum solution represents element number 192 and 18 mm depth as the optimum location of damage and its severity, respectively. Both of those values are close to the target values represented by element number 200 and 20 mm damage severity. Also, in this damage case, there is no need for the application of equivalent damage severity process due to the compatible length of damaged element in both experimental and numerical models.

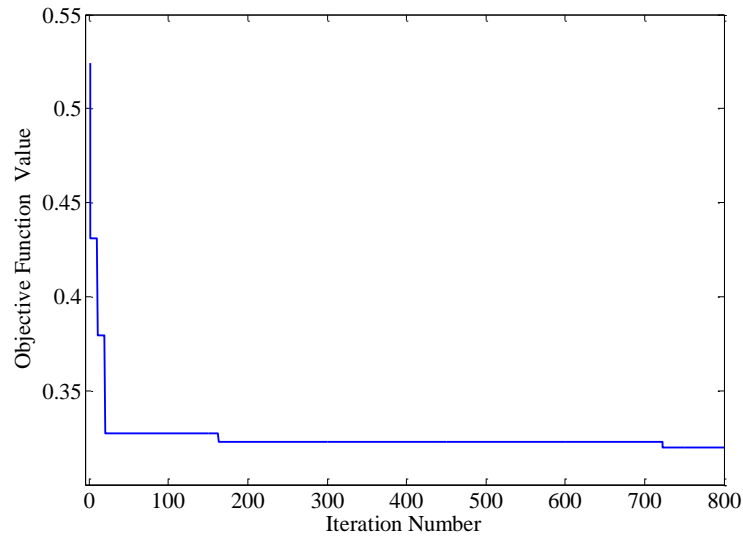


Figure 7.22: Improvement of objective function minimum value during iterations of the proposed TS based damage detection of the grid-bridge model in LAGDC-2M damage case

The distribution of the explored points during the optimization process is shown in Figure 7.23.

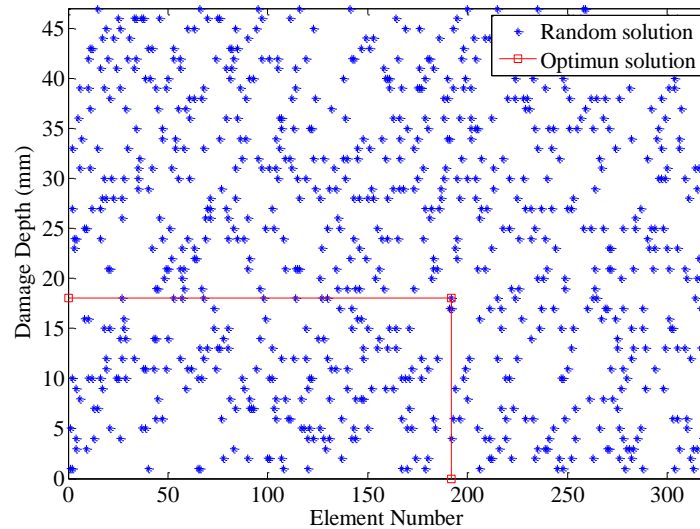


Figure 7.23: The distribution of the explored solutions in the tested space using TS optimization procedure for damage case LAGDC-2M

7.4 Damage detection in the Vierendeel bridge model

The steps of creating the form of objective function and application of damage detection procedure by TS optimization are implemented upon the Vierendeel bridge model in this paragraph.

7.4.1 Creating the form of objective function

The procedure of creating the proper form of objective function and its weighting factors that mentioned in *Figure 7.1* is considered in the Vierendeel bridge model. It is found that the proper form of objective function which produces global minimum close to the target damaged location is represented by equation (3.12) only. The participation of the normalized mode shapes of 3 and 5 modes are required to detect location of damage for both scenarios of damaged beam and column respectively. The weighting factor W_d will be 1.0 in the form of objective function which is in the form:

$$\text{Obj_Func} = W_d D \quad (7.3)$$

7.4.2 Application of the objective function

The application of objective function upon each case of damage is explained as following:

7.4.2.1 Objective function through damage case of AVDC-1

The proposed form of objective function is applied upon the first damage case AVDC-1 which is explained earlier in chapter-5. The first five mode shapes that extracted experimentally and computed numerically are used to calculate values of objective function under a certain damage severity which is randomly considered here as 20 mm depth.

Figure 7.24 shows the relationship between values of objective function and number of each damaged elements in the model. Behaviour of the objective function during the damage case AVDC-1 indicates that global minimum value is located at element number 334. This verifies the ability of use the proposed form of objective function under damage case AVDC-1 in the procedure of damage detection.

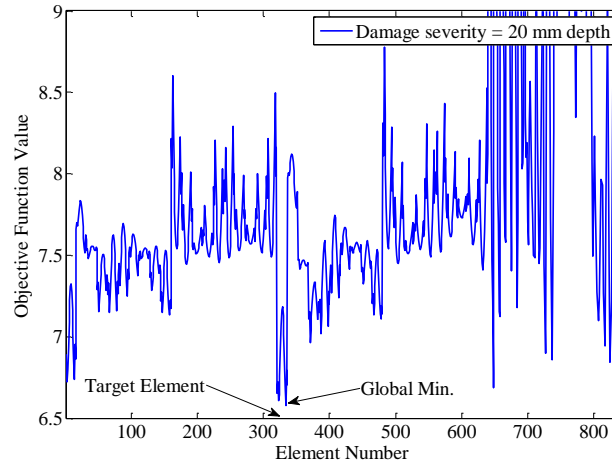


Figure 7.24: Behavior of objective function for damage case AVDC-1

7.4.2.2 Objective function through damage case of AVDC-1M

The proposed form of objective function is now applied upon the scenario of damaged column when the masses are added to the Vierendeel bridge model. In this case, only 3 modes should be used to provide the proper performance of the objective function. Damage severity of 20 mm depth is assumed for each damaged element to compute the corresponding value of objective function. All values of objective function are plotted with the corresponding number of damaged element as shown in *Figure 7.25*.

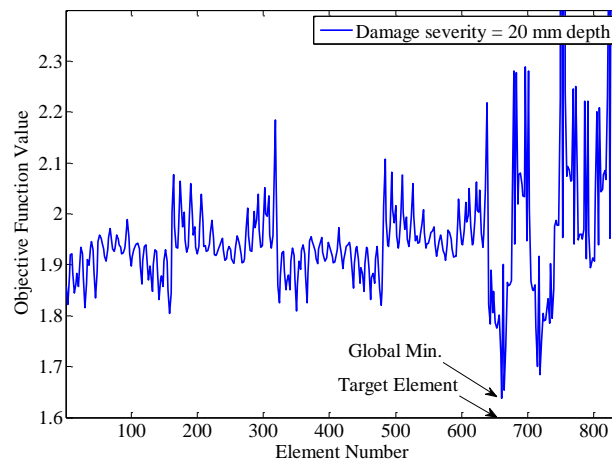


Figure 7.25: Behavior of objective function for damage case AVDC-1M

The location of global minimum value is at element number 661 which is very close to the target element number 660. This gives the ability of using the objective function with this damage case in the procedure of damage detection.

7.4.3 Damage detection in Vierendeel bridge model using the proposed TS optimization procedure

The adopted damage scenarios in the Vierendeel bridge model are investigated under the procedure of damage detection using the proposed TS optimization technique to detect location and damage severity. The range of possible damage severities that used during the TS optimization procedure is [1 - 47] mm which represents the damaged depth of element in the FE model. By trial and error method, the designed total number of iterations in the procedure of TS optimization is 1240 iterations. This value consists about 3.1% from the whole available searching space in the model that includes 838 elements. The application of the proposed TS optimization procedure to detect damage in each applicable damage case is implemented as following.

7.4.3.1 Application of TS procedure for damage detection of AVDC-1

During the application of TS optimization procedure of damage detection, the improvement of objective function values is progressed simultaneously with the iterations until reaching to the value of global minimum, as shown in *Figure 7.26*. The optimum solution is achieved after 889 iterations which produces the optimum location of damaged element exactly the same as the target element represented by number 332. The optimum damage severity during the optimization process represents the value of 36 mm damage depth. The procedure exhibits overestimation according to this damage value which has 16 mm difference relative to the target value of 20 mm depth. Nevertheless, the exact detected location of the damaged element during the optimization procedure indicates the ability of adopting the procedure of damage detection in this damage case.

Verification of the proposed numerical model, detection and localization of damage using Tabu-Search optimization method

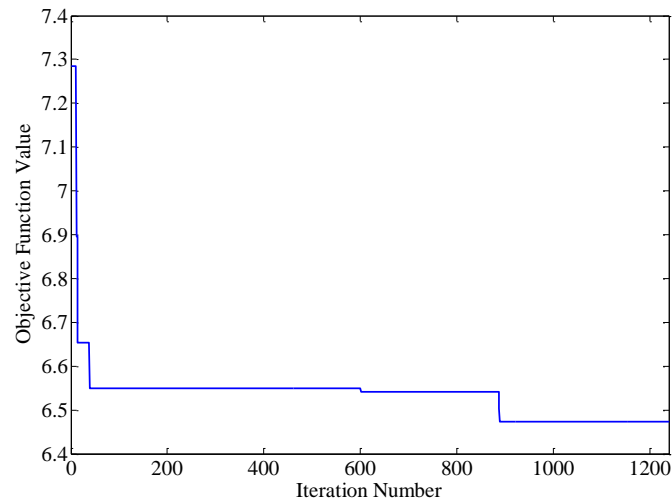


Figure 7.26: Improvement of objective function minimum value during iterations of the proposed TS based damage detection of the Vierendeel model in AVDC-1 damage case

The distribution of the checked solution during the optimization procedure is shown in *Figure 7.27*.

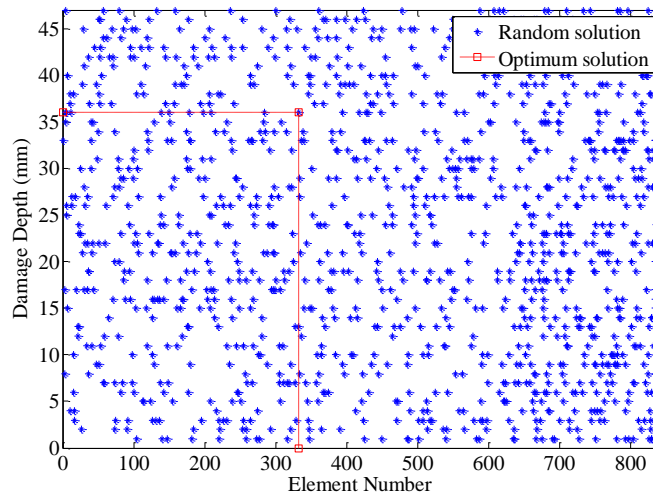


Figure 7.27: The distribution of the explored solutions in the tested space using TS optimization procedure for damage case AVDC-1

7.4.3.2 Application of TS procedure for damage detection of AVDC-1M

The case of damaged column in the model with additional mass state is investigated in the procedure of TS optimization for damage detection. During the optimization process, values of objective function are improved towards the minimum value. The progress of optimization is shown in *Figure 7.28*.

The optimum solution is achieved after 675 iterations, where the optimum damaged location is element number 659 which is very close to the target damaged element number 660. The resulted optimum damage severity is 32 mm depth, which is also within a reasonable limits when it is compared with the actual damage severity described in *Figure 5.43*. The shape of damage is irregular in this case because the size of damaged zone has 57 mm depth in on side and 5 mm in the other, *Figure 5.43*. So, if we consider the average depth of damaged zone, it could be considered as 31 $((57+5)/2)$ mm average depth. This is an approximate indication that could be used to describe the damage size in the real experimental case with the optimum result. Hence, it could be stated that both values of damage severities are close together and the optimum value of 32 mm depth is the best representative value for the experimental damage severity.

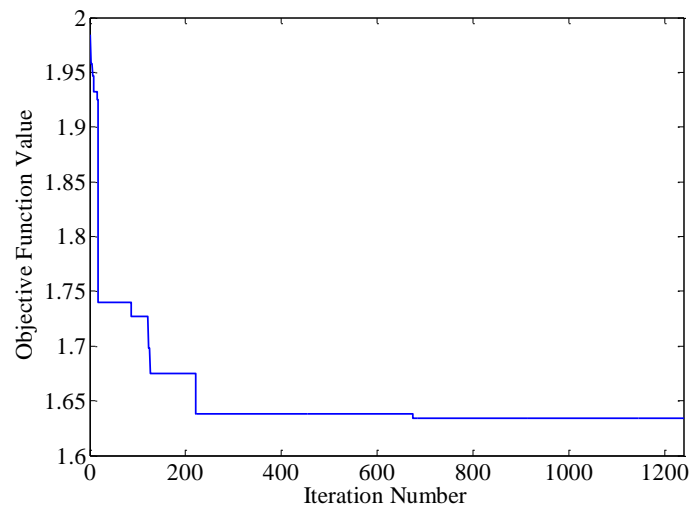


Figure 7.28: Improvement of objective function minimum value during iterations of the proposed TS based damage detection of the Vierendeel model in AVDC-1M damage case

The checked solutions during the optimization process are plotted in *Figure 7.29*.

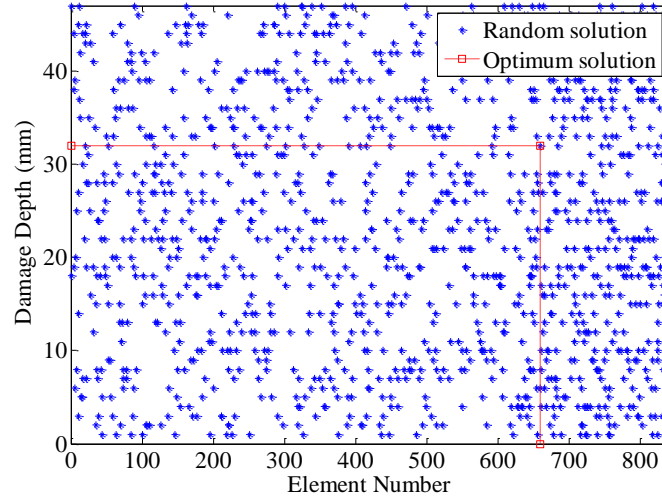


Figure 7.29: The distribution of the explored solutions in the tested space using TS optimization procedure for damage case AVDC-1M

The good distribution of the checked solutions in *Figure 7.29* reflects the adequate behaviour of the proposed TS optimization procedure during the searching process. In this behaviour, the whole searching space is explored within a limited number of iterations which guarantees to achieve the optimum solution properly.

7.5 Damage detection in the MSB model

The procedure of creating the form of objective function and its weighting factors is implemented upon the MSB model as the first part. The second part is applying the procedure of TS optimization to detect and localize the damage in the adopted model.

7.5.1 Creating the form of objective function

Using the procedure of creating the proper form of objective function that described in *Figure 7.1* and based on the adopted equations of (3.10) - (3.13), the following form is proposed:

$$\text{Obj_Func} = W_f F_r + W_d D + W_m M \quad (7.4)$$

where, the designed weighting factors W_f , W_d and W_m are 100, 1 and 100, respectively which are obtained by trial and error according to the information of the first five modes.

7.5.2 Application of the objective function during damage case ABDC-1

In order to verify the possibility of using the proposed form of objective function in the procedure of damage detection, the proposed form of objective function is applied upon the adopted damage case ABDC-1. Damage severity of 10 mm depth is assumed to be applied on the selected damaged elements in the FE model to compute the values of objective function at each damaged element. The relationship between values of objective function and the numbers of damaged column elements are plotted as shown in *Figure 7.30*.

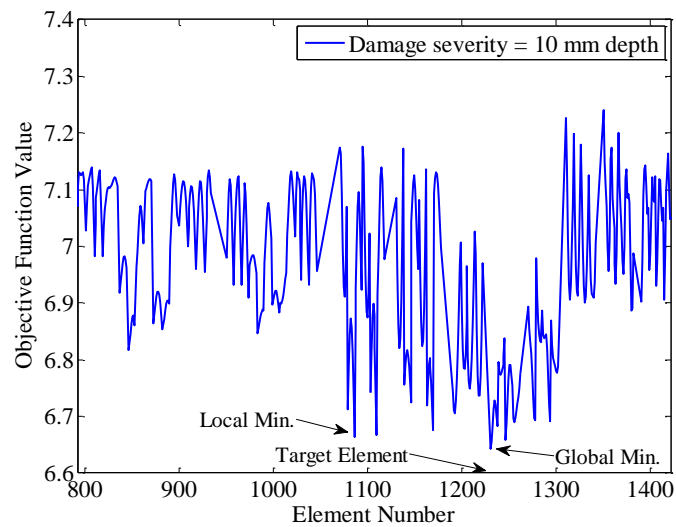


Figure 7.30: Behavior of the objective function for damage case ABDC-1

The global minimum value of objective function is located at element number 1233, as shown in *Figure 7.30*, which is exactly the same as the target element number. This behaviour reflects the efficiency of the proposed form of objective function which indicates that the objective function is able to be effectively used in the procedure of damage detection during the damage case of ABDC-1.

7.5.3 Damage detection in MSB model using the proposed TS optimization procedure

The proposed procedure of TS optimization is applied upon the damage case ABDC-1 for the sake of damage detection. The total included number of elements that likely to be damaged are 512 elements which represents the column elements only. This option is considered to avoid the complexity in calculations and to focus on the most important elements in the structure represented by the columns. Also, the probable damage severities are adopted in the range of [1:14] mm depth with 0.25 mm step which means that there are 57 value of damage severity likely to be used. Hence, the total searching space consists of 29184 (512x57) solutions but only 900 iterations are checked by the proposed TS optimization procedure. This means that the procedure of TS optimization during the damage detection process investigates only 3.1% (900/29184) from the whole searching space which is considerably small value. This also reflects the robustness and the efficiency of the proposed TS optimization procedure in the field of damage detection. The convergence of the objective function value toward global minimum value during the optimization procedure is shown in *Figure 7.31*.

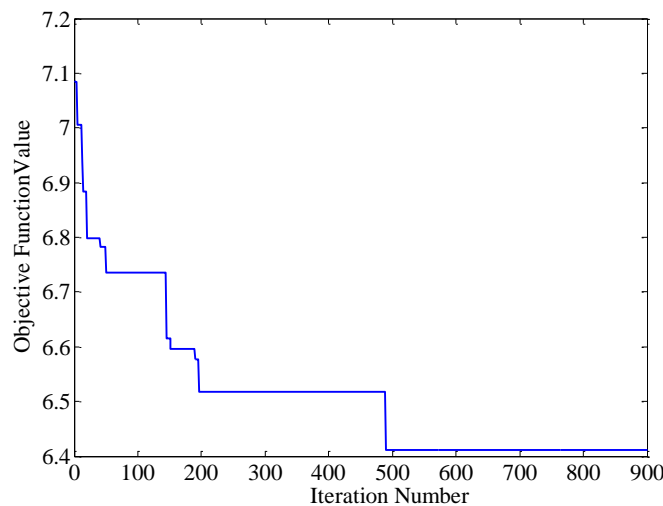


Figure 7.31: Improvement of objective function minimum value during iterations of the proposed TS based damage detection of the MSB model in damage case ABDC-1

The optimization process indicates that the optimum solution is achieved after 490 iterations with objective function value of 6.4106. At this value, the optimum solution includes optimum damage location at element number 1233 which is exactly the same location as the target element. On the other hand, the optimum solution gives optimum damage severity of 14 mm depth, which should be adjusted according to the equivalent damage process that described in *Figure 6.34*. In this figure, the equivalent damage severity of damage case (60x7.5) mm is (30x10.6) mm length by depth, respectively. Hence, the difference respect to the optimum damage severity of 14 mm is 3.4 mm (14 - 10.6). It is usually in any optimization process the solution is approximate, hence, the optimum damage severity indicates approximately to its corresponding value that implemented in the experimental model. The perfectly detected damaged location and the approximately detected damage severity indicate the efficiency of the proposed TS optimization procedure in damage detection process. Also, it exhibits the ability of this technique to avoid all traps of local minima and skip them towards global minimum value. The distribution of the checked solution during the optimization process can be shown in *Figure 7.32*.

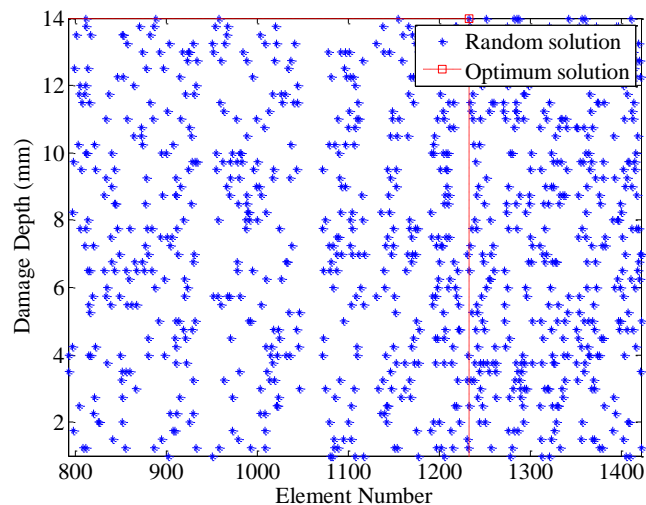


Figure 7.32: The distribution of the explored solutions in the tested space using TS optimization procedure for damage case ABDC-1

8. CONCLUSIONS AND RECOMMENDATIONS FOR FUTURE RESEARCH

Several conclusions can be observed in this work according to the aspects that taken into account during the study. The studied aspects include the use of AVM tests upon different models of steel structures to record the acceleration data that generated due to ambient vibrations. The recorded data are analysed to extract modal parameters of the adopted structures. Also, methods of modal extracting such as FDD, EFDD and SSI are highlighted in this work. The estimated modal parameters are used in the procedure of calibration by FE model updating process as well as damage detection process. Based on these aspects, the observed conclusions can be summarized as following:

1. Several techniques of damage detection are available in literature and the non-destructive techniques are the proper option to keep the integrity of structures without more damages during the detection process. As non-destructive inspection techniques, vibration based damage detection methods have significant features like the ability of dealing with damaged structure globally even when the damaged part is unreachable. Also, there is no need to prepare the detected parts before testing by cleaning them or installing the required test devices on these parts if it is difficult. These features encourage to use the base of vibration in the field of civil structure damage detection.
2. Ambient vibration measurements technique has several advantages when it is used as a base of structural modal identification, hence, this technique is suitable to be used in the field of structural damage detection. During the ambient vibration measurements, it is important to select proper locations for points of measurements depending on the type of structure. For the long-narrow structures, and when the torsional modes are insignificant, measurements points could be selected in line shape. For surfaces, plates or wide structures, a 2-D shape of measurements points should be implemented to produce the adequate modes of such structures. This 2-D shape of measurement points could be repeated in each level of the tall building to

form 3-D shape of measurements points which produce the required and representative modes.

3. ARTeMIS software provides several advantages in the field of extracting structural modal parameters based on AVM technique. It adopts FDD, EFDD and SSI techniques to extract modal parameters for any type of structure in simple way for the user with good accuracy. This is implemented with many options that verify the validity of the obtained results in order to be adoptable. On the other hand, ANSYS software is an adequate and efficient tool to perform modal structural analysis upon the FE model. It has several options that helps in creating and analysing models simultaneously with other softwares. Also, MATLAB software is an efficient tool that used in the programming of optimization procedure. The designed optimization procedure is processed in MATLAB which is integrated with ANSYS software to work as one unit. This unit could be then updated easily for any structure or any optimization procedure.
4. Using FDD technique to identify structural modal parameters is a suitable option due to its accuracy and simplicity. Unlike the SSI technique, implementing just few steps via FDD technique can lead to the requested values of modal parameters within relatively short time. Results could also be checked using EFDD technique. The SSI technique exhibits applicable behaviour to extract modal parameters in the case of one adopted set of measurements in the AVM test, like the case of overhang beam model. For the case of more than one adopted set of measurements, no sufficient structural (stable) modes are appeared in all sets of measurements which prevents estimating values of natural frequencies in some candidate locations. Thus, it is better to adopt FDD technique in modal identification instead of SSI technique in all models.
5. In the modal estimation procedure implemented by FDD peak-picking, it is adequate and accurately enough to use any of the frequency lines values of 2048, 4096 or 8192 to extract stable modes. This feature is considered for the complex structures while for simple structure the value of 1024 frequency lines is sufficient.

6. In literature, there are plenty of optimization methods deal with the field of structural damage detection in different ways. It is important to study each of them to make a decision about the proper one in damage detection. This reflects the importance of studying the untested techniques, like TS optimization, which allows the comparative academic studies to be implemented in the future.
7. It is more reliable to study different types of structural models which have one, two or three dimensional geometry when it is needed to apply new method of optimization such as TS procedure in the field of damage detection. The reliability is increased when the models are created and tested experimentally and numerically.
8. In experimental tests, the simulation of ambient vibration excitations using low level shaker excitation upon the tested models produces good compatible results with those obtained in the numerical analysis. This verify the ability of use such type of shaker devices to simulate ambient vibration in the laboratory.
9. The objective function plays the most important role in the procedure of damage detection. If the objective function is able to sense the changes in modal parameters sufficiently, then the damage could be detected. Otherwise, the detection according to the minimum value of objective function will not be accurate.
10. The first few modes in the range of 3 or 5 provide sufficient information about the changes in modal parameters due to the damage when applied in the objective function. Hence, using the first 3 or 5 modes is enough in the application of damage detection procedure.
11. In the calibration process of the Vierendeel bridge model, the same values of optimum structural parameters in both cases of using either 5 or 4 included modes in the calculations of objective function values are exactly obtained. This gives a conclusion that it is able to use any of them in the optimization procedure.
12. In damage detection optimization process, it is recommended to use equation 7.1 as an objective function for simple one dimensional structures while equation 7.2 is recommended for the grid-bridge model (2-D structure). For the bridge model with 3-D geometry, equation 7.3 is recommended as an objective function during the

optimization procedure and for the MSB equation 7.4 is recommended for the same purpose.

13. The proposed form of objective function of equation (3.12) and equation (3.13) facilitate the handling of normalized displacements of mode shapes that obtained by ARTeMIS software. ARTeMIS software produces only positive vectors of normalized displacements, hence, using the proposed forms gives solution to treat the displacement vectors of negative signs that obtained by ANSYS software for the corresponding modes.
14. In the objective function, the significant role of the changes in values of normalized displacements of mode shapes could be, sometimes, a sufficient parameter to perform the procedure of damage detection. The participation of natural frequencies could be sometime not included as in the case of Vierendeel bridge model, while the normalized displacements of mode shapes have the participation in all models. This indicates the important role of the information that provided by the mode shapes compared with the role of natural frequencies in the objective function.
15. According to process of the equivalent damage severity, it is possible to simulate any length of damaged element in the FE model that is shorter or longer than the actual damaged length in the experimental model.
16. In the calibration process of the Vierendeel bridge model, TS optimization procedure can achieve the optimum solution even in the low searching space ratio (0.11 - 4.25)%.
17. During the process of damage detection, the proposed TS optimization procedure achieves the optimum solution which represents the exact target value in some iterations while very close to the exact target value in other some iterations.
18. The proposed TS optimization procedure is an efficient technique that is able to avoid any existing local minima in the searching space and achieve the global optimum solution even with tiny difference between local and global minima.

According to present work, some recommendations for future researches are suggested as following:

1. Based on the same adopted models, applying damage detection procedure upon each case study under more than one damage location.
2. Including of more dynamic properties in the objective function, such as damping ratio, to increase the sensitivity towards the presence of damage.
3. Applying the same damage detection optimization procedure on concrete structures models.
4. Creating a formula of objective function that adopts the same number of included modes for the case of Vierendeel bridge model, without and with additional mass states, which can be used also for all other adopted models (case study) of this work.

9. REFERENCES

- [1] Dharma D., Keshab N., Chirayu T., Ramanjaneyulu G.: Different techniques of structural health monitoring, *International Journal of Civil, Structural, Environmental and Infrastructure Engineering*, ISSN 2249-6866, Vol. 3, No. 2, 2013, pp. 55-66.
- [2] Deraemaeker A., Reynders E., De Roeck G., Kullaa J.: Vibration based SHM: comparison of the performance of modal features vs features extracted from spatial filters under changing environmental conditions, *Proceedings of ISMA 2006, International Conference on Noise and Vibration Engineering*, Sas P. and De Munck M. (editors), Leuven, Belgium, 2006, pp. 849-863.
- [3] Turek, M., Thibert K., Ventura C., Kuan S.: Ambient vibration testing of three unreinforced brick masonry buildings in Vancouver, Canada, *Proceedings of (IMAC XXIV) the 24th International Modal Analysis Conference*, paper 77, St. Louis, Missouri, 2006.
- [4] ARTeMIS Extractor Pro, Release 3.41, Structural Vibration Solution A/S, NOVI Science Park, Niles Jernes Vej 10, DK-9229 Aalborg East, Denmark, 2004.
- [5] Ivanović S., Trifunac M., Todorovska M.: Ambient vibration tests of structures-a review, *ISET Journal of Earthquake Technology*, Paper No. 407, Vol. 37, No. 4, 2000, pp.165-197.
- [6] New Zealand Transport Agency, NZTA S6: 2015, Bridges and other significant highway structures inspection policy, SP/SS6: 2015 150220, 17 pages.
- [7] Design manual for road and bridges, *Inspection of Highway Structures*, BD 63/07, Vol. 3, Section 2, Part 4, February 2007, UK.
- [8] Zhu S., Levinson D., Liu H., Harder K.: The traffic and behavioral effects of the I-35W Mississippi river bridge collapse, *Transportation Research Part A*, Vol. 44, 2010, pp. 771-784, DOI: 10.1016/j.tra.2010.07.001.
- [9] Balageas D., Fritzen C., Guemes A.: *Structural health monitoring*, Wiley-ISTE, ISBN: 978-1-905209-01-9, 2006, 496 pages.
- [10] Melchor-Lucero O., Ferregut C.: Earthquake damage assessment of reinforced concrete members using an expert system, *11th World Conference on Earthquake Engineering*, Elsevier Science Ltd., ISBN: 0 08 042822 3, Paper No. 1263, 1996, 8 pages.
- [11] Bharadwaj N., Damodar M., Dipak K.: Vibration based structural damage detection Technique using Particle Swarm optimization with incremental swarm size, *International Journal of Aeronautical and Space Sciences*, Vol. 13, No.3, 2012, pp. 323-331, DOI: 10.5139/IJASS.2012.13.3.323.

References

- [12] Abu Husain N., Ouyang H.: Detection of damage in welded structure using experimental modal data, 9th International Conference on Damage Structures (DAMAS 2011) , IOP Publishing, Journal of physics, Conference series, Vol. 305, No. 1, 2011, pp. 1-11.
- [13] Farrar C., Worden K.: Structural health monitoring- a machine learning perspective, John Wiley & Sons, ISBN: 9781118443118, 1st edition, 2013, DOI: 10.1002/9781118443118.
- [14] Kahl K., Sirkis J. S.: Damage detection in beam structure using subspace rotation algorithm with strain data, American Institute of Aeronautics and Astronautics AIAA Journal, ISSN: 0001-1452, Vol. 34, No. 12, 1996, pp. 2609-2614.
- [15] Li B., Chen X., Ma J., He Z.: Detection of crack location and size in structures using wavelet finite element method, Journal of Sound and Vibration, Vol. 285, No. 4-5, 2005, pp. 767-782, DOI:10.1016/j.jsv.2004.08.040.
- [16] Schreurs P.: Fracture mechanics, Lecture notes - course 4A780, Concept version, Eindhoven University of Technology, Department of Mechanical Engineering, Materials Technology, Netherlands, 2012, 162 pages.
- [17] Erdogan F.: Fracture mechanics, International Journal of Solids and Structures, Vol. 37, No. 1-2, 2000, pp. 171-183, DOI:10.1016/S0020-7683(99)00086-4.
- [18] Shi ZY., Law S. S.: Structural damage localization from modal strain energy change, Journal of Sound and Vibration Vol. 218, No. 5, 1998, pp. 825-844, DOI:10.1006/jsvi.1998.1878.
- [19] Kumar M., Shenoj R.A., Cox S. J.: Experimental validation of modal strain energies based damage identification method for a composite sandwich beam, Journal of Composites and Science Technology, Vol. 69, No. 10, 2009, pp. 1635-1643, DOI:10.1016/j.compscitech.2009.03.019.
- [20] Cornwell P., Doebling S. W., Farrar C. R.: Application of the strain energy damage detection method to plate-like structures, Journal of Sound and Vibration Vol. 224, No. 2, 1999, pp. 359-374, DOI:10.1006/jsvi.1999.2163.
- [21] Esfandiari A., Nejad F. B., Rahai A.: Theoretical and experimental structural damage diagnosis method using natural frequencies through an improved sensitivity equation, International Journal of Mechanical Sciences, Vol. 70, 2013, pp. 79-89, DOI:10.1016/j.ijmecsci.2013.02.006.
- [22] Wang Y.: Vibration-based damage detection on a multi-girder bridge superstructure, PhD Thesis, University of Saskatchewan, Saskatoon, Canada, 2011.
- [23] Jean J. S.: A review of damage detection and health monitoring of mechanical systems from changes in the measurement of linear and non-linear vibrations, Mechanical

References

- Vibrations : Measurement, Effects and Control, Chapter 13, Nova Science Publishers, Inc., Editor: Robert R. Sapri, ISBN 978-1-60692-037-4, 2009, pp.643-702.
- [24] Doebling S. W., Farrar C. R., Prime M. B., Shevitz D. W.: Damage identification and health monitoring of structural and mechanical systems from changes in their vibration characteristics: a literature review, Los Alamos National Laboratory, University of California, LA-13070-MS, UC-900, 1996.
- [25] Sinou J., Lees A.: Influence of cracks in rotating shafts, *Journal of Sound and Vibration*, Vol. 285, No. 4-5, 2005, pp. 1015-1037, DOI:10.1016/j.jsv.2004.09.008.
- [26] Mosavi A., Dickey D., Seracino R., Rizkalla S.: Identifying damage locations under ambient vibrations utilizing vector autoregressive models and Mahalanobis distances, *Mechanical Systems and Signal Processing*, Vol. 26, 2012, pp. 254–267, DOI:10.1016/j.ymsp.2011.06.009.
- [27] Nahvi H, Jabbari M.: Crack detection in beams using experimental modal data and finite element model, *International Journal of Mechanical Sciences*, Vol. 47, No. 10, 2005, pp. 1477–1497, DOI:10.1016/j.ijmecsci.2005.06.008.
- [28] Owolabi G.M., Swamidass A.S.J., Seshadri R.: Crack detection in beam using changes in frequencies and amplitudes of frequency response function, *Journal of Sound and Vibration*, Vol. 265, No.1, 2003, pp. 1-22, DOI:10.1016/S0022-460X(02)01264-6.
- [29] Sierra J., Guemes A., Mujica L.: Damage detection by using FBGs and strain field pattern recognition techniques. *Smart Materials and Structures*, Vol. 22, No.2, 2013, pp. 1-10, DOI:10.1088/0964-1726/22/2/025011.
- [30] Alalikhani A., Al-Wazni S., Mišković Z., Salatić R.: Numerical test of damage detection using Tabu Search method, *Proceedings of 14th conference of ASEES – Association of Structural Engineering of Serbia*, (editors) M. Lazović, B. Stevanović, Novi Sad, Serbia, ISBN 978-86-85073-19-9, 2014, pp. 513-520.
- [31] Charles J. S.: Localization of vibration-based damage detection method in structural applications, Master thesis, University of Iowa, 2012.
- [32] Tung S. H., Shih M. H., Sung W. P.: Development of digital image correlation method to analyse crack variations of masonry wall, *Sadhana-Academy Proceeding in Engineering Sciences*, Vol. 33, No. 6, 2008, pp. 767-779.
- [33] Shih M. H., Sung W. P.: Developing dynamic digital image techniques with continuous Parameters to detect structural damage, *The Scientific World Journal*, Hindawi Publishing Corporation, Vol. 2013, Article ID 453468, 7 pages, <http://dx.doi.org/10.1155/2013/453468>.
- [34] Chen J. G., Wadhwa N., Cha Y. J., Durand F., Freeman W. T., Buyukozturk O.: Structural modal identification through high speed camera video: motion magnification, *Springer, Topics in Modal Analysis I*, Vol. 7, 2014, pp.191-197.

References

- [35] Yang C., Wu Z., Zhang Y.: Structural health monitoring of an existing PC box girder bridge with distributed HCFRP sensors in a destructive test, *Smart Materials and Structures*, IOP Publishing, Vol. 17, 2008, pp.1-10, DOI:10.1088/0964-1726/17/3/035032.
- [36] Bakis C. E., Nanni A., Terosky J. A., Koehler S. W.: Self-monitoring, pseudo-ductile, hybrid FRP reinforcement rods for concrete applications, *Composites Science and Technology*, Vol. 61, No. 6, 2001, pp.815-823, DOI:10.1016/S0266-3538(00)00184-6.
- [37] Muto N., Arai Y., Shin S. G., Matsubara H., Yanagida H., Sugita M., Nakatsuji T.: Hybrid composites with self-diagnosing function for preventing fatal fracture, *Composites Science and Technology*, Vol. 61, No. 6, 2001, p.p. 875-883, DOI:10.1016/S0266-3538(00)00165-2.
- [38] Wu Z. S., Yang C. Q., Harada T., Ye L. P.: Self-diagnosis of structures strengthened with hybrid carbon-fiber-reinforced polymer sheet, *Smart Material and Structures*, Institute of Physics Publishing, Vol. 14, 2005, pp. S39-S51, DOI:10.1088/0964-1726/14/3/006.
- [39] He R. S., Hwang S. F.: Identifying damage in spherical laminate shells by using a hybrid real-parameter genetic algorithm, *Journal of Composite Structures*, Vol. 80, No. 1, 2007, pp. 32-41, DOI:10.1016/j.compstruct.2006.02.035.
- [40] Estrada R. S.: Damage detection method in bridges through vibration monitoring: evaluation and application, PhD thesis, University of Minho, 2008.
- [41] He R. S., Hwang S. F.: Damage detection by an adaptive real-parameter simulated annealing genetic algorithm, *Journal of Computers and Structures*, Vol. 84, No. 31-32, 2006, pp. 2231-2243, DOI:10.1016/j.compstruc.2006.08.031.
- [42] Chou J. H., Ghaboussi J.: Genetic algorithm in structural damage detection, *Journal of Computers and Structures*, Vol. 79, No. 14, 2001, pp.1335-1353, DOI:10.1016/S0045-7949(01)00027-X.
- [43] Rucka M., Wilde K.: Crack identification using wavelets on experimental static deflection profiles, *Journal of Engineering Structures*, Vol. 28, No. 2, 2006, pp.279-288, DOI:10.1016/j.engstruct.2005.07.009.
- [44] Terradellas E., Morales G., Cuxart J., Yague C.: Wavelet method: application to the study of the stable atmospheric boundary layer under non-stationary conditions, *Dynamics of Atmospheres and Oceans*, Vol. 34, No. 2-4, 2001, pp. 225-244, DOI:10.1016/S0377-0265(01)00069-0.
- [45] Wang Q., Deng X.: Damage detection with spatial wavelets, *International Journal of Solids and Structures*, Vol. 36, No. 23, 1999, pp. 3443-3468, DOI:10.1016/S0020-7683(98)00152-8.

References

- [46] Kim H., Melhem H.: Damage detection of structures by wavelet analysis, *Journal of Engineering Structures*, Vol. 26, No. 3, 2004, pp. 347 - 362, DOI:10.1016/j.engstruct.2003.10.008.
- [47] Pandey A., Biswas M.: Damage detection in structures using changes in flexibility, *Journal of Sound and Vibration*, Vol. 169, No. 1, 1994, pp. 3-17, DOI:10.1006/jsvi.1994.1002.
- [48] Shih H. W., Thambiratnam D. P., Chan T. H.: Vibration based structural damage detection in flexural members using multi-criteria approach, *Journal of Sound and Vibration*, Vol. 323, No. 3-5, 2009, pp. 645-661, DOI:10.1016/j.jsv.2009.01.019.
- [49] Fan W., Qiao P.: Vibration-based damage identification methods: a review and comparative study, *Structural Health Monitoring*, Vol. 10, No.1, 2010, pp. 83-29, DOI: 10.1177/1475921710365419.
- [50] Wickramasinghe W. R., Thambiratnam, D. P., Chan T.: Modal flexibility method for structural damage detection in suspension bridges, 6th International Conference on Structural Health Monitoring of Intelligent Infrastructure, SHMII-6, 2013, Hong Kong.
- [51] Hwang H. Y., Kim C.: Damage detection in structures using a few frequency response measurements, *Journal of Sound and Vibration*, Vol. 270, No. 1-2, 2004, pp. 1-14, DOI:10.1016/S0022-460X(03)00190-1.
- [52] Nozarian M., Esfandiari A.: Structural damage identification using frequency response function, *Institute of Materials Engineering Australasia Ltd., Material Forum*, Vol. 33, 2009, pp.443-449.
- [53] Bandara R., Chan T., Thambiratnam D.: Structural damage detection method using frequency response functions, *Structural Health Monitoring*, 2014, pp. 1-12, DOI: 10.1177/1475921714522847.
- [54] He K., Zhu W.: Structural damage detection using changes in natural frequencies: theory and applications, *Journal of Physics*, 9th International Conference on Damage Assessment of Structures (DAMAS 2011), Conference Series 305, pp. 1-10, DOI:10.1088/1742-6596/305/1/012054.
- [55] Salawu O. S.: Detection of structural damage through changes in frequency: a review, *Engineering Structures*, Vol. 19, No. 9, 1997, pp.718-723, DOI:10.1016/S0141-0296(96)00149-6.
- [56] Wang L., Chan T.: Review of vibration-based damage detection and condition assessment of bridge structures using structural health monitoring, 2nd Infrastructure Theme Postgraduate Conference, 2009, Queensland University.
- [57] Farrar C., James III G.: System identification from ambient vibration measurements on a bridge, *Journal of Sound and Vibration*, Vol. 205, No. 1, 1997, pp.1-18, DOI:10.1006/jsvi.1997.0977.

References

- [58] Brincker R., Zhang L., Andersen P.: Modal identification of output-only systems using frequency domain decomposition, *Smart Materials and Structures*, Vol. 10, No. 3, 2001, pp. 441-445, DOI: 10.1088/0964-1726/10/3/303.
- [59] Brincker R., Frandsen J., Andersen P.: Ambient response analysis of the great belt bridge, *Proceedings of the 18th International Modal Analysis Conference (IMAC)*, San Antonio, Texas, 2000, pp. 26-32.
- [60] Roia D., Gara F., Balducci A., Dezi L.: Ambient vibration tests on a reinforced concrete school building before and after retrofitting works with external steel, dissipative towers, *Proceedings of the 9th International Conference on Structural Dynamics, Eurodyn*, (editors) Cunha A., Caetano E., Ribeir P., Müller G., Porto, Portugal, ISSN: 2311-9020, ISBN: 978-972-752-165-4, 2014, pp. 2509-2516.
- [61] Mišković Z., Alalikhani A., Al-Wazni S., Salatić R., Mišković L.: Vibration ambient test of Gazela bridge approach structure in Belgrade, *5th International Conference Civil Engineering - Science and Practice, Žabljak*, 2014, pp. 261-268.
- [62] Al-Wazni S., Mišković Z., Alalikhani A., Salatić R.: Comparison of FDD and SSI modal identification methods from ambient vibration data – case study, *5th International Conference Civil Engineering - Science and Practice, Žabljak*, 2014, pp. 3-10.
- [63] Zenunovic D., Topalovic M., Folic R.: Identification of modal parameters of bridges using ambient vibration measurements, *Shock and Vibration*, 2015, Article ID 957841, pp. 1-20.
- [64] Lord J. F., Ventura C., Dascotte E., Brinkler R., Andersen P.: FEM updating using ambient vibration data from a 48-storey building in Vancouver, British Columbia, Canada, *The 32nd International Congress and Exposition on Noise Control Engineering Jeju International Convention Center, Seogwipo, Korea*, 2003, No.1026, 8-pages.
- [65] Mahmoud M., Abe M., Fujino Y.: Analysis of suspension bridge by ambient vibration measurement using time domain method and its application to health monitoring, *Proceedings of SPIE, the International Society for Optical Engineering*, ISSN 0277-786X, Vol. 4359, No. 1, 2001, pp. 504-510.
- [66] Lu K. C., Wang Y., Lynch J. P., Loh C. H., Chen Y. J., Lin P. Y., Lee Z. K.: Ambient vibration study of the Gi-Lu cable-stay bridge: application of wireless sensing units, *Proceeding of SPIE 13th Annual Symposium on Smart Structural and Materials*, San Diego, CA, USA, 2006, Article No. 61741D, 11-pages.
- [67] Min K. W., Kim J., Parl S. A., Park C. S.: Ambient vibration testing for story stiffness estimation of a heritage timber building, *The Scientific World Journal*, Hindawi Publishing Corporation, Volume 2013, Article ID 198483, 9-pages.
- [68] Maral G.: *VSAT Networks*, Second Edition, John Wiley and Sons, ISBN 0-470-86684-5, 2nd edition, 2003.

- [69] Lamarche C., Paultre P., Proulx J., Mousseau S.: Assessment of the frequency domain decomposition technique by forced-vibration tests of a full-scale structure, *Earthquake Engineering and Structural Dynamics*, Vol. 37, No. 3, 2008, pp. 487-494, DOI: 10.1002/eqe.766.
- [70] Le T. H., Tamura Y.: Modal identification of ambient vibration structure using frequency domain decomposition and wavelet transform, *The 7th Asia-Pacific Conference on Wind Engineering*, Taipei, Taiwan, 2009, 8-pages.
- [71] Brincker R., Andersen P., Jacobsen N.: Automated frequency domain decomposition for operational modal analysis, *Proceedings of IMAC-XXIV, A Conference & Exposition on Structural Dynamics*, Society for Experimental Mechanics, No.25, 2007, 7-pages.
- [72] Freitas T. C., Pereira J. A.: Modal parameters identification using only response data-stochastic subspace identification and frequency domain decomposition, *Proceedings of COBEM, 19th International Congress of Mechanical Engineering*, Brasília, DF, 2007, 9-pages.
- [73] Jacobsen N., Andersen P., Brincker R.: Using enhanced frequency domain decomposition as a robust technique to harmonic excitation in operational modal analysis, *Proceedings of ISMA 2006, International Conference on Noise and Vibration Engineering*, Leuven, Belgium, Vol. 6, 2006, pp. 3129-3140.
- [74] Foti D., Gattulli V., Potenza F.: Output-only identification and model updating by dynamic testing in unfavorable conditions of a seismically damaged building, *Computer-Aided Civil and Infrastructure Engineering*, Vol. 29, No. 9, 2014, pp. 659–675, DOI: 10.1111/mice.12071.
- [75] Stevenson J. D.: Structural damping values as a function of dynamic response stress and deformation level, *Nuclear Engineering and Design*, Vol. 60, No. 2, 1980, pp. 211-237, DOI:10.1016/0029-5493(80)90238-1.
- [76] Agarwal A., Lang J. H.: *Foundations of Analog and Digital Electronic Circuits*, Department of Electrical Engineering and Computer Science, Massachusetts Institute of Technology, Elsevier, ISBN: 1-55860-735-8, 2005, p. 43.
- [77] Meninger S., Mur-Miranda J., Amirtharajah R., Chandrakasan A., Lang J.: Vibration - to- electric energy conversion, *IEEE Transactions on Very Large Scale Integration (VLSI) Systems*, Vol. 9, No. 1, 2001, pp. 64-76.
- [78] Emilio M. D. P.: *Data Aquisition Systems (Hardware): from fundamentals to applied design*, Chapter 2, Springer, ISBN: 978-1-4614-4213-4, 2013, pp.11-79, DOI 10.1007/978-1-4614-4214-1_2.
- [79] Sahin M., Sheno R. A.: Quantification and localization of damage in beam-like structures by using artificial neural networks with experimental validation, *Journal of*

References

- engineering structures, Vol. 25, No. 14, 2003, pp. 1785-1802, DOI:10.1016/j.engstruct.2003.08.001
- [80] Hui L., Kegui X., Quanquan Q.: Study of structural damage detection with multi-objective function genetic algorithms, SREE Conference on Engineering Modeling and Simulation, Procedia Engineering, Elsevier, Vol. 12, pp. 80–86, 2011, DOI:10.1016/j.proeng.2011.05.014
- [81] Meruane V., Heylen W.: An hybrid real genetic algorithm to detect structural damage using modal properties, Elsevier, Mechanical Systems and Signal Processing, Vol. 25, No. 5, 2011, pp. 1559 -1573, DOI:10.1016/j.ymsp.2010.11.020.
- [82] Nabeel H. H., Aveen A. A.: Damage detection and assessment of stiffness and mass matrices in curved simply supported beam using genetic algorithm, Journal of Engineering, University of Baghdad, Iraq, Vol. 18, No. 1, 2012, pp. 1-21.
- [83] Nagesh K. D.: Genetic algorithms, Water Resources Systems Planning and Management: Advanced Topics, NPTEL, Civil Engineering, IISc, Bangalore, M9L2, pp. 1 - 14.
- [84] Meruane V., Heylen W.: Damage detection by real-parameter hybrid genetic algorithm, European Workshop on Structural Health Monitoring, Poland, 2008, pp.1073-1080.
- [85] Aghabarati H., Tehranizadeh M.: Comparison study on neural networks in damage detection of steel truss bridge, Journal of Structural Engineering and Geotechnics, Vol. 1, No.1, 2011, pp. 37-48.
- [86] Meruane V., Heylen W.: Damage detection on a multi-cracked beam by parallel genetic algorithms using modal characteristics, Proceeding of ISMA 2008, International Conference on Noise and Vibration Engineering, Leuven, Belgium, 2008, pp. 3319-3332.
- [87] Heikki M., Kaisa M., Antti P.: On initial populations of a genetic algorithm for continuous optimization problems, Springer, Journal Global Optim, Vol. 37, No. 3, 2007, pp. 405–436, DOI:10.1007/s10898-006-9056-6.
- [88] Bashir L., Hasan R.: Solving banana (Rosenbrock) function based on fitness function, World Scientific News, EISSN 2392-2192, Vol. (12), 2015, pp. 41-56.
- [89] Iclanzan D., Dumitrescu D.: Overcoming hierarchical difficulty by hill-climbing the building block structure, GECCO'07 Proceedings of the 9th annual conference on Genetic and evolutionary computation, ISBN: 978-1-59593-697-4, 2007, pp. 1256-1263, DOI:10.1145/1276958.1277199.
- [90] Au F. T., Cheng Y. S., Tham L. G., Bai Z. Z.: Structural damage detection based on a micro-genetic algorithm using incomplete and noisy modal test data, Elsevier, Journal of Sound and Vibration, Vol. 259, No. 5, 2003, pp. 1081-1094, DOI:10.1006/jsvi.2002.5116.

References

- [91] Degertekin S.: A comparison of simulated annealing and genetic algorithm for optimum design of nonlinear steel space frames, *Structural and Multidisciplinary Optimization*, Springer, Vol. 34, No. 4, 2007, pp. 347–359, DOI 10.1007/s00158-007-0096-4.
- [92] Xia Y., Hao H.: A genetic algorithm for structural damage detection based on vibration data, *IMAC XIX, 19th International modal analysis conference*, Nanyang Technological University, Singapore, 2011, pp. 1381 - 1387.
- [93] Friswell M. I., Penny J. E., Garvey S. D.: A combined genetic and eigen-sensitivity algorithm for the location of damage in structures, *Journal of Computers and Structures*, Vol. 69, No. 5, 1998, pp. 547-556, DOI:10.1016/S0045-7949(98)00125-4.
- [94] Whitley D.: A genetic algorithm tutorial, *Statistics and Computing*, Springer, Vol. 4, No. 2, 1994, pp. 65 - 85, DOI:10.1007/BF00175354.
- [95] Panigrahi S., Chakraverty S., Mishra B.: Genetic algorithm based damage identification in non-homogenous structural members, *Challenges and Applications of Mathematical Modelling Techniques in Building Science and Technology (CAM2TBST)*, Central Building Research Institute, India, 2008, 9-pages.
- [96] Malhotra R., Singh N., Singh Y.: Genetic algorithms: concepts, design for optimization of process controllers, *Journal of Computer and Information Science*, Vol. 4, No. 2, 2011, pp. 39-54, DOI: <http://dx.doi.org/10.5539/cis.v4n2p39>.
- [97] Kirkpatrick S., Gelatt C. D., Vecchi M. P.: Optimization by simulated annealing, *Science*, New Series, Vol. 220, No. 4598, 1983, pp. 671-680.
- [98] Bertsimas D., Tsitsiklis J.: Simulated annealing, *Journal of Statistical Science*, Vol. 8, No. 1, 1993, pp. 10 - 15.
- [99] Tsallis C., Stariolo D.: Generalized simulated annealing, Elsevier, *Physica A: Statistical Mechanics and its Application*, Vol. 233, No. 1-2, 1996, pp. 395 - 406.
- [100] Alizamir S., Rebennack S., Pardalos P. M: Improving the neighbourhood selection strategy in simulated annealing using the optimal stopping problem, *Book of Simulated Annealing*, (editor) Tan C.M., ISBN 978-953-7619-07-7, I-Tech Education and Publishing, Vienna, Austria, 2008, pp. 363 - 382.
- [101] MATLAB software, Version 7.11.0.584 (R2010b), User's Guide, Option Reference, Simulated Annealing Options, Temperature Options.
- [102] Kirkegaard P. H., Rytter A.: Vibration based damage assessment of civil engineering structures using neural networks, *1st Workshop of the European Group for Structural Engineering Applications of Artificial Intelligence*, Lausanne, Denmark, ISSN 0902-7513 R9408, 1994, pp. 1-15.

- [103] Habib Y., Sadiq M., Hakim A.: Evolutionary algorithms, simulated annealing and tabu search: a comparative study, *Engineering Applications of Artificial Intelligence*, Vol. 14, No. 2, 2001, pp. 167–181, DOI:10.1016/S0952-1976(00)00065-8.
- [104] Norhisham B., Hong H., Andrew J.: Damage detection using artificial neural network with consideration of uncertainties, *Engineering Structures*, Vol. 29, No. 11, 2007, pp. 2806–2815, DOI:10.1016/j.engstruct.2007.01.013.
- [105] Mehrjoo M., Khaji N., Moharrami H., Bahreininejad A.: Damage detection of truss bridge joints using artificial neural networks, *Expert Systems with Applications*, Vol. 35, No. 3, 2008, pp. 1122–1131, DOI:10.1016/j.eswa.2007.08.008.
- [106] Gendreau M.: An introduction to Tabu Search: Chapter Handbook of Metaheuristics, *International Series in Operations Research & Management Science*, Springer, Kluwer Academic Publishers, ISBN: 0-306-48056-0, Vol. 57, 2003, pp. 37-54, DOI:10.1007/0-306-48056-5_2.
- [107] Glover, F.: Future paths for integer programming and links to artificial intelligence, *Computers & Operations Research*, Vol. 13, No. 5, 1986, pp. 533–549, DOI: 10.1016/0305-0548(86)90048-1.
- [108] Harris H. G., Sabnis G. M.: *Structural Modelling and Experimental Techniques*, Second Edition, CRC Press 1999.
- [109] Wickersheimer D.: The Vierendeel, *Journal of the Society of Architectural Historians*, University of California Press, Vol. 35, No. 1, 1976, pp. 54-60.
- [110] Soyoz S., Feng M. Q., Shinozuka M.: Structural reliability estimation with vibration-based identified parameters, *ASCE Journal of Engineering Mechanics*, Vol. 136, No. 1, 2010, pp. 100–106, DOI:10.1061/(ASCE)EM.1943-7889.0000066.
- [111] Sehgal S., Kumar H.: Structural dynamic model updating techniques: a state of the art review, Springer, *Archives of Computational Methods in Engineering*, 2015, pp. 1-19, DOI: 10.1007/s11831-015-9150-3.
- [112] Ruotolo R., Surace C.: Damage assessment of multiple cracked beams: numerical results and experimental validation, *Journal of Sound and Vibration*, Vol. 206 No. 4, 1997, pp. 567–588, DOI:10.1006/jsvi.1997.1109.
- [113] Alalikhhan A., Al-Wazni S., Mišković Z., Salatić R., Mišković Lj., Tests of heuristic optimization techniques in vibration- based damage detection, (Paper ID: 1410-2015 – under revision), *Građevinar – Jorunal of the Croatian Association of Civil Engineers*, ISSN (print) 0350-2465, ISSN (on-line) 1333-9095.
- [114] Mišković Z., Al-Wazni S., Alalikhhan A., Damage detection for civil structural health monitoring application – a case study of the steel grid bridge structural model, *Technical Gazette* (paper ID: TV-20160411065936 – under revision), ISSN 1330-3651 (print) ISSN 1848-6339 (On-line).

10. APPENDICES

APPENDIX A. Configuration input file (CFG)

The configuration input file consists of mainly six parts represent the flow charts of *Figure 5.5* or *Figure 5.26* as following:

1. The first part includes the title, symbol (T) followed by the value of sampling interval.

This is the header group with the title of the project.

The title can be a string of any length.

Header

Axi-symmetrical Pedestrian Bridge Model with Closely Spaced Modes

This is the sampling interval specified in sec.

T

0.0016666666

2. The second part includes the definition of nodes that forming the model which are arranged in x, y, and z coordinates after the number of each node.

This is the node definition group.

Node Number, X-coordinate, Y-coordinate, Z-coordinate.

Nodes

001 0 0 0

Appendices

002 670 0 0

003 1340 0 0

004 2010 0 0

005 2680 0 0

006 3350 0 0

007 4020 0 0

008 4690 0 0

009 5360 0 0

010 6030 0 0

011 6700 0 0

012 0 800 0

013 670 800 0

014 1340 800 0

015 2010 800 0

016 2680 800 0

017 3350 800 0

018 4020 800 0

019 4690 800 0

020 5360 800 0

021 6030 800 0

022 6700 800 0

023 4790 0 0

3. The third part contains the lions that connected between the nodes to form the model. Each number of node is written directly without ranking before and then the second node is written after one space to represent the two connected nodes by one line.

This is the line definition group.

From Node Number, To Node Number.

Lines

001 002

002 003

003 004

004 005

005 006

006 007

007 008

008 023

023 009

009 010

010 011

Appendices

012 013

013 014

014 015

015 016

016 017

017 018

018 019

019 020

020 021

021 022

001 012

002 013

003 014

004 015

005 016

006 017

007 018

008 019

009 020

010 021

011 022

4. Part number four represents the surfaces which represent the plates in the model (if they are existed). Each surface is surrounded by three lines to produce a triangular plate shape.

This is the surfaces definition group.

From first Node Number, second Node Number, to third Node Number.

Surfaces

001 002 012

002 013 012

002 003 013

003 014 013

003 004 014

004 015 014

004 005 015

005 016 015

005 006 016

006 017 016

006 007 017

007 018 017

007 008 018

008 019 018

008 023 019

023 009 019

009 020 019

009 010 020

010 021 020

010 011 021

011 022 021

5. The fifth part includes the ASC file which contains the readings of acceleration that recorded during the AVM tests. This part should be start by the name of the ASC file (with ASC extension) before the location and direction of each accelerometer within the set. The location is represented by the number of node which is in the start of the line. Then the direction is represented by three digits one of them is number ∓ 1 and the other are zeros. The numbers are ranked to represent the directions of x, y and z and the direction that the accelerometer is installed on is given the value of ∓ 1 while other two directions are given zeros. The plus-minus sign represent the opposite directions like upward or downward.

This is the definition group for the DOF information.

Description of the setups block

Setups

Measurement1

IntactBridgeDataSet 600-200-90-7-1.asc

Appendices

023 0 0 1 0.000001 m/s² Acceleration Transducer 1

023 0 -1 0 0.000001 m/s² Acceleration Transducer 2

010 0 0 1 0.000001 m/s² Acceleration Transducer 3

010 0 -1 0 0.000001 m/s² Acceleration Transducer 4

021 0 0 1 0.000001 m/s² Acceleration Transducer 5

011 0 0 1 0.000001 m/s² Acceleration Transducer 6

011 0 -1 0 0.000001 m/s² Acceleration Transducer 7

022 0 0 1 0.000001 m/s² Acceleration Transducer 8

Measurement2

IntactBridgeDataSet 600-200-90-7-2.asc

023 0 0 1 0.000001 m/s² Acceleration Transducer 1

023 0 -1 0 0.000001 m/s² Acceleration Transducer 2

008 0 0 1 0.000001 m/s² Acceleration Transducer 3

008 0 -1 0 0.000001 m/s² Acceleration Transducer 4

019 0 0 1 0.000001 m/s² Acceleration Transducer 5

009 0 0 1 0.000001 m/s² Acceleration Transducer 6

009 0 -1 0 0.000001 m/s² Acceleration Transducer 7

020 0 0 1 0.000001 m/s² Acceleration Transducer 8

Measurement3

IntactBridgeDataSet 600-200-90-7-3.asc

Appendices

023 0 0 1 0.000001 m/s² Acceleration Transducer 1

023 0 -1 0 0.000001 m/s² Acceleration Transducer 2

006 0 0 1 0.000001 m/s² Acceleration Transducer 3

006 0 -1 0 0.000001 m/s² Acceleration Transducer 4

017 0 0 1 0.000001 m/s² Acceleration Transducer 5

007 0 0 1 0.000001 m/s² Acceleration Transducer 6

007 0 -1 0 0.000001 m/s² Acceleration Transducer 7

018 0 0 1 0.000001 m/s² Acceleration Transducer 8

Measurement4

IntactBridgeDataSet 600-200-90-7-4.asc

023 0 0 1 0.000001 m/s² Acceleration Transducer 1

023 0 -1 0 0.000001 m/s² Acceleration Transducer 2

004 0 0 1 0.000001 m/s² Acceleration Transducer 3

004 0 -1 0 0.000001 m/s² Acceleration Transducer 4

015 0 0 1 0.000001 m/s² Acceleration Transducer 5

005 0 0 1 0.000001 m/s² Acceleration Transducer 6

005 0 -1 0 0.000001 m/s² Acceleration Transducer 7

016 0 0 1 0.000001 m/s² Acceleration Transducer 8

Measurement5

IntactBridgeDataSet 600-200-90-7-5.asc

023 0 0 1 0.000001 m/s² Acceleration Transducer 1

023 0 -1 0 0.000001 m/s² Acceleration Transducer 2

002 0 0 1 0.000001 m/s² Acceleration Transducer 3

002 0 -1 0 0.000001 m/s² Acceleration Transducer 4

013 0 0 1 0.000001 m/s² Acceleration Transducer 5

003 0 0 1 0.000001 m/s² Acceleration Transducer 6

003 0 -1 0 0.000001 m/s² Acceleration Transducer 7

014 0 0 1 0.000001 m/s² Acceleration Transducer 8

6. The last part includes the definition of equations which represent the relationship between the nodes that contain measurements and those without measurements. The nodes without measurements which are needed to be moved as those that contain measurements are in the left side of equation.

This is the definition group for slave node equations.

Left side node should move according to the right side equation.

Equations

node(011,2)=0

node(011,3)=0

node(022,2)=0

node(022,3)=0

node(013,2)=node(002,2)

node(014,2)=node(003,2)

node(015,2)=node(004,2)

node(016,2)=node(005,2)

node(017,2)=node(006,2)

node(018,2)=node(007,2)

node(019,2)=node(008,2)

node(020,2)=node(009,2)

node(021,2)=node(010,2)

node(022,2)=node(011,2)

The above configuration input file is designed for the intact grid-bridge model in the present work.

APPENDIX B. The acceleration data file (ASC file)

According to the configuration input file explained earlier, five sets are existed which contain the acceleration data that recorded during the AVM tests as ASC file form. A small part of the ASC file acceleration data in the first set of measurement that used in the grid-bridge model is listed in *Table 10.1*. The first column (from the left side) represent the time for recording data which has 0.001667 step as the value of sampling interval (T). Other columns represent the accelerometers and the data under each one are the acceleration that recorded during the test. *Table 10.1* lists the first 70 records of set 1 as a sample of recorded data according to the intact grid-bridge model without additional mass during AVM test.

Table 10.1: Acceleration data of the ASC file

Time	Accelero.1	Accelero.2	Accelero.3	Accelero.4	Accelero.5	Accelero.6	Accelero.7	Accelero.8
0.0000	10.1425	0.3687	10.2037	0.5445	10.2204	10.0201	0.2974	10.0181
0.0017	10.1449	0.3693	10.2049	0.5465	10.2211	10.0170	0.2953	10.0177
0.0033	10.1457	0.3679	10.2067	0.5425	10.2208	10.0197	0.2948	10.0177
0.0050	10.1455	0.3671	10.2067	0.5400	10.2174	10.0218	0.2937	10.0169
0.0067	10.1423	0.3690	10.2092	0.5417	10.2166	10.0185	0.2930	10.0167
0.0083	10.1416	0.3694	10.2142	0.5426	10.2174	10.0184	0.2937	10.0154
0.0100	10.1411	0.3713	10.2123	0.5393	10.2159	10.0188	0.2943	10.0155
0.0117	10.1435	0.3686	10.2089	0.5430	10.2167	10.0179	0.2941	10.0181
0.0133	10.1434	0.3694	10.2104	0.5448	10.2260	10.0187	0.2949	10.0185
0.0150	10.1477	0.3723	10.2113	0.5413	10.2282	10.0185	0.2952	10.0180
0.0167	10.1479	0.3715	10.2111	0.5450	10.2270	10.0205	0.2943	10.0148
0.0183	10.1452	0.3710	10.2084	0.5451	10.2265	10.0185	0.2957	10.0159
0.0200	10.1477	0.3719	10.2074	0.5435	10.2217	10.0179	0.2961	10.0184
0.0217	10.1475	0.3716	10.2108	0.5447	10.2221	10.0183	0.2921	10.0155
0.0233	10.1473	0.3709	10.2123	0.5429	10.2194	10.0189	0.2933	10.0164
0.0250	10.1482	0.3718	10.2147	0.5452	10.2167	10.0207	0.2962	10.0195
0.0267	10.1485	0.3718	10.2133	0.5445	10.2174	10.0167	0.2927	10.0180
0.0283	10.1516	0.3695	10.2078	0.5425	10.2159	10.0172	0.2924	10.0175
0.0300	10.1546	0.3667	10.2083	0.5446	10.2167	10.0191	0.2921	10.0152
0.0317	10.1531	0.3681	10.2059	0.5438	10.2207	10.0197	0.2933	10.0185
0.0333	10.1542	0.3696	10.2059	0.5435	10.2215	10.0232	0.2937	10.0178
0.0350	10.1556	0.3694	10.2074	0.5409	10.2231	10.0195	0.2928	10.0150
0.0367	10.1547	0.3721	10.2084	0.5409	10.2253	10.0180	0.2950	10.0170
0.0383	10.1537	0.3722	10.2103	0.5439	10.2268	10.0206	0.2927	10.0197
0.0400	10.1528	0.3723	10.2160	0.5450	10.2218	10.0204	0.2932	10.0168
0.0417	10.1483	0.3718	10.2192	0.5419	10.2208	10.0181	0.2927	10.0176
0.0433	10.1499	0.3737	10.2198	0.5439	10.2234	10.0197	0.2928	10.0155
0.0450	10.1537	0.3739	10.2171	0.5453	10.2199	10.0195	0.2947	10.0166

Appendices

0.0467	10.1555	0.3709	10.2159	0.5456	10.2251	10.0181	0.2955	10.0206
0.0483	10.1570	0.3731	10.2125	0.5441	10.2304	10.0169	0.2928	10.0181
0.0500	10.1590	0.3725	10.2084	0.5427	10.2242	10.0193	0.2975	10.0169
0.0517	10.1586	0.3698	10.2083	0.5414	10.2242	10.0192	0.2949	10.0158
0.0533	10.1603	0.3703	10.2107	0.5407	10.2244	10.0187	0.2958	10.0197
0.0550	10.1589	0.3658	10.2115	0.5408	10.2218	10.0185	0.2945	10.0167
0.0567	10.1570	0.3643	10.2147	0.5410	10.2217	10.0164	0.2911	10.0139
0.0583	10.1578	0.3647	10.2178	0.5412	10.2228	10.0192	0.2915	10.0149
0.0600	10.1561	0.3670	10.2161	0.5403	10.2216	10.0190	0.2895	10.0176
0.0617	10.1541	0.3694	10.2145	0.5419	10.2256	10.0187	0.2930	10.0168
0.0633	10.1567	0.3723	10.2112	0.5402	10.2264	10.0170	0.2961	10.0158
0.0650	10.1567	0.3727	10.2138	0.5413	10.2292	10.0185	0.2947	10.0176
0.0667	10.1557	0.3723	10.2111	0.5435	10.2316	10.0184	0.2942	10.0190
0.0683	10.1563	0.3756	10.2083	0.5474	10.2292	10.0180	0.2982	10.0161
0.0700	10.1591	0.3748	10.2093	0.5442	10.2289	10.0186	0.2965	10.0158
0.0717	10.1583	0.3710	10.2124	0.5444	10.2259	10.0175	0.2955	10.0146
0.0733	10.1558	0.3733	10.2149	0.5467	10.2221	10.0177	0.2934	10.0173
0.0750	10.1589	0.3718	10.2168	0.5434	10.2203	10.0186	0.2930	10.0191
0.0767	10.1581	0.3687	10.2157	0.5443	10.2180	10.0208	0.2937	10.0186
0.0783	10.1584	0.3662	10.2159	0.5419	10.2185	10.0204	0.2935	10.0158
0.0800	10.1591	0.3665	10.2130	0.5431	10.2195	10.0172	0.2930	10.0157
0.0817	10.1613	0.3678	10.2104	0.5425	10.2244	10.0182	0.2948	10.0174
0.0833	10.1613	0.3655	10.2079	0.5403	10.2260	10.0173	0.2935	10.0180
0.0850	10.1647	0.3678	10.2071	0.5415	10.2289	10.0214	0.2924	10.0145
0.0867	10.1607	0.3700	10.2109	0.5425	10.2328	10.0200	0.2937	10.0158
0.0883	10.1599	0.3688	10.2110	0.5431	10.2264	10.0193	0.2962	10.0180
0.0900	10.1588	0.3718	10.2175	0.5441	10.2268	10.0202	0.2951	10.0160
0.0917	10.1592	0.3714	10.2209	0.5447	10.2282	10.0217	0.2941	10.0191
0.0933	10.1574	0.3745	10.2162	0.5466	10.2280	10.0176	0.2940	10.0169
0.0950	10.1563	0.3734	10.2151	0.5456	10.2297	10.0189	0.2959	10.0162
0.0967	10.1600	0.3743	10.2153	0.5448	10.2299	10.0204	0.2971	10.0214
0.0983	10.1608	0.3723	10.2171	0.5469	10.2315	10.0190	0.2952	10.0163
0.1000	10.1625	0.3746	10.2161	0.5437	10.2336	10.0171	0.2965	10.0157
0.1017	10.1629	0.3749	10.2162	0.5418	10.2259	10.0158	0.2962	10.0162
0.1033	10.1611	0.3684	10.2133	0.5442	10.2291	10.0174	0.2943	10.0165
0.1050	10.1623	0.3694	10.2154	0.5446	10.2244	10.0221	0.2939	10.0147
0.1067	10.1643	0.3661	10.2152	0.5415	10.2232	10.0194	0.2928	10.0148
0.1083	10.1630	0.3672	10.2173	0.5412	10.2231	10.0210	0.2886	10.0174
0.1100	10.1587	0.3674	10.2158	0.5412	10.2232	10.0209	0.2881	10.0177
0.1117	10.1603	0.3699	10.2162	0.5420	10.2242	10.0172	0.2928	10.0176
0.1133	10.1611	0.3730	10.2138	0.5415	10.2312	10.0197	0.2919	10.0169
0.1150	10.1643	0.3727	10.2119	0.5431	10.2325	10.0179	0.2944	10.0166

APPENDIX C. Relations between recorded data and time of AVM tests

According to the grid-bridge model as a case study, the relations between the recorded acceleration and the time of AVM test for each accelerometer in one set of measurement are shown as following:

1. Model without additional mass

Figure 10.1: Acceleration measurements of set 1

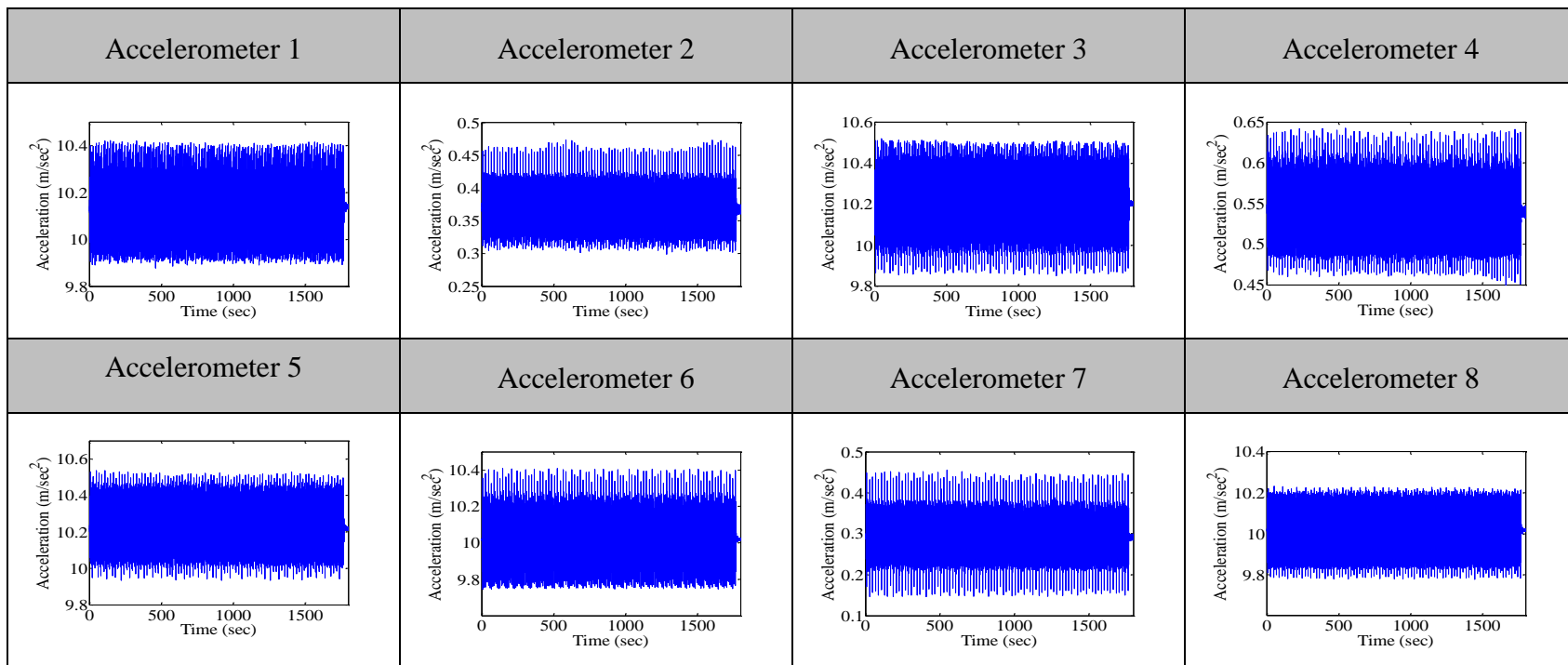


Figure 10.2: Acceleration measurements of set 2

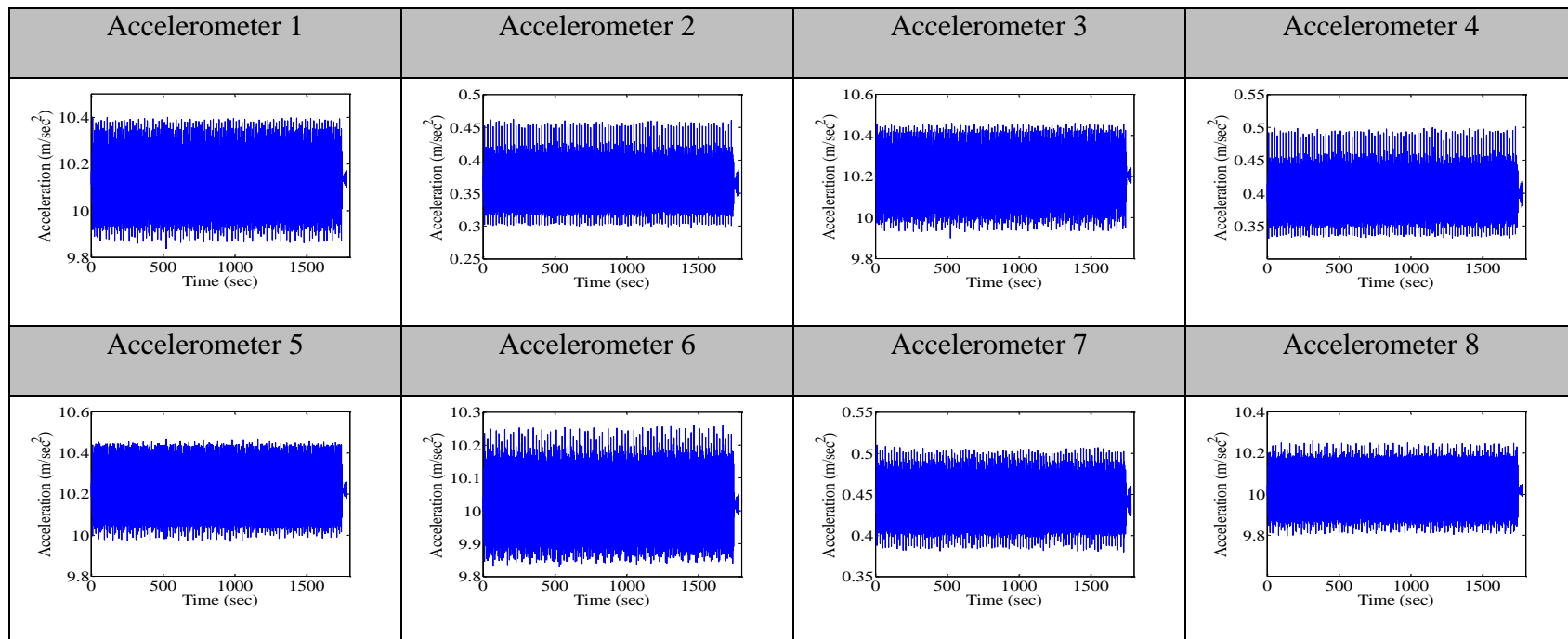


Figure 10.3: Acceleration measurements of set 3

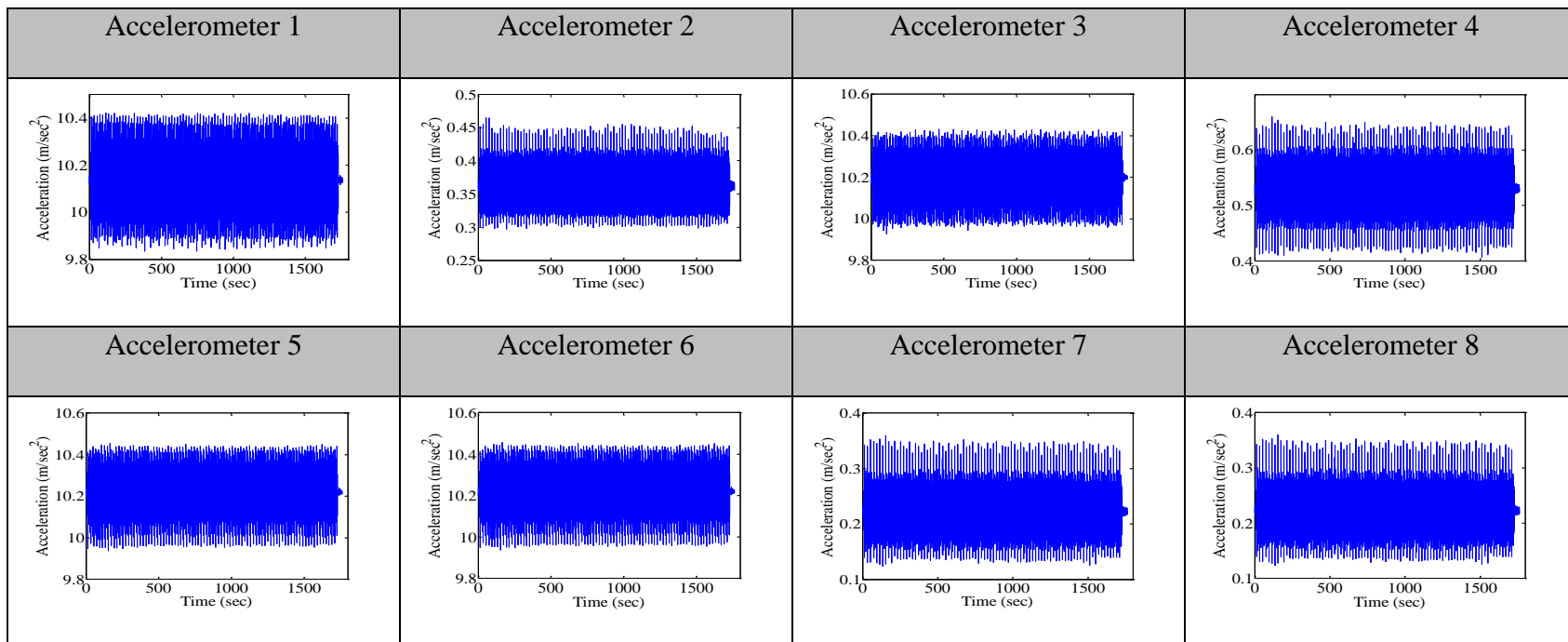


Figure 10.4: Acceleration measurements of set 4

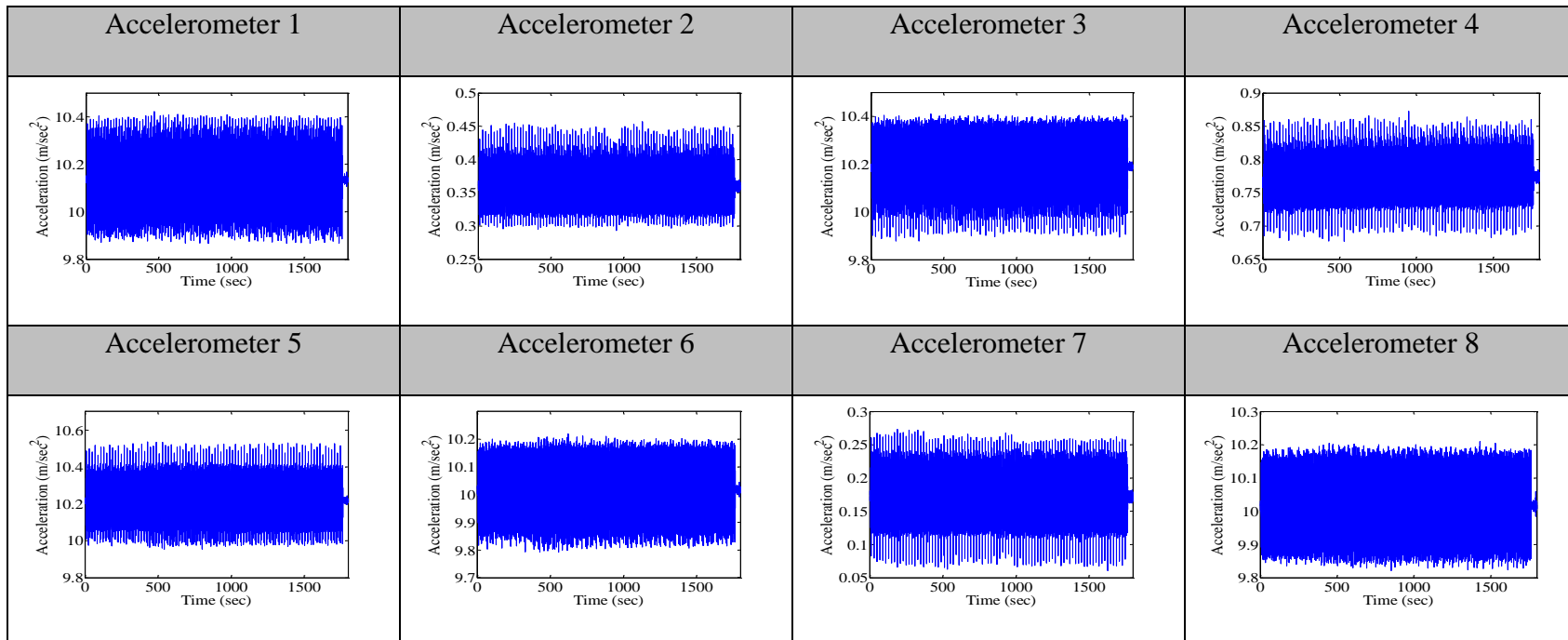
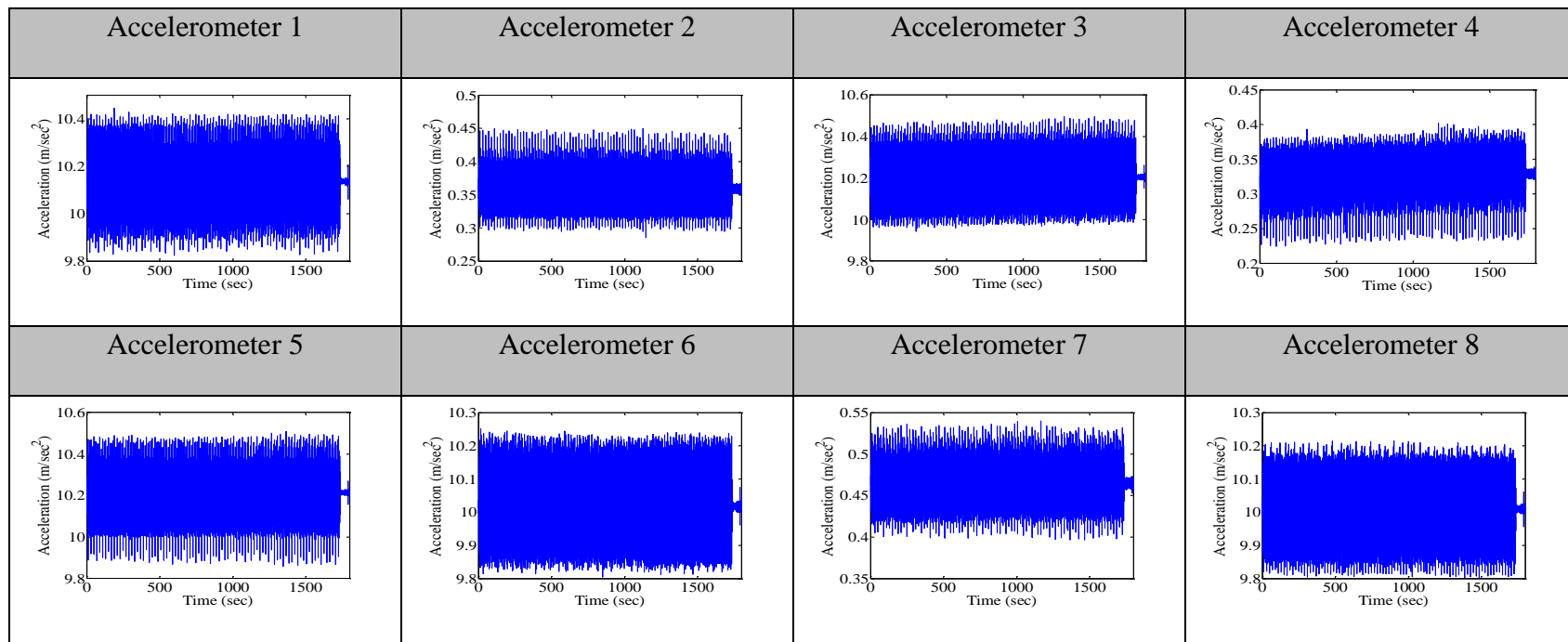


Figure 10.5: Acceleration measurements of set 5



2. Model with additional mass

Figure 10.6: Acceleration measurements of set 1

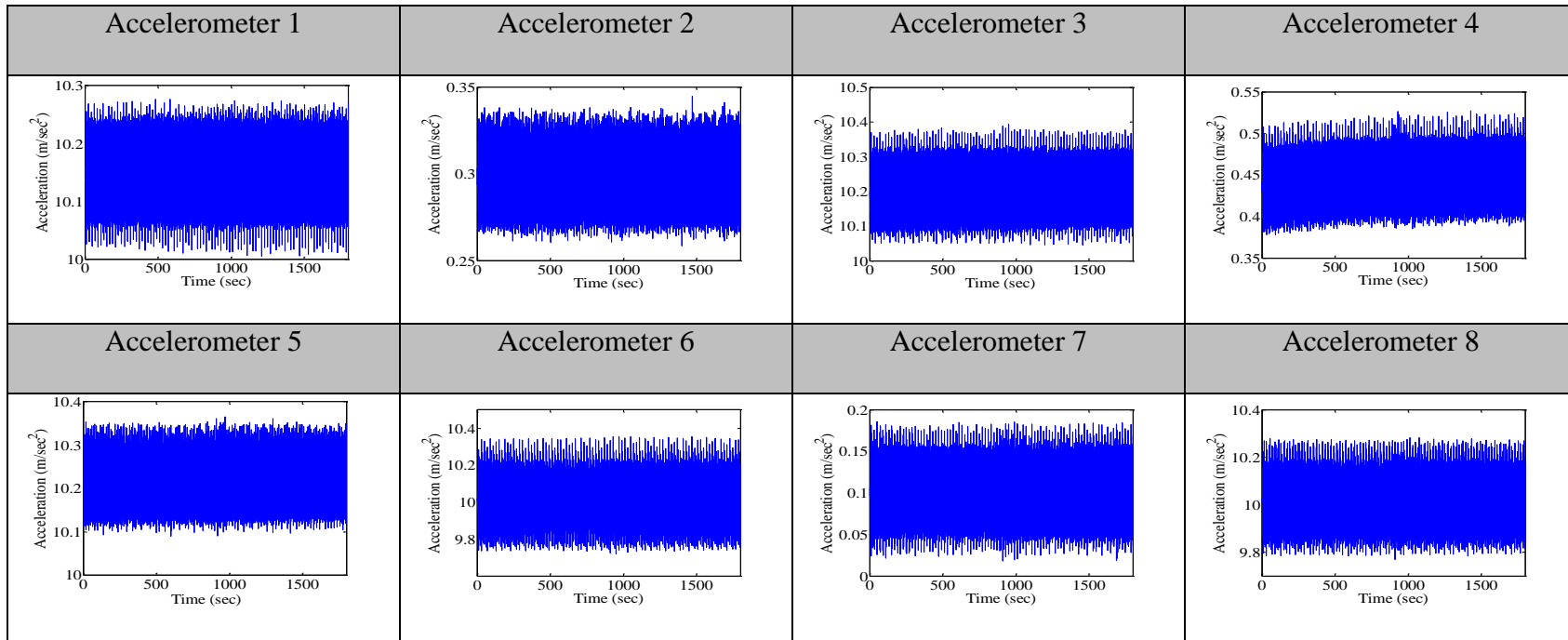


Figure 10.7: Acceleration measurements of set 2

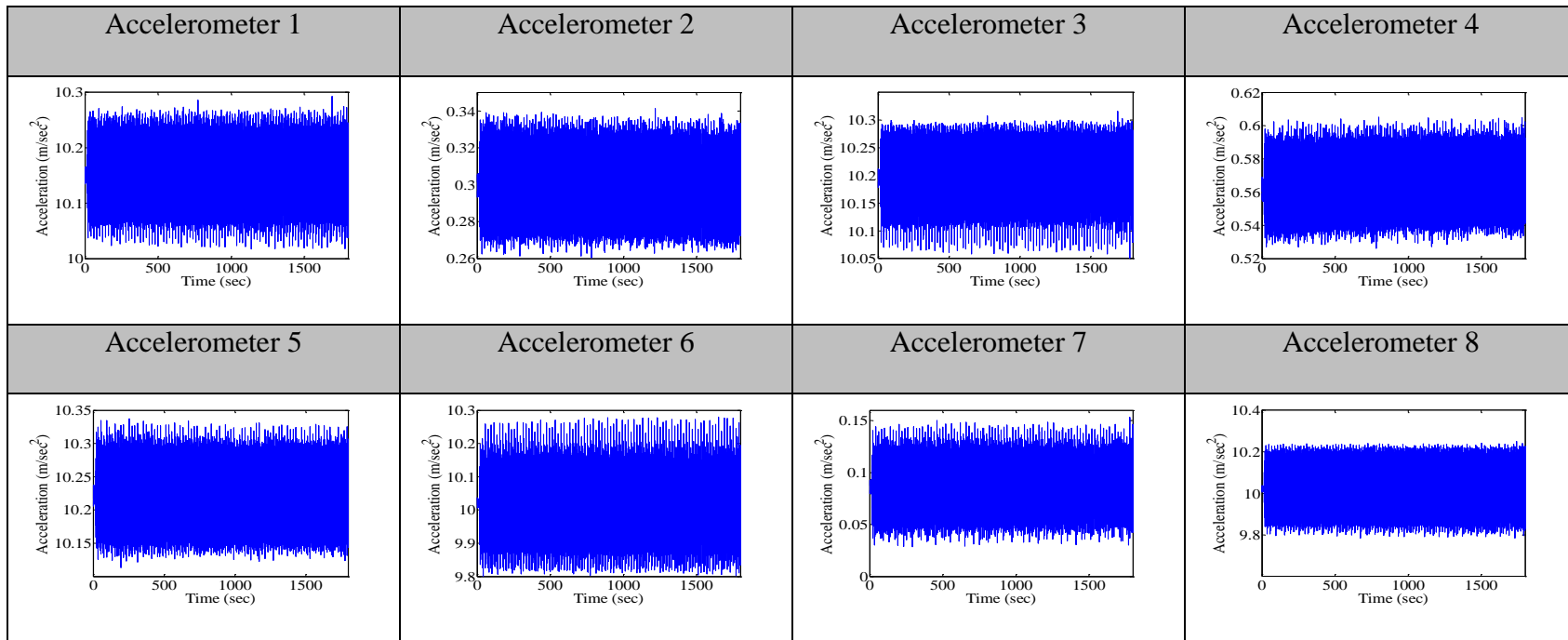


Figure 10.8: Acceleration measurements of set 3

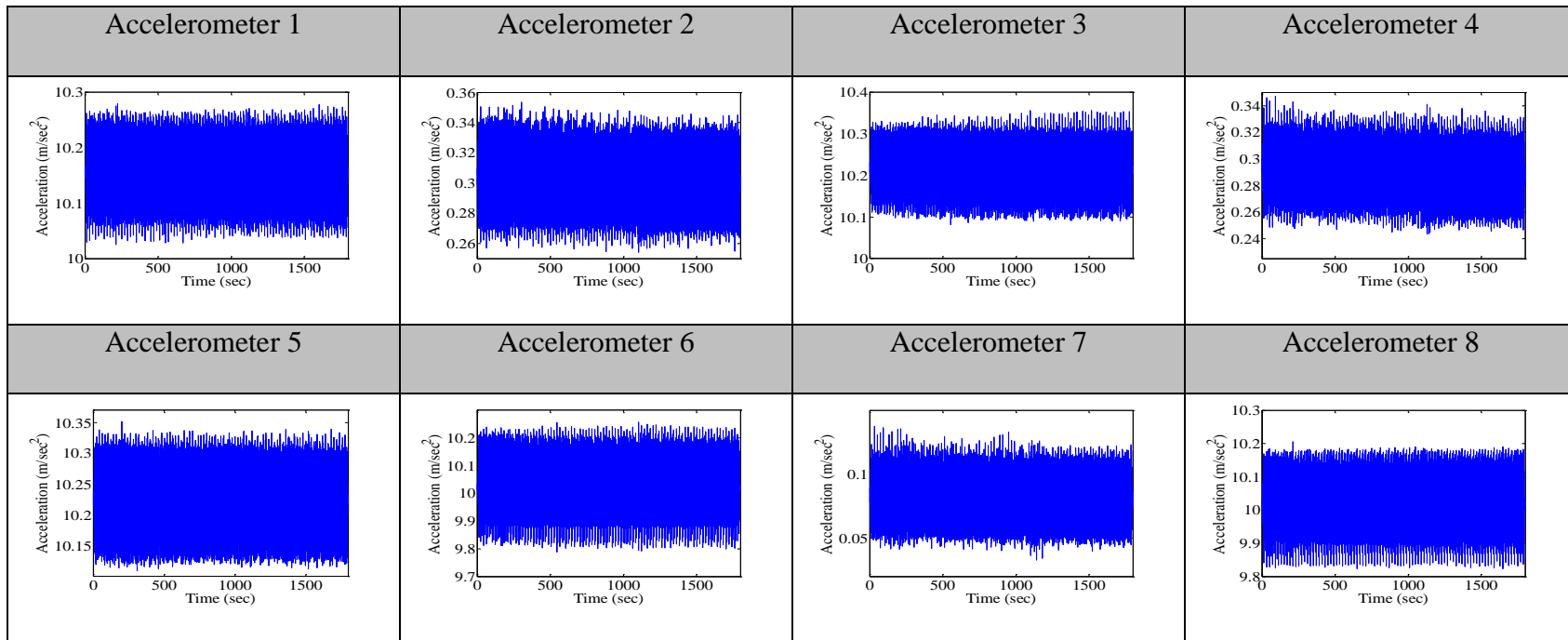


Figure 10.9: Acceleration measurements of set 4

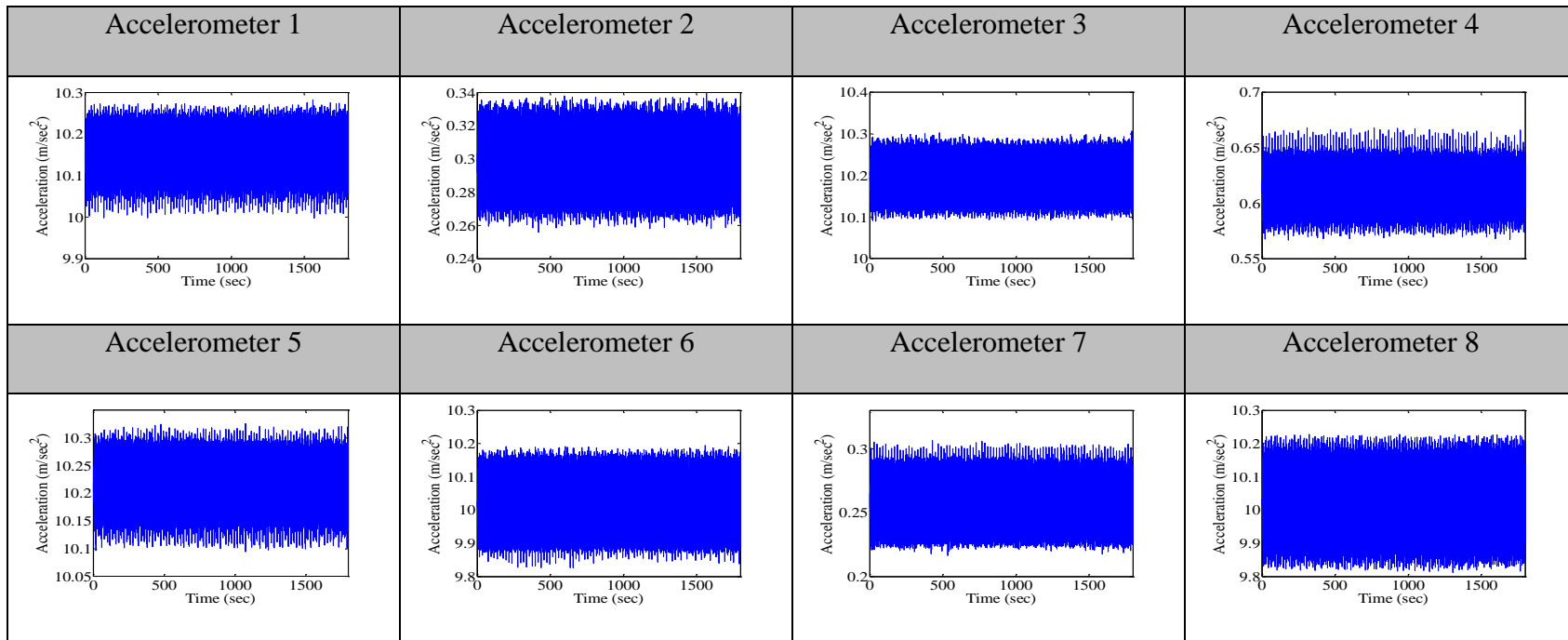
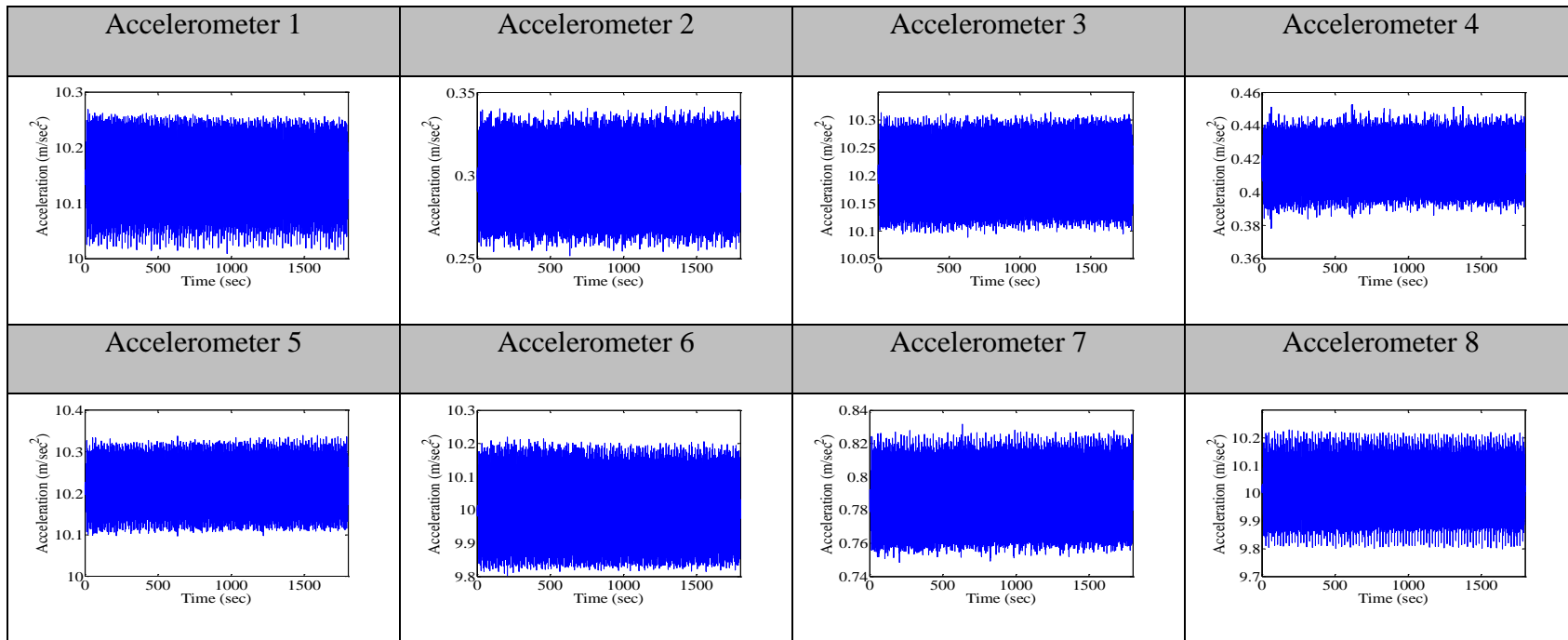


Figure 10.10: Acceleration measurements of set 5



AUTHOR BIOGRAPHY

Ahmed Alalikhhan was born in Najaf - Republic of Iraq 25. 04. 1976, where he completed his primary and secondary school. In 1994, he enrolled in Department of Civil Engineering, Faculty of Engineering, University of Kufa - Najaf - Iraq, and completed his undergraduate studies by defending his final BSc work entitled "Optimum design of rectangular concrete columns" in 1998. In 1998, the author started his MSc study in Department of Building and Construction Engineering, Faculty of Engineering, University of Technology - Baghdad - Iraq, which lasted three years. The author completed his MSc study in 2001 by defending his master thesis entitled "Design of reinforced concrete beams in shear with and without fibers" with an average score of 8.07. Then, the author was enrolled in 2011 at the Structural Engineering Department, Faculty of Civil Engineering, University of Belgrade to start his doctoral studies within the project of "World in Serbia".

Since 2002, the author had participations in several aspects during his service in the academic fields. He started as an assistant lecturer in the Department of Civil Engineering, Faculty of Engineering, University of Kufa - Najaf - Iraq by teaching Engineering Mechanics and Strength of Material for the first and second stages, respectively, as a main lecturer. In that period, the author was a member in several committees such as, Examination Committee, a member in the non-destructive (ultrasonic) tests committee, a designer of new buildings in the University of Kufa within the structural design committee and other else. The author is a member of the Iraqi Society of Engineers and holds the authority for the design and construction of civil engineering structures. Professional activities of the author includes, ordinary and fibrous reinforced concrete, steel constructions and building materials. Therefore, the author had participations in analyzing and designing of some famous constructions in Iraq such as, building of medicine deanship in Kufa University, structural steel frames in the French Kərbala cement plant and other else. The author has several published papers in the academic field, as author or co-author, which had been published through national or international journals.

The author is married and father for four Childs.

Прилог 1.

Изјава о ауторству

Потписани: Ахмед Алаликхан дипл. грађ. инж.

број индекса: 913/11

Изјављујем

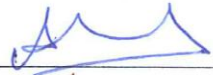
да је докторска дисертација под насловом

**„ДЕТЕКЦИЈА И ЛОКАЛИЗАЦИЈА ОШТЕЋЕЊА ГРАЂЕВИНСКИХ КОНСТРУКЦИЈА
НА ОСНОВУ РЕГИСТРОВАНИХ АМБИЈЕНТАЛНИХ ВИБРАЦИЈА“**

- резултат сопственог истраживачког рада,
- да предложена дисертација у целини ни у деловима није била предложена за добијање било које дипломе према студијским програмима других високошколских установа,
- да су резултати коректно наведени и
- да нисам кршио/ла ауторска права и користио интелектуалну својину других лица.

Потпис докторанда

У Београду, 2016.



Прилог 2.

Изјава о истоветности штампане и електронске верзије докторског рада

Име и презиме аутора: Ахмед Алаликхан дипл. грађ. инж.

Број индекса: 913/11

Студијски програм: Грађевинарство

Наслов рада: „ДЕТЕКЦИЈА И ЛОКАЛИЗАЦИЈА ОШТЕЋЕЊА
ГРАЂЕВИНСКИХ КОНСТРУКЦИЈА НА ОСНОВУ
РЕГИСТРОВАНИХ АМБИЈЕНТАЛНИХ ВИБРАЦИЈА“

Ментор: Др Зоран Мишковић, ванредни професор
Универзитет у Београду, Грађевински факултет

Потписани: Ахмед Алаликхан дипл. грађ. инж.

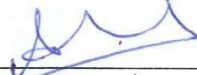
Изјављујем да је штампана верзија мог докторског рада истоветна електронској верзији коју сам предао за објављивање на порталу Дигиталног репозиторијума Универзитета у Београду.

Дозвољавам да се објаве моји лични подаци везани за добијање академског звања доктора наука, као што су име и презиме, година и место рођења и датум одбране рада.

Ови лични подаци могу се објавити на мрежним страницама дигиталне библиотеке, у електронском каталогу и у публикацијама Универзитета у Београду.

Потпис докторанда

У Београду, 2016.



Прилог 3.

Изјава о коришћењу

Овлашћујем Универзитетску библиотеку „Светозар Марковић“ да у Дигитални репозиторијум Универзитета у Београду унесе моју докторску дисертацију под насловом:

„ДЕТЕКЦИЈА И ЛОКАЛИЗАЦИЈА ОШТЕЋЕЊА ГРАЂЕВИНСКИХ КОНСТРУКЦИЈА НА ОСНОВУ РЕГИСТРОВАНИХ АМБИЈЕНТАЛНИХ ВИБРАЦИЈА“

која је моје ауторско дело.

Дисертацију са свим прилозима предао/ла сам у електронском формату погодном за трајно архивирање.

Моју докторску дисертацију похрањену у Дигитални репозиторијум Универзитета у Београду могу да користе сви који поштују одредбе садржане у одабраном типу лиценце Креативне заједнице (Creative Commons) за коју сам се одлучио/ла.

1. Ауторство

2. Ауторство - некомерцијално

3. Ауторство – некомерцијално – без прераде

4. Ауторство – некомерцијално – делити под истим условима

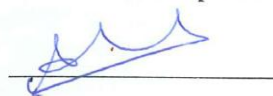
5. Ауторство – без прераде

6. Ауторство – делити под истим условима

(Молимо да заокружите само једну од шест понуђених лиценци, кратак опис лиценци дат је на полеђини листа).

У Београду, 2016.

Потпис докторанда



1. Ауторство - Дозвољаваате умножавање, дистрибуцију и јавно саопштавање дела, и прераде, ако се наведе име аутора на начин одређен од стране аутора или даваоца лиценце, чак и у комерцијалне сврхе. Ово је најслободнија од свих лиценци.

2. Ауторство – некомерцијално Дозвољаваате умножавање, дистрибуцију и јавно саопштавање дела, и прераде, ако се наведе име аутора на начин одређен од стране аутора или даваоца лиценце. Ова лиценца не дозвољава комерцијалну употребу дела.

3. Ауторство - некомерцијално – без прераде. Дозвољаваате умножавање, дистрибуцију и јавно саопштавање дела, без промена, преобликовања или употребе дела у свом делу, ако се наведе име аутора на начин одређен од стране аутора или даваоца лиценце. Ова лиценца не дозвољава комерцијалну употребу дела. У односу на све остале лиценце, овом лиценцом се ограничава највећи обим права коришћења дела.

4. Ауторство - некомерцијално – делити под истим условима. Дозвољаваате умножавање, дистрибуцију и јавно саопштавање дела, и прераде, ако се наведе име аутора на начин одређен од стране аутора или даваоца лиценце и ако се прерада дистрибуира под истом или сличном лиценцом. Ова лиценца не дозвољава комерцијалну употребу дела и прерада.

5. Ауторство – без прераде. Дозвољаваате умножавање, дистрибуцију и јавно саопштавање дела, без промена, преобликовања или употребе дела у свом делу, ако се наведе име аутора на начин одређен од стране аутора или даваоца лиценце. Ова лиценца дозвољава комерцијалну употребу дела.

6. Ауторство - делити под истим условима. Дозвољаваате умножавање, дистрибуцију и јавно саопштавање дела, и прераде, ако се наведе име аутора на начин одређен од стране аутора или даваоца лиценце и ако се прерада дистрибуира под истом или сличном лиценцом. Ова лиценца дозвољава комерцијалну употребу дела и прерада. Слична је софтверским лиценцама, односно лиценцама отвореног кода.